University of Southampton

EngD Thesis

A Paradigm to Maximise Performance and Profitability of Engineering Products in the Presence of Manufacturing Uncertainty

Author:
Christopher Stephen Dodd

Supervisors:
James Scanlan
Steve Wiseall
Rob Marsh

A thesis submitted in fulfilment of the requirements for the degree of Engineering Doctorate

in the

Computational Engineering Design Research Group
Faculty of Engineering and the Environment

April 2015

Declaration of Authorship

I, Christopher Dodd, declare that this thesis entitled 'A Paradigm to Maximise Performance and Profitability of Engineering Products in the Presence of Manufacturing Uncertainty' and the work presented in it are my own and has been generated by me as the result of my own original research.

- This work was done wholly or mainly while in candidature for a research degree at this University;
- Where any part of this thesis has previously been submitted for a degree or any other qualification at this University or any other institution, this has been clearly stated;
- Where I have consulted the published work of others, this is always clearly attributed;
- Where I have quoted from the work of others, the source is always given. With the exception of such quotations, this thesis is entirely my own work;
- I have acknowledged all main sources of help;
- Where the thesis is based on work done by myself jointly with others, I have made clear exactly what was done by others and what I have contributed myself;
- Two articles had been submitted to the International Journal of Production Economics and The International Journal of Advanced Manufacturing Technology, respectively. The articles are recommended for publication subject to revisions. The first article covers the material presented on the generalisation of the expected profit equations (Section 3.2.2 to Section 3.2.2.3). The second paper presents much of the material in Section 3.1.1 and Section 3.5.1.

Signed: _____

Date: _____

UNIVERSITY OF SOUTHAMPTON

Abstract

Engineering and the Environment
Computational Engineering Design Research Group

Engineering Doctorate

A Paradigm to Maximise Performance and Profitability of Engineering Products in the Presence of Manufacturing Uncertainty

by Christopher Dodd

Variation in the manufactured geometry of engineering components is perpetually present in production. Random variation can arise due to slight differences in material properties, machines and tools, processes and even climatic conditions in the factory. To guarantee the functionality or quality of individual components, features are inspected to verify they conform to the tolerance limits imposed. It is undesirable to produce non-conforming features, due to the cost of reworking features or scrapping components. In practice, it is not always feasible to improve manufacturing capability (reduce variation), or design components to be less susceptible to variation; in such a situation the cost of non-conformance should be minimised. Optimal Mean Setting, a methodology to maximise profit from a production system where the manufacturing variation is often greater than a feature's tolerance limits, can be applied in these circumstances.

Although the principle of Optimal Mean Setting dates back over 60 years, its application to engineering design is relatively undeveloped. A major part of this thesis was devoted to developing a robust, reliable and generalised framework to practice Optimal Mean Setting in engineering design. Errors were uncovered in previous attempts in the literature relating to Optimal Mean Setting of simple systems. Improvements to the maximum obtainable profit were also realised by implementing a new optimisation strategy to that developed in the literature. Another innovation developed in this thesis was the the application of copula function modelling to Optimal Mean Setting. Copulas allowed joint distributions to be created from non-parametric (or non family specific) feature variation distributions. This permitted Optimal Mean Setting to be applied to components with several quality characteristics where different distributions modelled the manufacturing variation. It also allowed the final geometry of a component to be modelled to access the distribution of performance of a batch of components. Numerical examples and the applications to real components are given.

Acknowledgements

I would like to express special thanks to my academic supervisory team, Jim Scanlan and Rob Marsh and my industrial supervisor Steve Wiseall who sadly passed away towards the end of last year. I have had the privilege of having tremendous freedom in the direction my research took, but always felt well supported in the work I was doing. I thank them for their trust and confidence in the path I was taking, particularly in the first three years of the EngD programme. Particular thanks must also go to Jim Scanlan who managed to orchestrate numerous regular review meetings with academic and Rolls-Royce personnel that regularly generated useful discussions and insights. Rob Marsh has provided insightful feedback on all my major written contributions throughout my thesis, I thank him greatly for the time he has taken doing this.

I am indebted to the numerous people in the Computational Engineering and Design Group at the University of Southampton for their discussions and expertise. Similarly, I thank the Product Cost Engineering group at Rolls-Royce who regularly attended my talks and presentations despite their busy schedules and were always open for a discussion. I will always be grateful to Steve Wiseall for his support at Rolls-Royce and his help with introducing me to the right people.

Particular thanks go to my mother and father for supporting my education and for their help proof reading sections of my thesis, as well as Bryony Meakins. Despite not having engineering backgrounds they persisted in trying to understand what I was attempting to articulate and this thesis is considerably improved due to them.

Contents

List of Figures

List of Tables

Definitions

Feature In this thesis a feature refers to a piece of geometry that requires inspection. Features are also referred to as *quality characteristics* in the literature. In general, features may be classified as manufacturing or design features, which are not necessarily equivalent. For example, the wall thickness of a turned pressure vessel may be a design parameter but it is created from the difference between two manufacturing features, the outer turned diameter and the inner turned diameter.

Rework Applies to a single feature of a component (although many features on the same component may be reworked). If a feature is found to be non-conforming but additional manufacturing operations can make that feature conform, the feature may be reworked.

Rework Cost Is the cost of reworking a feature. This includes all the economic resources required to get the component from the point at which it was deemed rework, reprocessed and place it back in the manufacturing sequence.

Scrap Applies to a whole component, but is due to non-conformance from a single feature. If a feature is found to be non-conforming, such that no additional manufacturing processes can be used to convert that feature into a conforming feature, the component is scrap.

Scrap Cost Is the difference between the residual value of the component deemed scrap, and the economic resources required to get the component to that particular stage in the manufacturing process.

Sequence Refers to the position of an inspection process relative to the order features are manufactured. For example, if two features were manufactured prior to being inspected, this is considered a different sequence compared to the manufacture and inspection of one feature followed by the manufacture and inspection of the second feature.

Stage Refers to the complete set of manufacturing processes required to manufacture a feature. In this thesis, stages are numbered using Roman numerals.

State Refers to part of a manufacturing stage that a component or feature is in. For example, within a manufacturing stage a rework loop may exist. Conforming and scrap states also exist within a manufacturing sequence depending on whether a feature conforms or does not conform from the preceding states or stages. States are referred to using Arabic numerals or C and S to denote conforming and scrap states.

Nomenclature

σ	standard deviation
ν	shape parameter (tLocation scale distribution)
$\mathbf{\Sigma}$	correlation matrix (Optimal Mean Setting)
ψ	correlation between two random variable (response surface)
$\mathbf{\Psi}$	correlation matrix (response surface modelling)
μ	mean
δ_{ij}	Kronecker delta
$\boldsymbol{\xi}$	noise in a system
U	upper specification limit
L	lower specification limit
$\boldsymbol{U}$	vector of upper specification limits
$\boldsymbol{L}$	vector of lower specification limits
SP	selling price (monetary units)
PC	processing cost (monetary units)
Sc	scrap cost (monetary units)
Rc	rework cost (monetary units)

Functions

$\phi(\bullet)$	standard normal probability distribution function
$\mathbf{\Phi}(\bullet)$	standard normal cumulative distribution function
$\xi(\bullet)$	error function
$\Gamma(\bullet)$	Gamma function
$C(\bullet)$	copula function
$F(\bullet)$	cumulative distribution function
$f(\bullet)$	probability distribution function

Film Cooling Hole

$\bar{u}$	mean component of velocity	(m/s)
$u^{'}$	fluctuating component of velocity	(m/s)
ρ	density	(kg/m^3)
κ	turbulent kinetic energy	J/kg
ε	turbulent dissipation rate	$J/kg\,s$
ν	kinematic viscosity	m^2/s
η	normalised cooling effectiveness	

Chapter 1

Introduction

1.1 Engineering Doctorate

The Engineering Doctorate (EngD) is a four year research programme combining Doctor of Philosophy (PhD) level research with taught components in an industrial setting. A proportion of these taught components are taken from a Masters of Business Administration (MBA) course while the remaining elements are technically biased to the EngD subject area. Each EngD programme is associated with an industrial sponsor with whom the candidate spends around 75% of their time.

The author is currently enrolled on an EngD programme run by the University of Southampton's Industrial Doctoral Training Centre (IDTC) and partnered by Rolls-Royce plc. Funding for this EngD programme is provided through the Engineering and Physical Sciences Research Council (EPSRC) and Rolls-Royce plc. The Rolls-Royce contribution is part of a Rolls-Royce led research programme; Strategic Investment in Low Carbon Engine Technology (SILOET), which was instigated in 2009 to accelerate the development of low carbon engine technologies. Support for SILOET has been provided by UK Government Department of Business, Innovation and Skills, managed by the Technology Strategy Board. The author and his academic supervisors are affiliated with the Computational Engineering and Design Group (CEDG) at the University of Southampton which is a Rolls-Royce University Technology Centre (UTC). At Rolls-Royce the author is based in the Product Cost Engineering (PCE) group which is part of the Rolls-Royce Design System Engineering (DSE) department.

1.2 Rolls-Royce

Rolls-Royce is a global provider of integrated power systems and services. The company operates in five main sectors:

- Civil aerospace
- Defence aerospace
- Marine
- Power Systems
- Nuclear

In these sectors as much as 50% of business comes from providing service support in the form of full-life care contracts between customers[1]. Rolls-Royce derives over 40% of its revenue from the civil aerospace sector (Hollinger and Powley [2014]) which primarily involves the design, manufacture and servicing of propulsive gas turbine engines. The SILOET programme is primarily focussed in the civil aerospace sector and the work undertaken in this report is contextualised around gas turbine engines.

1.3 Project Background

1.3.1 Cost Modelling

Part of the SILOET project, work package 2.5, relates to cost modelling which aims to:

"embed cost engineering processes, skills and tools into the organisation such that product cost is understood and 'traded', enabling optimum business solutions (product and supply chain) to be designed concurrently in a timely and efficient manner".

Cost modelling is one of the more immature engineering disciplines within Rolls-Royce and the overall objectives of SILOET work package 2.5 were to:

- *"Improve existing unit cost capability at process and component level through to whole engine level."*

[1] Retrieved from http://www.rolls-royce.com/careers/working_for_us/our_business/ - 21/10/2014

- *"Integrate this improved unit costing capability into design workflows; Key System at component and subsystem level and Enterprise/EPDS (Engine Preliminary Design System) at whole engine level."*

The development of accurate cost models enables cost to be a mainstream engineering parameter which, like stress, weight, aerodynamic flow and thermal transfer can be used in design optimisation as an objective function or constraint. The cost of Rolls-Royce engines is of fundamental economic importance to Rolls-Royce. Although the company enjoys a 50% market share in the wide-body aircraft engine market[2], it operates with a 9% to 14% profit margin compared to 19.8% from Rolls-Royce's main rival in the civil aerospace sector, General Electric (GE) (Hollinger and Powley [2014]). The calculation of profit margin is multifaceted, involving not only the unit cost of engines but the many operating costs of the company and profits derived from servicing operations. Nevertheless engine unit cost is clearly a significant contribution to profits achievable by the company. The importance of calculating unit cost concurrently during the design process was conceptually acknowledged by Miles and Swift [1998] as shown in Figure 1.1. Cost is committed very early in the design process, determined by the product concept which defines materials, geometry and to a large extent the manufacturing processes. It becomes increasingly hard to alter this as the design progresses. Unlike typical engineering variables, unit cost is not described by a governing physical equation, rather it is a measure of all the economic resources required to create a product. Ultimately, this manifests in a complex interrelationship between a supply chain and manufacturing processes and practices. Many of these challenges to unit cost estimation were addressed by a Rolls-Royce lead research programme DATUM (Design Analysis Tool for Unit-Cost Modelling) which began in 2002. This led to the development a broadly generative feature-based costing tool which linked design parameters and features to the method of manufacture, capturing the allocation of resources required to realise a product definition (Scanlan et al. [2006]). The issues regarding cost modelling are discussed in more detail in a review of the literature in Chapter 2, Section 2.6. The primary focus of this thesis is not on the cost models themselves, but on the cost of non-conformance and its impact on design.

1.3.2 Manufacturing Variability

Within the SILOET work package 2.5 one of the aims of task 2.5.2 - Tools and Methodology Development was to;

[2]Retrieved from http://www.rolls-royce.com/civil/customers/market_outlook/ 22/10/2014

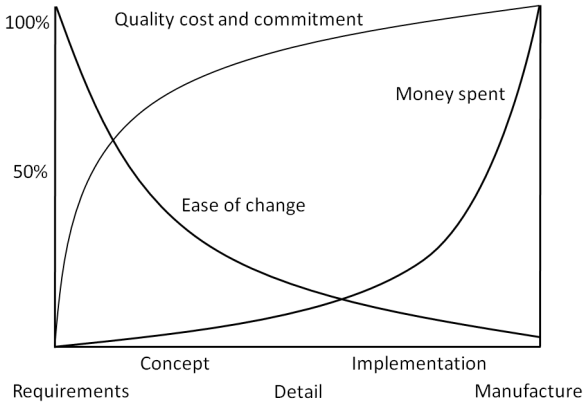

FIGURE 1.1: Cost incurred during product introduction (Miles and Swift [1998])

"relate more subtle 'quality' design parameters such as tolerances, surface finish and shape accuracy to the process capability and scrap and re-work costs".

Scrap and rework together with their associated costs arise due to non-conformance and the terms are defined formally under the Definitions section. Non-conformance occurs due to variation in the manufacturing process which results in features that do not comply with the tolerance limits imposed upon them. These tolerances may be in the form of dimensional constraints such as angles, thickness, diameters, lengths and positions or more general constraints such as surface quality.

There are two main sources of variation that can cause non-conformance during manufacturing; common cause variation and special cause variation (Shewhart [1931]). Common cause variation is constantly active within the system, it is probabilistically predicable and is often referred to as noise in the system. Special cause variation is an unanticipated phenomenon in the system and is probabilistically unpredictable. In manufacturing, tolerances are assigned to control the variability of a feature or product due to common cause variation. This type of variation is implicit in every manufacturing operation and is a fundamental property of nature[3]. Examples of common cause variation include temperature variation, variation in material properties and tool properties, and variations in how parts are loaded into holders. These uncertainties may conspire to cause variation in a measured manufacturing feature such as diameter, thickness or position relative to a datum. Special cause variation may also arise and a product may be deemed non-conforming because of it. However, non-conformance due to special cause variation is not necessarily due to a feature failing to conform within tolerance limits. By definition, tolerance limits cannot be used to control special cause variation as the variation, and the way it manifests in terms of variation to the geometry, is unpredictable. For example,

[3]Manufacturing a feature to an exact dimension was shown to require are infinite amount of information by Wilson [1980] using Shannon's theory of information (Shannon [1948]) and thus it is never possible to create an exact dimension.

a tool breakage during the manufacturing process and resulting surface imperfection it may cause would be considered special cause variation. This won't necessarily alter the diameter of the feature but the feature may still be deemed non-conforming on visual inspection[4]. Only common cause variation and the tolerances imposed to control it are considered in the research contained within this thesis.

In general, the form of manufacturing variation tends to obey the central limit theorem (according to Pyzdek [2001] from original studies by Shewhart [1931]), which states,

"*the average of the sum of a large number of independent, identically distributed random variables with finite means and variances converges "in distribution" to a normal random variable*[5]."

This permits common cause variation to be modelled using the normal distribution (Gaussian distribution), which is used as a default way to describe variation throughout this thesis. Nevertheless the normal distribution is not applicable in all cases (Pyzdek [2001] and Pyzdek [2002]) and as described in Section 1.4, one of the challenges of the research was to remove the reliance on the normal distribution to represent manufacturing variation.

1.3.3 Manufacturing Capability and Process Control

Manufacturing capability is used as a measure of how likely it is a manufacturing process will produce non-conforming features. There are a number of standard process capability measures as described in Natrella et al. [2012]. Generally, a manufacturing process is deemed capable if the variation is within the specification limits. The index C_{pk} is a commonly used metric where (Natrella et al. [2012]),

$$C_{pk} = \min\left[\frac{U-\mu}{3\sigma}, \frac{\mu-L}{3\sigma}\right]. \tag{1.1}$$

Most capability indices are variants of this form such as C_p, where the denominator is 6σ as opposed to 3σ, and C_{pm}, which takes into account the fact that the target mean may differ from the measured mean. The C_{pk} index is used in this thesis to indicate the relative capability of process, but any index which applies to normal distribution could be used. Figure 1.2(a) indicates $C_{pk} < 1$ as the manufacturing process variation is greater than the upper and lower specification limits, resulting in non-conformance.

[4] If such a variation occurs, often a component will be examined by the design team to establish if it will still perform its function as required, this is refereed to as a concession at Rolls-Royce.

[5] According to the definition given in the *issixsigma.com* dictionary. Retrieved from http://www.isixsigma.com/dictionary/central-limit-theorem/ 23/10/2014.

If the process variation is smaller than the upper and lower specification limits, $C_{pk} > 1$ and $> 99.73\%$ of items would conform[6].

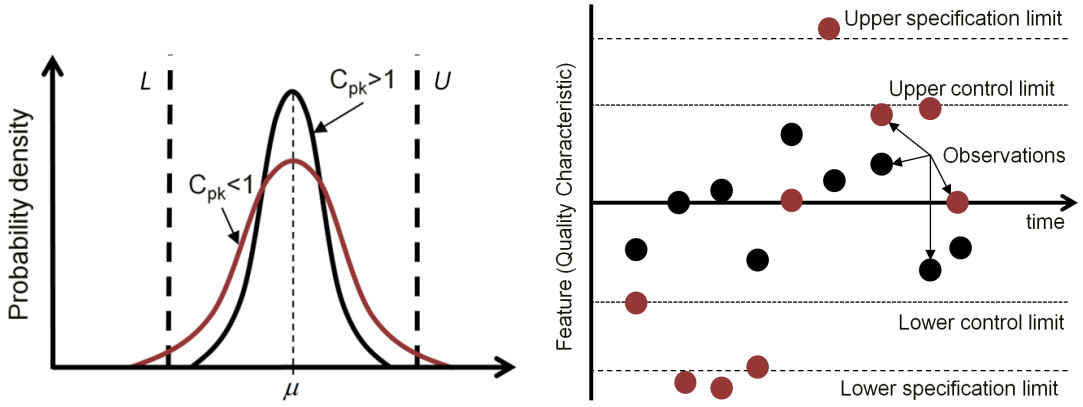

(a) Illustration of C_{pk} (b) Illustration of a control chart

FIGURE 1.2: Statistical process control

A prerequisite to using process capability incidences is ensuring the process is in-control. Shewhart [1931] was responsible for much of the early work on process control related to manufacturing. The aim being to monitor the feature values produced by the manufacturing process to ensure the process operates to its full potential (maximises conformance). Process control charts are commonly used to monitor the process (Natrella et al. [2012]) as illustrated by Figure 1.2(b). The x-axis represents time, while the y-axis corresponds to the value of the feature or quality characteristic. Upper and lower control limits are specified to define whether the process is in or out-of-control. Shewhart [1931] developed a set of rules, known as Western Electric Rules (Natrella et al. [2012]) which define these control limits and whether the observations support the notion of an in-control process. In essence, a process is deemed to be out-of-control if the observations are found not to come from the same distribution as the data originally used to set up the control chart. This implies the process has drifted, or the variance has changed, such that there must be other sources of uncertainty that are unaccounted for (special cause variation). The black points shown in Figure 1.2(b) (associated with the black distribution in Figure 1.2(a)) represent observations analogous of an in-control process. The points lie within the upper and lower control limits and there are no 'improbable' patterns amongst the points (they conform to the Western Electric Rules Natrella et al. [2012]). The process is also capable as the variation is well within the upper and lower specification limits, therefore $C_{pk} > 1$. No non-conforming features would be expected from this process. The observations illustrated by the red points (and red distribution)

[6]The larger the denominator in Equation 1.1 the greater the conformance. A property of the normal distribution is one standard deviation (σ) accounts for 68.27% of components, 2σ accounts for 95.54%, 4σ accounts for 99.994%, 5σ accounts for 99.99994% and 6σ accounts for 99.9999998% of components.

indicate an out-of-control process as there are points outside the control limits. In addition, some points fall outside the upper and lower specification limits, which would cause $C_{pk} < 1$ and non conforming features would be produced. It is possible to have an out-of-control but capable process ($C_{pk} > 1$) where the control limits may be exceeded but the observations lie within the specification limits. The scope of this thesis is delineated by in-control processes where $C_{pk} < 1$.

1.3.4 Performance, Capability and Cost

The interest in establishing the cost of non-conformance is not simply to offer better cost prediction to enhance the capability of cost models, but also an opportunity to maximise a component's performance whilst minimising cost. The design of today's gas turbine engines is fuelled by an ever increasing demand for quieter, more environmentally friendly engines with lower specific fuel consumption and reduced operating and running costs. This drives the design of components and subsystems closer to what is physically and materially possible, as a result variation can lead to an unwelcome degradation in performance. To maintain performance levels, more stringent tolerances must be applied and it is inevitable that in some cases the natural variations of some manufacturing processes will be greater than the tolerances. This is resolved by fully inspecting each component and reworking or scrapping the features and components that do not conform. In fact, regardless of how large the capability gap is between tolerances and manufacturing capability, it is always possible to produce components close to the optimum performance point, although the cost of doing so may be prohibitively high due to scrap and rework. Figure 1.3 illustrates the potential for improved profit for a component where performance varies in response to two features X_1 and X_2. There are two potential design points, design A and design B. Design A offers a higher average performance (marked A in the z-axis in Figure 1.3), provided the variation in the design parameters can be kept within $\Delta X_{1,A}$ and $\Delta X_{2,A}$. Failure to do this would result in a rapid degradation in Design A's performance and give no better or even worse performance than Design B, (due to the sensitivity of Design A's performance to the X_1 and X_2 design parameters). Design B illustrates the more robust of the two designs where the performance is considerably less sensitive to variations in the design parameters. The same manufacturing method is considered for Design A and B, however, only Design B can be manufactured without creating non-conformance. This indicates the manufacturing variation is almost as large as the range $\Delta X_{1,B}$ and $\Delta X_{2,B}$. Although it would be possible to produce design A, the cost of doing so would be considerably greater as the variation would be greater than $\Delta X_{1,A}$ and $\Delta X_{2,A}$. This would lead to costly scrap and rework.

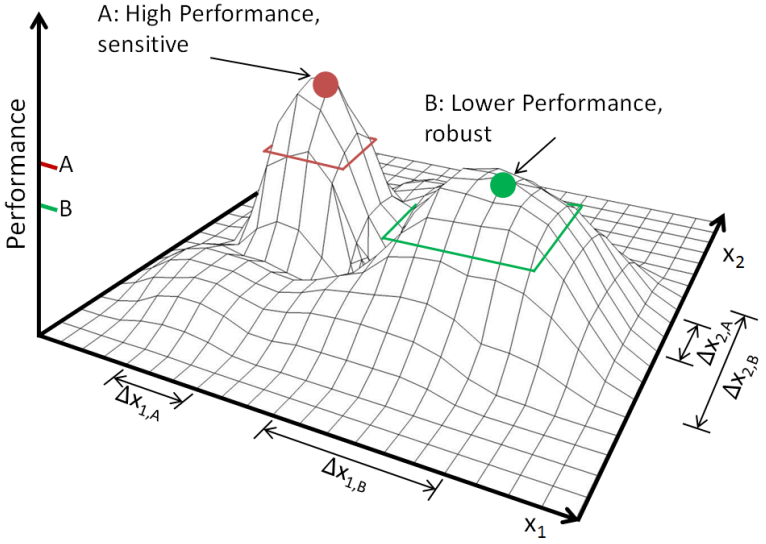

FIGURE 1.3: Illustration of the possibility of higher performance created by applying more stringent tolerances

A body of research known as Optimal Mean Setting explores the economic case of producing components to tolerances that are smaller than the manufacturing variation. The topic is reviewed in detail in Chapter 2, Section 2.5, although the fundamental principle is summarised by Figure 1.4. Reworking a feature is often less costly than scrapping a component, thus optimal mean setting aims to shift the manufacturing distribution mean in favour of rework, to reduce the overall cost of production. The terms U and L refer to the upper and lower specification limits and the difference between them corresponds to the ΔX range in Figure 1.3. The manufacturing variation is illustrated by the black curve. Scrap is produced, if on inspection, a feature is outside the design specification such that no additional manufacturing process can bring the feature within specification. Rework is required if a feature is found to be outside the specification limits but additional manufacturing operations are able to bring it within specification. By moving the mean of the manufacturing variation from μ_1 to μ_2 the probability of producing scrap can be reduced and the probability of rework increased. Since rework carries considerably less cost than scrap, it is likely setting the mean at μ_2 is less costly than in position μ_1. It would be possible to apply this technique to design A, from Figure 1.3, in a bid to reduce the cost of manufacture (but gain the performance benefit design A offers), thereby making it a more credible option. There are several challenges and implications of applying Optimal Mean Setting to practical engineering problems which are introduced in the following paragraphs (Section 1.4).

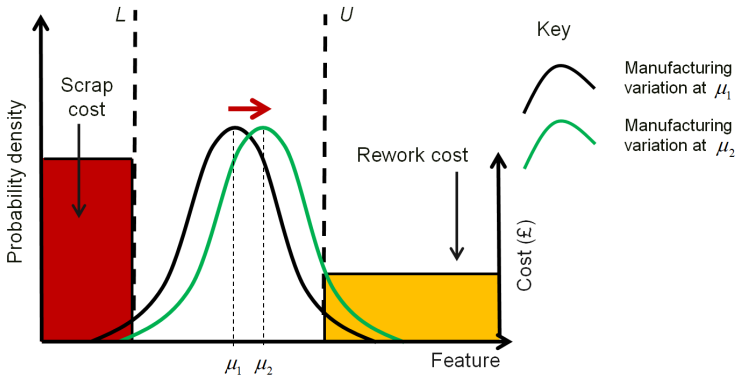

FIGURE 1.4: Effect of moving the mean of the distribution

1.4 Challenges

The challenges involved in this thesis can be divided into two main categories. The first challenge was to determine the cost of non-conformance itself. The second challenge was to remove the necessity to use normal distributions to characterise the variability of manufacturing processes.

Determine the cost of non-conformance: In accordance with SILOET work package 2.5 - task 2.5.2, a reliable method of calculating rework and scrap cost was required. Even in the simplest case, when manufacturing a component with a single feature, the cost of rework and scrap is not immediately obvious. Scrap and rework occurs due to manufacturing variation where it is possible to estimate the probability of producing scrap and rework by considering the area in the tails of the distribution above and below the upper and lower specification limits (Figure 1.4). However, if rework is produced, features are re-processed and there are additional probabilities of scrap, rework and conformance for these reworked components. In a batch of components, this reworking process would occur iteratively until all rework was complete. Determining the number of times components are reworked and the final probabilities of scrap and conformance is non-trivial, particularly where several features are considered. This problem has been studied in the literature, however, the method presented was found to be incorrect which is considered in more detail in Chapter 2, Section 2.5.

Non-normal distributions: Even if the manufacturing variation is normally distributed, feedback from the rework loop affects the shape of the final distribution of manufactured geometry to a variant of a normal distribution. If the variation of the manufacturing process is not normal or the inspectable feature (quality characteristic) is a combination of other manufacturing features (which may not be normally distributed), the manufactured geometry follows a variant of a normal distribution or a completely different distribution all together. This brings up two related problems.

- How to determine the scrap and rework probabilities if the manufacturing variation is not normally distributed, particularly if multiple features are considered where correlation exists between them.
- How to determine the distribution of the final geometry and how this influences the performance distribution of the component. This is a challenge even if the manufacturing variation is normally distributed due to the effect rework can have with regard to modifying the shape of the original normally distributed features.

Optimal Mean Setting can have a significant impact on the performance distribution by virtue of the fact the means are often biased towards rework. This point is illustrated in Figure 1.5. The function $f(x)$, known as a transfer function, illustrates the functional response due to changes in the feature (x). The variation in the feature (*Manufacturing distribution 1*) was mapped to the y-axis representing performance, via the transfer function $f(x)$, yielding *Performance distribution 1*. Optimal Mean Setting has the capacity to significantly skew the manufacturing distribution due to the shift in the mean and rework feedback, as represented by *Manufacturing distribution 2*. When this variation of the feature is mapped via the transfer function to the performance axis, the performance distribution is seen to vary from *Performance distribution 1* significantly. Although the total performance variation remains constant, the mean and the mode of *Performance distribution 2* would be greater than *Performance distribution 1*. This could have far-reaching implications particularly if the component was part of a larger assembly of similar components such as turbine blades. The performance of a turbine stage is dependent on the performance of each individual blade. If the mode and mean of the performance change there would be a knock-on effect to the realised performance of the turbine stage. In order to establish the performance variation, it is essential the distributions of the manufactured components be accurately known if Optimal Means Setting is applied.

1.5 Vision and Objectives

The overall objective of this thesis is to develop and apply the mathematical framework necessary to practice Optimal Mean Setting and analyse the consequence of doing so by establishing the resulting manufactured geometry distribution. Recall Optimal Mean Setting is a methodology that can be implemented to minimise production cost when the variation of the manufacturing processes is greater than the tolerances of the features or quality characteristics. It has an application where a performance gain is achievable from tolerance tightening. To achieve this vision, the challenges described in Section 1.4 must be overcome to accomplish the following objectives:

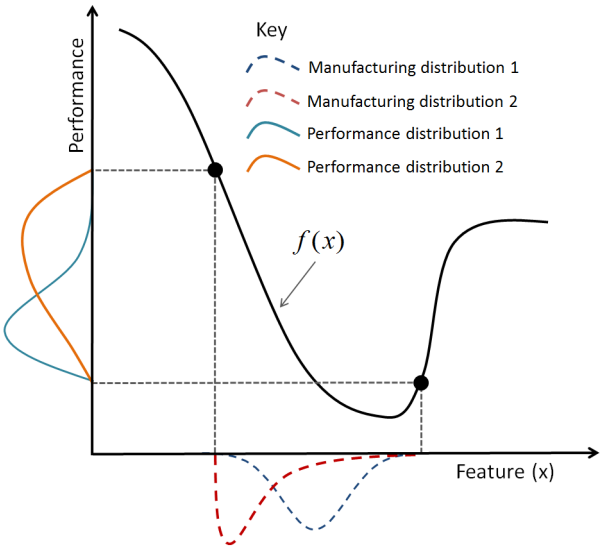

FIGURE 1.5: Effect of moving the mean of the distribution

1. Develop and implement a methodology to accurately determine the cost of production when the manufacturing variation is greater than the feature tolerance limits. This involves finding the probabilities of scrap and conformance after all rework cycles are complete as well as the average time features are reworked. The methodology must be applicable to one or several features, recognising there may be correlation between features.

2. It must be possible to achieve Objective 1, irrespective of the shape of the manufacturing process's variation. This applies even if multiple features must be inspected, each with different forms of variation (not all with normally distributed variation)[7].

3. The effect that rework has on the final distribution of the manufactured geometry must be considered such that it is possible to determine the associated effect on performance. It is more important to consider the variation in performance if Optimal Mean Setting is applied, as the resulting geometry distribution may be significantly skewed, which is also likely to skew the performance distribution.

1.6 Contributions

The contributions made by this research fall into four categories.

1. The first contribution is the development of a robust and generalised mathematical framework, enabling the conformance and scrap probabilities to be determined, as

[7]This implies standard multivariate parametric distribution functions cannot be used to find the joint probability of conformance, scrap and rework

well as the average time features spent being reworked. By extensively modelling and understanding rules governing the probability of components transferring between various states in the manufacturing process from first principles, errors were uncovered in the published research (Discussed in detail in Chapter 2, Section 2.5 and Chapter 4). The published literature used a Markovian model as a way to circumvent and simplify modelling from first principles. The new understanding that was gained from modelling from first principles allowed a correction to be derived for the original Markovian methodology.

2. There are two principle manufacturing regimes associated with Optimal Mean Setting. The first is where a feature is produced then immediately inspected, known as serial production. The second is where several features are produced before being inspected, known as parallel production. These concepts are explained in greater detail in Chapter 4. The original literature regarding parallel processes was restricted to considering just two features. This is generalised to n-features in Chapter 3. The generalisation was non-trivial due to the number of interactions that occur and ensuring all the possible probabilities of components transferring between states were accounted for. A set of equations were generated that enabled the probability of scrap, conformance and average time of rework to be computed for n-features, without having to formulate the specific equations for each problem. This method was combined with the serial production example for which an n-feature equation had already been developed. This involved re-formulating the serial equations such that they became a special case of the parallel equations rather than a separate form.

3. The knowledge gained from understanding the probabilities of features transferring between various states in the manufacturing process allowed an advancement in the optimisation methodology applied to Optimal Mean Setting. The new approach to Optimal Mean Setting outperformed the approach developed in the literature for parallel production. The improvements made by this new methodology are discussed in Chapter 3 - Section 3.5.1.

4. Copula functions are introduced to enable joint probability distributions to be created, where non-normal and dissimilar distributions described the manufacturing variation of the features (Chapter 4). This is vital to determine the conformance, scrap and rework probabilities for parallel production. Copula functions and their application to compute joint distributions is not novel, however, to the Author's knowledge this is the first time they have been applied to describe the variation of manufacturing features. The impact of using copula modelling is two-fold:

- There is no restriction on the shape of the distribution that describes the manufacturing variation. Custom distributions can be created or even data samples may be used, provided the shape of the distribution has an integral of one (it must classify as a probability). A practical example is given in Chapter 4 - Section 4.3 .
- Copulas enable the final geometry distribution to be found when optimal mean setting has been applied. This allows the performance distribution to be analysed. To the author's knowledge, such a technique to determine the distribution of the manufactured geometry has never been applied.

1.6.1 Software

Much of the work discussed in this project required the use of numerical simulations and calculations to validate analytical results and run numerical experiments. A significant proportion of the calculations required could not be expressed in closed form and the work drew heavily on the use of statistical and probabilistic methods. Matlab was chosen as the software package to develop simulations and experiments due to its highly capable statistical and optimisation packages. Additionally, as a high-level programming language it allows rapid development of functionally complex code.

In Chapter 4, a practical example of Optimal Means Setting was applied to a turbine blade cooling hole. Ansys workbench 14.5 and Fluent were used to model and solve the Navier-Stokes equations describing the flow of air through the hole and the cooling effect on the airfoil surface.

1.7 Description of Content

The motif of this thesis is the effect variation has on the function and cost of products. Quality Engineering embodies several paradigms that address this issue such as; Robust Design, Reliability Engineering and Axiomatic Design. Optimal Mean Setting is also a subset of Quality Engineering which specifically addresses the relationship between product cost and non-conformance. A literature review is given in Chapter 2 which discusses these various aspects of Quality Engineering. A comprehensive survey of cost modelling methodologies follows, which is essential to practice Optimal Mean Setting.

Chapter 3 onwards contains the Author's contributions to knowledge, expect where existing work is explicitly referenced . The Chapter opens with an introduction to the

mathematical basis Optimal Mean Setting. Initially, single feature and two feature serial and parallel cases are considered from first principles. The application of Markovian modelling to the Optimal Mean Setting problem is discussed in Section 3.2 and the errors in the literature (discovered from analysis from first principles) are examined. The following Sections 3.2.2.1 to 3.2.2.3 describe the generalisation of a Markovian method to establish the probability of scrap, conformance and the average time features spend being reworked for n-features in any combination of serial and parallel manufacturing stages. Section 3.4 offers a series of numerical examples utilising this new generalised methodology. Both serial and parallel production are considered, as well as a combination of both. This is not practical without the generalised methodology (developed in the preceding sections). The improved Optimal Mean Setting optimisation methodology is shown in Section 3.5, where it outperforms the methodology from the literature, yielding lower cost (higher profit). The impact of correlation between variables is also studied in this Section.

Chapter 4 furthers the Author's contribution to knowledge with the application of non-normal distribution and Copula statistics to the Optimal Mean Setting paradigm. Section 4.2.8 demonstrates how copulas apply to manufacturing distributions and Section 4.3 demonstrates how copulas can be used to model real manufacturing data. Their use in determining the resulting distributions of the manufactured geometry is also described. A practical example of Optimal Mean Setting, applied to a film cooling hole, (turbine blade or nozzle guide vane) is introduced in Section 4.4. An overview of film cooling holes, the manufacturing process and feasibility of applying Optimal Mean Setting to the manufacturing process are given in Sections 4.4.1 through to 4.4.3. Sections 4.4.4 through to 4.4.6 describe the hole geometry, experimental computation set-up and results.

Finally, a conclusion of the work is given and the future direction of Optimal Mean Setting is discussed in Chapter 5.

Chapter 2

Literature Review

2.1 Quality Engineering

Successfully engineered products perform their intended function well over a range of conditions in which they can reasonably be expected to operate. They are generally characterised by high levels of reliability and offer low risk and low unit and life-cycle cost. One of the greatest challenges to an engineer or designer is to ensure their product meets these objectives in the light of uncertainty. These uncertainties may arise from manufacturing, materials properties, operating environment or geometric changes over the lifetime of the component. Quality engineering is a generic term used to describe the methodologies aimed at reducing a product's variation to realise or partially realise these objectives, particularly with regard to minimising the effect of uncertainty.

There is no single reference for the origins of quality engineering but rather a number of related methodologies with the objective of reducing product variation to uncertainty. The origins of one of the most successful quality engineering practices Six Sigma, started with the development of statistical process control by Walter Andrew Shewhart of Western Electric. Later, Bill Smith of Motorola used Shewhart's ideas in the development of Six Sigma (Akpose [2010]). Walter Shewhart noted that the main cause of defects in manufactured devices was due to variation and that monitoring of the output was required to allow one to make adjustments to the process if the mean drifted too much. Bill Smith championed the concept that to attain defect-free (or close to defect free) production ± 6 standard deviations should lie between the mean and nearest specification limit. Over time, a 1.5 sigma shift may be expected, thus a defect rate of 3.4 parts per million could be expected corresponding, to a 4.5 sigma capability. Although the statistical aspects of Six Sigma are related to achieving a low defect rate, the overall aim is to achieve high levels of customer satisfaction. In many ways it is a cultural shift to

improve a company's level of customer satisfaction, profitability and to gain a competitive advantage. Indeed Pande et al. [2000] defined Six Sigma as "*A comprehensive and flexible system for achieving, sustaining and maximizing business success*". Variations on this are possible but Six Sigma was chosen as a useful starting metric. The application of Six Sigma methodologies to industry has been highly successful. To name a few examples of successful Six Sigma implementation (Anbari et al. [2004]); Motorola posted a $15 billion saving over 11 years, GE a saving of $2 billion after introducing Six Sigma in 1999 and Huges Aircraft's Missiles System Group reported 1000% increase in quality and 500% improved productivity.

Six Sigma practices involve following DMAIC, or DMADV strategies (Pande et al. [2000], Tutorialspoint [2014]) where

D : Define the problem and project goals,

M : Measure the problem and the responsible process,

A : Analyse the data and process to determine the root cause of the defect(s).

The last two letters are different for the DMAIC and DMADV methodologies respectively where,

I : Improve the process,

C : Control, ensure the process is under control such that the improvements are sustainable,

for the DMAIC, which is used for improving existing products or processes which are under-performing. The last two letters from DMADV refer to,

D : Design a process that fulfils the customer requirements

V : Verify the design fulfils the customer requirements.

The DMADV is used to design or redesign products and processes to ensure a reliable and defect free product. This is related to the concept of Design for Six Sigma (DFSS). The exact strategy for DFSS may vary, for example the second 'D' in DMADV may be replaced by 'O' referring to optimising the process capability and design.

The terminology used in Six Sigma is purposely equivocal as the methods are generic and may be applied to physical products as well as services. Nevertheless, many of the technical aspects of Six Sigma, such as design of experiment (DoE), optimisation and

manufacutring capability apply to the design of physical products which are of interest here. The following sections offer a general overview of Robust Design, reliability methods and Axiomatic Design methods. Robust Design principles have also been integrated to the area of Optimal Mean Setting (the main aspect of this research) and a detailed discussion of Robust Design in the context of Optimal Mean Setting is available in Section 2.5.

Robust designs are typically achieved by employing methods that characterise non-deterministic and uncertain parameters and their impact of the product. Two general approaches may be employed, Reliability Design or Robust Design as outlined by Taguchi (Taguchi [1986], Phadke [1989]). Reliability methods focus on the probability distribution of a system's response to uncertainty in parameters with known distributions. The aim is to minimise the risk of failure. This is fundamentally different to Robust Design where the objective is to optimise mean performance and minimise variation. In the latter, a system outside the specification limits is penalised but may be accepted, the focus is on the mean of the distribution of the system response. In a reliability based method a system outside the specification limits is not tolerated[1] and the focus is on the tails of the system response distribution.

2.2 Robust Design

Robust Design is a method of reducing the sensitivity of a product to variation. The concept is generally accredited to Dr. Genichi Taguchi who originally developed his ideas in Japan in the 1950s and 1960s. It wasn't until the 1980's when his work became known to Western academics with the English translation of his research, Taguchi [1986] and Phadke [1989]. However, Taguchi was not solely responsible for the concept of describing the statistical variation on an output or performance factor. In fact R.A Fisher with contributions from F. Yates (Fisher [1935], Yates [1964]) developed the definitive theory for accounting for variation in known and unknown factors and the impact on the experimental output. Fisher's method, known as Design of Experiment (DoE) was developed and refined primarily during his tenure at the Rothamsted Experimental Station in Harpenden, England. Rothamsted is an agricultural research establishment and during the 1920s a significant amount of research effort was devoted to determining the impact of various fertilisers on crops yields. Much of Fisher's work was aimed at efficient experimentation (Aldrich [2007]), "*to conduct experimental and observational inquiries so as to maximise the information obtained for a given expenditure*" (Fisher [1951]). Nevertheless, the long term aim of Rothamsted was to maximise crop yield in light of

[1] The probability of failure can never be eliminated but can be set very low, for example one failure event in 10 million.

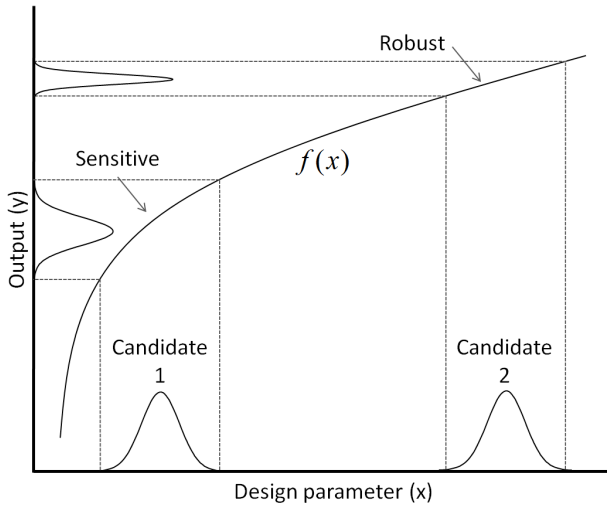

FIGURE 2.1: Graphical illustration of robust design where uncertainties are illustrated by typical input and output probability density functions (adapted from Keane and Nair [2005])

many uncontrollable factors (variations) such as rainfall, air quality, sunlight, soil quality and terrain gradients. This has many similarities to the concept of Robust Design, to minimise the sensitivity of the product output to variation, and indeed Fisher's DoE features heavily in modern day computational incarnations of Robust Design.

A robust design and a less robust design are illustrated in Figure 2.1. The horizontal axis represents a change in the control parameter (design parameter) and the vertical axis represents the output (performance). Two candidate solutions are shown where variability is present in the nominal value of x due to manufacturing variation. The manufacturing variation in both candidates is the same but, the first design (Candidate 1) suffers from greater variation in the output than Candidate 2 due to non-linearity in the function $f(x)$. Assuming low values of the output are desirable, the later design is more robust but has a slight performance deficit. In general, a small reduction in performance is acceptable if it results in a component that is more robust.

It is an engineer's task to find the design parameters that optimise the objective function. This can be expressed as a conventional optimisation problem (as described by Yao et al. [2011]), written as;

$$\begin{cases} \text{find:} & \boldsymbol{x} \\ \text{optimise:} & f(\boldsymbol{x}, \boldsymbol{s}) \\ \text{subject to:} & \boldsymbol{g}(\boldsymbol{x}, \boldsymbol{s}) \leq 0 \\ & \boldsymbol{L} \leq \boldsymbol{x} \leq \boldsymbol{U}. \end{cases} \tag{2.1}$$

The design parameters are given by the vector $\boldsymbol{x}$, $\boldsymbol{s}$ are signal factors and represent different configurations or operating conditions of the system. The objective function is

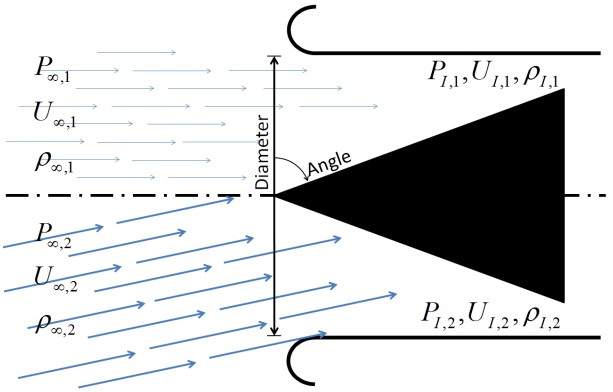

FIGURE 2.2: Ram air intake

$f(\boldsymbol{x}, \boldsymbol{s})$, $\boldsymbol{g}(\boldsymbol{x}, \boldsymbol{s})$ is an inequality constraint and $\boldsymbol{L}$ and $\boldsymbol{U}$ are the upper and lower bounds on the design space. Assuming the optimum can be found, or at least an acceptable output ($f(\boldsymbol{x}, \boldsymbol{s})$), it is also an engineers role to determine how the output may be affected by noise and explore other candidate solutions as in Figure 2.1. The objective function then becomes $f(\boldsymbol{x}, \boldsymbol{s}, \boldsymbol{\xi})$, where $\boldsymbol{\xi}$ are noise factors that may correspond to variations in the design parameters ($\boldsymbol{x}$) due to manufacturing variation or uncertainty in the system configuration or operating conditions ($\boldsymbol{s}$). For example, for the design of a ram air intake (Figure 2.2), the signal factors would be the pressure (P), velocity (U) and density (ρ) of the air prior to entering the intake from the free-stream (subscript ∞), and the output or response would be the pressure, velocity and density of the air inside the intake (subscript I). Control factors are parameters governing the design of the product the designer has control over. In the case of the intake, the control parameters would be the geometry of the intake, such as the inlet diameter (area) and the spike angle. Noise parameters are sources of variability in the system which may affect the signal or control factors. For example, the ram air intake would be susceptible to pressure, velocity and density changes due to altitude or Mach number. This is illustrated in the lower half of Figure 2.2 where the inlet flow is at an angle of attack relative to the free-stream and the velocity is greater. Manufacturing variation would affect the geometry of the duct, thus also affecting its response. These parameters are typically visualised on a P-diagram (Phadke [1989]) illustrated by Figure 2.3.

In a similar manner to Equation 2.1, a robust design can be written mathematically as (adapted from Yao et al. [2011]),

$$\begin{cases} \text{find:} & \boldsymbol{x} \\ \text{optimise:} & f(x, s) = f(\mu(\boldsymbol{x}, \boldsymbol{s}), \sigma(\boldsymbol{x}, \boldsymbol{s})) \\ \text{subject to:} & \boldsymbol{g}(\boldsymbol{x}, \boldsymbol{s}) \leq 0 \\ & \boldsymbol{L} \leq \boldsymbol{x} \leq \boldsymbol{U}. \end{cases} \tag{2.2}$$

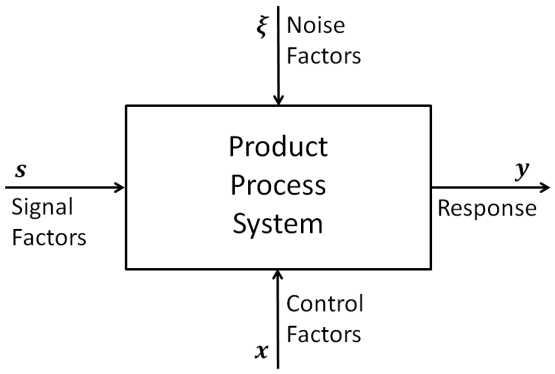

FIGURE 2.3: P-Diagram Phadke [1989]

Taguchi's method of robust design can be thought of as two distinct steps; parameter design and tolerance design. Parameter design is the process of exploiting non-linearities in the function $f(x)$ to reduce performance variation. Another way to improve average performance is to reduce the variability. In product design, it is generally possible to reduce the control parameter variation ($\sigma(x)$) by reducing the allowed manufacturing variation. This is achieved by tightening the tolerances, however, this is widely recognised to increase manufacturing cost proportional to the strictness of the tolerances (Spotts [1973], Chase [1988], Chase [1990]). This increased cost may come from longer run times (slower feed rates), increased non-conformance or investment to improve process capability. On the other hand, parameter design is 'free', choosing another point in the design space (moving to Candidate 2 rather than Candidate 1 in Figure 2.1) is generally considered not to incur extra cost[2]. In practice these two steps can be performed simultaneously as discussed by Li and Wu [1999]. In order to choose the correct parameters so that the design solution is robust, Taguchi [1986] introduced the concept of the quadratic loss function. Figure 2.4 illustrates this concept, where the quality loss (L) experienced by the average customer is,

$$L = k(f(\boldsymbol{x}) - t)^2 \quad \text{where} \quad k = A_0/\Delta_0^2.$$

Deviation from the target (t) is given by Δ_0 and A_0 is the loss experienced by the customer. The least loss is experienced by exactly meeting the target. To quantify the robustness of the design, Taguchi proposed using a signal-to-noise (SNR) ratio to measure the mean squared deviation (MSD) of the response comparative to the target.

[2]In reality different design configurations are unlikely to have exactly the same manufacturing costs, but the difference is generally considered to be less that the cost incurred through tolerance design Li and Wu [1999], Zang et al. [2005], Park et al. [2006]

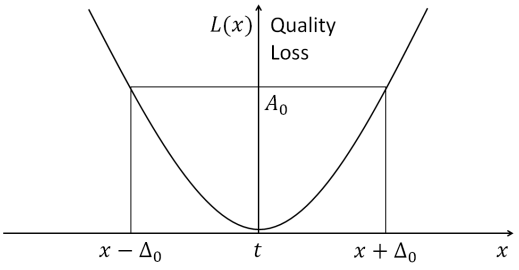

FIGURE 2.4: Illustration of a quality loss function Phadke [1989]

This gives a quantifiable measure of robustness written as,

$$\text{SNR} = -10\log_{10}\left(\frac{1}{n}\sum_{i=1}^{n}(f(\boldsymbol{x},\boldsymbol{\xi}_i)-t)^2\right)$$

where n represents the set of noise parameters that leads to the variability of the output, $f(\boldsymbol{x},\boldsymbol{\xi})$. This SNR is a nominal-the-best (NTB) type meaning that the loss is least when the design is on the nominal, half way between the bounds. Taguchi proposed two other possibilities; larger-the-better (LTB), where the design objective is to maximise the value of the quality characteristic (for example tensile strength or component life), and smaller-the-better (STB) where the design objective is to minimise the quality characteristic (weight for example). The mean squared deviation for each case is given by,

$$\text{SNR}_{\text{LTB}} = -10\log_{10}\left(\frac{1}{n}\sum_{i=1}^{n}(f(\boldsymbol{x},\boldsymbol{\xi}_i))^2\right)$$

and

$$\text{SNR}_{\text{STB}} = -10\log_{10}\left(\frac{1}{n}\sum_{i=1}^{n}(f(\boldsymbol{x},\boldsymbol{\xi}_i))^{-2}\right).$$

Since Taguchi [1986] and Phadke [1989] a number of other loss functions have been developed to meet specific requirements to different design problems. Asymmetric loss functions are discussed in the next paragraph and loss functions based on inverted probability distributions are discussed in Section 2.5.

In the original formulation of Robust Design, quality loss was only experienced by the customer. Since then researchers (Krishnaswami and Mayne [1994], Jeang [1997], Wu and Tang [1998]) considered the idea that the cost of a product could be broken down into two parts, the cost of manufacturing the product and the cost to the customer due to variations in quality. Jeang [1997] developed a model to trade the increased manufacturing cost of tight tolerances and the accompanying low quality loss. Wu and Tang [1998] illustrated the fact that the quality loss may not be symmetric both sides of the design nominal, such that if the design was off-nominal it would be preferable to be one side of the nominal, than the other, in order to minimise quality loss. Wu and

Tang [1998] utilised the reduced quality loss gradient one side of the nominal to shift the target to minimise quality loss as well and manufacturing cost. Wu et al. [1998] also considered asymmetric quality loss functions to minimise quality loss and manufacturing cost with tolerance design. Jeang [2001] proposed the optimization of manufacturing cost and quality loss. In this model, the optimal values of the process means and process tolerances as well as the design tolerances were defined, giving the designer the ability to specify the product parameters as well as the process parameters required to manufacture it. Jeang [2010] offered an all encompassing model for manufacture and quality loss cost by including machining cost, inspection cost, reworking cost and replacement cost if a component were scrapped. Jeang and Lin [2013] extended the optimisation of quality under a cost constraint to multiple features, again the optimum process means, process tolerances and the design tolerances were computed by the model.

Process capability indices are widely used (Jeang and Chung [2008]) to quantify the performance of a manufacturing process in terms of the relationship between the process variation and the tolerance bounds. Naidu [2008] used a process capability index as the basis for manufacturing and quality cost optimisation for a NTB case. Jeang and Chung [2008] and Abdolshah et al. [2009] developed a new capability measure which incorporated quality loss. A review of loss based capability indices are reviewed by Abdolshah et al. [2011].

One limitation of these works is their applicability to multi-response systems, where one wishes to consider two or more functional or quality characteristics simultaneously [Abdul-Kader et al., 2010]. Practical design problems often have more than one goal, in aerospace design it is common to aim for light weight, low cost and high performance systems, all of which tend to be in tension with one-another. Engineering judgement is often used to differentiate between different quality characteristics but this is ambiguous and does not guarantee the same result from two different engineers. There are several methods for systematically accounting for multiple quality responses, a detailed review is provided by Jeyapaul et al. [2004], however a general overview is given here.

Assignment of weights: Shiau [1990], Tai et al. [1992] Antony [2001]assigned weighting to each S/N ratio where the summation for all the weighted S/N ratios gave the overall quality loss of the system. In a similar vain Wu and Chyu [2004] accounted for multiple correlated quality characteristics by minimising the total average quality loss. A drawback of assigning weights is the process is inherently based on engineering judgement.

Principle Component Analysis (PCA): PCSA is a technique used to transform a set of correlated responses in to a smaller number of uncorrelated parameters or design variables. Antony [2000] used this technique on a submerged arc-welding process with

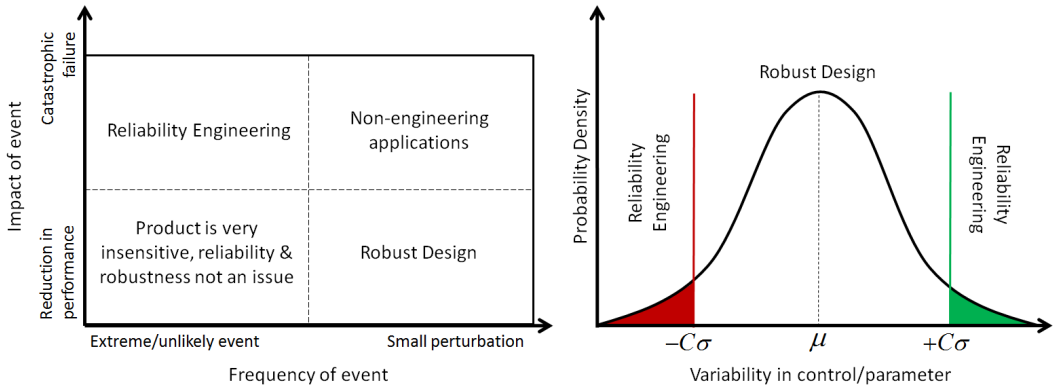

FIGURE 2.5: Illustration of the differences between Robust Design and Reliability Engineering adapted from Huyse [2001]

two responses. In general, the principle component has an eigenvalue greater than one, however, it is possible to have multiple eigenvalues greater than one. In this case a weighting has to be applied which is not desirable. Additionally the uncorrelated parameters or design variables do not necessarily account for all the variability in the response so it is possible the design will not be fully optimised.

Interpretation of Customer Requirements Quality function deployment (QFD) was proposed by Akao [1972] to transform a set of qualitative customer requirements into quantitative design parameters. The method was used by Kovach and Cho [2008] to weight each quality characteristic. The relative importance of the design parameters could then be ranked and the systems optimised based on relative importance.

2.3 Reliability Engineering

An area closely related to Robust Design is Reliability Engineering. The principle difference between the two methodologies is illustrated in Figure 2.5. Failure of a system is not permitted in Reliability Engineering. The failure of a system in Robust Design would be permitted, although the cost in terms of quality loss is high, the main objective is to minimise overall loss. The left plot in Figure 2.5 shows reliability based designs are engineered against failure when encountering infrequent but large perturbations to their operating conditions, or in manufacturing, where a failure of the design would be catastrophic. For example, the design of a building against collapse in an earthquake. When the impact of small perturbations in operating conditions or manufacturing leads to degradation in performance, but not catastrophic failure, Robust Design principles are utilised. Thus, in terms of the probability density function, Robust Design is concerned with the mean of the distribution whereas Reliability Engineering is concerned with the red and green tails of the distribution, as illustrated by the right plot in Figure

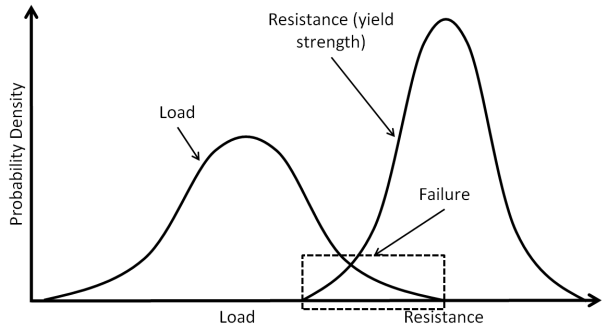

FIGURE 2.6: Illustration of the probability of failure adapted from Zang et al. [2002]

2.5. The value C is a constant, setting the number of standard deviations from the mean (μ) to the upper and lower specification limits.

Traditionally the risk of catastrophic failure has been mitigated against by using Factors of Safety for loads and knockdown factors for strengths, in the field of structural design. However, this approach gives no indication of the likelihood of a load exceeding the nominal design limit or the strength of the design being less than the nominal design. Invariably, this leads to over-engineered and suboptimal design solutions, as it is not possible to determine the relative importance of various design decisions on the reliability and robustness of the design (Zang et al. [2002]). Reliability Engineering resolves these shortcomings by using a probabilistic approach to determine the likelihood of the system failing due to the variability of two or more uncertain factors as illustrated by Figure 2.6. The area enclosed by the overlapping tails of the load and strength distribution defines the probability of the design failing. Such techniques have been used in civil engineering for many decades (Sundararajan [1995]), where engineering projects are governed by standard design codes. These codes designate the reliability of structures in extreme events of a given frequency, such as a 1 in 100 year earthquake. This specifies the size of the overlapping region between load and reliability in Figure 2.6.

A limit state function is commonly used to specify the conditions at which the system will fail and is illustrated in Figure 2.7. There are two design parameters x_1 and x_2, where the goal is to ensure the design is as far away from the failure region as possible (given by the limit state function $g(x, s)$) whilst optimising an objective function. Mathematically this can be written as,

$$\begin{cases} \text{find:} & \boldsymbol{x} \\ \text{optimise:} & f(x,s) = \mu(\boldsymbol{x}, s) \\ \text{subject to:} & P[g(\boldsymbol{x}, s) \leq 0] \leq r \\ & \boldsymbol{L} \leq \boldsymbol{x} \leq \boldsymbol{U}. \end{cases} \tag{2.3}$$

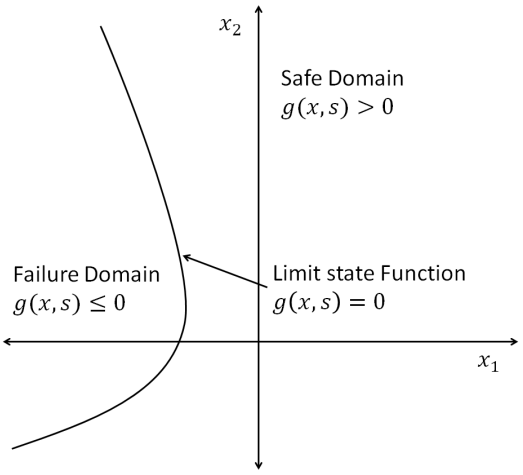

FIGURE 2.7: Illustration of a limit state function on the design space, adapted from Keane and Nair [2005]

as described by Yao et al. [2011]. The function $P[\bullet]$ is the probability that the bracketed statement is true, while r is a scalar specifying the reliability requirement (i.e. the system may fail once in 10^6 cycles). Thus, $P[g \leq 0]$ is the probability of failure for a given set of design parameters $\boldsymbol{x}$, which must be less than a specified reliability level r.

Determining the probability of failure,

$$P_F = P[\boldsymbol{g(x, s)} \leq 0] = \int_{\boldsymbol{g(x)} \leq \boldsymbol{0}} f_{\boldsymbol{x}}(\boldsymbol{x})\, \mathrm{d}\boldsymbol{x}, \tag{2.4}$$

is often computationally expensive due to the number of dimensions in the design domain $\boldsymbol{x}$, the complexity of the domain boundary $\boldsymbol{g}(\boldsymbol{x} = 0)$ and it is often not possible to express the failure domain analytically (Zang et al. [2002], Keane and Nair [2005]). Monte Carlo simulation can be used to approximate the P_F, however a large number of samples are required to estimate P_F to a reasonable degree of accuracy. To approximate P_F to an order of magnitude 10^{-6}, over one million samples are required as the error scales as $\mathcal{O}1/\sqrt{N}$ where N is the number of samples. This is not practical if $f(x)$ is a computationally expensive function to evaluate. An alternative approach is the use of First-Order and Second-Order Reliability Methods, FORM and SORM respectively. There are four principal stages as cited in Zang et al. [2002],

1. Transform the physical space into standard normal space.
2. Determine the most probable point (MMP).
3. Approximate the limit state function at the MMP.
4. Determine the probability of failure using the approximate limit state function from the previous step.

The FORM method is less computationally expensive than the SORM approach as the limit state function is approximated by a tangent whereas a quadratic approximation is used by SORM. Consequently SORM gives a more accurate estimate of the probability of failure. A detailed review of FORM and SORM methods are available from Robinson [1998] and Rackwitz [2001]. Langley [1999] showed that reliability methods were special cases of an asymptotic formulation based on the Laplace approximation. The reduction of this asymptotic approximation to the FORM and SORM methods is illustrated by Keane and Nair [2005].

In an analogous way to the Taguchi method of improving product quality Savage and Swan [2001] proposed a reliability based quality improvement approach. The model determines the nominal design parameter values to maximise the probability of multiple quality characteristics being within the upper and lower specification limits. Since there is no loss function, the quality of the design is the same, provided the design parameter lies between the limits. Savage and Seshadri [2003] proposed a binary loss function to account for the scrap and rework costs if a design was outside the specification limits. The objective was to minimise the sum of the production cost (including inspection cost) and cost of scrap and rework. Savage et al. [2006] further developed the concept of quality optimisation through conformance-based design by introducing the NTB, STB and LTB quality characteristics. The basic principles of Reliability Engineering, to minimise the probability of failure are inversely analogous to another design methodology, Axiomatic Design, where the objective is to maximise the probability of conformance. This design method is discussed in the following section.

2.4 Axiomatic Design

Axiomatic Design was introduced by Nam Suh in the 1980s and provides a framework, mapping the functional requirements (quality functions) of a system to the design parameters. These design parameters can also be mapped to manufacturing processes. The methodology offers a scientific approach to design (Suh [1978], Suh [1990] and Suh [2001]). The mainstays of the approach are the first and second axioms; the independence axiom relating to how function requirements map to design parameters and the information axiom relating to the likelihood of the system satisfying its functional requirements when manufactured. Information reduction is analogous to the Taguchi methodology of optimising the means to minimise variation in the performance outputs. The reduction of information is also similar to reducing the probability of failure in reliability based methods.

Axiomatic design maps the functional requirements (FRs) of the system through a design matrix (A) to the design parameters (DPs) as demonstrated in Equation 2.5,

$$\begin{Bmatrix} FR_1 \\ FR_2 \\ \vdots \\ FR_i \end{Bmatrix} = \begin{bmatrix} A_{11} & A_{12} & \cdots & A_{1j} \\ A_{21} & A_{22} & \cdots & A_{2j} \\ \vdots & \vdots & \ddots & \vdots \\ A_{i1} & A_{i2} & \cdots & A_{ij} \end{bmatrix} \begin{Bmatrix} DP_1 \\ DP_2 \\ \vdots \\ DP_j \end{Bmatrix}. \tag{2.5}$$

The subscripts i and j are the numbers of FRs and DPs in the system. It is a necessary condition of Axiomatic design that the numbers of FRs equal the number of DPs. The system is said to be uncoupled if the elements $A_{ij} = 0 \; \forall \; i = j$, so that every FR is satisfied by exactly one DP. Such a design is easy to optimise as each FR can be determined independently of all the others. The design matrix A can also exist in upper or lower triangular form representing a decoupled design, where some FRs depend on two or more DPs. Nevertheless, at least one FR is mapped to only one DP. Again it is possible to satisfy each FR, although the order each is solved is important. One must first satisfy the independent FR and DP pair before satisfying the next FR, which will depend on two DPs. If the design matrix A cannot be resolved into upper or lower triangular form and it is not uncoupled, the system is said to be coupled. Such a system is hard to optimise, since any change in one DP will affect multiple FRs. Figure 2.8 illustrates a coupled and uncoupled design solution for the pitch and yaw control of aircraft. With reference to Equation 2.5, FR_1 and FR_2 are the pitch and yaw functionalities respectively. The DP_1 and DP_2 parameters correspond to the control surfaces facilitating the yaw and pitch motions. The V-tail configuration of a General Atomics Altair unmanned aircraft in the top of Figure 2.8 is a coupled design as a deflection of the control surface would result in both pitch and yaw, thus A_{11}, A_{12}, A_{21} and A_{22} would be non-zero. The DC-8 aircraft in pictured in the lower half of Figure 2.8 has an uncoupled tail-plane design solution where the pitch and yaw functionalities are satisfied independently by different control surfaces.

The information axiom states that the best design is the one with the least information (Suh [1990], Suh [2001], Park [2004] and Park et al. [2006]), which is always an uncoupled design. However, most practical cases involve coupled or decoupled designs (Park [2007] provides an extensive discussion regarding the application of Axiomatic Design). Suh [2001] states it is generally possible to reduce coupled designs to decoupled ones by setting the least sensitive elements in the A matrix to zero. The information axiom is closely related to the probability of failure integral from reliability based methods (Equation 2.4). It requires the computation of the probability of success given by,

$$P_s = \int_{\Omega} \dots \int P_{\delta DP_j} \, \mathrm{d}\delta DP_j \dots P_{\delta DP_1} \, \mathrm{d}\delta DP_1$$

FIGURE 2.8: Illustration of the a coupled and independent design solution for pitch and yaw control of aircraft (NASA [2015])

where Ω is the feasible design domain and $P_{\delta DP_n}$ is the probability density function of the n^{th} design parameter. The term δDP_n is the range on the manufacturing variability of DP_j such that $-\Delta DP_j \leq \delta DP_j \leq \Delta DP_j$. The design domain is prescribed by the mapping (matrix A) between the FRs and the DPs. For a two variable problem, the probability of success is given by,

$$P_s = \int_a^b \int_c^d P_{\delta DP_2} P_{\delta DP_1} \, \mathrm{d}\delta DP_2 \, \mathrm{d}\delta DP_1$$

where the limits are,

$$a = -\frac{\Delta FR_1}{A_{11}}, \quad b = \frac{\Delta FR_1}{A_{11}}, \quad c = \frac{-\Delta FR_2 - A_{21}\delta DP_1}{A_{22}} \quad \text{and} \quad d = \frac{\Delta FR_2 - A_{21}\delta DP_1}{A_{22}}.$$

The term δFR_i is the acceptable range of the i^{th} functional requirement specified by the customer such that $-\Delta FR_i \leq \delta FR_i \leq \Delta FR_i$. Figure 2.9 shows the functional domain mapping for a two variable problem. The design domain is contained within the parallelogram illustrated on Figure 2.9. The functional domain is indicated by the partially obscured blue rectangle contained within $-\Delta FR_1 \leq \delta FR_1 \leq \Delta FR_1$ and $-\Delta FR_2 \leq \delta FR_2 \leq \Delta FR_2$. The probability of success is the area of the common range, where the functional domain overlaps the design domain, indicated by the green rectangle. If the functional domain were to increase in size, or the design domain decrease in size, the probability of success would tend to zero at the point where the common range was fully enclosed. Solving the P_s integral for a decoupled design was outlined

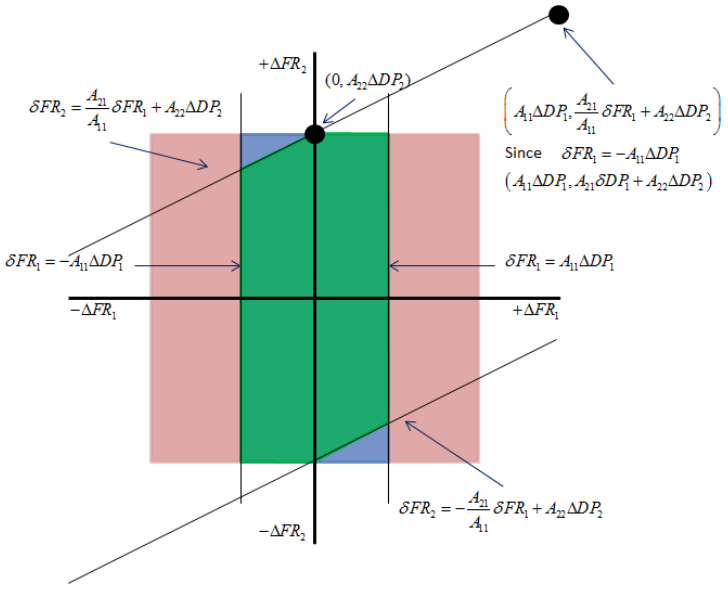

FIGURE 2.9: Illustration of the functional and design spaces on functional domain (adapted from Suh [2001])

by Frey et al. [2000] and Park [2004]. Park [2007] also offers an in-depth discussion of Axiomatic Design, particularly regarding the information axiom, including worked examples.

Axiomatic Design, like reliability based methods, is well suited for accounting for multiple system responses (quality characteristics) and design parameters. Optimisation of the probability of success or probability of failure for the two respective approaches determines the 'best' design. The 'best' design being the one that fulfils the functional requirements with the least likelihood of producing non-conforming products or components. With Axiomatic and reliability methods, the effect variability has on the functional performance is minimised. However, unlike Taguchi based robust design methods, there is no built-in mechanism for trading functional performance with increased production cost from tolerance tightening.

2.5 Optimal Mean Setting Literature

Canning problem

Springer [1951] is widely credited with introducing the concept of Optimal Mean Setting with the proposition of the *can filling problem*. The objective of Springer's model was to determine the optimum level to fill a can to minimise production cost. Under-filling the can below a threshold level resulted in the contents being discarded or sold at a reduced price. If the can were overfilled, it could be brought to market but would fetch the same

price as cans with the 'correct' content level. Therefore, the extra amount by which the can was overfilled resulted in lost revenue. In a general sense, the extra content in the can is comparable to rework, while discarding a can's contents or selling at a 'knock-down' price due to under-filling, is comparable to scrap. Production cost was minimised by slightly over filling the cans on average, to reduce the probability of discarding the contents and accepting the small loss in revenue from over filling. Subsequent literature on the canning problem can be subdivided into two main methodologies:

1 Those that define conforming and non-conforming items based on a lower specification limit.

2 Those which define a movable upper limit in addition to the lower limit, i.e. containers with a contents above a threshold level are also non-conforming in addition to those with a contents lower than the lower specification limit.

The methodology developed by Hunter and Kartha [1977] falls into the first category. They specified two potential markets. Conforming items were those that fell above the lower specification limit and were sold in the 'primary' market. Items that fell under the lower specification limits were non-conforming and would be sold at a reduced price in a secondary market. The optimal mean setting in Hunter and Kartha [1977] was based on maximising profit rather than the minimisation of production cost as in Springer [1951]. Profit was defined as the income from conforming items, the income from the rejected items and the cost of contents or material. A similar model was presented by Nelson [1978]. Considerably later, Das [1995] developed a faster solution methodology, replacing the graphical-tabular solution from Hunter and Kartha [1977] with a numerical technique based on standard lookup tables. Carlsson [1984] applied the optimal mean setting approach to the steel beam industry and modified the profit function from Hunter and Kartha [1977]. A premium was added for high quality beams, while a discount was offered for low quality beams. Thus, there were an infinite range of prices for the beams, reflecting how much greater or lower the manufactured quality was compared to the target quality. Bisgaard et al. [1984] further developed the secondary market paradigm and proposed that non-conforming items should be sold at a price proportional to how much content was missing, (in a similar manner to lower quality beams fetching lower prices from Carlsson [1984]). This ensured the price of secondary market items were based on the level of ingredient, which prevented a situation where nearly empty cans could be sold at the same price as almost full cans. The concept of a secondary market was completely dropped by Golhar [1987], he proposed cans with content below the lower limit should be emptied and re-filled and the sold in the regular market. This was motivated by considering pharmaceutical products where there was no secondary market.

The motivation for the second category stems from the desire to reduce the cost of overfilled containers being sold at a regular price. This was especially important for products such as pharmaceuticals, liquor and perfume where the cost per millilitre or gram is high. Bettes [1962] originally introduced the concept of defining an upper limit such that items with 'too much' ingredient would be reprocessed at a fixed cost in a similar manner to under-filled containers. The lower specification limit was set by legislation or legal requirements. The process mean and the upper specification limit were optimised simultaneously. Setting the upper specification limit too high resulted in loss due to ingredients going into the market free of charge. However, setting the upper specification limit too close to the lower specification limit resulted in high reprocessing cost as there was a high probability items would fall outside this range. The mean was adjusted to maximise the probability of items falling in the range between the lower and upper specification limits. Golhar and Pollock [1988] addressed the same problem as Bettes [1962] but had a more systematic approach rather than the trial and error methodology used by Bettes [1962]. Schmidt and Pfeifer [1991] also optimised both the mean and upper specification limit where the filling capacity was limited such that the profit was maximised per fill attempt. The paper also quantifies the increase in profit achieved relative to only optimising the process mean. Liu and Raghavachari [1997] showed optimising both the mean and upper specification limit always outperforms optimising only one of these variables where the variability follows a continuous distribution. They also considered normal, truncated normal, and truncated logistic distributions.

Both the first and second category approaches require 100% inspection plans. This is not always economically viable as it is time consuming and costly to inspect every quality characteristic. Sample inspection is an alternative strategy where a number of representative items are inspected from a larger lot. The number of non-conforming items from the sample determines whether the lot is deemed to conform.

Sampling Plans

Boucher and Jafari [1991] considered a lot-by-lot sampling plan based on attributes[3]. Two price structures existed for items from accepted and rejected lots, where items from rejected lots were sold to a secondary market. In addition to an attribute based sampling plan Arcelus and Rahim [1990] developed a sampling plan for attributes and variables. Carlsson [1989] considered a system where products were produced in lots and subject to lot-by-lot inspection based on variables. The selling price for items was based on

[3]Sample inspection based on attributes is used where the measured characteristic either passes or fails inspection (binary decision). Alternatively the measured characteristic may produce a discrete value, thus it is possible to quantify by how much a characteristic misses or exceeds a quality requirement. Such an inspection plan is referred to as inspection by variables.

whether they were from an accepted or rejected lot and also proportional to quality. Thus, a customer would pay one price for items from an accepted lot plus an extra amount proportional to the extent to which the items exceeded the quality requirements. Another price existed for items from a rejected lot where customers would pay even less proportional to the extent individual items missed the required quality characteristic. The price items were sold for is analogous to the principle set out by Carlsson [1984]. A similar principle, where the price of items in the market is determined by their quality relative to the target quality, was considered by Hong [1999]. They jointly optimised the mean as well as the screening limits. Pulak and Al-Sultan [1996] modified the model by Boucher and Jafari [1991] by implementing a rectifying inspection plan, where all rejected lots underwent 100% inspection and all non-conforming items were reworked or scrapped and replaced. This is applicable where a secondary market does not exist or where other manufacturing stages follow, in a multi-stage manufacturing system. Al-Sultan [1994] considered setting the means to maximise profit, where each product had two attributes produced by two different machines in series. A sampling plan was used to determine whether the attributes fell above or below a lower specification limit. A two stage surrogate screening process was proposed by Lee and Elsayed [2002] where the inspectable variable (weight of a cement bag) was not measured directly but by a surrogate variable correlated with the inspectable variable (mil-ampere of the load cell) instead. In this case it was considerably quicker to measure the amperage of the load cell than determine the weight of the cement bag. Duffuaa et al. [2009] used a sampling plan for two quality characteristics produced in series and recently Peng and Khasawneh [2014] used a screening method (outlined in Montgomery [2009]) to determine the defect rate for serial production systems. Peng's article is considered in more detail in Section 2.5.2

Non-canning problems

In a departure from the filling of containers, Dodson [1993] considered the production of rolled aluminium sheet. Undersized sheet would result in the scrapping of the whole roll, the excess from an oversized sheet was removed and scrapped. Scrapping the excess material was considerably less costly than scrapping the whole sheet. This is directly analogous to rework in a material removal manufacturing operation. Wen and Mergen [1999] were the first to consider optimal mean setting in the context of processing a feature or component where the variability of the process is greater than the fixed specification limits. Wen and Mergen [1999] optimised the mean setting to minimise 'loss'. They used an example of the production of an inner ring of a bearing race (grinding

process). This was a high precision component where the manufacturing variability was normally distributed and greater than the specification limits.

Taguchi Quality Loss

Taguchi introduced the concept that the further a product was away from a desirable quality target, the greater the economic loss. This concept was introduced to the field of optimal mean setting by Arcelus and Rahim [1996], Arcelus [1996], Elsayed and Chen [1993]. The introduction of the loss function generates a tension to pull the mean towards the target quality and limits the extent the mean might move towards rework. Mukhopadhyay and Chakraborty [1995] investigated the effect of increased variance due to general ageing and wear over time. A Taguchi loss function was used to balance acceptable variance (which could be improved through machine and tool replacement) with reduction in quality. Rahim and Al-sultan [2000] furthered the work by Mukhopadhyay and Chakraborty [1995] to also optimise the mean in addition to the variance. Both Chen et al. [2002] and Ho and Quinino [2003] used the single feature optimal mean model from Wen and Mergen [1999] and introduced a Taguchi quality loss function. Chen et al. [2002] demonstrated a ± 0.003 change in the mean and 3.4% to 26.0% difference in total loss compared to the numerical example given by Wen and Mergen [1999] depending on the type of quality loss function used. Teeravaraprug and Cho [2002] studied a multivariate quality loss function to capture customer dissatisfaction with product quality. The mean settings for two quality characteristics were then optimised to determine the most profitable mean values. Chen and Chou [2003] offered a similar paper where the methodology was based on the single feature model by Wen and Mergen [1999]. Chen and Lai [2007a] modified the sampling plan model from Pulak and Al-Sultan [1996] under the quadratic quality loss condition. Duffuaa and El-Ga'aly [2013] developed a multi-objective feature mean optimal setting methodology to maximise profit, income and product uniformity, where Taguchi quadratic loss was used as a surrogate for product uniformity.

An asymmetric quality loss function can be used as an alternative to the quadratic loss function, where the loss is not equal both sides of the target. Kapur and Wang [1987] were the first to introduce Optimal Mean Setting with an asymmetric loss function, where a log-normal distribution was used to define the quality characteristic. Kapur and Cho [1994] claimed using a Weibull distribution improved the flexibility of the asymmetric distribution which better represented real situations. Similarly Moorhead and WU [1998] practised optimal mean setting with an asymmetric loss function. Chen et al. [2002] applied an asymmetric loss function to the Optimal Mean Setting model proposed by Wen and Mergen [1999]. (Chen [2004]) took a similar approach but used

a rectifying inspection plan proposed by Pulak and Al-Sultan [1996]. Chen and Lai [2007b] applied an asymmetric quality loss function to the sampling plan model from Pulak and Al-Sultan [1996], building on an earlier work (Chen and Lai [2007a]). They also quantified the optimum lot size to maximise profit. Chen [2010] brought together the literature by Al-Sultan [1994], Pulak and Al-Sultan [1996], Chen and Lai [2007a,b] to determine the economic manufacturing quantity and optimum process mean under the rectifying inspection plan with an asymmetric loss function for product in serial production (multiple quality characteristics per product).

The quadratic loss function introduced by Taguchi and the derivative asymmetric loss function assume that loss varies smoothly with deviations from the target quality. Mixed quality loss functions allow transitions in the quality loss, for example a step change in quality loss when the characteristic falls outside the upper or lower specification limits. Cho and Leonard [1997] represented quality loss with a piecewise linear function where loss was roughly proportional to the deviation from the quality target. Chen [2005] used a mixed quality loss function that was quadratic inside the specification limits and a piecewise linear loss function outside the specification limits. Cho [2002] and Teeravaraprug [2006] tailored the loss function for a particular product based on historical data concerning the performance of products with customers loss. Both articles used statistical regression analysis to construct the loss function.

Another way to represent quality loss was proposed by Spiring [1993] who used a reflected normal distribution function (Figure 2.10). The curve is useful because the loss is not unbounded like the quadratic loss function. Drain and Gough [1996] applied this loss function to a semi-conductor manufacturing process. They also extended its formulation to include two quality characteristics, specifying a bivariate inverted normal quality loss function. Sun et al. [1996] suggested the losses due to a feature being off-target were too severe and modified the function accordingly. Other types of inverted probability density functions were investigated as candidates for loss functions. Spiring and Yeung [1998] considered the Gamma, the Tukey lambda and Laplace distributions. The inverted beta function was considered by Leung and Spiring [2002] which allowed both symmetric and asymmetric quality loss to be described. A comprehensive review of the use of inverted probability functions as loss functions is given by Leung and Spring [2004].

2.5.1 Multiple Quality Characteristics

Products often have multiple quality characteristics. In general, there are two ways in which quality characteristics can be manufactured. Each quality characteristic requires a manufacturing stage followed by an inspection stage. However, multiple quality

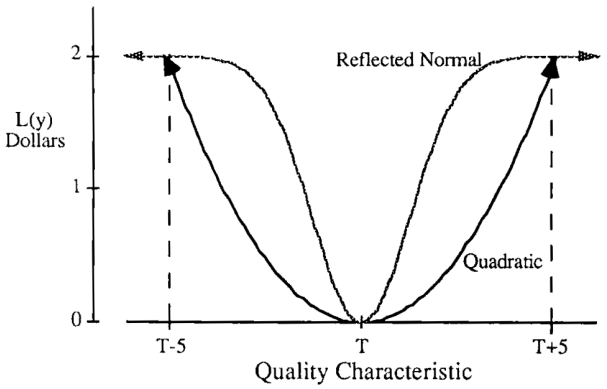

FIGURE 2.10: The reflected normal loss function from Spiring [1993]

characteristics could be manufactured before an inspection process, known as parallel production: alternatively an inspection stage could be applied after each quality characteristic, known as serial production.

The principle complication between the manufacture of quality characteristics in a serial production system, and in a parallel production system is illustrated by Figure 2.11. For a single quality characteristic, there is a cost (I) for being outside the specification limits. The cost of being over the upper specification limit (C_U) and the cost of being under the lower specification limit (C_L) can also be differentiated as described by Wen and Mergen [1999]. In a two feature parallel case, an additional cost is introduced (II) to account for two features being outside the specification limits. In general the cost of II is greater than I due to the added valued of manufacturing and then reworking or scrapping two features, as opposed to the added value of just one feature (Teeravaraprug and Cho [2002],Chan and Ibrahim [2004]). Elsayed and Chen [1993], Kapur and Cho [1996] and Drain and Gough [1996] were the first to consider quality loss for parallel production, where quality loss for two characteristics were modelled using the bivariate normal distribution function. Chen and Chou [2003] used the bivariate quality characteristics from Kapur and Cho [1996] but expanded the model by allowing for different non-conformance costs, depending on whether a quality characteristic fell above or below the upper and lower specification limits respectively, for each quality characteristic (x_1 and x_2). Khasawneh et al. [2008] developed a similar model which led to six different non-conformance costs, illustrated in greater detail in Figure 3.6 under Section 3.1.2. Cho [2002] used the bivariate model with two non-conformance costs (I and II) to construct a regression-based loss function. Teeravaraprug [2006] presented a similar paper but extended the approach to multiple quality characteristics. Duffuaa et al. [2009] developed an optimal mean model for two quality characteristics in series utilising a sampling plan.

The optimal means for two manufacturing processes in series was studied by Al-Sultan

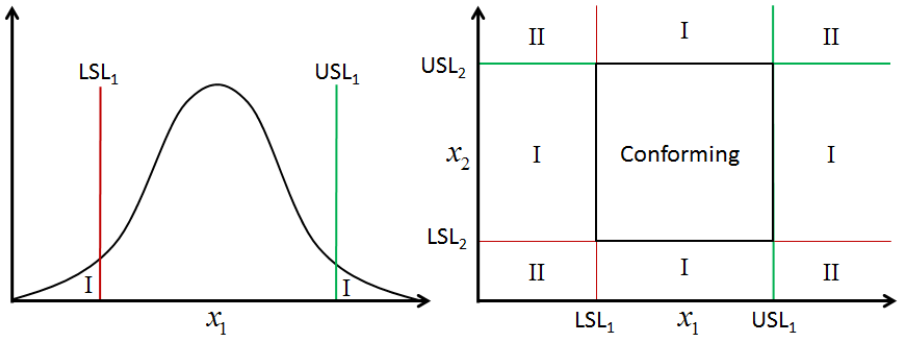

FIGURE 2.11: The Differences between the non-conformance costs between single and dual quality characteristics, adapted from Teeravaraprug and Cho [2002] and Chan and Ibrahim [2004]

and Pulak [2000], which is an extension of Golhar [1987], but for two stages. Bowling et al. [2004] developed models for one, two and n quality characteristics produced in series. The work introduced Markov modelling to predict the long-term probabilities of components conforming or being deemed scrap, and the average time features spent being reworked. This more closely models reality, where features designated rework may be re-processed several times. Previous literature essentially gave a snap-shot of the short-term probability of features conforming, being scrapped or requiring rework. Markovian modelling allowed the final proportion of scrap and conformance, as well as average number of rework cycles to be calculated. Bowling et al. [2004] was the first in a selection of articles (Bowling et al. [2004], Khasawneh et al. [2008], Selim and Al-Zu'bi [2011] and Peng and Khasawneh [2014]) that utilised Markovian modelling. The Markovian approach to Optimal Mean Setting is discussed in greater detail in Section 3 and 3.2. Some errors in the Markovian-based equation for expected profit from Bowling's 2004 paper were uncovered by Selim and Al-Zu'bi [2011] (Section 3.1) who reformulated the n stage model originally proposed by Bowling et al. [2004]. Peng and Khasawneh [2014] introduced an Optimal Mean Setting model for a mixture of parallel and serial production based on the models from Bowling et al. [2004] and Khasawneh et al. [2008]. A numerical example was given with four quality characteristics, two in parallel following serially from another two produced in parallel. A sampling plan was used as opposed to 100% inspection.

2.5.2 Summary of Optimal Mean Setting

Optimal Mean Setting is the basis for the research in this thesis, therefore its key features are summarised below, prior to the main literature review summary. The original use of Optimal Mean Setting, to determine the optimum fill levels of containers to maximise profit, is slightly different to its application to engineering design parameters in the

presence of manufacturing variability. Wen and Mergen [1999] were the first to translate the problem to the paradigm of engineering design. The next significant advancement was the introduction of Markovian modelling (Bowling et al. [2004] and Selim and Al-Zu'bi [2011]) to find the eventual probabilities of scrap and conformance accounting for the possibility it could take several rework cycles to convert features requiring rework into conforming or scrap components. The Markovian approach was applied to parallel production systems by Khasawneh et al. [2008], although errors remain in this work. The major limitations on the current state-of-the-art are errors in the Markovian model for parallel features and the inability to account for more than two features in parallel production. Furthermore there is no real generalisation between serial and parallel processes [4]. This makes it impractical to apply Optimal Mean Setting to the variety of features and manufacturing sequences that exist for the production of a real product. A more robust, correct and generalised framework to practice Optimal Mean Setting is required which is the subject of Chapter 3 - Section 3. Before this, a review of the literature encompassing cost modelling is undertaken. Optimal Mean Setting relies on an accurate unit cost estimate as the procedure is essentially a cost balancing exercise.

2.6 Cost Modelling

Most design and optimisation methods do not include cost as a design parameter, either as a constraint or as an objective function. A major reason for this is the inaccuracies present in calculating the cost, particularly during the early stages of design, where an exact geometry and method of manufacture have yet to be defined (Scanlan et al. [2006]). Where cost modelling is used in Robust Design and Optimal Mean Setting methodologies, it often applies only to a single or very few feature(s). Typically, these are design features as they are connected with the quality or functional performance of the product. However, design features are not necessarily the same as manufacturing features which actually drive the cost of manufacturing a component. For example, the wall thickness of a pressure vessel may be a design feature relating to the maximum pressure a vessel can safely contain. Assuming the vessel was made from a metal billet, a possible manufacturing method would be to turn the outer diameter and bore the inner diameter to result in a wall thickness. Thus, two manufacturing features are required to produce the design feature, which in turn relates to the quality or performance parameter. Typically, a gas turbine component will have several high level quality characteristics that must be met, driven by many design parameters, which themselves will

[4] Peng and Khasawneh [2014] did offer an example for the production of four features in two stages (serial production) with two features per stage (parallel production). However, a new set of equations would have to be generated if one wanted to consider only three features or five features, or produce three in parallel and only one in series.

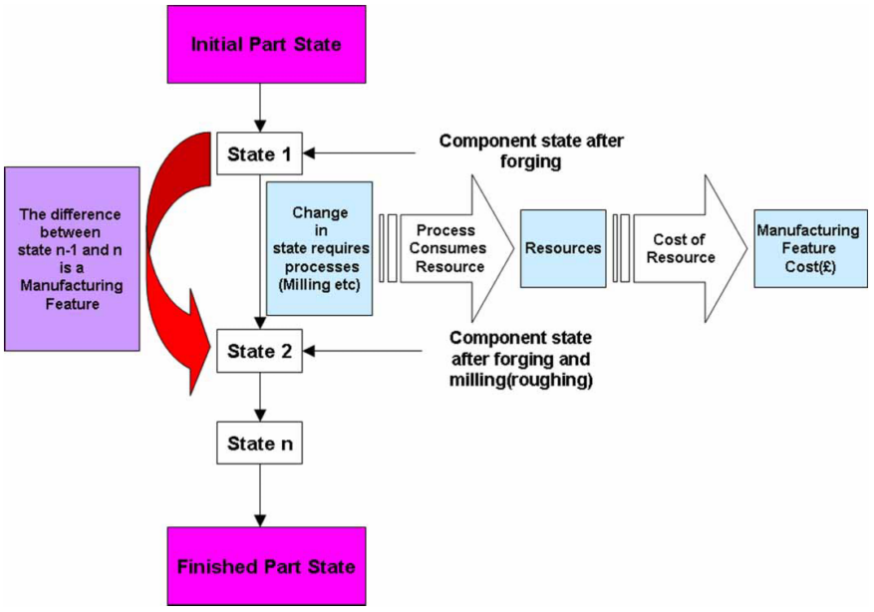

FIGURE 2.12: Illustration of manufacturing feature cost from Tammineni et al. [2009]

consist of several manufacturing features. Figure 2.12 indicates the costs associated with each manufacturing process, which sum together to determine the total production cost. A change in the design feature nominals will alter these manufactured features, as well as filtering back to the condition of supply and raw material states as follows:

- Change in the design parameter nominal
  - leads to changes in the manufacturing features
    - which will modify the condition of supply (COS)
      - and alters the required raw material state

A gas turbine component may have hundreds or thousands of manufacturing features, thus generating a cost model to this level of detail is a considerable undertaking. Not surprisingly there are several cost modelling methodologies that aim to circumvent this level of detail.

2.6.1 Data Mining and Regression Based Costing Methods

Data mining cost methods attempt to find statistical relationships between product cost and one or more parameters, often through linear regression. They are typically

beneficial in the conceptual stages of design where little geometric detail exists. Parametric and neural network models have been popular in cost modelling literature and are discussed within this Section.

2.6.1.1 Parametric Costing

The use of parametric cost models in aerospace can be traced back to Wright [1936] and an observation that the unit cost of an aircraft decreased with the number of aircraft produced. The Rand Corporation's work in the 1950s introduced the idea of cost estimating relations (CERs), which were developed to aid the Department of Defence (US) in estimating the cost of new military projects (Younossi et al. [2002]). Stahl [2010] investigated the use of parametric models where several variables were found to influence the cost of space telescopes. The Value Improvement team at Rolls-Royce also employed parametric methods to predict component cost based on typical high level design parameter of a component. An example of this type of technique is shown in Figure 2.13 (Langmaak et al. [2013]), where the milling operation time was scaled against the perimeter of a bladed disk (blisk). The red points indicate the known milling times for five blisks that had previously been manufactured. The black line was fitted to using R^2 regression and the red dashed lines indicate the confidence limits of the regression lines. These confidence limits denote the boundaries in which 95% of the points would be expected to fall if more data was collected. Although a statistically significant relationship may be found between cost and a parameter or parameters, it is not implicitly causal. If enough data is available a proportion of a data set can be used to generate a scaling parameter and the remaining portion can be used to test the relationship. Variables are selected which are believed to have some significance to driving the cost of a product. Rush and Roy [2001] discuss the application of 'expert judgement' for variable selection, else variables may be chosen based on statistical or casual proof they affect cost. Analysis, correlation and regression follow from which CERs can be selected. Processes of verification and validation are required before the predictions are used. Curran et al. [2004] offers a more extensive review of these parametric costing methods.

The level of geometric detail within Optimal Mean Setting is high as it is applied to individual design and manufacturing features. In contrast, regression is an approximation as to how many individual parameters change, in response to a principle driving parameter or CER. Thus, a parametric model may not be sufficiently detailed for Optimal Mean Setting where one is interested in how cost varies in response to a few very specific features.

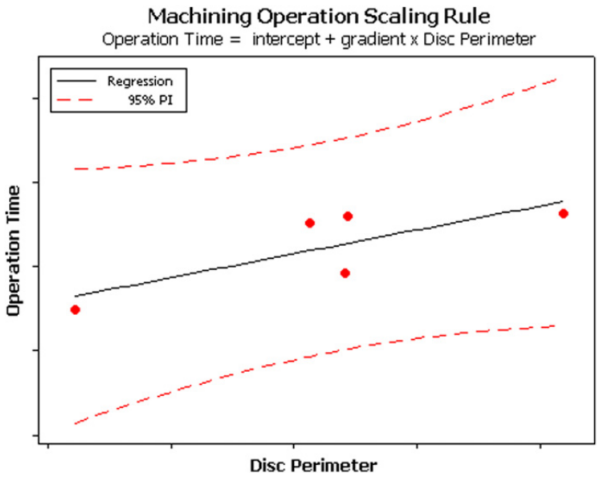

FIGURE 2.13: Illustration of parametric scaling from Langmaak et al. [2013]

2.6.1.2 Neural Networks

A popular model from the general arena of data mining is a neural network, which is an attempt to mimic human brain functionality originally devised as a method of pattern recognition. An implementation of such a method involves a network of nodes, representing neurons, which are linked by weighted connections, symbolic of synapses. The general arrangement is shown in Figure 2.14 from Cavalieri [2004]. To be useful as a cost model, a data set is required to train the model. A set of inputs (design parameters) are connected to the input layer and the weighted connections adjusted until the output (cost) is correct. The model will then 'know' how the costs of previous components were related to the inputs and can be used to make predictions about the cost for a new product, provided the new product is a derivative of the components in the training data set. Zhang et al. [1996] used a neural net approach to estimate the cost of packing products based on geometric characteristics of the products. Cavalieri [2004] also used the neural net method to estimate unit cost of brake disks. Both studies found neural nets outperformed parametric regression type analysis, particularly with regard to flexibility. As referred to by Cavalieri [2004], if a new production facility was implemented, a neural net can simply be re-trained on the new data set, whereas a parametric method would require rebuilding and validating. This is due to the fact that a neural net will automatically find cost estimating relationships in a data set during training, whereas a parametric model requires expert knowledge to define such relationships.

A primary disadvantage of the neural net approach to cost estimating is that an extensive data set is required to train the model, particularly when relationships are non-linear. Typically, the Aerospace industry does not produce enough derivative products to enable this. Additionally there is no necessity for causal relations between inputs and

outputs and the exact relationship can be hard to extract and comprehend. If a new product is clearly outside the existing dataset, the model may not be able to produce any worthwhile predictions. Again this type of approach is better suited to the early stages of design, where one is willing to accept a 'ballpark' cost figure rather than an exact calculation.

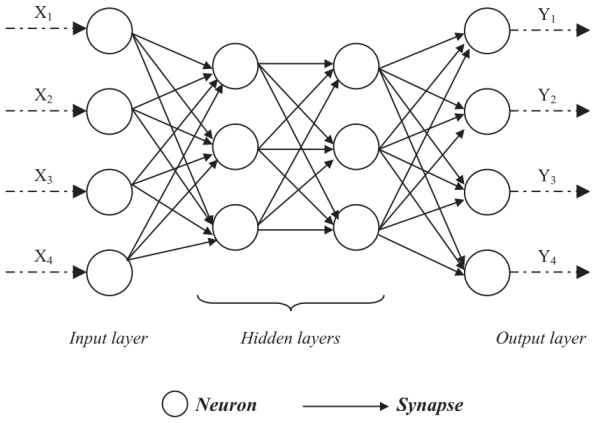

FIGURE 2.14: A typical neural net, Cavalieri [2004]

2.6.2 Analogous Costing

Analogous costing, like parametric costing, is typically used in the early design stages where there is a lack of detailed geometry information (Rehman and Guenov [1998]). The principle of an analogous costing technique is to adjust the cost of a target product based on the differences between the target product and a similar known product. Taylor [1997] applied such a technique to the cost of an engine nose-cowl. The effectiveness of the method relies on the ability to differentiate between the two cases. Typically, analogous estimates utilise a single historical data point as the basis for the new cost estimate. This implicitly assumes the new product is similar technologically and discounts any significant advances in manufacturing technology. A degree of 'expert judgement' is also required, although the results are generally held in higher esteem than parametric methods (Myrtveit and Stensrud [1999]). The generic form of an analogous cost estimate is, $C_N = C_P\, F_C\, F_M\, F_P$, Curran et al. [2004]. An initial estimate is based on the historic cost, C_P and modified by the three F ratios. Differences in complexity between the historical component and the target component are accounted for by F_C. Jenab and Liu [2010] offer a concise account of determining the relative complexity between two products. Miniaturisation factors, such as reducing subsystem size (for weight saving), are accounted for by F_M. Miniaturisation usually increases the cost. The term F_P relates to productivity improvements between the historical data point and the target. Generally these factors are estimated through expert opinion.

As with parametric methods, analogous cost methods are generally better suited to the concept design phase as a cost prediction can be generated without specific geometric detail. As a design becomes more detailed, geometry linked cost models may be created which are preferable to analogous methods. Nevertheless, the principle of using previous components as a basis for a new part cost is powerful. This principle is actually used in generative feature-based cost models (discussed later) whereby the costs of common manufacturing features are used and scaled to determine the cost of new components.

2.6.3 Detailed Costing Methods

Detailed costing methods include any method that attempts to model cost from the bottom-up based on the manufacturing features of the component's geometry. These include; activity based costing (ABC), bottom-up and feature-based methods. Modelling cost in this way ensures that there is a causal relationship between cost, and CERs. The necessity for this is summarised by Collopy and Curran [2005a] and Collopy and Curran [2005b]. Furthermore, changes in geometry explicitly relate to manufacturing features enabling scrap and rework modelling, although this is not common-place.

To support Optimal Mean Setting analysis cost models are required that allow the cost of individual design changes to be calculated and allow scrap and rework calculations to be executed. Feature-based cost methods are inherently based on the manufacturing process, inferring the time (and hence cost) required to manufacture a feature. The cost is acquired by multiplying the manufacturing time by cost rates, dependent on the operation. It was noted by Rush and Roy [2000] that manufacturers tend to have large numbers of three dimensional CAD (Computer Aided Design) models that can be decomposed into particular features required by the function of the part. These design features can be decomposed into manufacturing features to allow one to assess the cost of a design feature in terms of the constituent manufacturing features. Thus, during design it would be possible to infer the manufacturing features and operations and subsequently calculate the cost of the new design. Marx et al. [1995] noted this required information was typically associated with detailed design and needed to be pushed upstream. To facilitate such a capability Scanlan et al. [2006] outlined the creation of an assessable library of knowledge that contains processes, work centres, materials and historical components. These tools were developed by the Rolls-Royce project, DATUM (Design Analysis Tool for Unit Cost Modelling). Tammineni et al. [2009] outlined the way in which the knowledge was captured and used by the cost model (Figure 2.15), as proposed by DECODE. As part of the DECODE programme, Vanguard Studio was identified as a useful tool to create cost models. Figure 2.16 indicates a typical model where inputs are geometric features pertinent to the component. The geometry is

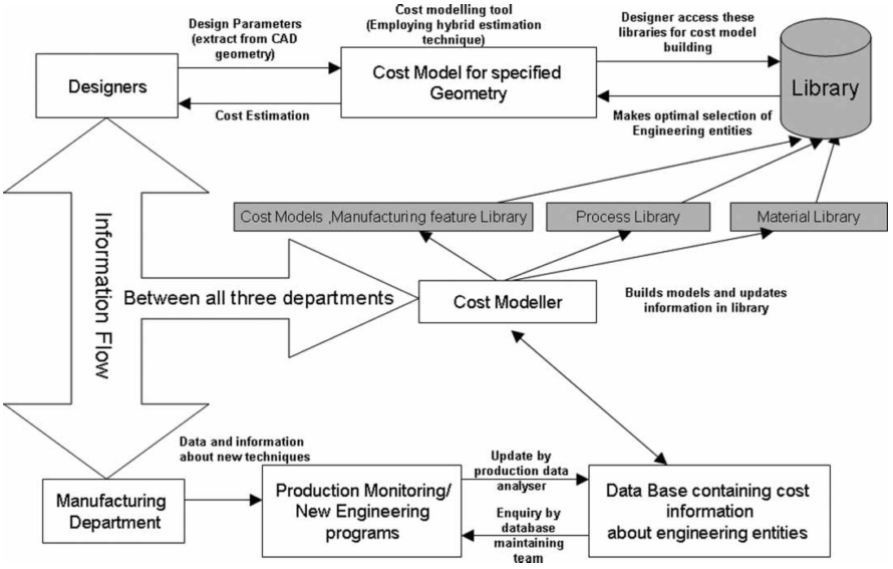

FIGURE 2.15: Cost model information flow [Tammineni et al., 2009]

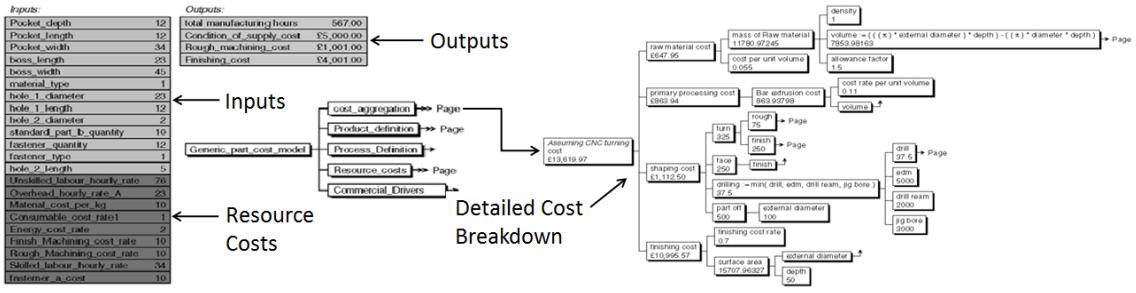

FIGURE 2.16: Example of a Vanguard Studio cost model

parametrised thus changes to the 'Inputs' such as 'Pocket Depth' or 'Boss Length' apply to the geometry of the whole component. The resource costs are high level parameters that are generally independent of the geometry of a design, such as material cost rates, energy cost rate and hourly wage. Outputs are costs and/or manufacturing times for the overall process and sub-processes. The model has a horizontal tree breakdown structure, where each node represents part of the total cost. For example, the 'cost aggregation node' divides into four lower level costs; raw material cost, primary processing cost, shaping cost and finishing cost. Each of these breaks-down further. For example, raw material cost for a forged component (such as a turbine disk) is calculated from the total volume of the forging. In the Vanguard Studio cost model, the forging volume is determined by applying rules to the finish part volume. A change in the 'Inputs' will bring about a change in the finished parts volume and consequently the forging volume which changes the raw material cost. The other three costs are similarly affected by changes to the input values. Knowledge, such as determining a forging volume and a condition of supply from the finished part geometry are contained within the

model. Manufacturing knowledge relating to the cost of manufacturing a feature is also contained within the model. For example, the cost of some features such as 'Pocket Depth' may be related to the volume of material removed, whereas other features such as 'Hole Diameter' may be a function of the material thickness. Several other articles use Vanguard Studio to build a cost model. Keane and Scanlan [2007] gave an example of the trade-off between the aerodynamic performance of an airliner wing and cost, where wing cost was calculated using a Vanguard Studio cost model. Rao et al. [2007] applied a cost and weight multi-objective optimisation to the design of a turbine disk. Cheung et al. [2010] proposed the use of Vanguard Studio cost models in the calculation of manufacture cost for a Value Driven Design application for gas-turbine design. Langmaak et al. [2013] applied Vangaurd Studio cost model to determine the cost of bladed disks (blisks) for gas-turbine engines.

The development of feature-based cost models within Rolls-Royce has allowed the vision presented in Figure 2.15 to be realised. A featured-based cost tool, using data from the manufacturing process, has been integrated into a geometry tool (Siemens NX) as illustrated by Figure 2.17[5]. A set of design features are presented on the left window which can be scaled. The right window outputs the cost of each feature. This method is somewhat constrained to scaled variations on existing components. Nevertheless, a considerable proportion of new engine components are derivatives of past designs. The

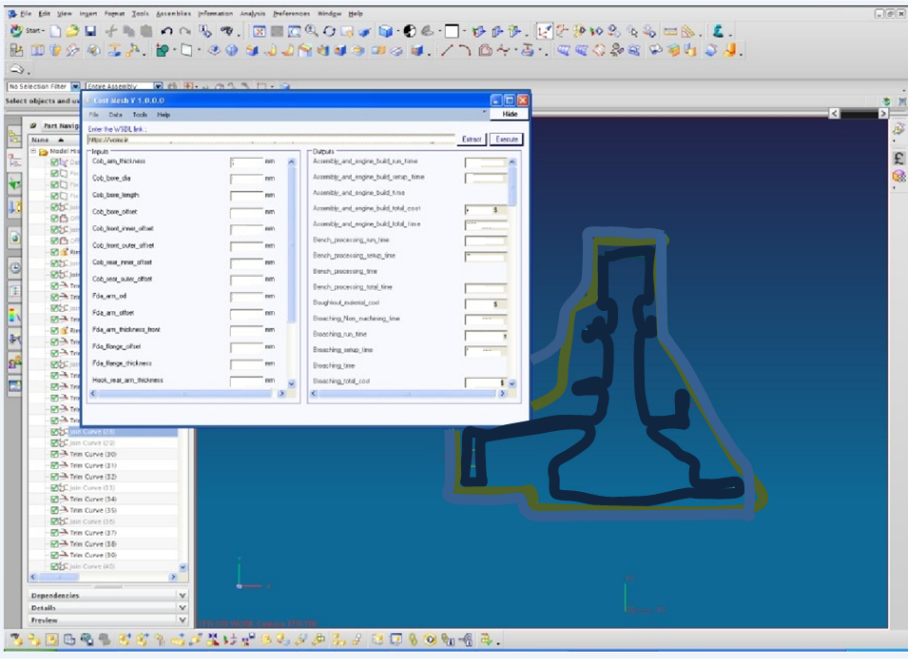

FIGURE 2.17: Illustration of a cost model linked to a computer geometry tool.

cost of a component is driven by a detailed cost model. The level of detail present in

[5]Provided by Product Cost Engineering, Rolls-Royce

these feature-based cost models and their integration into the computer geometry tool, allow the geometry to be optimised for functional performance as well as cost.

Optimal Mean Setting requires a cost modelling capability to determine the manufacturing cost for design features and enable cost to update in response to changes in the mean location. Detailed bottom-up costing methods fulfil this criteria and the tools and methodology present in the literature required have been discussed (Section 2.6.3). This thesis does not contribute to cost modelling methodologies, however, the concept of attributing cost to specific features is used to determine scrap, rework and conformance cost within the realm of Optimal Mean Setting.

2.7 Summary of Literature

A number of techniques and design principles around the area of Robust Design and Reliability Engineering deal with the propagation of uncertainty to characterise the variation in the performance or functionality of products and systems (Sections 2.1 to 2.4). These methods acknowledge manufacturing variability and all are united in maximising the allowable amount of variability. Performance is sacrificial, provided the sensitivity of the product to variation can be reduced (and product safety can be maintained). In contrast, the research in this thesis asks how might performance be preserved or maximised most efficiently (in an economic sense) if the manufacturing variation is not seen as a constraint. Reliability Engineering is the closest to this philosophy where a system is not permitted to fail (performance must be maintained), however, there is no mechanism to reduce manufacturing cost, nor consequently to improve economic efficiency. Optimal Mean Setting offers a mechanism to reduce manufacturing costs when tolerances remain tight to guarantee high performance. There are several areas of Optimal Mean Setting which have not been tackled by existing research, listed below:

- There are errors in Khasawneh et al. [2008], relating to the numbers of components moving between stages for parallel production systems. These are explained and rectified in Section 3.2.2.
- Current literature only accounts for the possibility of two features being manufactured before inspection in a Markovian based Optimal Mean Setting framework (Khasawneh et al. [2008] and Peng and Khasawneh [2014]). A generalised case is developed in Section 3.2.2.1. There is also a difference in the way serial and parallel processes are modelled in the literature (Bowling et al. [2004] and Selim and Al-Zu'bi [2011] versus Khasawneh et al. [2008] and Peng and Khasawneh [2014],

respectively). Section 3.2.2.3 develops a unified method of considering both serial and parallel processes with one equation.

- A detailed understanding of how correlation affects the optimal mean and expected profit for parallel operations is not present in the literature. This is considered under Section 3.5.2.

- No papers exist that consider the impact of Optimal Mean Setting on the manufactured geometry distribution of the component. As Optimal Mean Setting tends to bias rework, the manufactured geometry distribution tends to be skewed towards the rework specification limit. This is considered in Chapter 4. A case study applied to film cooling holes is presented in Section 4.4.2, which links the change in the manufactured geometry distribution to the expected performance distribution of the component. Again this has not been considered in the literature.

Chapter 3

Optimal Mean Setting

As discussed in the Introduction, Optimal Mean Setting is the principle of shifting the process mean to maximise profit, when the variance of a manufacturing process is larger than the tolerance limits. It relies on an asymmetry between the cost of scrap and rework such that non-conformance may be biased towards one or other, (usually rework). The objective of Optimal Mean Setting is illustrated by Equation 3.1 where profit is maximised by changing the process mean.

$$\begin{aligned} \text{Profit} &= \text{Items Sold} - \text{Processing Cost} \\ &- \text{Scrap Cost} - \text{Rework Cost}. \end{aligned} \tag{3.1}$$

The principle contribution to knowledge of this Chapter is the development of a generalised expression for expected profit (item 2 from Section 1.6 in Chapter 1). The process of generating a generalised methodology involved consideration of three major elements; serial production (Section 3.1.1), production of multiple features (Section 3.1.2) and Markovian modelling (Section 3.2). Each of these elements had been considered in literature previously but were not brought together in a generalised approach. Detailed consideration from first principles of these elements also led to new and improved understanding, correcting errors in the parallel model (item 1 from Section 1.6 in Chapter 1) and developing an improved optimisation methodology (item 3 from Section 1.6 in Chapter 1). Where this research draws from or compares against existing work is explicitly referenced. The Chapter closes with the application of the new generalised approach to model problems (Section 3.4).

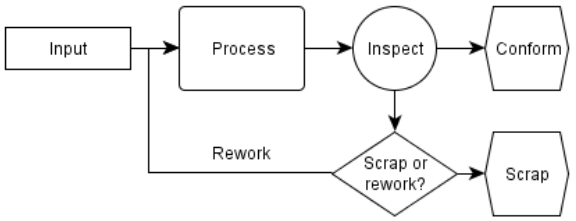

FIGURE 3.1: Process flow diagram with a rework loop

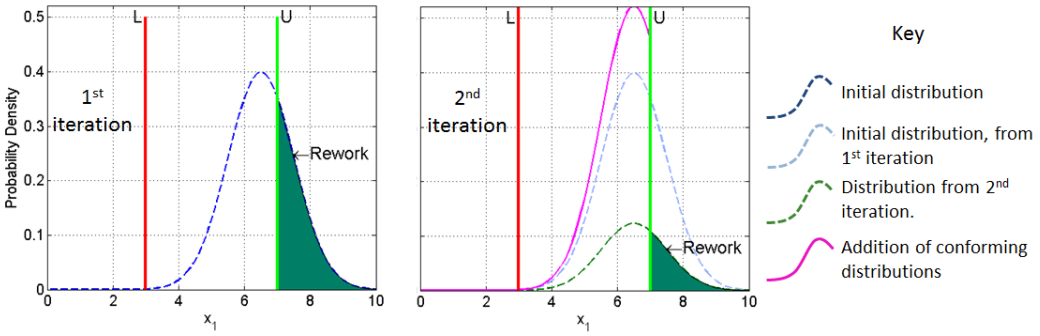

FIGURE 3.2: Two iterations of an iterative manufacturing process

3.1 Iterative Manufacturing Processes

The principle objective in this section is to derive an expression for total profit for the production of a feature which can be maximised by adjusting the process mean(s). It is possible to manufacture one or multiple features in sequence, one after another with an inspection process after each. This is known as ***serial production***. Alternatively, several features may be processed prior to inspection. This is known as ***parallel production***, although this does not imply features have to be manufactured simultaneously, it is the location of the inspection process relative to the processing of features that is important.

3.1.1 Single-Feature Iterative Manufacturing From First Principles

An iterative manufacturing method involves a rework loop which passes rework items back for re-processing. The process starts with an initial manufacturing operation which generates features in three states; rework, conforming and scrap. Several subsequent iterations convert the rework into just two states, conforming and scrap. An inspection process is used at each iteration to determine whether parts conform, are scrap, or require rework. Figure 3.1 indicates these iterative steps and the final states; conformance or scrap.

The process is examined in more detail in Figure 3.2, where the distribution of each iteration is assumed to be normally distributed. The dashed blue line, on the right plot of Figure 3.2, indicates the distribution of manufactured geometry due to manufacturing variation if the initial cut was set at 6.5 units. The red and green vertical lines locate the lower and upper specification limits respectively. The target value for this process would be five (mid way between the USL and LSL). Here, the mean was shifted to reduce scrap in favour of increased rework. The green area represents the components requiring rework. The green dashed line, on the right plot of Figure 3.2, shows the resulting distribution from re-processing the rework parts. The solid magenta line, on the right plot of Figure 3.2, is the sum of the conforming components from the first and second iteration and represents the distribution of manufactured geometry after this second iteration. The light blue dashed line, on the right plot of Figure 3.2, indicates the original distribution from the first iteration. The dark green shaded region, on the right plot of Figure 3.2, clearly indicates further rework is required, although less than after the initial cut. Subsequent iterations would steadily reduce this area until the integral of the magenta curve was equal to one, indicating all components were either conforming or scrap.

To maximise profit from such a process, an optimal reworking strategy must be identified specifically the mean values for each iteration. It would be feasible to alter the mean values for each iteration such that the initial mean may be $\mu_{x_1} = 6.5$, followed by a different mean for subsequent iterations. However, it can be shown for the production of a single feature only one optimal mean exists for the initial manufacturing stage and all subsequent rework operations. There are several assumptions detailed as follows.

Assumptions

1. Products or features are produced continuously.
2. All manufacturing processes are under statistical control.
3. The manufacturing variation of the initial operation and all rework operations are the same.
    a. Assumes the same or similar machines are used for rework operations. For low production volumes this is practical provided the machines are free, (not fully utilised). It is also practical where rework is expected and the manufacturing route is designed as such.
    b. Assumes the manufacturing variation will not change with the differing volumes of material to be removed, added or manipulated between components. Typically the features requiring rework will be close to the target geometry

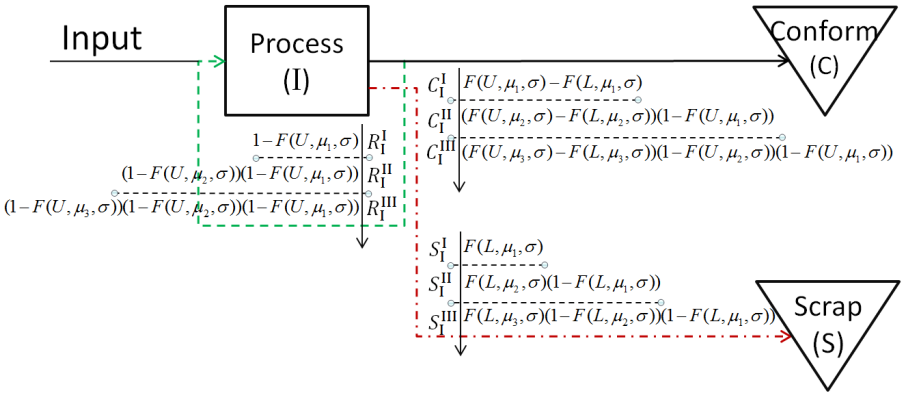

FIGURE 3.3: Probabilities of components in the rework, scrap and conforming states for three iterations

(within a few standard deviations of conformance) and so there are unlikely to be great geometric differences between the components that require feature rework.

4. The specification limits for the initial operation and all rework operations are the same, i.e. the nominal geometry of the feature(s) are unchanged. In practical situations this applies unless special authorisation is given, as the geometry will differ from the original design specification (concessions).

5. The flow of features through the rework stages in a parallel manufacturing operation has a standard form discussed in Section 3.1.2 and further in Section 3.2.2. If the manufacture of a specific product or features doesn't exactly fit this standard form the link between rework states may be broken as shown by worked examples in Section 4.4 and Appendix F.

6. The inspection process used to determine whether a feature is scrap, rework or conforming is assumed to be 100% accurate. Practically this implies the variation of the inspection process is very much smaller than the variation of the manufacturing process.

The expected profit for the production of a single feature follows the general form given by Equation 3.1. The probabilities of components occupying the three states (confirming, scrap and rework), for three iterations, is given by Figure 3.3. This diagram is representative of Figure 3.1 except the inspection and decision stages are implicit in the Process (I) box. The values R, C and S are the rework, conforming and scrap states respectively. A superscript represents an iteration, while the subscripts indicate where the features in that state originated (all from state I in this case). The function $F(\bullet)$ is

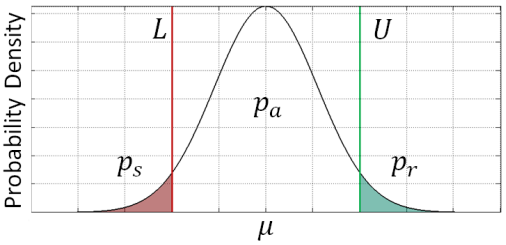

FIGURE 3.4: Single variable normal manufacturing variation

the cumulative normal distribution function (CDF) given by,

$$F(X, \mu, \sigma) = \Pr[X \leq x] = \int_{-\infty}^{x} f_X \, \mathrm{d}t, \tag{3.2}$$

where f_X is the normal distribution function given by,

$$f(x, \mu, \sigma) = \frac{1}{\sigma\sqrt{2\pi}} \exp\left(-\frac{(x-\mu)^2}{2\sigma^2}\right). \tag{3.3}$$

The first terms (first iteration) for the rework, conformance and scrap states in Figure 3.3 correspond to the areas of the red, white and green regions in Figure 3.4. The second iterations for the rework, conformance and scrap states are also the areas of the red, white and green regions in Figure 3.4 but with a different target mean μ_2. The terms are also regulated by the probability of rework from the first iteration $1 - F(U, \mu_1, \sigma)$. The rework, conformance and scrap for the third iteration again involve a different target mean μ_3 and are regulated by the probability of rework from the first and second iterations. For n iterations the expected profit is given by,

$$\begin{aligned} E(PR) = SP \Bigg[\sum_{i=1}^{n} \overbrace{[F(U, \mu_i, \sigma) - F(L, \mu_i, \sigma)]}^{\text{Conformance}} \prod_{i=2}^{n} \\ \underbrace{[1 - F(U, \mu_{i-1}, \sigma)]}_{\text{Rework (previous iter.)}} \Bigg] - PC - \Bigg[\sum_{i=1}^{n} \Bigg(Sc \underbrace{[F(L, \mu_i, \sigma)]}_{\text{Scrap}} \\ + Rc \underbrace{[1 - F(U, \mu_i, \sigma)]}_{\text{Rework}} \Bigg) \prod_{i=2}^{n} \underbrace{[1 - F(U, \mu_{i-1}, \sigma)]}_{\text{Rework (previous iter.)}} \Bigg]. \end{aligned} \tag{3.4}$$

The first term in the square parenthesis is the probability of conformance after n iterations. This will reproduce the terms in the conformance state (C) in Figure 3.3 The second term in square parenthesis gives the probabilities of scrap and rework after n iterations, reproducing the terms under the rework (R) and scrap (S) states in Figure 3.3. The constants, SP, PC, Sc, and Rc are the selling price, processing cost, scrap cost

and rework cost respectively. The means, μ_i for $i = 1, 2, \ldots, \infty$, are the target means for each iteration. The initial operation is $i = 1$ and $i \geq 2$ are rework iterations. For practical situations n is a large number defining the total number of iterations necessary to complete all the rework such that only scrap and conforming items remain. The standard deviation is given by σ.

Equation 3.4 determines the difference between the income generated from the components that can be sold (first term) and the total production cost. The total production cost includes the cost of scrap and rework, enclosed within the second set of large square parenthesis and the initial processing cost (PC).

It is conjectured that to maximise the profit an optimal mean can be found which is the same for every iteration (the initial processing and all rework iterations). This is proven here.

Theorem 3.1. *There is only one μ_{opt} that satisfies*

$$\max_{\boldsymbol{\mu} \in \mathbb{R}} \left\{ PR(\boldsymbol{\mu}) \right\},$$

where $\boldsymbol{\mu} = [\mu_1, \mu_2, \ldots, \mu_\infty]$. Such that $\mu_i = \mu_{opt}$, $\forall\, i \,\exists\, [1, \infty]$.

. To avoid confusion with bracketed terms, let total profit (TP) be equivalent to expected profit term ($E(PR)$) in Equation 3.4 (for this theorem and proof). Differentiating Equation 3.4 with respect to each μ_i and setting to zero, $\partial TP_i / \partial \mu_i$ gives the stationary point (maximum)[1] for each iteration i. A general expression for the maximum for each iteration is sought. Although $i \to \infty$, in general the number of rework iterations for a batch of components will be finite. However, there is always a diminishingly small probability that rework will exist and more iterations will be required. Let the total number of rework iterations be n, where in practical cases n will be a large number but in the general case $n = \infty$. Consider the optimal means for the last three rework iterations[2],

$$\mu_{\text{opt}_n} = \frac{1}{2(L-U)} \left\{ 2\sigma^2 \ln \left[\frac{SP + Rc}{SP + Sc} \right] + L^2 - U^2 \right\}, \tag{3.5}$$

[1] The stationary point is shown to be a maximum after the proof is completed, rather than showing each stationary point for ever i is a maximum. This is shown in Appendix A

[2] The three expressions for μ_{opt_n}, $\mu_{\text{opt}_{n-1}}$ and $\mu_{\text{opt}_{n-2}}$ (Equations 3.5 to 3.7) are derived in Appendix B by first considering a finite number of rework operations.

$$\mu_{\text{opt}_{n-1}} = \frac{1}{2(L-U)}\left\{2\sigma^2 \ln\left[\frac{1}{2\alpha}\left(\xi(\varphi_n)\alpha + \xi(\upsilon_n)\beta + 3Rc + 2SP + Sc\right)\right] + L^2 - U^2\right\}, \tag{3.6}$$

$$\mu_{\text{opt}_{n-2}} = \frac{1}{2(L-U)}\left\{2\sigma^2 \ln\left[\frac{1}{4\alpha}\left(\left(-\xi(\varphi_n)\alpha - \xi(\upsilon_n)\beta - 3Rc - 2SP - Sc\right)\xi(\upsilon_{n-1}) + \xi(\varphi_n)\alpha + \xi(\upsilon_n)\beta - 2\xi(\varphi_{n-1})\alpha + 7Rc + 4SP + 3Sc\right)\right] + L^2 - U^2\right\}. \tag{3.7}$$

There are two cost terms defined as $\alpha = SP + Rc$ and $\beta = SP + Sc$ and ξ is the error function given by,

$$\xi(\varphi_i) = \frac{2}{\sqrt{\pi}}\int_0^{\varphi_i} e^{-t}\,\mathrm{d}t \;\text{ and }\; \xi(\upsilon_i) = \frac{2}{\sqrt{\pi}}\int_0^{\upsilon_i} e^{-t}\,\mathrm{d}t \tag{3.8}$$

where,

$$\varphi_i = \frac{\sqrt{2}(-\mu_i + L)}{2\sigma} \;\text{ and }\; \upsilon_i = \frac{\sqrt{2}(-\mu_i + U)}{2\sigma} \tag{3.9}$$

For $i = n$, μ_{opt_n} is purely a function of the relative costs and relationship between the specification limits (L and U) and the manufacturing variation σ. The second to last optimal mean, $\mu_{\text{opt}_{n-1}}$, is a function of the costs, specification limits, σ and the last optimal mean, μ_{opt_n}. The third to last optimal mean, $\mu_{\text{opt}_{n-2}}$, is a function of the costs, specification limits, σ and the last two optimal means, $\mu_{\text{opt}_{n-1}}$ and μ_{opt_n}. Notice that the earlier optimal means are functions of all subsequent optimal means; thus to establish the value of the first optimal mean, one must first establish the value of the last optimal mean, then the second to last optimal mean and so on. Accordingly a new subscript j is defined such that $j = [n, n-1, \ldots, 1]$. From Equations 3.5 to 3.7 a general expression for μ_{opt_j} can be constructed where,

$$\mu_{\text{opt}_j} = \frac{1}{2(L-U)}\left\{2\sigma^2 \ln\left[\frac{\Gamma_j}{2^{n-j}\alpha}\right] + L^2 - U^2\right\} \tag{3.10}$$

and Γ_j is given by,

$$\begin{aligned}\Gamma_j = &-1[\Gamma_{j+1}\,\xi(\upsilon_{j+1})] \\ &+ \Gamma_{j+1} + 2^{n-(j+1)}\xi(\varphi_{j+1})\alpha \\ &+ 2^{n-j}Rc + 2^{n-(j+1)}SP + 2^{n-(j+1)}Sc.\end{aligned} \tag{3.11}$$

The n^{th} term is always

$$\mu_{\text{opt}_n} = \frac{1}{2(L-U)}\left\{2\sigma^2 \ln\left[\frac{\beta}{\alpha}\right] + L^2 - U^2\right\}. \tag{3.12}$$

Lemma 3.2. *Given that L, U and σ remain constant for each iteration, to prove the conjecture, $\mu_i = \mu_{opt}$, $\forall\, i\, \exists\, [1, \infty]$, it must be shown,*

$$\begin{aligned}\frac{\Gamma_j}{2^{n-j}\alpha} &= \frac{\Gamma_{j+1}}{2^{n-j+1}\alpha}\bigg|_{n\to\infty} \textit{ which reduces to} \\ \Gamma_j &= 2\Gamma_{j+1}\big|_{n\to\infty}.\end{aligned} \tag{3.13}$$

The last three terms of Γ (Equation 3.11) increase as a factor of two for each iteration. The third term, $2^{n-(j+1)}\xi(\varphi_{j+1})\alpha$, can increase up to a maximum of a factor of two for each iteration, when $\varphi_{j+1} = 1$. Thus, it remains to be shown the maximum rate of increase, per iteration, for the first two terms of Γ is two, in the limit $n \to \infty$. This is shown by applying linear stability analysis. A new subscript m is defined where $m = [n-1, n-2, \ldots, 1]$ where m is the next point after $m+1$. Let $f(\Gamma) = \Gamma_m/2^{n-m}\alpha$ and let a fixed point be defined such that

$$\Gamma_m = \Gamma_{m+1} = \Gamma^* = f(\Gamma^*). \tag{3.14}$$

A small deviation from this fixed point is,

$$\Gamma_{m+1} = \Gamma^* + \delta\Gamma_{m+1}.$$

Therefore at the next step,

$$\begin{aligned}\delta\Gamma_m &= \Gamma_m - \Gamma^* \\ &= f(\Gamma_{m+1}) - \Gamma^* \\ &= f(\Gamma^* + \delta\Gamma_{m+1}) - \Gamma^*.\end{aligned} \tag{3.15}$$

Since $\delta\Gamma_{m+1} << \Gamma^*$ a Taylor series expansion around Γ^* can be implemented giving,

$$f(\Gamma^* + \delta\Gamma_{m+1}) = \Gamma^* + \delta\Gamma_{m+1}\left(\frac{\mathrm{d}f}{\mathrm{d}\Gamma}\right)_{\Gamma=\Gamma*} + \mathcal{O}(\delta\Gamma_{m+1}^2).$$

Close to the fixed point the second order terms $\mathcal{O}(\delta\Gamma_{m+1}^2)$ are very small and can be neglected. Recognising $f(\Gamma^*) = \Gamma^*$, from Equation 3.14, the above equation can be rewritten as

$$\delta\Gamma_m = f'(\Gamma^*)\,\delta\Gamma_{m+1}$$

where $f' = \mathrm{d}f/\mathrm{d}\Gamma$ and

$$f'(\Gamma^*) = -\xi(\upsilon) + 1. \tag{3.16}$$

The maximum value of Equation 3.16 is $f'(\Gamma^*) = 2$ for all values $\mu \exists \mathbb{R}$. Thus, the equality in Equation 3.13 is satisfied in the limit as $n \to \infty$ proving the lemma and completing the proof, confirming the same optimal mean must be applied for each rework iteration to maximise profit. Thus the Markovian method (outlined by Bowling et al. [2004] and Selim and Al-Zu'bi [2011]) which implicitly uses the same mean for every iteration, is justified and greatly simplifies the expression for total profit, given in Equation 3.4 in iterative form. □

3.1.2 Multiple-Feature Iterative Manufacturing from First Principles

A logical extension to Optimal Mean Setting with one feature is the production of multiple features. If multiple features are created in series the optimal mean for each stage is the same as considering each one individually. However, several features may be produced in one stage (parallel processing). This is fundamentally different as there are multiple rework routes for each feature. The simplest type of parallel processing is dual feature processing, where two features are created prior to inspection, a specific case of a general parallel system.

Figure 3.5 indicates the processing of two features prior to inspection, reminiscent of the one feature case in Figure 3.1. Inspection processes are implicit at the end of the initial state and the three rework stages. The three rework states are initially fed from the first manufacturing operation (I), which can also cause scrap and conformance. After initial processing, the single feature rework states (2) and (3) may receive components from themselves (i.e. items are reworked but still don't conform and require further rework) or from the dual feature rework state (4) (i.e. only one feature conforms when reworked in state 4). The dual feature reworking state (4) may only receive components from the initial operation and from itself, if after dual feature rework both features still require rework. As in the single feature rework case, all components eventually conform or

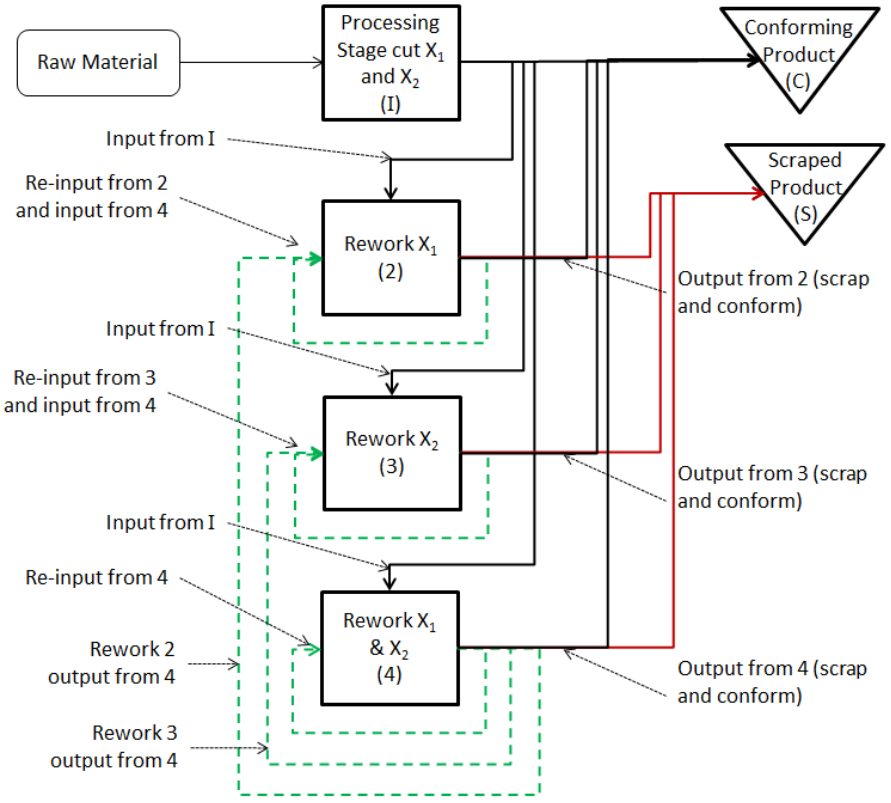

FIGURE 3.5: Manufacturing flow in two-feature parallel process

are scrapped. The initial probabilities of scrap ($p_{\mathrm{I,S}}$), conformance ($p_{\mathrm{I,C}}$) and the three rework states ($p_{\mathrm{I},2}$, $p_{\mathrm{I},3}$ and $p_{\mathrm{I},4}$) are illustrated on Figure 3.6. The S_{X_i} and R_{X_i} terms indicate scrap and rework respectively for features where i defines the specific feature. There are three separate probabilities for the rework region, $p_{\mathrm{I},2}$ to $p_{\mathrm{I},4}$, whilst the scrap regions are grouped into one probability $p_{\mathrm{I,S}}$, irrespective of what feature caused the scrap. Scrap for any one feature results in the whole component being scrapped, whereas one or more features can be reworked. Khasawneh et al. [2008] was the first to define the probabilities of rework, scrap and conformance for dual features in this way, however, their method does not allow for correlation between features, which may occur particularly if two or more features are produced on the same machine or a single machining operation is responsible for the creation of multiple features. For example, the diameter and eccentricity of a hole may be inspectable features but produced from a single drilling operation. The bivariate normal distribution allows for the possibility

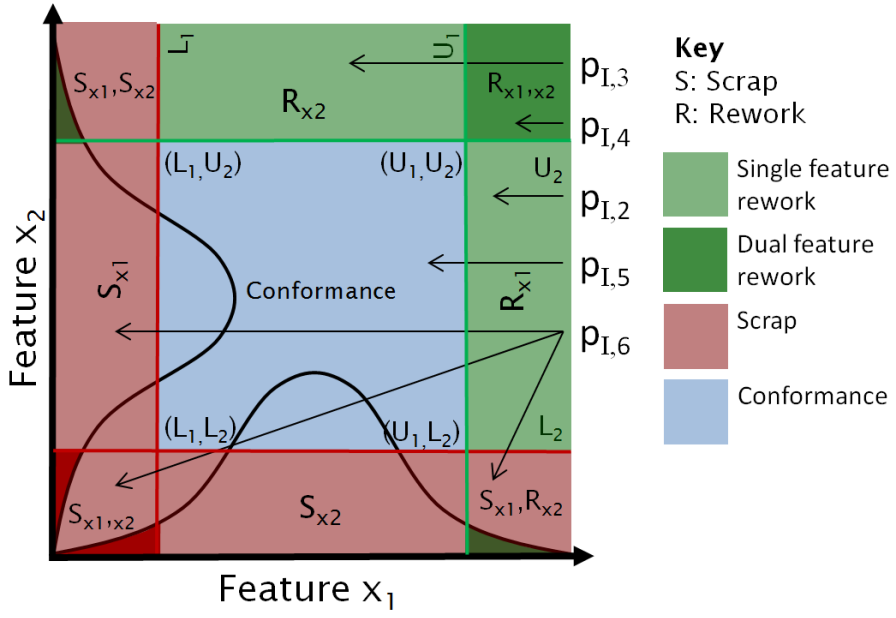

FIGURE 3.6: Dual feature rework, conformance and scrap

of correlation and is given by,

$$f(x_1,x_2) = \frac{1}{2\pi\sigma_1\sigma_2\sqrt{1-\rho^2}} \exp\left\{\frac{-1}{2(1-\rho^2)}\left[\left(\frac{x_1-\mu_1}{\sigma_1}\right)^2 + \left(\frac{x_2-\mu_2}{\sigma_2}\right)^2 - 2\rho\left(\frac{x_1-\mu_1}{\sigma_1}\right)\left(\frac{x_2-\mu_2}{\sigma_2}\right)\right]\right\} \tag{3.17}$$

where $\rho = \text{corr}(x_1,x_2) = \text{cov}(x_1,x_2)/\sigma_1\sigma_2$. The cumulative distribution of this function allows the rework, conformance and scrap probabilities to be calculated and is given by,

$$F(x_1,x_2) = \int_{-\infty}^{x_1}\int_{-\infty}^{x_2} f(t_1,t_2)\ \mathrm{d}t_2\ \mathrm{d}t_1$$

In general there are no closed form solutions to this equation, but solutions exist in terms of the error function and this form of integral is well supported in numerical packages such as Matlab's *mvncdf* function (Mathworks [2012]). The probabilities $p_{I,2}$ to $p_{I,S}$ are

computed as follows:

$$
\begin{aligned}
p_{\mathrm{I},2} = \int_{\mathrm{U}_1}^{\infty}\int_{\mathrm{L}_2}^{\mathrm{U}_2} f(t_1,t_2)\,\mathrm{d}t_2\,\mathrm{d}t_1 \quad &= \quad F(\infty,\mathrm{U}_2) - F(\mathrm{U}_1,\mathrm{U}_2)\\
&- \quad F(\infty,\mathrm{L}_2) + F(\mathrm{U}_1,\mathrm{L}_2),\\
p_{\mathrm{I},3} = \int_{\mathrm{L}_1}^{\mathrm{U}_1}\int_{\mathrm{U}_2}^{\infty} f(t_1,t_2)\,\mathrm{d}t_2\,\mathrm{d}t_1 \quad &= \quad F(\mathrm{U}_1,\infty) - F(\mathrm{U}_1,\mathrm{U}_2)\\
&- \quad F(\mathrm{L}_1,\infty) + F(\mathrm{L}_1,\mathrm{U}_2),\\
p_{\mathrm{I},4} = \int_{\mathrm{U}_1}^{\infty}\int_{\mathrm{U}_2}^{\infty} f(t_1,t_2)\,\mathrm{d}t_2\,\mathrm{d}t_1 \quad &= \quad F(\infty,\mathrm{U}_2) - F(\mathrm{U}_1,\infty)\\
&+ \quad F(\mathrm{U}_1,\mathrm{U}_2),\\
p_{\mathrm{I},C} = \int_{\mathrm{L}_1}^{\mathrm{U}_1}\int_{\mathrm{L}_2}^{\mathrm{U}_2} f(t_1,t_2)\,\mathrm{d}t_2\,\mathrm{d}t_1 \quad &= \quad F(\mathrm{U}_1,\mathrm{U}_2) - F(\mathrm{L}_1,\mathrm{U}_2)\\
&- \quad F(\mathrm{U}_1,\mathrm{L}_2) + F(\mathrm{L}_1,\mathrm{L}_2),\\
p_{\mathrm{I},S} = \int_{-\infty}^{\mathrm{L}_1}\int_{-\infty}^{\infty} f(t_1,t_2)\,\mathrm{d}t_2\,\mathrm{d}t_1 \quad &+ \quad \int_{-\infty}^{\infty}\int_{-\infty}^{\mathrm{L}_2} f(t_1,t_2)\,\mathrm{d}t_2\,\mathrm{d}t_1\\
-\int_{-\infty}^{\mathrm{L}_1}\int_{-\infty}^{\mathrm{L}_2} f(t_1,t_2)\,\mathrm{d}t_2\,\mathrm{d}t_1 \quad &= \quad F(\mathrm{L}_1,\infty) + F(\infty,\mathrm{L}_2)\\
&- \quad F(\mathrm{L}_1,\mathrm{L}_2).
\end{aligned}
\tag{3.18}
$$

These initial probabilities determine the proportion of items going into the various states illustrated in Figure 3.5. In total there are eight CDF evaluations in Equation 3.18 which increase as 2^{n+1}, where n is the number of features. Although the computational expense of evaluating CDF functions is relatively low, owing to the speed-up methods detailed by Genz and Bretz [2002] and Genz [2004], it is simple to half the number of CDF evaluations by rearranging the univariate distribution axes. The univariate axes can be reversed so the axes run from ∞ to $-\infty$[3], such that rework occurs towards the origin as shown in Figure 3.7.

For n-features, the rework, scrap and conformance probabilities can be calculated using

[3]Generally one would expect positive dimesnions for features, but since the dimension of a feature is a function of the refernce measurement location, negative dimensions are possilbe. This justifies the extension of the axes to $-\infty$.

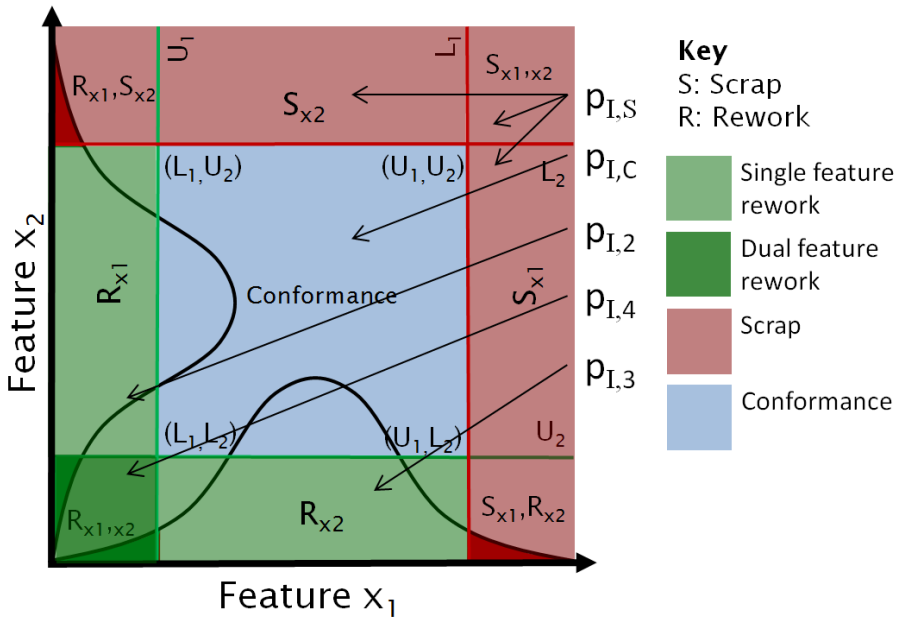

FIGURE 3.7: Dual feature rework, conformance and scrap with rearranged axes

the approach to determine rectangular probabilities discussed in Nelsen [2006]. A rectangular region can be defined by $\boldsymbol{L} = (L_1, \ldots, L_n)$ and $\boldsymbol{U} = (U_1, \ldots, U_n)$, where $\boldsymbol{L}_i \leq \boldsymbol{U}_i$ $\forall\ i = 1, 2, \ldots, n$ and where $(\boldsymbol{L}, \boldsymbol{U})$ is an n-dimensional rectangle (n is the number of features at a given stage). The vectors $\boldsymbol{L}$ and $\boldsymbol{U}$ represent the lower and upper specification limits for each feature as indicated on Figure 3.7. Taking the Cartesian product of n intervals, $A = (L_1, U_1) \times (L_2, U_2) \times, \ldots, \times (L_n, U_n)$. A cumulative distribution function (CDF) F: $\mathbb{R}^n \to [0, 1]$ is given by the integral of the multivariate distribution function,

$$F(\boldsymbol{x}, \boldsymbol{\mu}, \boldsymbol{\Sigma}) = \int_{-\infty}^{x_n} \cdots \int_{-\infty}^{x_1} \frac{1}{\sqrt{(2\pi)^k |\boldsymbol{\Sigma}|}} \exp\left\{ -\frac{(\boldsymbol{t} - \boldsymbol{\mu})^T \boldsymbol{\Sigma}^{-1} (\boldsymbol{t} - \boldsymbol{\mu})}{2} \right\} \mathrm{d}t_1 \ldots \mathrm{d}t_n, \tag{3.19}$$

where $\boldsymbol{X}$ is a k-dimensional random vector $\boldsymbol{X} = [X_1, \ldots, X_k]$, $\boldsymbol{\mu}$ is a k-dimensional mean vector $\boldsymbol{\mu} = [E[X_1], \ldots, E[X_k]]$ and $\boldsymbol{\Sigma}$ is a $k \times k$ covariance matrix, $\boldsymbol{\Sigma} = [\mathrm{Cov}[X_i, X_j]]$, $i = 1, \ldots, k$; $j = 1, \ldots, k$. The probability enclosed in the rectangle $A = (\mathbf{L}, \mathbf{U})$ is given by:

$$P_A = P(L_1 < X_1 \leq U_1, \ldots, L_n < X_n \leq U_n),$$

which can be expressed as,

$$P_A = \sum_{i_1=0}^{1} \sum_{i_2=0}^{1} \cdots \sum_{i_n=0}^{1} (-1)^{i_1 + i_2 + \cdots + i_n} F\left(\boldsymbol{x}_{i_1}, \boldsymbol{x}_{i_2}, \ldots, \boldsymbol{x}_{i_n}\right). \tag{3.20}$$

where,

$$\begin{cases} \boldsymbol{x}_{ij} = \boldsymbol{L}_j & \text{if } i_j = 0, \\ \boldsymbol{x}_{ij} = \boldsymbol{U}_j & \text{if } i_j = 1 \end{cases} \qquad \forall \quad j = 1, 2, \ldots, n.$$

The probability of rework is simply,

$$P_{Rw} = F(\boldsymbol{U}, \boldsymbol{\mu}, \boldsymbol{\Sigma}) - P_A$$

and the probability of scrap,

$$P_{Sr} = 1 - F(\boldsymbol{U}, \boldsymbol{\mu}, \boldsymbol{\Sigma}). \tag{3.21}$$

The mechanics of Equation 3.20 are illustrated in Figure 3.8 for a two feature example with features X_1 and X_2. Let $\boldsymbol{L} = [L_1, L_2]$ and $\boldsymbol{U} = [U_1, U_2]$ be the lower and upper specification limits respectively. The means and covariance matrix are $\boldsymbol{\mu} = [\mu_1, \mu_2]$ and $\boldsymbol{\Sigma} = [\sigma_1^2, \rho\sigma_1\sigma_2; \rho\sigma_1\sigma_2, \sigma_2^2]$. Thus, the probability of conformance is,

$$\begin{aligned} p_{1,C} &= (-1)^2 F(U_1, U_2) \\ &+ (-1)^1 F(L_1, U_2) \\ &+ (-1)^1 F(U_1, L_2) \\ &+ (-1)^0 F(L_1, L_2). \end{aligned} \tag{3.22}$$

The first line of Equation 3.22 refers to calculating the probability enclosed within the blue rectangle, shown in Figure 3.8(a). The second line of Equation 3.22 refers to calculating the probability enclosed by the magenta rectangle in Figure 3.8(b) and likewise for the remaining lines and figures. It follows that $p_{\mathrm{I},2} = F(L_1, U_2) - F(L_1, L_2)$, $p_{\mathrm{I},3} = F(U_1, L_2) - F(L_1, L_2)$, $p_{\mathrm{I},4} = F(L_1, L_2)$ and $p_{\mathrm{I},S} = 1 - F(U_1, U_2)$. The number of CDF evaluations increase by 2^n using this method. Therefore, only four CDF evaluations are required in this two-dimensional case, as opposed to eight using Equation 3.18.

The profit equation for two features follows the same principles as the one feature profit equation given in Equation 3.4, albeit the rework and scrap terms are more complex. The flow of components through a dual feature manufacturing system and the probabilities of components occupying each state for four iterations are illustrated by Figure 3.9. Theorem 3.1 demonstrated there was only one optimal mean to maximise profit for the production of one feature. However, Assumption 3 is not upheld in the case of manufacturing dual features. This is because there are three varieties of rework, where only dual feature rework (state 4), is equivalent to the initial manufacturing operation (State I). The single feature rework states, (2) and (3), are each equivalent to the example presented in Theorem 1, but the dual feature rework state (4) is clearly different as two

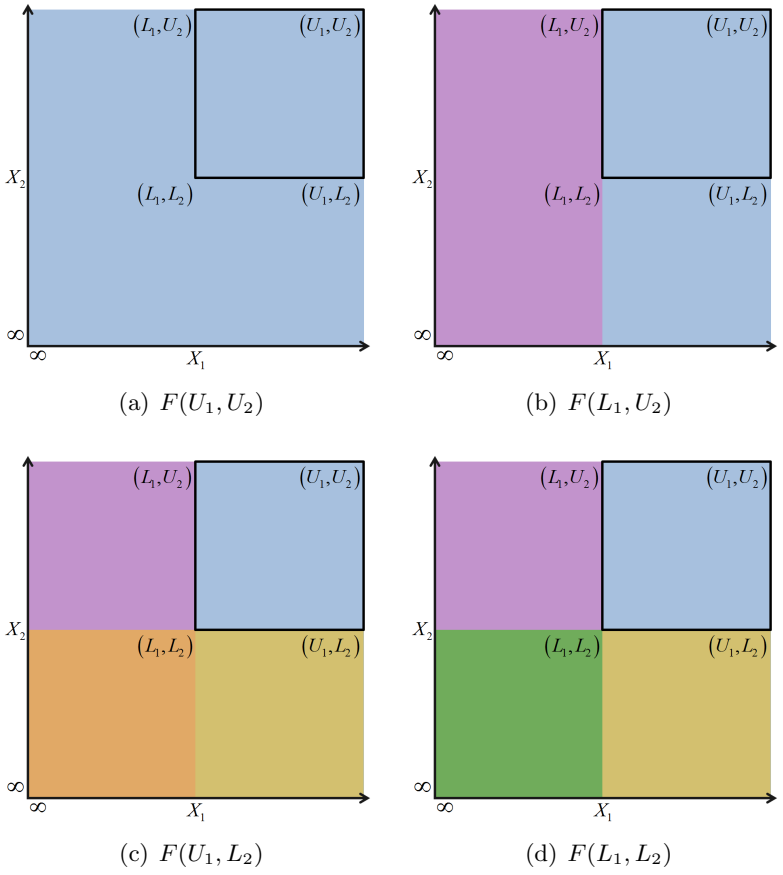

(a) $F(U_1, U_2)$ (b) $F(L_1, U_2)$

(c) $F(U_1, L_2)$ (d) $F(L_1, L_2)$

FIGURE 3.8: Evaluation of 2D rectangular probability

features are involved. By considering the flow of features through the manufacturing process in Figure 3.9, it becomes clear the means for dual feature rework are different to the means for single feature rework, even though the features are the same. The first iteration (Figure 3.9) (superscript I), produces conformance, scrap and three varieties of rework, represented by the blue, red and green regions in Figure 3.7. For the second iteration (II), the probability term for the X_1 rework state (2) is represented by the R_{X_1} rectangle in Figure 3.7. Similarly the probability term for X_2 rework state (3) is represented by the R_{X_2} rectangle in Figure 3.7. The first probability value for the dual feature rework stage (4) is given by the R_{X_1,X_2} rectangle in Figure 3.7. Features processed by the single feature rework states (2) and (3) may require additional rework even after processing. Thus, iteration III and IV for states (2) and (3) contain functions of $\mu_{2,1}$, $\mu_{2,2}$ and σ, corresponding to processing a feature independently of the other feature (i.e. only one feature required rework). Additionally, one or other of the features reworked by the dual feature rework stage (4) may require single feature rework even after dual feature processing. Therefore, iteration III and IV for states (2) and (3) also contain functions of $\boldsymbol{\mu}$ and $\boldsymbol{\Sigma}$ corresponding to features manufactured in parallel (dual feature rework). It may also take several rework iterations to convert dual feature

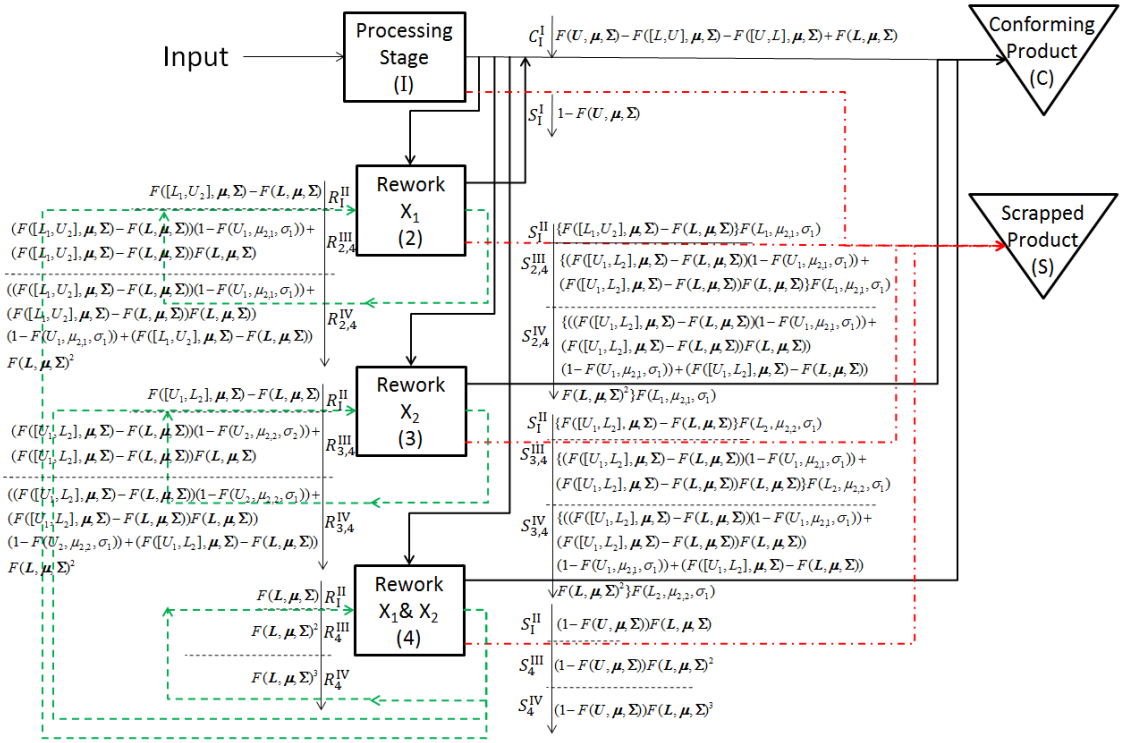

FIGURE 3.9: Probabilities of components in the scrap and rework states for four iterations

rework to scrap or conformance, hence the squared and cubic powers for iterations III and IV in state (4). The scrap terms for each iteration are the products between the relevant rework terms and the probability of scrap for that rework state, $F(L_1, \mu_{2,1}, \sigma_1)$, $F(L_2, \mu_{2,2}, \sigma_2)$ and $F(\boldsymbol{L}, \boldsymbol{\mu}_1, \boldsymbol{\Sigma})$ for state (2), (3) and (4) respectively. The scrap and rework terms for each rework state for n iterations, which are required to express the

expected profit for a dual feature manufacturing system are given by,

$$\begin{aligned} RwP_2 &= F([U_1, L_2], \boldsymbol{\mu}, \boldsymbol{\Sigma}) - F(\boldsymbol{L}, \boldsymbol{\mu}, \boldsymbol{\Sigma}) \\ &+ \sum_{i=2}^{\infty} RwP_{2_{i-1}} \left[1 - F(U_1, \mu_{2,1}, \sigma_1)\right] + F(\boldsymbol{L}, \boldsymbol{\mu}, \boldsymbol{\Sigma})^{i-1} \\ &\left[F([U_1, L_2], \boldsymbol{\mu}, \boldsymbol{\Sigma}) - F(\boldsymbol{L}, \boldsymbol{\mu}, \boldsymbol{\Sigma})\right], \\ \\ RwP_3 &= F([L_1, U_2], \boldsymbol{\mu}, \boldsymbol{\Sigma}) - F(\boldsymbol{L}, \boldsymbol{\mu}, \boldsymbol{\Sigma}) \\ &+ \sum_{i=2}^{\infty} RwP_{3_{i-1}} \left[1 - F(U_2, \mu_{2,2}, \sigma_2)\right] + F(\boldsymbol{L}, \boldsymbol{\mu}, \boldsymbol{\Sigma})^{i-1} \\ &\left[F([L_1, U_2], \boldsymbol{\mu}, \boldsymbol{\Sigma}) - F(\boldsymbol{L}, \boldsymbol{\mu}_1, \boldsymbol{\Sigma})\right], \\ \\ RwP_4 &= \sum_{i=2}^{\infty} F(\boldsymbol{L}, \boldsymbol{\mu}, \boldsymbol{\Sigma}) F(\boldsymbol{L}, \boldsymbol{\mu}, \boldsymbol{\Sigma})^{i-1}. \end{aligned} \tag{3.23}$$

The scrap probabilities generated from the three rework states are given by Equation 3.24,

$$\begin{aligned} SrP_2 &= \{F([L_1, U_2], \boldsymbol{\mu}, \boldsymbol{\Sigma}) - F(\boldsymbol{L}, \boldsymbol{\mu}, \boldsymbol{\Sigma}) \\ &+ \sum_{i=2}^{\infty} SrP_{2_{i-1}} \left[1 - F(U_1, \mu_{2,1}, \sigma_1)\right] + F(\boldsymbol{L}, \boldsymbol{\mu}, \boldsymbol{\Sigma})^{i-1} \\ &\left[F([L_1, U_2], \boldsymbol{\mu}, \boldsymbol{\Sigma}) - F(\boldsymbol{L}, \boldsymbol{\mu}, \boldsymbol{\Sigma})\right]\} F(L_1, \mu_{2,1}, \sigma_1) \\ \\ SrP_3 &= \{F([U_1, L_2], \boldsymbol{\mu}, \boldsymbol{\Sigma}) - F(\boldsymbol{L}, \boldsymbol{\mu}, \boldsymbol{\Sigma}) \\ &+ \sum_{i=2}^{\infty} SrP_{3_{i-1}} \left[1 - F(U_2, \mu_{2,2}, \sigma_2)\right] + F(\boldsymbol{L}, \boldsymbol{\mu}, \boldsymbol{\Sigma})^{i-1} \\ &\left[F([U_1, L_2], \boldsymbol{\mu}, \boldsymbol{\Sigma}) - F(\boldsymbol{L}, \boldsymbol{\mu}, \boldsymbol{\Sigma})\right]\} F(L_2, \mu_{2,2}, \sigma_2), \\ \\ SrP_4 &= SC_4 \sum_{i=1}^{\infty} \left(1 - F(\boldsymbol{U}, \boldsymbol{\mu}, \boldsymbol{\Sigma})\right) F(\boldsymbol{L}, \boldsymbol{\mu}, \boldsymbol{\Sigma})^i. \end{aligned} \tag{3.24}$$

To condense the notation let $TSrP = SrP_2 + SrP_3 + SrP_4$. Also the initial scrap can be written,

$$SrP_{\text{I}} = 1 - F(\boldsymbol{U}, \boldsymbol{\mu}, \boldsymbol{\Sigma}), \tag{3.25}$$

The total profit for this two feature example can be written as,

$$\begin{aligned} TP_2 = SP[1 - SrP_{\text{I}}(\boldsymbol{\mu}) - (TSrP(\boldsymbol{\mu}, \mu_{2,1}, \mu_{2,2})] \\ - [Rc_2\, RwP_2(\boldsymbol{\mu}, \mu_{2,1}) + Rc_3\, RwP_3(\boldsymbol{\mu}, \mu_{2,2}) \\ + Rc_4\, RwP_4(\boldsymbol{\mu}) + ScP_2SrP_2(\boldsymbol{\mu}, \mu_{2,1}) \\ + Sc_3SrP_3(\boldsymbol{\mu}, \mu_{2,2}) + Sc_4SrP_4(\boldsymbol{\mu})] - PC. \end{aligned} \tag{3.26}$$

The single feature rework and scrap probabilities (RwP_2, RwP_3, SrP_2 and SrP_2) are functions of four means, $\boldsymbol{\mu} = [\mu_{1,1}, \mu_{1,2}]$ for dual feature rework, and $\mu_{2,1}$ and $\mu_{2,2}$ for the two single feature reworks. The initial scrap probability (SrP_{I}) and dual feature rework state (4) are functions of two means $\boldsymbol{\mu} = [\mu_{1,1}, \mu_{1,2}]$. Although $\mu_{1,1}$ and $\mu_{2,1}$ both apply to the feature X_1, the first mean only applies when the second feature is also processed along with the first feature, prior to inspection. The second mean ($\mu_{2,1}$), only applies when the first feature is processed and inspected independently from the second feature. This similarly applies to the X_2 feature means. The distinction between the dual and single feature means can be graphically illustrated by considering Figure 3.10, which shows the scatter of 2000 points drawn randomly from a joint normal distribution. The mean of the scattered points lies in the centre of the conformance region but due to the geometry of the scrap and rework regions, a greater proportion of these points lie in the scrap region since the scrap region is larger by $2\text{L}_1\text{L}_2$ (difference between the scrap and rework areas). To ensure equal scrap and rework probabilities for the illustration in Figure 3.10, $\mu_{x_1} = \mu_{x_2} = 5.0617$. For a single feature (Figure 3.4) there are equal probabilities of scrap and rework with the mean centred, $\mu = 5$. To further complicate the balance between scrap and rework cost, the various rework regions (Figure 3.10) may have different costs associated with them and the cost of dual feature rework is likely to be the sum of the single feature rework costs. Therefore, to maximise Equation 3.26, which has a mixture of dual feature and single feature rework, a total of four means must be adjusted such that,

$$\hat{\boldsymbol{\mu}}_{\text{opt}} = \max_{\hat{\boldsymbol{\mu}} \in \mathbb{R}} \left\{ TP_2(\mu_{1,1}, \mu_{1,2}, \mu_{2,1}, \mu_{2,2}) \right\}. \tag{3.27}$$

The vector, $\hat{\boldsymbol{\mu}}_{\text{opt}}$, is the four element vector containing the optimal means for the dual features as well as the single features. Note that the dual feature scrap and rework equation (RwP_4 and SrP_4) only involve dual feature probabilities and thus only the first two means of $\hat{\boldsymbol{\mu}}_{\text{opt}}$ apply to these states. Clearly the exact values of the optimal

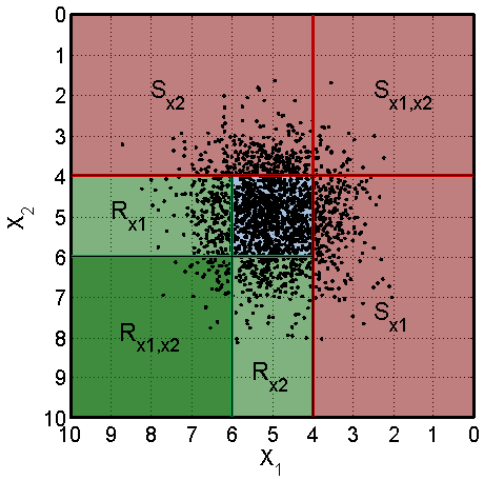

FIGURE 3.10: Scatter plot

means depends on the relative scrap and rework costs associated with the probabilities.

3.2 Markovian Modelling

The transitions of features and the associated components from one state to another can be modelled using Markov chains. Bowling et al. [2004] introduced Markovian modelling to the Optimal Mean Setting problem with subsequent contributions from Khasawneh et al. [2008] for dual features and Selim and Al-Zu'bi [2011] for multiple features manufactured in series. A Markovian approach allows the iterative expressions for conformance, rework, scrap and ultimately expected profit (derived in Sections 3.1.1 and 3.1.2), to be simplified. Markovian modelling also allows a generalised expression for expected profit to be derived, accounting for any number of features in any combination of serial and parallel operations. Such a generalised expression has not been derived in the literature.

This section introduces Markovian modelling to the problem of determining the expected profit for manufactured features. This thesis makes no contribution to the field of Markovian modelling but does to the application of Markovian modelling to Optimal Mean Setting, specifically the contributions and objectives of this Section are:

1. Following existing literature, develop a Markovain model for the expected profit from a single feature.

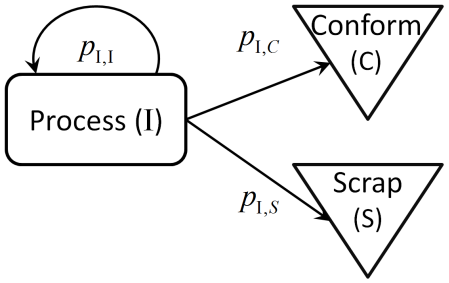

FIGURE 3.11: Random walk for the production of a single feature

2. Following existing literature, expand the single feature model to the production of two features in series with reference to Bowling et al. [2004] and the corrections made by Selim and Al-Zu'bi [2011].

3. Develop a new Markovian model for two features produced in parallel (dual features), correcting the errors made by Khasawneh et al. [2008]. A numerical comparison between the re-formulated method and Khasawneh et al. [2008] methods is made.

4. Generalise the new Markovian model to enable expected profit co be calculated for any number of features in any combination of parallel and serial manufacturing sequences or a combination of both. This new expression is then applied to a numerical example in Section 3.4.

3.2.1 Markov Modelling of Serial Production Systems

3.2.1.1 Single Feature - Serial Production

A serial production system strictly involves the manufacture of a single inspectable feature prior to an inspection process. A component may comprise of several inspectable features, which are created sequentially in a serial production system with an inspection process at each stage. At each stage there are three possible states; conforming, scrap and rework, which can be thought of as states of a random walk. The conforming and scrap states are absorbing, such that if a component enters one of these states it cannot move to another state. Rework is a transient state, since a component in a rework state may move to a conforming, scrap or another rework state. Figure 3.1 illustrates the manufacturing flow for a single feature, which can be depicted as a group of transient and absorbing states shown in Figure 3.11. The arrows indicate the possible flow of components from the input to the various states, conforming (C), Scrap (S) and rework back into the initial state (I). The p values give the probability of transferring between these states. All components entering at the input eventually end up in the scrap or

conforming states. Once in an absorbing state it is impossible to leave it. The presence of these absorbing states and the fact it is possible to enter the absorbing states from the other state in a finite number of steps, make this an absorbing Markov chain. The average time components spend being reworked and the final conformance and scrap probabilities can be extracted from the fundamental matrix, ($\boldsymbol{M}$) and the long-run absorption matrix, ($\boldsymbol{F}$). The construction of these matrices is outlined by Bowling et al. [2004], but elaborated here, drawing detail from Grinstead and Snell [2006].

The probabilities or going from one state to another (short term probabilities) in Figure 3.11 can be represented by the transition matrix $\boldsymbol{P}$, given by,

$$\boldsymbol{P} = \begin{array}{c} \\ \mathrm{I} \\ C \\ S \end{array} \begin{array}{c} \begin{array}{ccc} \mathrm{I} & C & S \end{array} \\ \begin{bmatrix} p_{\mathrm{I,I}} & p_{\mathrm{I},C} & p_{\mathrm{I},S} \\ 0 & 1 & 0 \\ 0 & 0 & 1 \end{bmatrix} \end{array}, \tag{3.28}$$

where the values $p_{\mathrm{I,I}}$, $p_{\mathrm{I},C}$ and $p_{\mathrm{I},S}$ are the probability of rework, conformance and scrap respectively. These correspond to the areas noted in Figure 3.4. These probabilities are given by,

$$\begin{aligned} p_{\mathrm{I,I}} &= \int_{L}^{\infty} \frac{1}{\sqrt{2\pi\sigma^2}} e^{\frac{-(x-\mu)^2}{2\sigma^2}} \, \mathrm{d}x \\ p_{\mathrm{I},C} &= \int_{L}^{U} \frac{1}{\sqrt{2\pi\sigma^2}} e^{\frac{-(x-\mu)^2}{2\sigma^2}} \, \mathrm{d}x \\ p_{\mathrm{I},S} &= \int_{-\infty}^{L} \frac{1}{\sqrt{2\pi\sigma^2}} e^{\frac{-(x-\mu)^2}{2\sigma^2}} \, \mathrm{d}x \end{aligned} \tag{3.29}$$

These expressions correspond to the terms from the first iteration for the rework, conforming and scrap states on Figure 3.3. As already stated, an absorbing Markov chain must have at least one state, i, that is absorbing such that $\boldsymbol{P}(i,i) = 1$. Consequently $\boldsymbol{P}(i,j) = 0, \ \forall\, j \neq i$ since each row of the transition matrix $\boldsymbol{P}$ must sum to 1. States C and S in Equation 3.31 satisfy this property. The transition matrix can be written in canonical form,

$$\begin{array}{c} \\ \mathrm{TRS} \\ \mathrm{ABS} \end{array} \begin{array}{c} \begin{array}{cc} \mathrm{TRS} & \mathrm{ABS} \end{array} \\ \left[\begin{array}{c|c} \boldsymbol{Q} & \boldsymbol{R} \\ \hline 0 & \boldsymbol{I} \end{array}\right] \end{array}. \tag{3.30}$$

The sub-matrix $\boldsymbol{Q}$ is a t-by-t matrix giving the probabilities of going from a transient to another/same transient state, where t is the number of transient states. The sub-matrix $\boldsymbol{R}$ is a t-by-r matrix giving the probabilities of going from a transient to absorbing state. The value r is the number of absorbing states. The 0 sub-matrix is a r-by-t zero matrix and $\boldsymbol{I}$ is a r-by-r identity matrix. Iterated multiplication of the $\boldsymbol{P}$ matrix gives the

probabilities of items transferring to other states for each iteration. For the first, second and third iterations $\boldsymbol{P}$ is:

$$\boldsymbol{P}^1 = \begin{bmatrix} \boldsymbol{Q} & \boldsymbol{R} \\ 0 & \boldsymbol{I} \end{bmatrix},$$

$$\boldsymbol{P}^2 = \begin{bmatrix} \boldsymbol{Q} & \boldsymbol{R} \\ 0 & \boldsymbol{I} \end{bmatrix} \begin{bmatrix} \boldsymbol{Q} & \boldsymbol{R} \\ 0 & \boldsymbol{I} \end{bmatrix} = \begin{bmatrix} \boldsymbol{Q}^2 & \boldsymbol{R}+\boldsymbol{Q}\boldsymbol{I} \\ 0 & \boldsymbol{I} \end{bmatrix},$$

$$\boldsymbol{P}^3 = \begin{bmatrix} \boldsymbol{Q}^2 & \boldsymbol{R}+\boldsymbol{Q}\boldsymbol{I} \\ 0 & \boldsymbol{I} \end{bmatrix} \begin{bmatrix} \boldsymbol{Q} & \boldsymbol{R} \\ 0 & \boldsymbol{I} \end{bmatrix} = \begin{bmatrix} \boldsymbol{Q}^3 & \boldsymbol{R}+\boldsymbol{Q}\boldsymbol{R}+\boldsymbol{Q}^2\boldsymbol{R} \\ 0 & \boldsymbol{I} \end{bmatrix}.$$

Let n be the number of iterations required such that all the components end up in either the scrap of conforming states [4]. Thus, by induction $\boldsymbol{P}^n$ is[5],

$$\boldsymbol{P}^n = \begin{bmatrix} \boldsymbol{Q}^n & (I+\boldsymbol{Q}+\boldsymbol{Q}^2+\cdots+\boldsymbol{Q}^{n-1})\boldsymbol{R} \\ 0 & \boldsymbol{I} \end{bmatrix}.$$

In the limit[6] as $n \to \infty$, the term $\boldsymbol{Q}^n \to 0$. Let M be the infinite sequence,

$$\boldsymbol{M} = I+\boldsymbol{Q}+\boldsymbol{Q}^2+\cdots+\boldsymbol{Q}^{\infty} = \frac{1}{I-\boldsymbol{Q}}.$$

Thus, in the limit as $n \to \infty$, the $\boldsymbol{P}$-matrix becomes,

$$\boldsymbol{P}^{\infty} = \begin{bmatrix} 0 & \boldsymbol{M}\boldsymbol{R} \\ 0 & \boldsymbol{I} \end{bmatrix}.$$

The matrix $\boldsymbol{M}$ in known as the fundamental matrix and gives the expected number of times item spend in a transient state j, given they started in a transient state i. In the context of Figure 3.11, this is the average number of times items are in the rework state. The long term absorption probabilities are calculated from the product of the $\boldsymbol{R}$-matrix (probabilities of going from a transient to an absorbing state) and the $\boldsymbol{M}$-matrix,

$$\boldsymbol{F} = \boldsymbol{M}\boldsymbol{R}.$$

The $\boldsymbol{F}$-matrix gives the long run absorption probability of items ending up in state j after starting in state i. The $\boldsymbol{M}$ and $\boldsymbol{F}$ matrices are used to attribute the cost of rework and scrap as well as determine the total number of conforming items that may be sold. For the manufacturing sequence in Figure 3.11, given the transition matrix in Equation

[4] The $\boldsymbol{Q}\boldsymbol{R}$ terms are always the same size as the $\boldsymbol{R}$-matrix (t-by-r), hence matrix addition is valid.

[5] Note a second identity matrix (I) appears when the like terms of $\boldsymbol{R}$ are collected outside the brackets for the (1,2)44 entry of $\boldsymbol{P}^n$. This identity matrix (I) is the same size as $\boldsymbol{Q}\boldsymbol{R}$ rather than the $\boldsymbol{I}$-matrix which has size r-by-r.

[6] Since the rows of $\boldsymbol{Q}$ are strictly less than one. The largest eigenvalue of $\boldsymbol{Q}$ is less than one, thus $\boldsymbol{Q}^n \to 0$ as $n \to \infty$

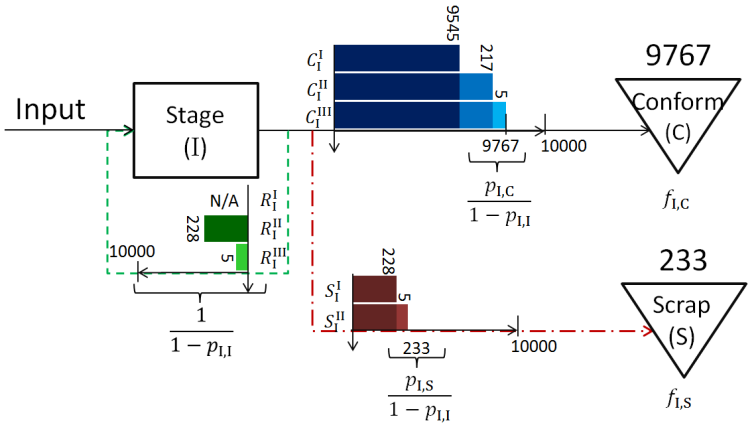

FIGURE 3.12: The flow of 10,000 components with one inspectable feature through a single stage serial production system

3.28, the average time the feature is reworked and the final probabilities of conformance and scrap are,

$$\boldsymbol{M} = (\boldsymbol{I} - \boldsymbol{Q})^{-1} = \begin{matrix} \\ \text{I} \end{matrix} \begin{matrix} \text{I} \\ \left[\; m_{\text{I,I}} \; \right] \end{matrix} = \frac{1}{1 - p_{\text{I,I}}}$$

and

$$\boldsymbol{F} = \boldsymbol{M} \times \boldsymbol{R} = \begin{matrix} \\ \text{I} \end{matrix} \begin{matrix} C & S \\ \left[\; \dfrac{p_{\text{I},C}}{1 - p_{\text{I,I}}} & \dfrac{p_{\text{I},S}}{1 - p_{\text{I,I}}} \; \right] \end{matrix}.$$

The mechanism that generates the values determined by the $\boldsymbol{M}$ and $\boldsymbol{F}$ matrices can be illustrated using a numerical example, shown in Figure 3.12. The figure describes the flow of 10,000 components, with one inspectable feature, through a single stage serial production system. The process means, variances and lower and upper specification limits were arbitrarily chosen as $\mu = 5$, $\sigma = 1$, $L = 3$ and $U = 7$ respectively. The numbers of components in each state are illustrated by the length of the bars (Figure 3.12). The initial manufacturing operation produced 228 scrap and rework items while 9545 conformed. Of the 228 rework items, five were scrapped after the second iteration and the remaining 223 conformed after two rework iterations. The average time the items spent being reworked is the sum of the probabilities of items entering the rework state, which is given by the geometric series,

$$p_{\text{I,I}} + p_{\text{I,I}}^2 + p_{\text{I,I}}^3 + \ldots \sum_{r=1}^{\infty} p_{\text{I,I}}^r = \frac{1}{1 - p_{\text{I,I}}} \Leftrightarrow |p_{\text{I,I}}| < 1.$$

This is the same value given by the $\boldsymbol{M}$-matrix which corresponds to items spending an average 1.0233 times being processed by Stage I (this can be verified from the numerical values given in Figure 3.12). Similar sequences exist for the final conformance

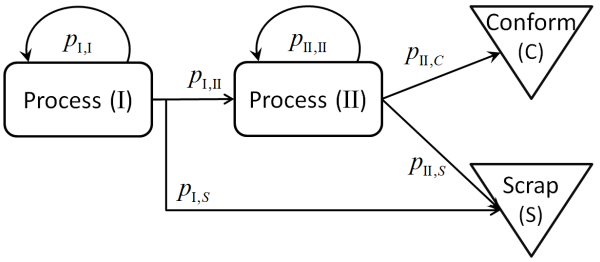

FIGURE 3.13: Random walk for the production of a two features in a serial production system

probability,

$$p_{\mathrm{I,C}} + p_{\mathrm{I,C}}\, p_{\mathrm{I,I}} + p_{\mathrm{I,C}}\, p_{\mathrm{I,I}}^2 + \ldots \sum_{r=0}^{\infty} p_{\mathrm{I,C}}\, p_{\mathrm{I,I}}^r = \frac{p_{\mathrm{I,C}}}{1 - p_{\mathrm{I,I}}} \Leftrightarrow |p_{\mathrm{I,I}}| < 1,$$

and the final scrap probability,

$$p_{\mathrm{I,S}} + p_{\mathrm{I,S}}\, p_{\mathrm{I,I}} + p_{\mathrm{I,S}}\, p_{\mathrm{I,I}}^2 + \ldots \sum_{r=0}^{\infty} p_{\mathrm{I,S}}\, p_{\mathrm{I,I}}^r = \frac{p_{\mathrm{I,S}}}{1 - p_{\mathrm{I,I}}} \Leftrightarrow |p_{\mathrm{I,I}}| < 1,$$

where both expressions are given by the $\boldsymbol{F}$-matrix. Markovian modelling allows these expressions to be determined without having to generate them from first principles, which would get overwhelmingly complex for a larger numbers of features. The same expressions can be found by generalising the iterations shown in Figure 3.3 providing the mean μ is kept constant for each iteration, in accordance with Theorem 3.1. The expected profit for this one feature, serial manufacturing example is given by,

$$E(PR) = SP\, f_{\mathrm{I},C} - PC - SC\, f_{\mathrm{I},3} - RC(m_{\mathrm{I,I}} - 1),$$

where RC, SC and PC are the rework, scrap and processing cost rates. The elements, $f_{\mathrm{I},j}$ and $m_{\mathrm{I},j}$ are the elements of the $\boldsymbol{M}$ and $\boldsymbol{F}$ matrices.

3.2.1.2 Two Features - Serial Production

The errors made by Bowling et al. [2004] (corrected by Selim and Al-Zu'bi [2011]) for the production of two features in series are explained in this Section.

Figure 3.13 shows the flow of components and the transition probabilities of items transferring between states for a two stage serial production system. The transition matrix

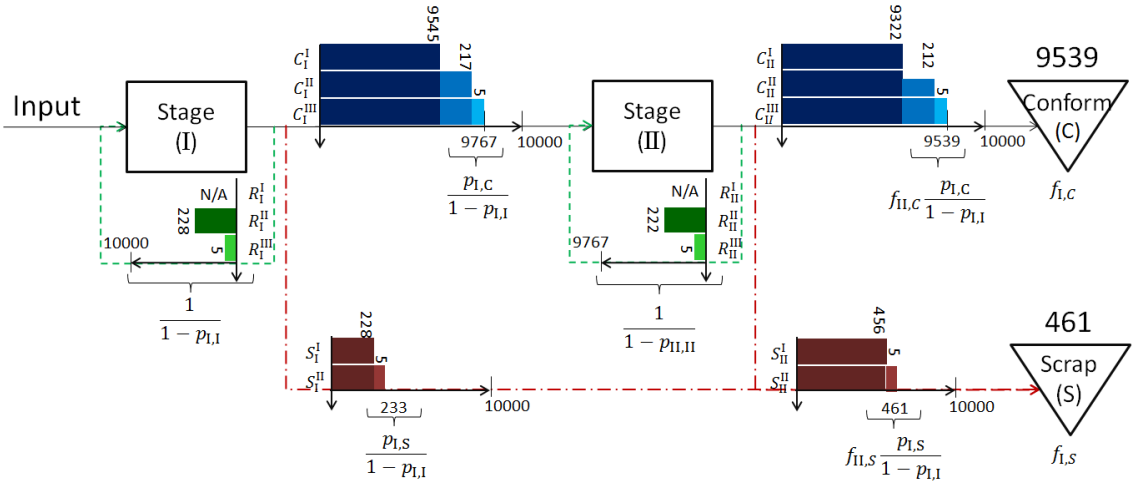

FIGURE 3.14: The flow of 10,000 components with two inspectable features through a two stage serial production system

is given by,

$$\boldsymbol{P} = \begin{array}{c} \\ \mathrm{I} \\ \mathrm{II} \\ C \\ S \end{array} \begin{array}{c} \begin{array}{cccc} \mathrm{I} & \mathrm{II} & C & S \end{array} \\ \begin{bmatrix} p_{\mathrm{I,I}} & p_{\mathrm{I,II}} & 0 & p_{\mathrm{I},S} \\ 0 & p_{\mathrm{II,II}} & p_{\mathrm{II,C}} & p_{\mathrm{II,S}} \\ 0 & 0 & 1 & 0 \\ 0 & 0 & 0 & 1 \end{bmatrix} \end{array}. \tag{3.31}$$

Following the analysis outlined for a single feature in Section 3.2.1.1 the $\boldsymbol{M}$ and $\boldsymbol{F}$ matrices are,

$$\boldsymbol{M} = \begin{array}{c} \\ \mathrm{I} \\ \mathrm{II} \end{array} \begin{array}{c} \begin{array}{cc} \mathrm{I} & \mathrm{II} \end{array} \\ \begin{bmatrix} \dfrac{1}{1-p_{\mathrm{I,I}}} & \dfrac{p_{\mathrm{I,C}}}{(1-p_{\mathrm{I,I}})(1-p_{\mathrm{II,II}})} \\ 0 & \dfrac{1}{1-p_{\mathrm{II,II}}} \end{bmatrix} \end{array} \tag{3.32}$$

and

$$\boldsymbol{F} = \begin{array}{c} \\ \mathrm{I} \\ \mathrm{II} \end{array} \begin{array}{c} \begin{array}{cc} \mathrm{C} & \mathrm{S} \end{array} \\ \begin{bmatrix} \dfrac{p_{\mathrm{I,II}}\,p_{\mathrm{II,C}}}{(1-p_{\mathrm{I,I}})(1-p_{\mathrm{II,II}})} & \dfrac{p_{\mathrm{I,S}}}{1-p_{\mathrm{I,I}}} + \dfrac{p_{\mathrm{I,II}}\,p_{\mathrm{II,S}}}{(1-p_{\mathrm{I,I}})(1-p_{\mathrm{II,II}})} \\ \dfrac{p_{\mathrm{II,C}}}{1-p_{\mathrm{II,II}}} & \dfrac{p_{\mathrm{II,S}}}{1-p_{\mathrm{II,II}}} \end{bmatrix} \end{array}. \tag{3.33}$$

Figure 3.14 illustrates the flow of 10,000 components through a two stage serial production system where the process means and variances were chosen as $\mu_1 = \mu_2 = 5$ and $\sigma_1 = \sigma_2 = 1$. The lower and upper specification limits for each stage were chosen as $L_1 = L_2 = 3$ and $U_1 = U_2 = 7$. The quotients under the conformance and scrap bar charts (Figure 3.14) give the total numbers of scrap and conforming components

after stage I (geometric series). As can be seen from the bar charts, only three iterations were required to convert all 10,000 items into scrap or conforming items. Only the 9767 (out of 10,000) conforming items from Stage I entered Stage II. Again three iterations were required to convert these features into scrap and conforming items. The total conforming and scrapped items from Stage II can be calculated from the $\boldsymbol{F}$ matrix terms, $f_{\mathrm{II,C}}$ and $f_{\mathrm{II,S}}$. The values of these terms requires careful interpretation as they were wrongly interpreted by Bowling et al. [2004]. The $f_{\mathrm{II,C}}$ and $f_{\mathrm{II,S}}$ values give the long term probability items passed to the conforming and scrap states from Stage II, relative to the number of items that entered State II. However, $f_{\mathrm{I,C}}$ gives the long term probability that items successfully passed through both Stages I and II, the final conformance probability and not just the probability they successfully pass through Stage I. In a similar manner, the $f_{\mathrm{I,S}}$ term not only gives the probability items were scrapped after Stage I, but also the probability that items passed Stage I before being scrapped at Stage II. This clarification was originally given by Selim and Al-Zu'bi [2011]. Because the $f_{\mathrm{II,C}}$ and $f_{\mathrm{II,S}}$ terms are relative to the number of items that entered Stage II, each are multiplied by the quotient $p_{\mathrm{I,C}}/(1-p_{\mathrm{I,I}})$, determining the total input from Stage I into Stage II. The quotient from the $\boldsymbol{M}$ matrix, which gives the average time items spent in rework for Stages I and II, is also displayed in Figure 3.14.

The expected profit for the system is,

$$\begin{aligned} E(PR) = SP\, f_{\mathrm{I,C}} &- \left[PC_1 + PC_2 \quad \overbrace{\frac{p_{\mathrm{I,II}}}{1-p_{\mathrm{I,I}}}}^{\text{Confrom from I}} \right] \\ &- \left[SC_1 \underbrace{\frac{p_{\mathrm{I,S}}}{1-p_{\mathrm{I,I}}}}_{\text{Scrap from I}} + SC_2 \underbrace{\frac{p_{\mathrm{I,C}}}{1-p_{\mathrm{I,I}}}}_{\text{Conform from I}} \quad f_{\mathrm{II,S}} \right] \\ &- \left[RC_1\,(m_{\mathrm{I,I}}-1) + RC_2\,(m_{\mathrm{II,II}}-1) \quad \underbrace{\frac{p_{\mathrm{I,C}}}{1-p_{\mathrm{I,I}}}}_{\text{Conform from I}} \right]. \end{aligned} \tag{3.34}$$

This equation is different to Equations 1 and 2 from Selim and Al-Zu'bi [2011]. All three solutions are correct however, the interpretation of the second scrap cost gives rise to the difference in form. The scrap cost at Stage II in Selim and Al-Zu'bi [2011] is the summation $SC_1 + SC_2$. In Equation 3.34 of this paper, SC_2 is considered to be the cost of scrapping an item at Stage II, which may or may not include the cost

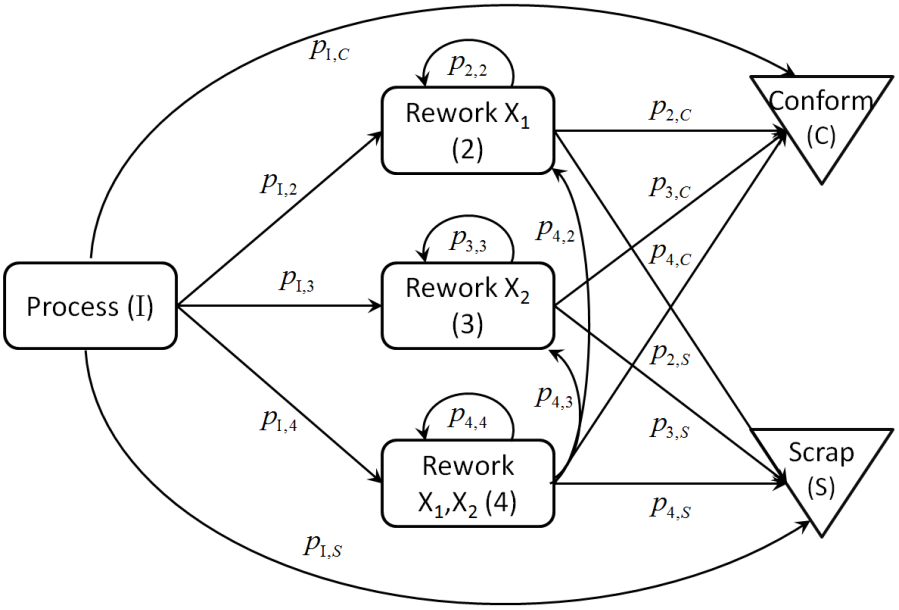

FIGURE 3.15: Random walk for the manufacture of two features in a parallel production system

of scrap at Stage I[7]. Additionally the scrap value maybe rework dependent, such that the scrap value may increase or decrease depending on the number of rework iterations. For example, an additive rework operation may increase the scrap value of an item with successive rework iterations. Provided the scrap costs are appropriately assigned Equation 3.34 agrees with the solution presented in Selim and Al-Zu'bi [2011].

3.2.2 Markovian Modelling of Parallel Production Systems

The simplest form of a parallel system is the production of two features in parallel, dual feature production. Figure 3.15 depicts the flow of items with dual features through the initial processing stage (I) to the conforming or scrap states, C, and S respectively. Items can pass directly into these absorbing states from state I, or via one of three types of rework (transient states, 2, 3 and 4) associated with a transition probability $p_{i,j}$. The three rework states correspond to rework for the X_1 feature, the X_2 feature or both X_1 and X_2 features together. The associated transition matrix is,

[7]This is a decision that must be taken depending on the processes and the value assigned to the item at various stages in the manufacturing route. The scrap value may depend on factors such as the potential use for the item in another application or the amount of material that can be redeemed.

$$\boldsymbol{P} = \begin{array}{c} \\ \mathrm{I} \\ 2 \\ 3 \\ 4 \\ C \\ S \end{array} \begin{array}{c} \begin{array}{cccccc} \mathrm{I} & 2 & 3 & 4 & C & S \end{array} \\ \begin{bmatrix} p_{\mathrm{I},\mathrm{I}} & p_{\mathrm{I},2} & p_{\mathrm{I},3} & p_{\mathrm{I},4} & p_{\mathrm{I},C} & p_{\mathrm{I},S} \\ 0 & p_{2,2} & 0 & 0 & p_{2,C} & p_{2,S} \\ 0 & 0 & p_{3,3} & 0 & p_{3,C} & p_{3,S} \\ 0 & p_{4,2} & p_{4,3} & p_{4,4} & p_{4,C} & p_{4,S} \\ 0 & 0 & 0 & 0 & 1 & 0 \\ 0 & 0 & 0 & 0 & 0 & 1 \end{bmatrix} \end{array}. \tag{3.35}$$

The $p_{i,j}$ values are given from Equation 3.20 where $i = \mathrm{I}, 2, \ldots, C, S$, $j = \mathrm{I}, 2, \ldots, C, S$ for dual feature processing (the initial state (I) and dual feature rework state (4)). The p-values for single feature rework probabilities are given by,

$$\begin{aligned} p_{2,2} &= 1 - \boldsymbol{\Phi}(\mathrm{U}_1), \\ p_{2,C} &= \boldsymbol{\Phi}(\mathrm{U}_1) - \boldsymbol{\Phi}(\mathrm{L}_1), \\ p_{2,S} &= \boldsymbol{\Phi}(\mathrm{L}_1), \\ p_{3,3} &= 1 - \boldsymbol{\Phi}(\mathrm{U}_2), \\ p_{3,C} &= \boldsymbol{\Phi}(\mathrm{U}_2) - \boldsymbol{\Phi}(\mathrm{L}_2), \\ p_{3,S} &= \boldsymbol{\Phi}(\mathrm{L}_2), \\ p_{4,i} &= p_{\mathrm{I},i} \quad \text{for} \quad i = [2, 3, \ldots, C, S]. \end{aligned} \tag{3.36}$$

Following the method outlined in Section 3.2.1.1 the $\boldsymbol{M}$ and $\boldsymbol{F}$ matrices are:

$$\boldsymbol{M} = \begin{array}{c} \\ \mathrm{I} \\ 2 \\ 3 \\ 4 \end{array} \begin{array}{c} \begin{array}{cccc} \mathrm{I} & 2 & 3 & 4 \end{array} \\ \begin{bmatrix} 1 & \dfrac{p_{\mathrm{I},2}}{(1-p_{2,2})(1-p_{4,4})} & \dfrac{p_{\mathrm{I},3}}{(1-p_{3,3})(1-p_{4,4})} & \dfrac{p_{\mathrm{I},4}}{1-p_{4,4}} \\ 0 & \dfrac{1}{1-p_{2,2}} & 0 & 0 \\ 0 & 0 & \dfrac{1}{1-p_{3,3}} & 0 \\ 0 & \dfrac{p_{4,2}}{(1-p_{2,2})(1-p_{4,4})} & \dfrac{p_{4,3}}{(1-p_{3,3})(1-p_{4,4})} & \dfrac{1}{1-p_{4,4}} \end{bmatrix} \end{array} \tag{3.37}$$

and

$$\boldsymbol{F} = \begin{array}{c} \\ \text{I} \\ 2 \\ 3 \\ 4 \end{array} \begin{array}{c} \begin{array}{cc} C & S \end{array} \\ \begin{bmatrix} f_{\text{I},C} & f_{\text{I},S} \\ \dfrac{p_{2,C}}{1-p_{2,2}} & \dfrac{p_{2,S}}{1-p_{2,2}} \\ \dfrac{p_{3,C}}{1-p_{3,3}} & \dfrac{p_{3,S}}{1-p_{3,3}} \\ f_{4,C} & f_{4,S} \end{bmatrix} \end{array} \tag{3.38}$$

where,

$$\begin{aligned} f_{\text{I},C} &= p_{\text{I},C} + \frac{p_{\text{I},2}p_{2,C}}{(1-p_{2,2})\,(1-p_{4,4})} + \frac{p_{\text{I},3}p_{3,C}}{(1-p_{3,3})\,(1-p_{4,4})} + \frac{p_{\text{I},4}p_{4,C}}{1-p_{4,4}}, \\ f_{\text{I},S} &= p_{\text{I},S} + \frac{p_{\text{I},2}p_{2,S}}{(1-p_{2,2})\,(1-p_{4,4})} + \frac{p_{\text{I},3}p_{3,S}}{(1-p_{3,3})\,(1-p_{4,4})} + \frac{p_{\text{I},4}p_{4,S}}{1-p_{4,4}}, \\ f_{4,C} &= \frac{p_{4,2}p_{2,C}}{(1-p_{2,2})(1-p_{4,4})} + \frac{p_{4,3}p_{3,5}}{(1-p_{3,3})\,(1-p_{4,4})} + \frac{p_{4,C}}{1-p_{4,4}}, \\ f_{4,S} &= \frac{p_{4,2}p_{2,S}}{(1-p_{2,2})(1-p_{4,4})} + \frac{p_{4,3}p_{3,S}}{(1-p_{3,3})\,(1-p_{4,4})} + \frac{p_{4,6}}{1-p_{4,4}}. \end{aligned} \tag{3.39}$$

Although Khasawneh et al. [2008] specified the system in this way, the meaning of the entries in the $\boldsymbol{F}$-matrix were incorrectly interpreted leading to an incorrect definition of expected profit. The columns in the $\boldsymbol{F}$-matrix correspond to the absorbing states, conforming (C) and scrap (S). The rows in the $\boldsymbol{F}$-matrix correspond to a particular transient state; the initial processing stage, or one of three rework states. The first entry in the $\boldsymbol{F}$-matrix ($f_{\text{I},C}$), is the probability items eventually conform given the number of items in the initial processing state (which is all the items). It gives the final probability of conformance and the adjacent entry $f_{\text{I},S}$ gives the final probability of scrap. Entry $f_{2,C}$ is the probability items eventually conform given the total number of items that went into the X_1-feature rework state (state 2). This won't be all the items, some will have conformed or been scrapped directly from the initial process and others will only require X_2 rework or X_1, X_2 rework. The same principles apply to state 3, and the entry in the $\boldsymbol{F}$-matrix, $f_{3,C}$. The entry, $f_{4,C}$, defines the probability of components conforming given the number of components in state 4, but irrespective of the path taken. Therefore, $f_{4,C}$ is not only the probability of items going directly from state 4 to conformance but also includes components that go from state 4 to state 2 or state 3 before finally conforming.

The expected profit for a dual feature case is defined in general terms as,

$$\begin{aligned} E(PR) &= SP\, D_{\mathrm{I,C}} - PC - (SC_1\, D_{\mathrm{I,S}} + \\ &+ SC_2\, D_{2,\mathrm{S}} + SC_3\, D_{3,\mathrm{S}} + SC_4\, D_{4,\mathrm{S}}) \\ &- (RC_1\, m_{\mathrm{I},2} + RC_1\, m_{\mathrm{I},3} + RC_1\, m_{\mathrm{I},4}), \end{aligned} \tag{3.40}$$

where SP is the selling price, PC is processing cost, SC and RC are the scrap and rework costs respectively. The subscripts refer to the costs at a given state. The D values are the final probabilities of items going directly from one state (first subscript) to the conforming or scrapped states (second subscript). The crucial difference between D and the $\boldsymbol{F}$-matrix values is that the D values only apply to the number of items in a state going **directly** to an absorbing state. For the first term in Equation 3.40, we wish to determine the income generated from the numbers of components that eventually conform. Since all the components start in state I, $D_{\mathrm{I},C} = f_{\mathrm{I},C}$. However, this pattern is not repeated for the other D probabilities. For example, $D_{2,\mathrm{S}}$ and $D_{3,\mathrm{S}}$ are the probabilities items go from states 2 and 3 to the scrap state. The equivalent $f_{2,\mathrm{S}}$ and $f_{3,\mathrm{S}}$ terms give the probabilities of items going from states 2 and 3 to the scrap state, assuming they originally started in these states. This is not the case since all components initially go through state I, and state 4 may feed states 2 and 3. To determine the total proportion of items in the various states, the feed-ins and feed-outs of each state must be known. Since the processing of rework is dynamic (it takes several iterations before all rework is converted to conforming or scrapped items), a numerical illustration is helpful to illustrate the flow of items through the system. Figure 3.16 describes the paths of 10,000 components where $\mu_1 = \mu_2 = 5$, $\sigma_1 = \sigma_2 = 1.55$ and the specification limits were set at $L_1 = L_2 = 3$ and $U_1 = U_2 = 7$. The quantities represented by each D value are explained with reference to Figure 3.16 under the bold headings below.

Explanation of the $D_{\mathrm{I},S}$ value

Multiple subscripts separated by a semicolon (Figure 3.16) indicate items have come from more than one source. For example, $C^{\mathrm{III}}_{2;3;4}$ indicates the conforming items at the third iteration where the items have come from the second, third and fourth states. Figure 3.16 shows the first iteration produced 1872 scrapped items and 6449 conforming items. Therefore, the $D_{\mathrm{I},S}$ value is the initial probability of scrap, given by $p_{\mathrm{I},S}$ which is illustrated by Figure 3.7, such that,

$$D_{\mathrm{I},S} = p_{\mathrm{I},S}.$$

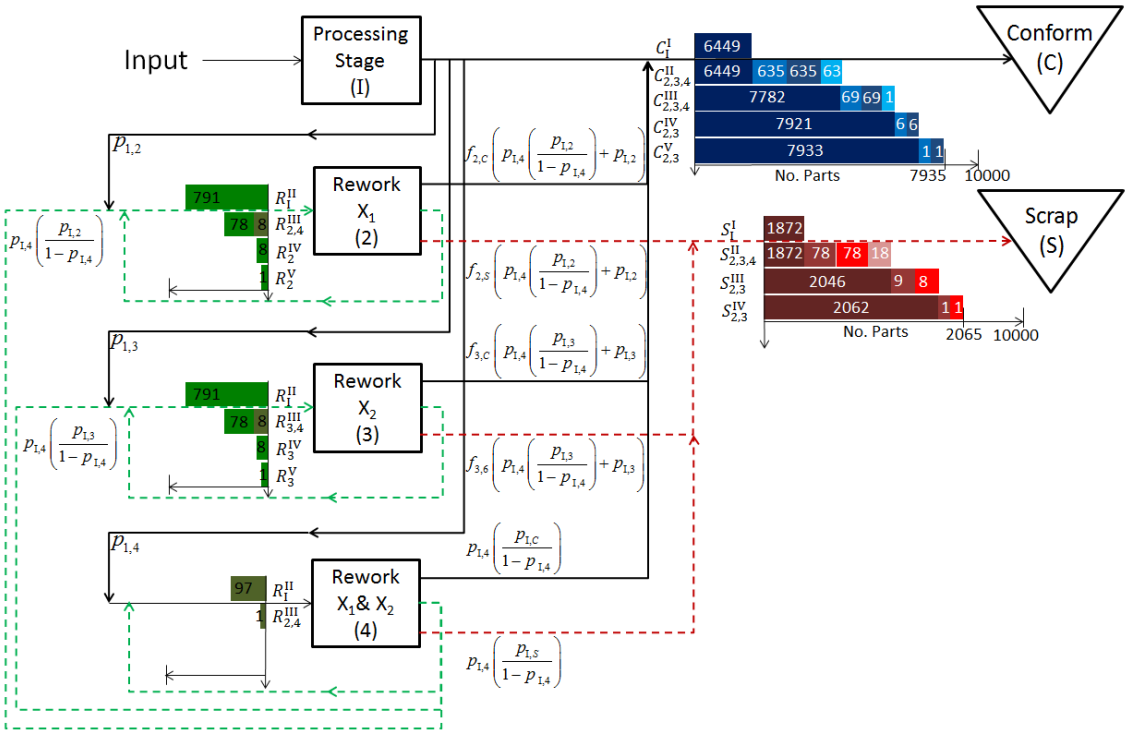

FIGURE 3.16: The flow of 10,000 components with two inspectable features through a dual stage production system

Explanation of the $D_{2,S}$ and $D_{3,S}$ values

Additionally, during the first iteration all three varieties of rework totalling 1679 rework items were produced. The probabilities of items entering the rework states (2, 3, and 4) are $p_{\mathrm{I},2}$, $p_{\mathrm{I},2}$ and $p_{\mathrm{I},4}$ (Figure 3.7). These inputs into states 2 and 3 only apply during the first iteration however, there are other inputs during the second iteration. Processing the single feature rework (states 2 and 3) during the second operation generated 78 scrap and 635 conforming items. There were also 78 items each, feeding back into states 2 and 3 from the states themselves (rework requiring further rework). The stacked bar graphs, $R^{\mathrm{II}}_{2;4}$ and $R^{\mathrm{II}}_{3;4}$ also indicate there was an additional smaller input of items from state 4. This occurred as there was the possibility that after reworking the dual features, one feature would conform but the other would require additional rework. The probability that items fed into state 2 from state 4 is given by $p_{\mathrm{I},4}\,p_{\mathrm{I},2}$. The total probability of components from state 4 feeding state 2, over all iterations, is given by,

$$p_{\mathrm{I},4}\,p_{\mathrm{I},2} + p_{\mathrm{I},4}\,p^2_{\mathrm{I},2} + p_{\mathrm{I},4}\,p^3_{\mathrm{I},2} + \cdots = \sum_{r=1}^{\infty} p_{\mathrm{I},4}\,p^r_{\mathrm{I},2},$$

where r is the iteration number[8]. This a geometric series which can be written,

$$\sum_{r=1}^{\infty} p_{\mathrm{I},4}\, p_{\mathrm{I},2}^{r} = p_{\mathrm{I},4}\, \frac{p_{\mathrm{I},2}}{1-p_{\mathrm{I},2}} \Leftrightarrow |p_{\mathrm{I},2}| < 1. \tag{3.41}$$

A similar argument exists for components feeding into state 3 from state 4. Iterations III and IV convert the remaining single feature rework components into scrap and conforming items. The final output from states 2 and 3 into the absorbing states (scrap and conformance) must account for the two inputs, one from the first iteration and another from state 4. The output into the scrap state from state 2 ($D_{2,S}$) is given by,

$$D_{2,S} = f_{2,S}\left(\frac{p_{\mathrm{I},4}p_{\mathrm{I},2}}{(1-p_{\mathrm{I},2})} + p_{\mathrm{I},2}\right). \tag{3.42}$$

Similar terms apply to state 3 and the probability of items conforming from these single feature rework states (the terms are shown in Figure 3.16 to the right of the rework stages).

Explanation of the $D_{4,S}$ value

The dual feature rework state (4) initially received items from the first iteration with probability $p_{I,4}$. There were no other feed-ins to this state. The final output from state 4 into the absorbing scrap state must subtract the feed-outs into the two transient single feature rework states (2 and 3). Recall the $\boldsymbol{F}$-matrix value, $f_{4,S}$, includes these feed-out probabilities to states 2 and 3. The output from state 4 into the scrap state follows a similar principle defined in Equation 3.41, given by,

$$D_{4,S} = p_{\mathrm{I},4}\left(\frac{p_{\mathrm{I},2}}{1-p_{\mathrm{I},4}}\right). \tag{3.43}$$

A similar equation exists to define the probability of components going straight from state 4 to conformance, as illustrated in Figure 3.16.

The interpretation of the $\boldsymbol{M}-$matrix elements by Khasawneh et al. [2008] was correct. Never-the-less, the interpretation of the elements are restated here for clarity. The entry $m_{\mathrm{I},2}$ is the number of times the second state is occupied given the first state as the starting point (hence $m_{\mathrm{I},2} < 1$). The same argument follows for $m_{\mathrm{I},3}$ and $m_{\mathrm{I},4}$. These elements are used to determine the rework cost of the three rework states. The same proportions can be found from $m_{4,2}$ and $m_{4,3}$ as the process is identical to the first state,

[8] In this discrete example, there are no further feed-outs from state 4 into states 2 and 3 after the second iteration, however in a continuous production system there is always a diminishing probability of feed-outs after r-iterations.

Stats.	Values	**Costs**	Values
$\boldsymbol{L}$	$[8, 13]$	SP	$[120]$
$\boldsymbol{U}$	$[12, 17]$	PC	$[45]$
$\boldsymbol{\sigma}$	$\sigma_{x_1} = \sigma_{x_2} = 1$	RC	$[0, 15, 12, 20]$
		SC	$[8, 9, 11, 14]$

TABLE 3.1: Specification limits, process variation and cost from the numerical example from Section 4 Khasawneh et al. [2008]

albeit with fewer components. Note, $m_{4,4}$ is the probability the fourth state is occupied, given the starting point is the fourth state, hence $m_{4,4} \geq 1$, due to rework.

The final form of the expected profit for this dual feature process is given by,

$$\begin{aligned} E(PR) &= SP\, f_{\mathrm{I},C} - PC - SC_1\, p_{\mathrm{I},S} \\ &- SC_2 \left(p_{\mathrm{I},4} \left(\frac{p_{\mathrm{I},2}}{1 - p_{\mathrm{I},4}} \right) + p_{\mathrm{I},2} \right) f_{2,S} \\ &- SC_3 \left(p_{\mathrm{I},4} \left(\frac{p_{\mathrm{I},3}}{1 - p_{\mathrm{I},4}} \right) + p_{\mathrm{I},3} \right) f_{3,S} \\ &- SC_4 \left(\frac{p_{\mathrm{I},S}}{1 - p_{\mathrm{I},4}} \right) p_{\mathrm{I},4} - RC_2\, m_{\mathrm{I},2} \\ &- RC_3\, m_{\mathrm{I},3} - RC_4\, m_{\mathrm{I},4}. \end{aligned} \tag{3.44}$$

The probability terms multiplying the four scrap costs (SC_{I} to SC_4 in Equation 3.44) are the difference between this correct expression for expected profit and Equation 5 from Khasawneh et al. [2008].

The impact of this revision on the optimal mean values and the expected profit was investigated by comparing the revision with the numerical example detailed under Section 4 from Khasawneh et al. [2008]. Table 3.1 outlines the specification limits, process variation and costs related to the numerical example. Figure 3.17 illustrates the expected profit surfaces versus the process means, μ_{X_1} and μ_{X_2}. The expected profit from Khasawneh et al. [2008] is represented by Case I and the expected profit given by Equation 3.44 is represented by Case II. The Case I expected profit was 71.1592 where the optimal mean locations were $\mu_{x_1} = 10.5514$ and $\mu_{x_2} = 15.6080$ (Figure 3.17). The Case II expected profit was 0.38% higher at 71.4287 with optimal means 0.38% and 0.27% lower at $\mu_{x_1} = 10.5115$ and $\mu_{x_2} = 15.5651$, respectively. Although the impact of the feed-in and feed-out terms is of the order 0.1%, the terms become more significant depending on the relative costs and the capability of the manufacturing processes. Figures 3.18 to 3.20 illustrate the difference between the optimal means and expected profit from Case

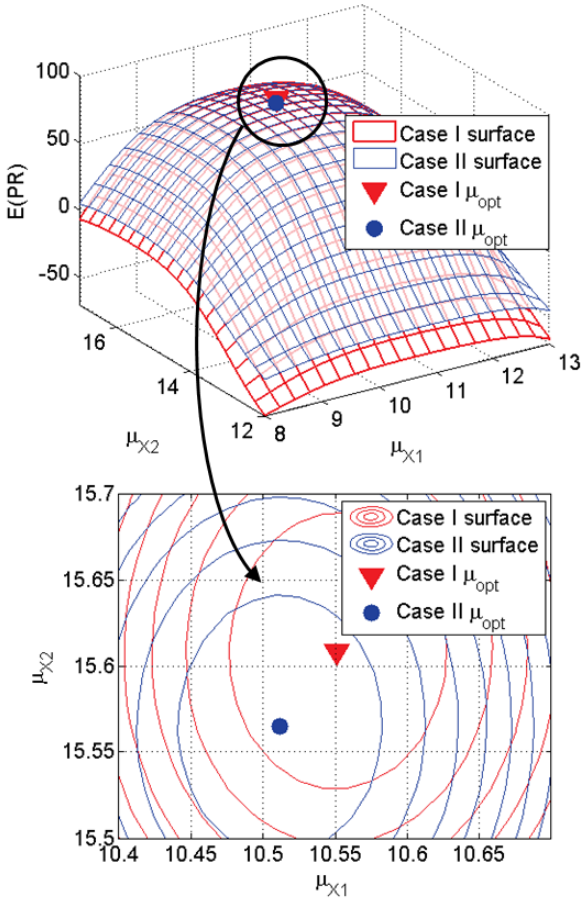

FIGURE 3.17: Comparison of profit surfaces between Khasawneh et al. [2008] and Equation 3.44

II compared to the Case I model for: (1) increased process variation (σ), (2) increased scrap cost, (3) correlation between features (ρ). The numerical example detailed in Khasawneh et al. [2008] was used as a reference set-up. The optimal means for each case were found by maximising the expected profit (using Matlab's *fmincon* function). Each point on Figures 3.18 to 3.20 was created by finding the maximum expected profit and corresponding optimal means for each case. The difference between the expected profits between Case II and Case I is defined as $\Delta E(PR) = E(PR)^{\text{II}} - E(PR)^{\text{I}}$ where the superscript defines the case. The difference between the optimal means is defined as $\Delta\tilde{\mu}_{X_1} = \tilde{\mu}^{\text{II}}_{X_1} - \tilde{\mu}^{\text{I}}_{X_1}$, where the tilde notation is used to represent the optimal mean. A similar argument applies to the X_2 feature.

The difference between the Case I and Case II expected profit increased by 4% when the process variation was doubled (Figure 3.18(a)). An accompanying change of 1% to the optimal means was also observed, illustrated by Figure 3.18(a). These changes were driven by increased rework, due to higher process variation, making the impact of the feed-in and feed-out terms more significant. Figure 3.18(b) clearly indicates that the D

terms are around an order of magnitude less than the f terms, (note the $D_{2,S}$ and $D_{3,S}$ curves are very similar). This reduced the impact of the scrap costs for Case II compared to Case I, ensuring Case II yielded a higher profit. The magnitude of $\Delta E(PR)$ and $\Delta\tilde{\mu}$ were small for $\sigma \approx 1$, since both D and f terms were small which limited the effect scrap costs had on expected profit (Equation 3.44). Therefore, the introduction of feed-in and feed-out modelling had less impact on the $\Delta E(PR)$ and $\Delta\tilde{\mu}$ when process variation was low. The same effect would be seen by adjusting upper and lower specification limits (U and L). This would also alter the rework probability and therefore the significance of the feed-in and feed-out modelling.

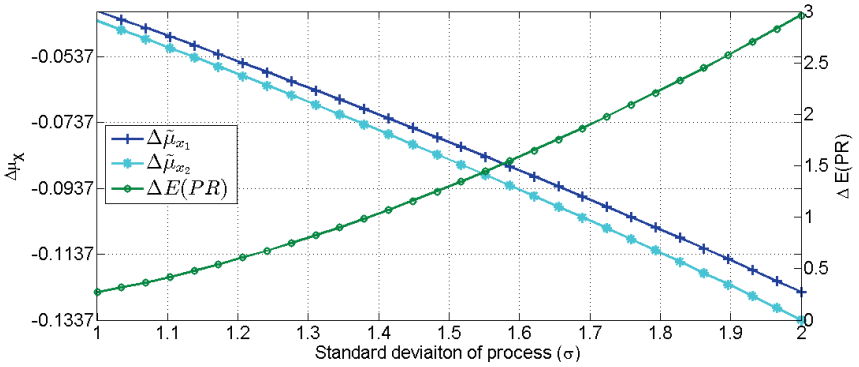

(a) Expected profit and optimal means versus process variation (σ)

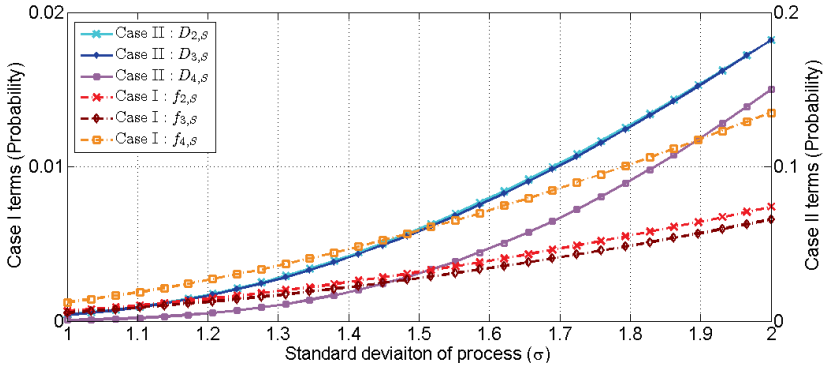

(b) Transient state to scrap state probabilities for Case I and Case II versus process variation (σ)

FIGURE 3.18: Sensitivity of Cost and feed-in and feed-out probabilities to versus process variation (σ)

The relationship between scrap cost, $\Delta E(PR)$ and $\Delta\tilde{\mu}$ was explored in Figure 3.19. A scrap cost ratio multiplied each of the scrap cost constants (SC_1 to SC_4). There was a 1.4% difference in expected profit between the two cases for a scrap cost ratio of five (Figure 3.19(a)). This was accompanied by a difference in the order of 1% between the optimal means. The values of the D and f terms in Figure 3.19(b) remained small, only changing between 0.3% to 13% compared to the changes of between $\sim$ 1200% and $\sim$ 50000% for the D and f terms in Figure 3.18(b). These small variations were due

to changes in the optimal means, which affected the rework probability and hence the values of the D and f terms. Never-the-less, the two orders of magnitude absolute difference between the D and f terms lead to differences between the Case II and Case I expected profit and optimal mean values.

Varying the other cost values, SP, PC and RC also influenced the difference between the Case II and Case I optimal means and expected profit. However, the influence is orders of magnitude less than changes to the scrap costs so the results are not shown as they are deemed insignificant[9].

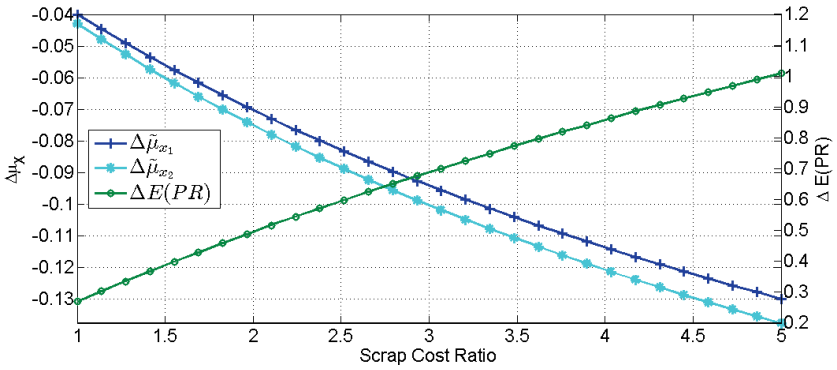

(a) Expected profit and optimal means versus scrap cost

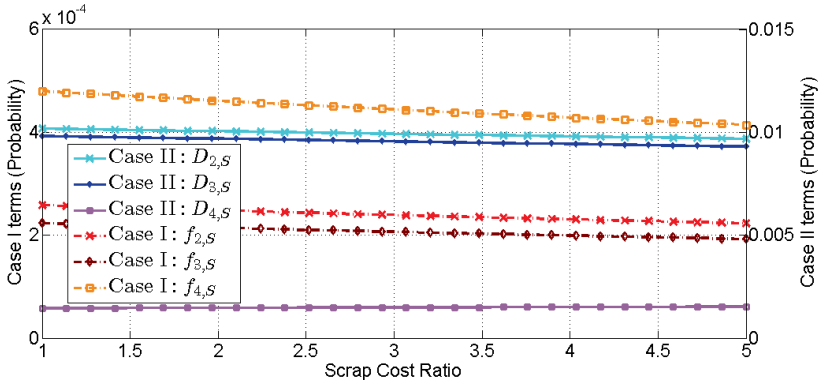

(b) Transient state to scrap state probabilities for Case I and Case II versus scrap cost

FIGURE 3.19: Sensitivity of Cost and feed-in and feed-out probabilities to versus scrap cost

Correlation between the features where, $-1 \leq \rho \leq 1$, affected $\Delta E(PR)$ between 0.24 and 0.3, decreasing with increased correlation. (Figure 3.20(a)). The values of $\Delta E(PR)$ were an order of magnitude less sensitive to variations in correlation than with variations in process standard deviation and scrap costs. The effect on $\Delta\tilde{\mu}$ was also an order of magnitude less, with the greatest values at slight negative correlation (Figure

[9]The feed-in and feed-out terms affect the total scrap cost and therefore how far the means shift towards rework. Altering the other costs will affect the cost balance and accordingly adjust the optimal means. However, the effect is not very significant as the other costs are not directly related to the feed-in and feed-out terms (Equation 3.44).

3.20(a)). Figure 3.20(b) indicates the values of the D terms are an order of magnitude less than the f terms. The values of the $D_{2,S}$ and $D_{3,S}$ terms initially rose with increased correlation before reducing to close to zero. The inverse trend occurred with the $f_{2,S}$ and $f_{3,S}$ terms. The $f_{4,S}$ and $D_{4,S}$ exhibited similar contrary behaviour. This implies the $D_{2,s}/f_{2,S}$, $D_{3,S}/f_{3,S}$ and $D_{4,S}$ terms are more significant than the $f_{2,S}$, $f_{3,S}$ and $f_{4,S}$ terms, highlighting the importance of feed-in and feed-out modelling. Although the $\Delta E(PR)$ and $\Delta\tilde{\mu}$ values were small compared to the values in Figures 3.18(a) and 3.20(a), increased process standard deviation or greater scrap cost values would lead to greater $\Delta E(PR)$ and $\Delta\tilde{\mu}$ values. The exact difference feed-in and feed-out modelling makes in Equation 3.40, compared to Equation 5 from Khasawneh et al. [2008], depends on the exact parameters of the problem.

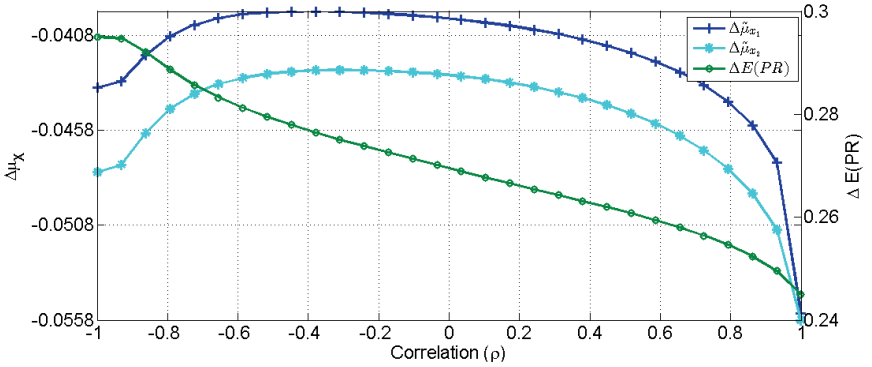

(a) Expected profit and optimal means versus correlation (ρ)

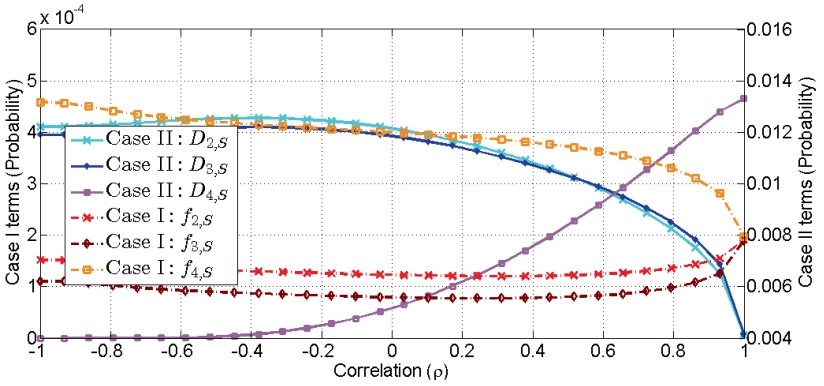

(b) Transient state to scrap state probabilities for Case I and Case II versus correlation (ρ)

FIGURE 3.20: Sensitivity of Cost and feed-in and feed-out probabilities to correlation (ρ)

In all three sensitivity analyses (Figures 3.18 to 3.20), the $\Delta E(PR)$ values remained positive while the $\Delta\tilde{\mu}$ values were negative. The maximum value of $D_{2,S}/f_{2,S}$, $D_{3,S}/f_{3,S}$ and $D_{4,S}$ is one or less, thus the D terms are smaller than the f terms. As a consequence, $E(PR)^{\mathrm{II}} - E(PR)^{\mathrm{I}} > 0$. Since the cost of scrap in Equation 3.40 is less than Equation

5 from Khasawneh et al. [2008] (given the same costs and process variances), the Case II optimal means are more scrap biased (lower) than the Case I optimal means.

It has been shown that correctly modelling the flow of components feeding in and out of rework states affects the expected profit and optimal means. The impact that these feed-in and feed-out terms have depends on the process variation, the relative costs (particularly scrap costs) and correlation. Hitherto, only feed-in and feed-out modelling for dual features have been considered. As the number of features increases, these feed-in and feed-out terms increase exponentially as $3^n - 2^n$, where n is the number of features. It quickly becomes impractical to work out which feed-ins and feed-outs apply to which state and non-trivial to determine the expected profit equation. For just four features produced in parallel, one must calculate 65 feed-in and feed-out terms and apply them to the correct rework states. The next section develops a method for defining these terms for n-features processed in parallel and applying them correctly to the correct rework state. This method allows the expected profit equation to be written directly for n-features processed in parallel.

3.2.2.1 General Solution for Parallel Production

The primary difficulty in developing a generalised solution was establishing the combinations of rework states and feed-ins, and the probability of components entering or transitioning between states. This difficulty was overcome by setting up two types of matrix. The $\boldsymbol{S}$-matrix is a binary matrix and indicates the existence of rework states and whether components could enter a particular state from another state. The $\boldsymbol{D}$-matrix has a similar form to the $\boldsymbol{S}$-matrix but determines the number of components transferring into each rework state. The combination of $\boldsymbol{S}$ and $\boldsymbol{D}$ matrices correctly defines the feed-ins to each rework state, dependent on the number of features. For example, consider the dual feature production system shown in Figure 3.15. There are two possible types of rework, single feature and dual feature, and there are separate $\boldsymbol{S}$ and $\boldsymbol{D}$ matrices for each. For single feature rework, the x_1-feature rework in state 2 can only feed into itself. This gives a '1' in the first entry in the ${}^1\boldsymbol{S}$ matrix (Equation 3.45), the second entry is zero since the second state cannot receive x_2-feature rework. Similarly the x_2-feature rework in state 3 can only feed into itself. However, the dual feature rework state (state 4) can output both x_1-feature and x_2-feature rework, hence the two '1' entries in the last row of the ${}^1\boldsymbol{S}$ matrix. For dual feature rework, the dual feature rework state (4) can only feed itself and there are no other combinations of dual

feature rework. Therefore, ${}^{2}\boldsymbol{S}$ only contains one entry, a '1'.

$$ {}^{1}\boldsymbol{S} = \begin{matrix} \\ 2 \\ 3 \\ 4 \end{matrix} \begin{matrix} \begin{matrix} x_1 & x_2 \end{matrix} \\ \begin{bmatrix} 1 & 0 \\ 0 & 1 \\ 1 & 1 \end{bmatrix} \end{matrix} \begin{matrix} \\ (x_1) \\ (x_2) \\ (x_1, x_2) \end{matrix} \quad \text{and} \quad {}^{2}\boldsymbol{S} = \begin{matrix} \\ 4 \end{matrix} \begin{matrix} x_1, x_2 \\ \begin{bmatrix} 1 \end{bmatrix} \end{matrix} \begin{matrix} \\ (x_1, x_2) \end{matrix} \tag{3.45} $$

The $\boldsymbol{D}$-matrix entries follow a standard pattern and get turned on or off by combining with the $\boldsymbol{S}$-matrix. The $\boldsymbol{D}$-matrix entries for single feature and dual feautre rework are shown in Equation 3.46. Multiplying each matrix entry from the $\boldsymbol{S}$-matrix with the corresponding entry in the $\boldsymbol{D}$-matrix gives the total probabilities of feed-ins to each rework state for all rework varieties (single or dual feature for this two feature example). Here the entries in the standard form of the $\boldsymbol{D}$-matrix are the same as the '1s' in the $\boldsymbol{S}$-matrix, however, this is not the case when there are more than two features. Therefore, the $\boldsymbol{S}$-matrix acts to filter out impossible rework transfers.

$$ {}^{1}\boldsymbol{D} = \begin{matrix} \\ 2 \\ 3 \\ 4 \end{matrix} \begin{matrix} \begin{matrix} 2 & 3 \end{matrix} \\ \begin{bmatrix} p_{\mathrm{I},2} & 0 \\ 0 & p_{\mathrm{I},3} \\ \frac{p_{\mathrm{I},4}p_{\mathrm{I},2}}{1-p_{\mathrm{I},4}} & \frac{p_{\mathrm{I},4}p_{\mathrm{I},3}}{1-p_{\mathrm{I},4}} \end{bmatrix} \end{matrix} \quad \text{and} \quad {}^{2}\boldsymbol{D} = \begin{matrix} \\ 4 \end{matrix} \begin{matrix} 4 \\ \begin{bmatrix} p_{\mathrm{I},4} \end{bmatrix} \end{matrix} . \tag{3.46} $$

The remainder of this Section shows how the $\boldsymbol{S}$ and $\boldsymbol{D}$ matrix are generalised to a standard form, such that when the number of features (n) is changed the correct matrices are generated. The generalised form is given first and then applied to a three feature problem. The final paragraph in this Section explains how the probabilities of feed-outs are determined and how the $\boldsymbol{S}$ and $\boldsymbol{D}$ matrices are combined with the selling price, scrap and rework costs.

Let $\boldsymbol{X} = [x_1, x_2, \ldots, x_N]$ be a vector of inspectable features, where N is the total number of inspectable features. The total number of processing states, including the initial processing state is given by:

$$ \eta = 1 + \sum_{k=1}^{N} \frac{N!}{k!(N-k)!} \tag{3.47} $$

where k is the number of features requiring rework at each state. Thus, a process with three inspectable features requires an initial processing state, three single feature reworks, three dual feature reworks and one triple feature rework. Let ${}^{k}\boldsymbol{C} =$

$\{^k c_{\beta+1}, ^k c_{\beta+2}, \ldots, ^k c_{\beta+m}\}$ be the set containing the k-type combinations where m determines the cardinality of the set,

$$m = \frac{N!}{k!(N-k)!}, \tag{3.48}$$

corresponding to the number of k-type combinations. The value, β, determines the starting element for each k-type set where,

$$\beta = \sum_{k=1}^{k-1} \frac{N!}{k!(N-k)!}. \tag{3.49}$$

For $k-1=0$, the β term is zero. Examining the combinations when $k=1$ a three feature process, $\boldsymbol{X} = [x_1, x_2, x_3]$, gives $^1\boldsymbol{C} = \{^1c_1, ^1c_2, ^1c_3\} = \{[x_1], [x_2], [x_3]\}$. For $k=2$ the combinations are $^2\boldsymbol{C} = \{^2c_4, ^2c_5, ^2c_6\} = \{[x_1, x_2], [x_1, x_3], [x_2, x_3]\}$ and $^3\boldsymbol{C} = \{^3c_7\} = \{[x_1, x_2, x_3]\}$ for $k=3$. All the possible combinations are given by $\boldsymbol{\Upsilon}$ where $\left\{^k\boldsymbol{C} \subset \boldsymbol{\Upsilon}\right\}_{\forall\, k \in \{1,2,\ldots,k\}}$. The set $\boldsymbol{\Upsilon}$ is monotonic in k such that the first subset of combinations, $^1\boldsymbol{C}$ always represents single feature rework(s). The second subset of combinations, $^2\boldsymbol{C}$, always contains dual feature rework and so on. In general form $\boldsymbol{\Upsilon} = \{^1\boldsymbol{C}, ^2\boldsymbol{C}, \ldots, ^k\boldsymbol{C}\}$. Thus, for three inspectable features,

$$\begin{aligned} \boldsymbol{\Upsilon} &= \{\{^1\boldsymbol{C}\}, \{^2\boldsymbol{C}\}, \{^3\boldsymbol{C}\}\} \\ &= \{\{^1c_1, ^1c_2, ^1c_3\}, \{^2c_4, ^2c_5, ^2c_6\}, \{^3c_7\}\} \\ &= \{[x_1], [x_2], [x_3], [x_1, x_2], [x_1, x_3], \ldots \\ &\quad [x_2, x_3], [x_1, x_2, x_3]\}. \end{aligned} \tag{3.50}$$

It is possible to construct a matrix whose elements determine the inputs into the various rework states. The generalised form of such a matrix $\boldsymbol{S}$ is given by Equation 3.51. To condense the subscript notation let $\delta = \beta + m$. Each column in Equation 3.51 represents a k-type combination while the rows represent each rework state.

$$^k\boldsymbol{S} = \begin{array}{c} \\ \alpha \\ \alpha+1 \\ \vdots \\ \eta \end{array} \begin{array}{c} \begin{array}{cccc} ^k c_{\beta+1} & ^k c_{\beta+2} & \cdots & ^k c_{\delta} \end{array} \\ \begin{bmatrix} \lambda_{\alpha-1,\beta+1} & \lambda_{\alpha-1,\beta+2} & \cdots & \lambda_{\alpha-1,\delta} \\ \lambda_{\alpha,\beta+1} & \lambda_{\alpha,\beta+2} & \cdots & \lambda_{\alpha,\delta} \\ \vdots & \vdots & \ddots & \vdots \\ \lambda_{\eta-1,\beta+1} & \lambda_{\eta-1,\beta+2} & \cdots & \lambda_{\eta-1,\delta} \end{bmatrix} \end{array} \begin{array}{l} \\ (\boldsymbol{\Upsilon}_{\alpha-1}) \\ (\boldsymbol{\Upsilon}_{\alpha}) \\ \vdots \\ \boldsymbol{\Upsilon}_{\eta-1} \end{array} \tag{3.51}$$

Note the matrix rows start from α, given by,

$$\alpha = 2 + \sum_{k=1}^{N} \frac{N!}{k!(N-k)!} - \left[\sum_{k=N}^{k} \frac{N!}{k!(N-k)!}\right], \tag{3.52}$$

where the minimum value of α is two, corresponding to the first possible rework state as shown in Figures 3.15 and 3.16 . The matrix elements are given by,

$$\lambda_{i,j} = \begin{cases} 0 & \iff {}^{k}c_j \nexists \{\boldsymbol{\Upsilon}_i\}\,; \\ 1 & \iff {}^{k}c_j \exists \{\boldsymbol{\Upsilon}_i\}\,, \end{cases} \tag{3.53}$$

where i and j refer to row and column number respectively. The $\boldsymbol{\Upsilon}$ elements on the right side of Equation 3.51 refer to the subsets of $\boldsymbol{\Upsilon}$. For a three feature production system the values $\lambda_{i,j}$ are populated as follows: For $k = 1$, Equation 3.48 indicates there are three $k = 1$ type combinations. The first $k = 1$ combination gives ${}^{1}c_1 = [x_1]$ and $\boldsymbol{\Upsilon}_1 = [x_1]$ thus Equation 3.53 indicates $\lambda_{1,1} = 1$. The second element $\lambda_{1,2} = 0$, as ${}^{1}c_2 = [x_2]$ is not part of the set $\boldsymbol{\Upsilon}_1 = [x_1]$ and similarly for ${}^{1}c_3$. All the λ values for the ${}^{1}\boldsymbol{S}$ are displayed in Equation 3.54 where the c-values along the top row and $\boldsymbol{\Upsilon}$-combinations on the right column are written out.

$${}^{1}\boldsymbol{S} = \begin{array}{c} \\ 2 \\ 3 \\ 4 \\ 5 \\ 6 \\ 7 \\ 8 \end{array} \begin{array}{c} \begin{array}{ccc} x_1 & x_2 & x_3 \end{array} \\ \left[\begin{array}{ccc} 1 & 0 & 0 \\ 0 & 1 & 0 \\ 0 & 0 & 1 \\ 1 & 1 & 0 \\ 1 & 0 & 1 \\ 0 & 1 & 1 \\ 1 & 1 & 1 \end{array}\right] \end{array} \begin{array}{l} (x_1) \\ (x_2) \\ (x_3) \\ (x_1, x_2) \\ (x_1, x_3) \\ (x_2, x_3) \\ (x_1, x_2, x_3). \end{array} \tag{3.54}$$

An $\boldsymbol{S}$-matrix exists for all k, where the size of the matrix is $(\eta - 1) \times m$ where m is k-dependent. The $\boldsymbol{S}^k$-matrix for $k = 2$ is given by,

$${}^{2}\boldsymbol{S} = \begin{array}{c} \\ 5 \\ 6 \\ 7 \\ 8 \end{array} \begin{array}{c} \begin{array}{ccc} x_1,x_2 & x_1,x_3 & x_2,x_3 \end{array} \\ \left[\begin{array}{ccc} 1 & 0 & 0 \\ 0 & 1 & 0 \\ 0 & 0 & 1 \\ 1 & 1 & 1 \end{array}\right] \end{array} \begin{array}{l} (x_1, x_2) \\ (x_1, x_3) \\ (x_2, x_3) \\ (x_1, x_2, x_3). \end{array} \tag{3.55}$$

For $k = 3$ the $\boldsymbol{S}$-matrix is,

$${}^{3}\boldsymbol{S} = \begin{array}{c} \\ 8 \end{array} \begin{array}{c} \begin{array}{c} x_1,x_2,x_3 \end{array} \\ \left[\begin{array}{c} 1 \end{array}\right] \end{array} \begin{array}{l} (x_1, x_2, x_3). \end{array} \tag{3.56}$$

The $\boldsymbol{S}$-matrix determines where the rework feed-ins come from for each rework state. The probabilities for each of these feed-ins is given by the $\boldsymbol{D}$-matrix which has the

general form,

$$
{}^{k}\boldsymbol{D} = \begin{array}{c} \\ \alpha \\ \alpha_w{+}1 \\ \vdots \\ \delta{+}1 \\ \delta{+}2 \\ \vdots \\ \eta \end{array}
\begin{array}{c}
\begin{array}{cccc} \alpha & \alpha{+}1 & \cdots & \delta{+}1 \end{array} \\
\left[\begin{array}{cccc}
p_{w,\alpha_w} & 0 & \cdots & 0 \\
0 & p_{w,\alpha_w+1} & \cdots & 0 \\
\vdots & \vdots & \ddots & \vdots \\
0 & 0 & \cdots & p_{w,\delta_w+1} \\
\frac{p_{w,\delta_w+2}p_{w,\alpha_w}}{1-p_{w,\delta_w+2}} & \frac{p_{w,\delta_w+2}p_{w,\alpha_w+1}}{1-p_{w,\delta_w+2}} & \cdots & \frac{p_{w,\delta_w+2}p_{w,\delta_w+1}}{1-p_{w,\delta_w+2}} \\
\vdots & \vdots & \ddots & \vdots \\
\frac{p_{w,\eta_w}p_{w,\alpha_w}}{1-p_{w,\eta_w}} & \frac{p_{w,\eta_w}p_{w,\alpha_w+1}}{1-p_{w,\eta_w}} & \cdots & \frac{p_{w,\eta_w}p_{w,\delta_w+1}}{1-p_{w,\eta_w}}
\end{array}\right]
\end{array}. \tag{3.57}
$$

where a manufacturing stage is given by $w = [\mathrm{I}, \mathrm{II}, \mathrm{III}, \ldots, W]$, where W is the final manufacturing stage. Where only one manufacturing stage is present the w subscripts can be ignored. The $\boldsymbol{D}$-matrix is the same size as the $\boldsymbol{S}$-matrix where the top layer of the matrix is a $m \times m$ matrix with only leading diagonal elements. These probabilities relate to the probability of feed-ins to a rework state from the initial processing state. The lower layer of the matrix has size $(\eta - \delta - 1) \times m$, where the probabilities in each element refer to rework feed-ins from other rework states. The $\boldsymbol{D}$-matrices for $k = [1, 2, 3]$, for a three feature system are given below:

$$
{}^{1}\boldsymbol{D} = \begin{array}{c} \\ 2 \\ 3 \\ 4 \\ 5 \\ 6 \\ 7 \\ 8 \end{array}
\begin{array}{c}
\begin{array}{ccc} 2 & 3 & 4 \end{array} \\
\left[\begin{array}{ccc}
p_{\mathrm{I},2} & 0 & 0 \\
0 & p_{\mathrm{I},3} & 0 \\
0 & 0 & p_{\mathrm{I},4} \\
\frac{p_{\mathrm{I},5}p_{\mathrm{I},2}}{1-p_{\mathrm{I},5}} & \frac{p_{\mathrm{I},5}p_{\mathrm{I},3}}{1-p_{\mathrm{I},5}} & \frac{p_{\mathrm{I},5}p_{\mathrm{I},4}}{1-p_{\mathrm{I},5}} \\
\frac{p_{\mathrm{I},6}p_{\mathrm{I},2}}{1-p_{\mathrm{I},6}} & \frac{p_{\mathrm{I},6}p_{\mathrm{I},3}}{1-p_{\mathrm{I},6}} & \frac{p_{\mathrm{I},6}p_{\mathrm{I},4}}{1-p_{\mathrm{I},6}} \\
\frac{p_{\mathrm{I},7}p_{\mathrm{I},2}}{1-p_{\mathrm{I},7}} & \frac{p_{\mathrm{I},7}p_{\mathrm{I},3}}{1-p_{\mathrm{I},7}} & \frac{p_{\mathrm{I},7}p_{\mathrm{I},4}}{1-p_{\mathrm{I},7}} \\
\frac{p_{\mathrm{I},8}p_{\mathrm{I},2}}{1-p_{\mathrm{I},8}} & \frac{p_{\mathrm{I},8}p_{\mathrm{I},3}}{1-p_{\mathrm{I},8}} & \frac{p_{\mathrm{I},8}p_{\mathrm{I},4}}{1-p_{\mathrm{I},8}}
\end{array}\right]
\end{array},
$$

$$
{}^{2}\boldsymbol{D} = \begin{array}{c} \\ 5 \\ 6 \\ 7 \\ 8 \end{array}
\begin{array}{c}
\begin{array}{ccc} 5 & 6 & 7 \end{array} \\
\left[\begin{array}{ccc}
p_{\mathrm{I},5} & 0 & 0 \\
0 & p_{\mathrm{I},6} & 0 \\
0 & 0 & p_{\mathrm{I},7} \\
\frac{p_{\mathrm{I},8}p_{\mathrm{I},5}}{1-p_{\mathrm{I},8}} & \frac{p_{\mathrm{I},8}p_{\mathrm{I},6}}{1-p_{\mathrm{I},8}} & \frac{p_{\mathrm{I},8}p_{\mathrm{I},7}}{1-p_{\mathrm{I},8}}
\end{array}\right]
\end{array},
$$

$$
{}^{3}\boldsymbol{D} = \begin{array}{c} \\ 8 \end{array}
\begin{array}{c}
\begin{array}{c} 8 \end{array} \\
\left[\begin{array}{c} p_{\mathrm{I},8} \end{array}\right]
\end{array}.
$$

The product of $\boldsymbol{D}$-matrix columns and $\boldsymbol{S}$-matrix columns determines the probability of components entering rework states from other rework states and the initial processing state. The expected profit for multiple features from a single-stage can be written as,

$$E(PR) = SP\, f_{\mathrm{I},C} - PC - Sr - Rw, \tag{3.58}$$

where,

$$\begin{aligned} Sr_w =& SC_w\, p_{w,S} - \sum_{k=1}^{N} \sum_{j=\alpha}^{\delta+1} \Bigg(SC_{j_w} \sum \Big[{}^{k}\boldsymbol{S}_{\forall\,[\alpha,\eta],j} \\ & {}^{k}\boldsymbol{D}_{\forall\,[\alpha,\eta],j}\, \frac{p_{j_w,S}}{1 - p_{j_w,j_w}} \Big] \Bigg), \end{aligned} \tag{3.59}$$

$$Rw_w = \sum_{j=2}^{\eta} RC_{j_w}\, m_{w,j_w}.$$

For the scrap (Sr) term in Equation 3.59, i is the manufacturing stage (e.g. stage I or stage II) and the column numbering of the $\boldsymbol{S}$-matrices is the same as the $\boldsymbol{D}$-matrices. The fraction term (last term) of the scrap equation in Equation 3.59 determines the output from each rework state. One will recall from Section 3.2.2, the terms in the $\boldsymbol{F}$-matrix refer to the probability that items passing though the i^{th} stage will eventually conform or become scrap. However, the exact route items take after passing through the i^{th} stage is not given. This is not an issue for single feature rework states but is for multiple feature rework states. The fraction term discussed above strictly accounts for items passing from the i^{th} state to scrap or conformance.

3.2.2.2 Transition probabilities

The transition matrix is required to compute $f_{\mathrm{I},C}$ and the $m_{\mathrm{I},j}$ values in Equations 3.58 and 3.59. A generalised $\boldsymbol{P}$-matrix is presented which can be determined from the $\boldsymbol{S}$-matrix. Computationally it is easy to generate the k-type combinations to find $\boldsymbol{\Upsilon}$ using a combination package such as '*combinator*' for Matlab (Fig [2009]). Thus, the $\boldsymbol{S}$-matrix is readily computable and the $\boldsymbol{P}$-matrix can be found without further logical operations.

The general form of the $\boldsymbol{P}$-matrix is given by Equation 3.60.

$$\boldsymbol{P}_w = \begin{array}{c} \\ w \\ 2 \\ \vdots \\ \vdots \\ \vdots \\ \eta \\ C \\ S \end{array} \begin{array}{c} \begin{array}{ccccccccccc} \text{I} & 2 & 3 & \cdots & \cdots & \cdots & \cdots & \eta & C & S \end{array} \\ \begin{bmatrix} 0 & p_{w,2} & p_{w,3} & \cdots & \cdots & \cdots & \cdots & p_{w,\eta} & p_{w,C} & p_{w,S} \\ 0 & & & & \cdots & \cdots & \cdots & 0 & p_{2,C} & p_{2,S} \\ \vdots & & & & \cdots & \cdots & \cdots & \vdots & \vdots & \vdots \\ \vdots & & {}^1\boldsymbol{\Gamma}_w & & & & & \vdots & \vdots & \vdots \\ \vdots & & & & & {}^2\boldsymbol{\Gamma}_w & & \vdots & \vdots & \vdots \\ 0 & & & & & & {}^k\boldsymbol{\Gamma}_w & p_{\eta_w,C} & p_{\eta_w,S} \\ 0 & 0 & 0 & \cdots & \cdots & \cdots & \cdots & \cdots & 1 & 0 \\ 0 & 0 & 0 & \cdots & \cdots & \cdots & \cdots & \cdots & 0 & 1 \end{bmatrix} \end{array} \tag{3.60}$$

for every w stage. The $\boldsymbol{\Gamma}$ terms are k dependent such that,

$$^{\boldsymbol{k}}\boldsymbol{\Gamma}_w = \sum {}^k\boldsymbol{S}_{\forall\,[\alpha,\eta],j}\; {}^k\boldsymbol{J}_{\forall\,[\alpha,\eta],j} \tag{3.61}$$

where j is the column number. The ${}^k\boldsymbol{J}$ terms are given by,

$${}^k\boldsymbol{J}_w = \begin{array}{c} \\ \alpha \\ \alpha{+}1 \\ \vdots \\ \eta \end{array} \begin{array}{c} \begin{array}{cccc} \alpha & \alpha{+}1 & \cdots & \delta{+}1 \end{array} \\ \begin{bmatrix} p_{\alpha_w,\alpha_w} & p_{\alpha_w,\alpha_w+1} & \cdots & p_{\alpha_w,\delta_w+1} \\ p_{\alpha_w+1,\alpha_w} & p_{\alpha_w+1,\alpha_w+1} & \cdots & p_{\alpha_w+1,\delta_w+1} \\ \vdots & \vdots & \ddots & \vdots \\ p_{\eta_w,\alpha_w} & p_{\eta_w,\alpha_w+1} & \cdots & p_{\eta_w,\delta_w+1} \end{bmatrix} \end{array}, \tag{3.62}$$

where both the subscripts α and δ are k-dependent. For a three feature example, the following $\boldsymbol{J}$-matrices are obtained (the w is dropped as only 1 stage is present):

$${}^{1,2}\boldsymbol{J} = \begin{array}{c} \\ 2 \\ 3 \\ 4 \\ 5 \\ 6 \\ 7 \\ 8 \end{array} \begin{array}{c} \begin{array}{ccc} 2 & 3 & 4 \end{array} \\ \begin{bmatrix} p_{2,2} & p_{2,3} & p_{2,4} \\ p_{3,2} & p_{3,3} & p_{3,4} \\ p_{4,2} & p_{4,3} & p_{4,4} \\ p_{5,2} & p_{5,3} & p_{5,4} \\ p_{6,2} & p_{6,3} & p_{6,4} \\ p_{7,2} & p_{7,3} & p_{7,4} \\ p_{8,2} & p_{8,3} & p_{8,4} \end{bmatrix} \end{array}, \quad \begin{array}{c} \\ 5 \\ 6 \\ 7 \\ 8 \end{array} \begin{array}{c} \begin{array}{ccc} 5 & 6 & 7 \end{array} \\ \begin{bmatrix} p_{5,5} & p_{5,6} & p_{5,7} \\ p_{6,5} & p_{6,6} & p_{6,7} \\ p_{7,5} & p_{7,6} & p_{7,7} \\ p_{8,5} & p_{8,6} & p_{8,7} \end{bmatrix} \end{array}$$

and

$$ {}^{3}\boldsymbol{J} = \begin{matrix} \\ 8 \end{matrix} \overset{8}{\begin{bmatrix} p_{8,8} \end{bmatrix}}. $$

Multiplying each column of ${}^{k}\boldsymbol{J}$ by each column of ${}^{k}\boldsymbol{S}$ gives the ${}^{k}\boldsymbol{\Gamma}$ entries of the transition matrix (Equation 3.60). For a three feature example the transition matrix is given in Equation 3.63.

$$ \boldsymbol{P} = \begin{array}{c} \\ \text{I} \\ 2 \\ 3 \\ 4 \\ 5 \\ 6 \\ 7 \\ 8 \\ C \\ S \end{array} \begin{array}{c} \begin{array}{cccccccccc} \text{I} & 2 & 3 & 4 & 5 & 6 & 7 & 8 & C & S \end{array} \\ \begin{bmatrix} 0 & p_{\text{I},2} & p_{\text{I},3} & p_{\text{I},4} & p_{\text{I},5} & p_{\text{I},6} & p_{\text{I},7} & p_{\text{I},8} & p_{\text{I},C} & p_{\text{I},S} \\ 0 & p_{2,2} & 0 & 0 & 0 & 0 & 0 & 0 & p_{2,C} & p_{2,S} \\ 0 & 0 & p_{3,3} & 0 & 0 & 0 & 0 & 0 & p_{3,C} & p_{3,S} \\ 0 & 0 & 0 & p_{4,4} & 0 & 0 & 0 & 0 & p_{4,C} & p_{4,S} \\ 0 & p_{5,2} & p_{5,3} & 0 & p_{5,5} & 0 & 0 & 0 & p_{5,C} & p_{5,S} \\ 0 & p_{6,2} & 0 & p_{6,4} & 0 & p_{6,6} & 0 & 0 & p_{6,C} & p_{6,S} \\ 0 & 0 & p_{7,3} & p_{7,4} & 0 & 0 & p_{7,7} & 0 & p_{7,C} & p_{7,S} \\ 0 & p_{8,2} & p_{8,3} & p_{8,4} & p_{8,5} & p_{8,6} & p_{8,7} & p_{8,8} & p_{8,C} & p_{8,S} \\ 0 & 0 & 0 & 0 & 0 & 0 & 0 & 0 & 1 & 0 \\ 0 & 0 & 0 & 0 & 0 & 0 & 0 & 0 & 0 & 1 \end{bmatrix} \end{array} \tag{3.63} $$

Khasawneh et al. [2008] show how to translate the $\boldsymbol{P}$-matrix into the $\boldsymbol{M}$ and $\boldsymbol{F}$ matrices required for the $f_{1,C}$ and $m_{1,j}$ values in Equations 3.58 and 3.59.

3.2.2.3 General Solution for n-stage Serial and Parallel Production

A multi-stage production system may involve several parallel processes following serially from one another, or parallel processes mixed with serial processes. Multi-stage serial production systems were discussed by Bowling et al. [2004] and Selim and Al-Zu'bi [2011] but could not deal with parallel production. A small but significant change is made here, such that the formulation of the serial transition matrix and subsequent formulations of the $\boldsymbol{M}$ and $\boldsymbol{F}$ matrices, are consistent with the methodology for parallel systems discussed in the previous section. Figure 3.21 shows an initial processing stage (I), from which scrap, rework and conforming items are generated. A distinction is made between the rework state (2) and initial processing (I) such that rework is a separate operation to the initial processing stage. This may or may-not accurately describe the flow through a real production process (rework may occur on the same machine as the initial cut) but only the cost value is relevant. This is conceptually different from past literature where rework simply fed back into the initial processing stage. Figure 3.21 indicates the feed-ins and feed-outs of each state. The transition matrix for this process is,

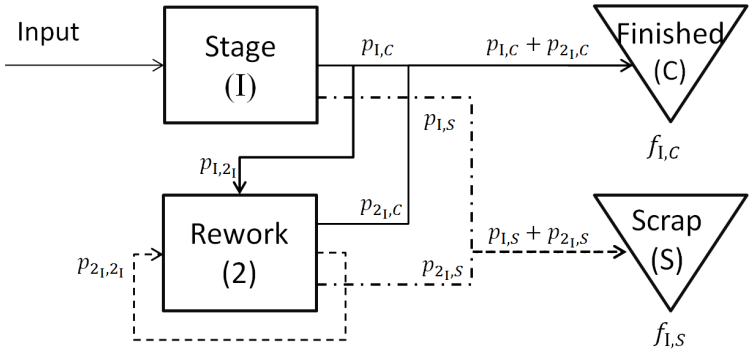

FIGURE 3.21: Single-stage process

$$\boldsymbol{P} = \begin{array}{c} \\ \mathrm{I} \\ 2 \\ C \\ S \end{array} \begin{array}{c} \begin{array}{cccc} \mathrm{I} & 2 & C & S \end{array} \\ \begin{bmatrix} 0 & p_{\mathrm{I},2_\mathrm{I}} & p_{\mathrm{I},C} & p_{\mathrm{I},S} \\ 0 & p_{2_\mathrm{I},2_\mathrm{I}} & p_{2_\mathrm{I},C} & p_{2_\mathrm{I},S} \\ 0 & 0 & 1 & 0 \\ 0 & 0 & 0 & 1 \end{bmatrix} \end{array}, \tag{3.64}$$

where 2_I indicates stage one rework (state 2). For a single rework state process, the probabilities of conformance, rework and scrap are identical to the initial probabilities of conformance, rework and scrap. Therefore, the following simplifying conditions are met,

$$p_{\mathrm{I},2_\mathrm{I}} = p_{2_\mathrm{I},2_\mathrm{I}}, \quad \text{and} \quad p_{\mathrm{I},\mathrm{C}} = p_{2_\mathrm{I},\mathrm{C}}. \tag{3.65}$$

The corresponding $\boldsymbol{F}$ and $\boldsymbol{M}$ matrices are,

$$\boldsymbol{M} = \begin{array}{c} \\ \mathrm{I} \\ 2 \end{array} \begin{array}{c} \begin{array}{cc} \mathrm{I} & 2 \end{array} \\ \begin{bmatrix} 1 & \frac{p_{\mathrm{I},2_\mathrm{I}}}{1-p_{\mathrm{I},2_\mathrm{I}}} \\ 0 & \frac{1}{1-p_{\mathrm{I},2_\mathrm{I}}} \end{bmatrix} \end{array}. \tag{3.66}$$

and

$$\boldsymbol{F} = \begin{array}{c} \\ \mathrm{I} \\ 2 \end{array} \begin{array}{c} \begin{array}{cc} C & S \end{array} \\ \begin{bmatrix} \frac{p_{\mathrm{I},C}}{1-p_{\mathrm{I},2_\mathrm{I}}} & \frac{p_{\mathrm{I},S}}{1-p_{\mathrm{I},2_\mathrm{I}}} \\ \frac{p_{\mathrm{I},C}}{1-p_{\mathrm{I},2_\mathrm{I}}} & \frac{p_{\mathrm{I},S}}{1-p_{\mathrm{I},2_\mathrm{I}}} \end{bmatrix} \end{array}. \tag{3.67}$$

The expected profit for this one feature example is,

$$\begin{aligned} E(PR) = & \overbrace{SP\,\frac{p_{\text{I},C}}{1-p_{2_\text{I},2_\text{I}}}}^{\text{Conformance}} - PC_1 - \overbrace{SC_\text{I} p_{\text{I},S}}^{\text{Scrap } 1^{\text{st}} \text{ state}} \\ & - \underbrace{SC_{2_\text{I}} \frac{p_{\text{I},2_\text{I}}\, p_{2_\text{I},S}}{1-p_{2_\text{I},2_\text{I}}}}_{\text{Scrap } 2^{\text{nd}} \text{ state}} - \underbrace{RC_\text{II}\,\frac{1}{1-p_{2_\text{I},2_\text{I}}}}_{\text{Rework } 2^{\text{nd}} \text{ state}}. \end{aligned} \tag{3.68}$$

Equation 3.68 reduces to Equation 3.70 by acknowledging the scrap terms can be reduced by writing,

$$C = SC_\text{I}\, p_{\text{I},S} + SC_{2_\text{I}} \frac{p_{\text{I},2_\text{I}} p_{2_\text{I},S}}{1-p_{2_\text{I},2_\text{I}}}$$

where the cost of scrap is the same from state I and from state 2_I hence, $SC_\text{I} = SC_{2_\text{I}}$. The probability of scrap from state I is the same as the probability of scrap from state 2_I hence, $p_{\text{I},S} = p_{2_\text{I},S}$. The probability of rework components feeding into state 2_I from state I is the same as the probability of rework from state 2_I back to state 2_I hence, $p_{\text{I},2_\text{I}} = p_{2_\text{I},2_\text{I}}$, therefore,

$$\begin{aligned} C(1-p_{\text{I},2_\text{I}}) =& (1-p_{\text{I},2_\text{I}}) SC_\text{I}\, p_{\text{I},S} - SC_\text{I}\, p_{\text{I},2_\text{I}}\, p_{\text{I},S} \\ C(1-p_{\text{I},2_\text{I}}) =& SC_\text{I}\, p_{\text{I},S}(1-p_{2_\text{I},2_\text{I}} + p_{\text{I},2_\text{I}}) \\ C =& SC_\text{I} \frac{p_{\text{I},S}}{1-p_{\text{I},2_\text{I}}}. \end{aligned} \tag{3.69}$$

Hence the expected profit is,

$$\begin{aligned} E(PR) =& SP\,\frac{p_{\text{I},C}}{1-p_{\text{I},2_\text{I}}} - PC - SC_\text{I} \frac{p_{\text{I},S}}{1-p_{\text{I},2_\text{I}}} \\ & - RC_\text{II}\,\frac{p_{\text{I},2_\text{I}}}{1-p_{\text{I},2_\text{I}}}, \end{aligned} \tag{3.70}$$

which is identical in form to Equation 2 from Bowling et al. [2004] and Selim and Al-Zu'bi [2011].

The format shown in Figure 3.21 can easily be extended to a multi-stage process. An absorbing Markov chain was developed for a two-stage example as shown by Figure 3.22. As in Figure 3.21, the probability feed-ins and feed-outs to each stage are illustrated. Examination of the $\boldsymbol{F}$ and $\boldsymbol{M}$ matrices from this two-stage process reveal a general method by which the scrap, rework and conformance terms in Equation 3.59 can be used recursively to model a multi-stage process where each stage can have multiple features produced in parallel. The transition matrices for the two stage I and II are given by Equation 3.71,

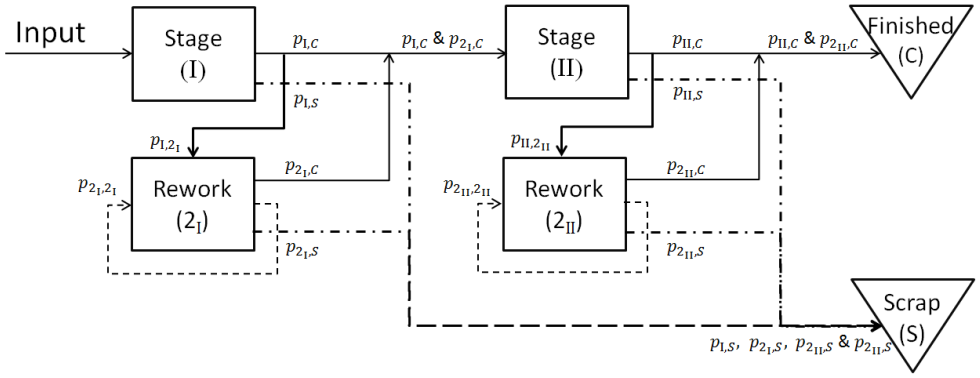

FIGURE 3.22: A two-stage serial production process

$$\boldsymbol{P}_\mathrm{I} = \begin{array}{c} \\ \mathrm{I} \\ 2 \\ C \\ S \end{array} \begin{array}{c} \begin{array}{cccc} \mathrm{I} & 2 & C & S \end{array} \\ \begin{bmatrix} 0 & p_{\mathrm{I},2_\mathrm{I}} & p_{\mathrm{I},C} & p_{\mathrm{I},S} \\ 0 & p_{2_\mathrm{I},2_\mathrm{I}} & p_{2_\mathrm{I},C} & p_{2_\mathrm{I},S} \\ 0 & 0 & 1 & 0 \\ 0 & 0 & 0 & 1 \end{bmatrix} \end{array}, \quad \text{and} \quad \boldsymbol{P}_\mathrm{II} = \begin{array}{c} \\ \mathrm{I} \\ 2 \\ C \\ S \end{array} \begin{array}{c} \begin{array}{cccc} \mathrm{I} & 2 & C & S \end{array} \\ \begin{bmatrix} 0 & p_{\mathrm{II},2_\mathrm{II}} & p_{\mathrm{II},C} & p_{\mathrm{II},S} \\ 0 & p_{2_\mathrm{II},2_\mathrm{II}} & p_{2_\mathrm{II},C} & p_{2_\mathrm{II},S} \\ 0 & 0 & 1 & 0 \\ 0 & 0 & 0 & 1. \end{bmatrix} \end{array} \tag{3.71}$$

where 2_I indicates the rework state from the first stage and 2_II is the rework state from the second stage. Additionally to Equation 3.65, the probabilities of conformance, scrap and rework in the rework state (2) for the second stage are identical to the initial stage probabilities such that,

$$p_{\mathrm{II},2_\mathrm{II}} = p_{2_\mathrm{I},2_\mathrm{II}} \quad \text{and} \quad p_{\mathrm{II},\mathrm{C}} = p_{2_\mathrm{II},\mathrm{C}}. \tag{3.72}$$

The $\boldsymbol{F}$ and $\boldsymbol{M}$ matrices for both stages are,

$$\boldsymbol{F}_\mathrm{I} = \begin{array}{c} \\ \mathrm{I} \\ 2_\mathrm{I} \end{array} \begin{array}{c} \begin{array}{cc} C & S \end{array} \\ \begin{bmatrix} \frac{p_{\mathrm{I},C}}{1-p_{\mathrm{I},2_\mathrm{I}}} & \frac{p_{\mathrm{I},S}}{1-p_{\mathrm{I},2_\mathrm{I}}} \\ \frac{p_{\mathrm{I},C}}{1-p_{\mathrm{I},2_\mathrm{I}}} & \frac{p_{\mathrm{I},S}}{1-p_{\mathrm{I},2_\mathrm{I}}} \end{bmatrix} \end{array} \text{for stage I} \quad \boldsymbol{F}_\mathrm{II} = \begin{array}{c} \\ \mathrm{II} \\ 2_\mathrm{II} \end{array} \begin{array}{c} \begin{array}{cc} C & S \end{array} \\ \begin{bmatrix} \frac{p_{\mathrm{II},C}}{1-p_{\mathrm{II},2_\mathrm{II}}} & \frac{p_{\mathrm{II},S}}{1-p_{\mathrm{II},2_\mathrm{II}}} \\ \frac{p_{\mathrm{II},C}}{1-p_{\mathrm{II},2_\mathrm{II}}} & \frac{p_{\mathrm{II},S}}{1-p_{\mathrm{II},2_\mathrm{II}}} \end{bmatrix} \end{array} \text{for stage II} \tag{3.73}$$

and

$$\boldsymbol{M}_\mathrm{I} = \begin{array}{c} \\ \mathrm{I} \\ 2_\mathrm{I} \end{array} \begin{array}{c} \begin{array}{cc} \mathrm{I} & 2_\mathrm{I} \end{array} \\ \begin{bmatrix} 1 & \frac{p_{\mathrm{I},2_\mathrm{I}}}{1-p_{\mathrm{I},2_\mathrm{I}}} \\ 0 & \frac{1}{1-p_{\mathrm{I},2_\mathrm{I}}} \end{bmatrix} \end{array} \text{for stage I} \quad \boldsymbol{M}_\mathrm{II} = \begin{array}{c} \\ \mathrm{II} \\ 2_\mathrm{II} \end{array} \begin{array}{c} \begin{array}{cc} \mathrm{I} & 2_\mathrm{II} \end{array} \\ \begin{bmatrix} 1 & \frac{p_{\mathrm{II},2_\mathrm{II}}}{1-p_{\mathrm{II},2_\mathrm{II}}} \\ 0 & \frac{1}{1-p_{\mathrm{II},2_\mathrm{II}}} \end{bmatrix} \end{array} \text{for stage II.} \tag{3.74}$$

The expected profit is given by,

$$E(PR) = \overbrace{SP\, f_{\text{I},C}\, f_{\text{II},C}}^{\text{Final conformance}} - PC_{\text{I}} - \overbrace{SC_{\text{I}}\, p_{\text{I},S}}^{\text{Scrap I 1}^{\text{st}}\text{ state}} - \overbrace{SC_{2_{\text{I}}} \frac{p_{\text{I},2_{\text{I}}}\, p_{2_{\text{I}},S}}{1 - p_{\text{I},2_{\text{I}}}}}^{\text{Scrap I 2}^{\text{nd}}\text{ state}}$$
$$- \overbrace{RC_{2_{\text{I}}} \frac{1}{1 - p_{\text{I},2_{\text{I}}}}}^{\text{Rework I 2}^{\text{nd}}\text{ state}} - \Bigg[PC_{\text{II}} - \underbrace{SC_{\text{II}}\, p_{\text{II},S_{\text{I}}}}_{\text{Scrap II 1}^{\text{st}}\text{ state}} \tag{3.75}$$
$$- \underbrace{SC_{2_{\text{II}}} \frac{p_{\text{II},2_{\text{II}}}\, p_{2_{\text{II}},S}}{1 - p_{\text{II},2_{\text{II}}}}}_{\text{Scrap II 2}^{\text{nd}}\text{ state}} - \underbrace{RC_{2_{\text{II}}} \frac{1}{1 - p_{\text{II},2_{\text{II}}}}}_{\text{Rework II 2}^{\text{nd}}\text{ state}} \Bigg] f_{\text{I},C}$$

In the same manner to Equation 3.69, the scrap terms related to the scrap from stage I are reduced to,

$$SC_{\text{I}} \frac{p_{\text{I},S}}{1 - p_{\text{I},2_{\text{I}}}}.$$

The scrap terms related to scrap from stage II can be written as follows,

$$C = SC_{\text{II}}\, p_{\text{II},S} + SC_{2_{\text{II}}} \frac{p_{\text{II},2_{\text{II}}}\, p_{2_{\text{II}},S}}{1 - p_{2_{\text{II}},2_{\text{II}}}},$$

where the cost of scrap is the same irrespective whether the scrap originates from state II or 2_{II}, $SC_{\text{II}} = SC_{2,\text{II}}$. The probability of scrap from state II is the same as the probability of scrap from state 2_{II} hence, $p_{\text{II},S} = p_{2_{\text{II}},S}$. The probability of rework components feeding into state 2_{II} from state II is the same as the probability of rework from state 2_{II} back to state 2_{II} hence, $p_{\text{I},2_{\text{II}}} = p_{2_{\text{I}},2_{\text{I}}}$, therefore,

$$\begin{aligned} C(1 - p_{\text{II},2_{\text{II}}}) &= (1 - p_{2_{\text{II}},2_{\text{II}}})\, SC_{\text{II}}\, p_{\text{II},S} - SC_{\text{II}}\, p_{\text{II},2_{\text{II}}}\, p_{\text{II},S} \\ C(1 - p_{\text{II},2_{\text{I}}}) &= SC_{\text{II}}\, p_{\text{II},S}(1 - p_{2_{\text{II}},2_{\text{II}}} + p_{\text{II},2_{\text{II}}}) \\ C &= SC_{\text{II}} \frac{p_{\text{II},S}}{1 - p_{\text{II},2_{\text{II}}}}. \end{aligned} \tag{3.76}$$

Therefore Equation 3.75 can be written in a reduced form as,

$$\begin{aligned} E(PR) = {} & SP\, f_{\text{I},C} f_{\text{II},C} - (PC_{\text{I}} + PC_{\text{II}}\, f_{\text{I},C}) \\ & - \left[SC_{\text{I}} \left(\frac{p_{\text{I},S}}{1 - p_{2_{\text{I}},2_{\text{I}}}} \right) + SC_{\text{II}} \left(\frac{p_{\text{II},S}}{1 - p_{\text{II},2_{\text{II}}}} \right) f_{\text{I},C} \right] \\ & - RC_{2_{\text{I}}}\, m_{\text{I},2_{\text{I}}} - RC_{2_{\text{II}}}\, m_{\text{II},2_{\text{II}}}\, f_{\text{I},C} \end{aligned} \tag{3.77}$$

This Equation also corresponds to Selim's Equation 2 for two features which is illustrated

in Appendix C since the two equations are not as obviously equivalent as the one feature case (Equation 3.70). Notice that the second stage scrap and rework terms are multiplied by the final conformance probability from the previous stage $p_{\mathrm{I},C}/(1-p_{\mathrm{I},2_{\mathrm{I}}})$. This allows each stage to be modelled as a single-stage process reminiscent of Equations 3.64, 3.66 and 3.67. In essence, the scrap, rework and conformance probabilities from each stage are multiplied by the final conformance from the previous stage (for the first stage this is one). Thus, the expected profit can be written as

$$\begin{aligned} E(PR) =& SP\prod_{i=\mathrm{I}}^{w} f_{i,C} \\ &- \sum_{i=\mathrm{I}}^{w}\{(PC_i + Sr_i + Rw_i)\}\prod_{l=\mathrm{I}}^{l-\mathrm{I}} f_{l,C}, \end{aligned} \tag{3.78}$$

where W is the total number of stages. This Equation is similar to Equation 2 from Selim and Al-Zu'bi [2011], however, it is necessary to use the $f_{i,C}$ and $f_{l,C}$ terms to allow for a multi-state stage (a stage with parallel processing). The Sr_i and Rw_i terms are given from Equation 3.78.

3.3 Codification of Equation 3.78

The calculations and logic required to determine Equation 3.78 (detailed in Sections 3.2.2.1, 3.2.2.2 and 3.2.2.3) were codified in Matlab to enable automatic computation of expected profit for a given number for features with a combination of serial of parallel operations. The Matlab code is given in Appendix E. The main function, *StageCostFun*, requires the following inputs;

MU: The means for each feature

sigs: Standard deviation of the manufacturing process for each feature

rho: Correlation matrix determining the correlation between features

U: Upper specification limit for each feature

L: Lower specification limits for each feature

R_Cost: Rework cost vector for the rework costs for each state of each feature

S_Cost: Scrap cost vector for the scrap costs for each state of each feature

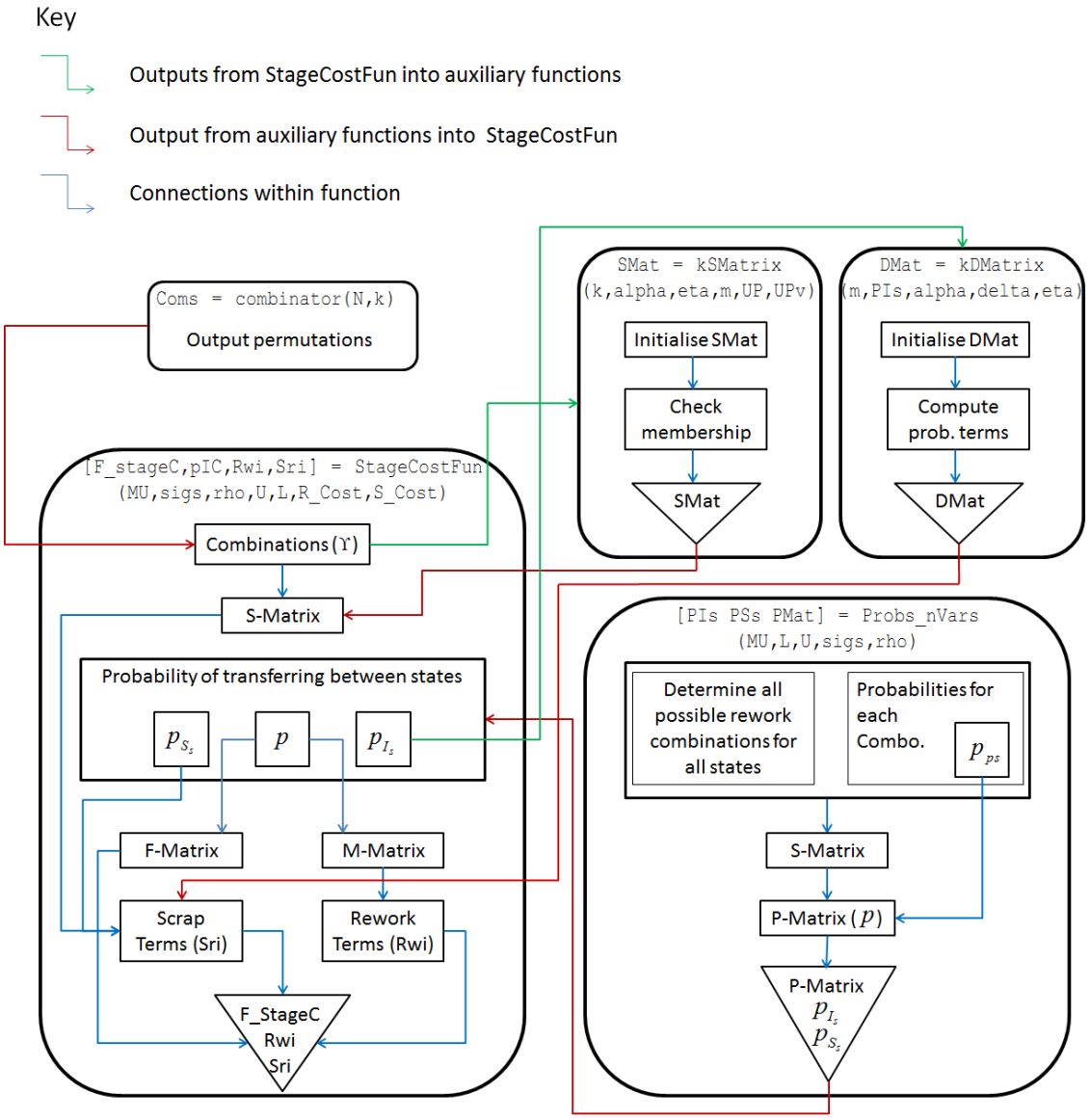

FIGURE 3.23: Diagrammatic overview of the code developed to calculate expected profit

StageCostFun

The main function, *StageCostFun*, returns the elements necessary to compute Equation 3.78 where the major elements of the function are shown in Figure 3.23. The first operation determines all possible permutations of rework, as shown in mathematical form in Equation 3.50. The Matlab function *combinator* (Fig [2009]) is used to determine all permutations given the total number of features (N) and the number of features requiring rework (k). From this the $\boldsymbol{S}$-matrix can be found and the binary γ-values determined (Equations 3.51 and 3.53). The probabilities of components transferring between sates is computed by an axillary function, *Probs_nVars*, which is explained in more detail under the proceeding headings. The three outputs from the *Probs_nVars*

function feed back to the *StageCostFun* function. The first, p_{S_s}, is a vector containing the probabilities components are scrapped. This is used by the Scrap terms (Sri) section of the code, which is a codified version of the Sr_w term given in Equation 3.59. The second output, P, is the transition matrix which is used to generate the $\boldsymbol{F}$ and $\boldsymbol{M}$-matrices as described by Equation 3.30 and the description in Section 3.2. The $\boldsymbol{F}$-matrix terms are used to define the final conformance from a particular stage and the scrap quantities. The Rework terms section of the code requires the $\boldsymbol{M}$-matrix (Rw_w, Equation 3.59). The third output from *Probs_nVars*, P_{I_s}, contains all the probabilities of components going from a stage I, II, III, ... to another state. These terms are required by the *kDMatrix* function, discussed below. The three outputs from this *StageCostFun* function correspond to the Sr_i, Rw_i, $F_{i,C}$ and $F_{l,C}$ terms in Equation 3.78.

kSMatrix

The function *kSMatrix* is an auxiliary function that takes inputs relating to all the possible rework permutations (UP and UPv) and returns the $\boldsymbol{S}$-matrix into *StageCostFun*. The other inputs are constants given in Section 3.2. The function uses the permutations provided by *combinator* (Fig [2009]), from within *StageCostFun*, and determines the binary values of the γ elements of the $\boldsymbol{S}$-matrix (Equations 3.51 and 3.53).

kDMatrix

This auxiliary function is used by *StageCostFun* to determine the $\boldsymbol{D}$-matrix which is used in the computation of the scrap terms, Sr_w, in Equation 3.59. The probabilities of components transferring between states is given by the P_{I_s} vector which is present in *StageCostFun* and computed by *Probs_nVars*.

Probs_nVars

The principle purpose of this function is to return the transition matrix ($\boldsymbol{P}$) to the *StageCostFun* function. The P_{I_s} and P_{S_s} vectors, which are also outputs, are part of the complete transition matrix. The code first determines all the possible probabilities of transferring from one state to another (P_{P_S} vector). The Matlab function *mvncdf* (Mathworks [2012]) is used to determine the values of these probabilities, which assumes the distributions are normally distributed. This is a codified version of Equation 3.19 which utilises the procedures illustrated by Genz and Bretz [2002] and Genz [2004]. Although normal distributions are assumed, this is not a limiting assumption and the *mvncdf* function (Mathworks [2012]) can be replaced by another function to compute

probabilities for distributions that are non-normal (see Chapter 4). The $\boldsymbol{S}$-matrix is used in conjunction with the P_{P_S} vector to generate the transition matrix for a given number of features.

3.4 Optimal Mean Setting Using Equation 3.78 - Numerical Examples

To demonstrate the use and application of Equation 3.78 and the code described in Section 3.3, a series of numerical examples are given.

a. Single stage, single feature, serial production.

b. Two stage, two feature, serial production.

c. Single stage, two feature, parallel production.

d. Multiple stages, multiple features, combined serial and parallel production.

Section 3.1.2 showed in order to find optimal means for the processing of dual features, the means for single feature rework and dual feature rework must be optimised separately. This was contrary to the literature where no distinction was made between single feature and dual feature rework. The numerical examples given in items a to d do not use this new method (single and dual feature rework are not optimised independently), which is covered in detail in the proceeding Section 3.5.

For each example the steps involved in obtaining the expected profit equation are detailed. This is intended as a useful reference on the application of Equations 3.78 and 3.59 as well as demonstrating the effectiveness of these equations over the methodology in the current literature; which are wrong for parallel cases and require the expected profit equations to be derived from first principles for serial cases.

3.4.1 Serial Production

a. Single Feature Numerical Example

For the production of a single feature in a single manufacturing stage, $w = \mathrm{I}$ and the constants in Table 3.2 from Section 3.2.2.1 apply.

1-feature	m	β	α	η	δ
k= 1	1	0	2	2	1

TABLE 3.2: Constants for one stage, one feature example

Equation 3.78 is,

$$E(PR) = SP \prod_{i=\mathrm{I}}^{\mathrm{I}} f_{i,C} - \sum_{i=\mathrm{I}}^{\mathrm{I}} \{(PC_i + Sr_i + Rw_i)\} \prod_{l=\mathrm{I}}^{0} f_{l,C},$$

where the $\boldsymbol{S}$ and $\boldsymbol{D}$ matrices required for Sr_{I} are,

$${}^{1}\boldsymbol{S} = {}^{x_1}{}_{2} \begin{bmatrix} 1 \end{bmatrix} (x_1) \quad \text{and} \quad {}^{1}\boldsymbol{D} = {}^{2}{}_{2} \begin{bmatrix} p_{\mathrm{I},2_{\mathrm{I}}} \end{bmatrix} (2).$$

This makes the Sr_{I} and Rw_{I} terms,

$$Sr_w = SC_w\, p_{w,S} - \sum_{k=1}^{1} \sum_{j=2}^{2} \left(SC_j \left[{}^{k}\boldsymbol{S}_{2,j}\, {}^{k}\boldsymbol{D}_{2,j} \frac{p_{j,S}}{1 - p_{j,j}} \right] \right),$$

$$Sr_{\mathrm{I}} = SC_{\mathrm{I}}\, p_{\mathrm{I},S} - \left(SC_2 \left[p_{\mathrm{I},2} \frac{p_{\mathrm{I},S}}{1 - p_{2,2}} \right] \right),$$

$$Rw_{\mathrm{I}} = RC_2\, m_{\mathrm{I},2}.$$

Therefore, the expected profit as generated by Equations 3.78 and 3.59 is

$$E(PR) = SP\, f_{\mathrm{I},C} - PC_1 - SC_{\mathrm{I}} p_{\mathrm{I},S} - SC_2 \frac{p_{\mathrm{I},2_{\mathrm{I}}}\, p_{2_{\mathrm{I}},S}}{1 - p_{2_{\mathrm{I}},2_{\mathrm{I}}}} - RC_2\, m_{\mathrm{I},2}. \tag{3.79}$$

The $\boldsymbol{F}$ and $\boldsymbol{M}$ matrices are found using the method described in Section 3.2, which contains the f and m terms in Equation 3.79. The transition matrix (P), which is necessary for the computation of the $\boldsymbol{F}$ and $\boldsymbol{M}$ matrices, is found using Equation 3.61 from Section 3.2.2.2 where,

$${}^{\mathbf{1}}\boldsymbol{\Gamma} = \sum {}^{1}\boldsymbol{S}_{\forall\,[2,2],2}\, {}^{1}\boldsymbol{J}_{\forall\,[2,2],2} \quad \text{and} \quad {}^{1}\boldsymbol{J} = {}^{2}{}_{2} \begin{bmatrix} p_{2,2} \end{bmatrix}.$$

Substituting this value into the general formulation for the transition matrix (Equation 3.60), gives the Transition matrix shown in Equation 3.64 in Section 3.2.2.3. The $\boldsymbol{F}$ and $\boldsymbol{M}$ matrices (Equations 3.66 and 3.66) are also given providing all the elements required to compute Equation 3.79.

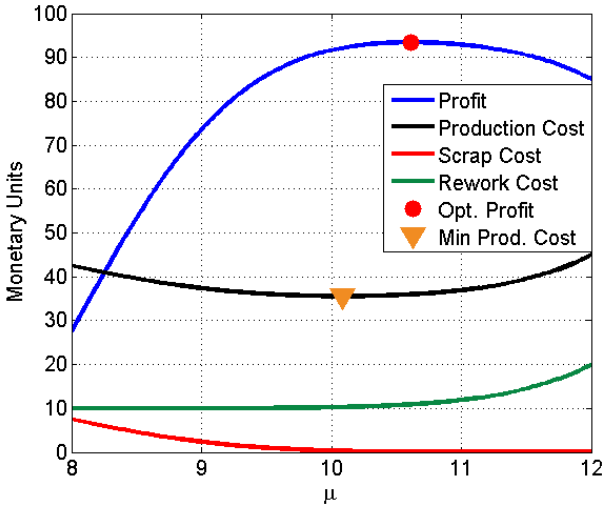

FIGURE 3.24: Variation of expected profit, scrap, rework, and total production costs with the mean (μ)

The specification limits, process variability and costs are shown in Table 3.3. These values are the same as 'Numerical example - 5.1 Single-Stage system' from Bowling et al. [2004] and the numerical example from Selim and Al-Zu'bi [2011]. The profit, scrap cost, rework cost and total production cost (from Equation 3.79) are plotted in Figure 3.24 versus the mean (μ). Production cost is $E(PR) - SP\, f_{\mathrm{I},C}$, rework cost is $RC_2\, m_{\mathrm{I},2}$ and scrap cost $SC_{\mathrm{I}} p_{\mathrm{I},S} + SC_2 \frac{p_{\mathrm{I},2_{\mathrm{I}}}\, p_{2_{\mathrm{I}},S}}{1-p_{2_{\mathrm{I}},2_{\mathrm{I}}}}$. The plot clearly reveals the optimal mean to minimise the production cost, $\mu_{\mathrm{opt}} = 10.09$ (obtained using Matlab's *fmincon* function (Mathworks [2012])), is not the same as the optimum mean for maximum profit, $\mu_{\mathrm{opt}} = 10.61$, located by the markers. Thus, finding the optimal mean to minimise the scrap and rework cost will not maximise the profit since it may pay to have a greater rework cost if it increases the number of conforming components that can be sold (reducing scrap).

Variable	**Value**	**Costs**	**Value**
U	12	SP	120
L	8	PC	25
$\boldsymbol{\sigma}$	1	RC	10
		SC	15

TABLE 3.3: Inputs for the plot in Figure 3.24

b. Two Features, Two Stage Numerical Example

For the production of two features in two manufacturing stages $W = \mathrm{II}$ and the following constants from Section 3.2.2.1 apply.

1-feature	m	β	α	η	δ
$k=1$	2	0	2	0	2

TABLE 3.4: Constants for one stage, one feature example

The general equation for expected profit becomes,

$$E(PR) = SP \prod_{i=\mathrm{I}}^{\mathrm{II}} f_{i,C} - \sum_{i=\mathrm{I}}^{\mathrm{II}} \{(PC_i + Sr_i + Rw_i)\} \prod_{l=\mathrm{I}}^{\mathrm{I}} f_{l,C}. \tag{3.80}$$

The $\boldsymbol{S}$ and $\boldsymbol{D}$ matrices for each of the stages, I and II, have the same form as the single feature case given by,

$$^{1}\boldsymbol{S} = {}^{x_1}{}_{2}\left[\begin{array}{c} \\ 1 \\ \\ \end{array}\right](x_1) \quad \text{and} \quad {}^{1}\boldsymbol{D} = {}^{2}{}_{2}\left[\begin{array}{c} \\ p_{\mathrm{I},2_{\mathrm{I}}} \\ \\ \end{array}\right](2),$$

for the first stage (I) and

$$^{1}\boldsymbol{S} = {}^{x_1}{}_{2}\left[\begin{array}{c} \\ 1 \\ \\ \end{array}\right](x_1) \quad \text{and} \quad {}^{1}\boldsymbol{D} = {}^{2}{}_{2}\left[\begin{array}{c} \\ p_{\mathrm{II},2_{\mathrm{II}}} \\ \\ \end{array}\right](2),$$

for the second stage (II). The Sr_w terms are given by,

$$Sr_w = SC_w\, p_{w,S} - \sum_{k=1}^{1}\sum_{j=2}^{2}\left(SC_j\left[{}^{k}\boldsymbol{S}_{2,j}\,{}^{k}\boldsymbol{D}_{2,j}\frac{p_{j_w,S}}{1-p_{j_w,j_w}}\right]\right),$$

where the unbounded summation term is not present as there is only one term inside the square brackets. Each of the iterations for the I and II stages are,

$$Sr_{\mathrm{I}} = SC_{\mathrm{I}}\, p_{\mathrm{I},S} - \left(SC_{2_{\mathrm{I}}}\left[p_{\mathrm{I},2_{\mathrm{I}}}\frac{p_{\mathrm{I},S}}{1-p_{2_{\mathrm{I}},2_{\mathrm{I}}}}\right]\right) \qquad \text{for stage I}$$

$$Sr_{\mathrm{II}} = SC_{\mathrm{II}}\, p_{\mathrm{II},S} - \left(SC_{2_{\mathrm{II}}}\left[p_{\mathrm{II},2_{\mathrm{II}}}\frac{p_{\mathrm{II},S}}{1-p_{2_{\mathrm{II}},2_{\mathrm{II}}}}\right]\right) \qquad \text{for stage II}$$

The rework terms for the two stages are,

$$Rw_{\mathrm{I}} = RC_{2_{\mathrm{I}}}\, m_{\mathrm{I},2_{\mathrm{I}}} \quad \text{and} \quad Rw_{\mathrm{II}} = RC_{2_{\mathrm{II}}}\, m_{\mathrm{II},2_{\mathrm{II}}}.$$

For both manufacturing stages (I and II), the expected profit Equation 3.80 becomes,

$$\begin{aligned} E(PR) =& SP\, f_{\mathrm{I},C}\, f_{\mathrm{II},C} - PC_{\mathrm{I}} - SC_{\mathrm{I}}\, p_{\mathrm{I},S} - SC_{2_{\mathrm{I}}}\frac{p_{\mathrm{I},2_{\mathrm{I}}}\, p_{2_{\mathrm{I}},S}}{1-p_{\mathrm{I},2_{\mathrm{I}}}} - RC_{2_{\mathrm{I}}}\, m_{\mathrm{I},2_{\mathrm{I}}} \\ &- \left[PC_{\mathrm{II}} - SC_{\mathrm{II}}\, p_{\mathrm{II},S_{\mathrm{I}}} - SC_{2_{\mathrm{II}}}\frac{p_{\mathrm{II},2_{\mathrm{II}}}\, p_{2_{\mathrm{II}},S}}{1-p_{\mathrm{II},2_{\mathrm{II}}}} - RC_{2_{\mathrm{II}}}\, m_{\mathrm{II},2_{\mathrm{II}}}\right] f_{\mathrm{I},C}. \end{aligned} \tag{3.81}$$

As in the previous example, a single feature and a single manufacturing stage, the transition matrix (P) is required to establish the $\boldsymbol{F}$ and $\boldsymbol{M}$ matrices which contain the f and m terms. As there are two stages, there are two transition matrices and hence two Γ values given by,

$$^{1}\boldsymbol{\Gamma}_{w} = \sum {}^{1}\boldsymbol{S}_{\forall[2,2],2}\, {}^{1}\boldsymbol{J}_{\forall[2,2],2},$$

where

$$^{1}\boldsymbol{J}_{\mathrm{I}} = {}_{2}\begin{bmatrix} {}^{2} \\ p_{2\mathrm{I},2\mathrm{I}} \end{bmatrix} \quad \text{for stage I and} \quad {}^{1}\boldsymbol{J}_{\mathrm{II}} = {}_{2}\begin{bmatrix} {}^{2} \\ p_{2_{\mathrm{II}},2_{\mathrm{II}}} \end{bmatrix} \quad \text{for stage II.}$$

Substituting these value into the general formulation for the transition matrix (Equation 3.60), gives the Transition matrices shown in Equation 3.71 in Section 3.2.2.3. The $\boldsymbol{F}$ and $\boldsymbol{M}$ matrices (Equations 3.73 and 3.74) are also given, providing all the elements required to compute Equation 3.81.

The process specification limits, variability and costs are shown in Table 3.5. The data is the same as 'Numerical example - 5.2 Two-stage system' from Bowling et al. [2004] the numerical example in Selim and Al-Zu'bi [2011]. Note the scrap cost from the second stage in the literature is defined as $\mathrm{SC}'_2 = \mathrm{SC}'_1 + \mathrm{SC}_2 = 10 + 12 = 27$.[10] Figure 3.25

Variable	**Value**	**Costs**	**Value**
U	[12 17]	SP	120
L	[8 13]	PC	[25 20]
$\boldsymbol{\sigma}$	$\sigma_{x_1} = \sigma_{x_2} = 1$	RC	[15 12]
		SC	[10 27]

TABLE 3.5: Inputs for the plot in Figure 3.24

illustrates the production, scrap and rework costs as well as profit in a two-dimensional version of the plot in Figure 3.24. Profit is given from Equation 3.81, where production cost is $E(PR) - SP\, f_{\mathrm{I},C}\, f_{\mathrm{II},C}$. Rework costs and scrap costs are associated with $RC_{2_{\mathrm{I}}}$ and $RC_{2_{\mathrm{II}}}$, and SC_{I}, $SC_{2_{\mathrm{I}}}$, SC_{II} and $SC_{2_{\mathrm{II}}}$ respectively. The highest profit (71.41) was obtained from Matlab's *fmincon* function (Mathworks [2012]) with $\mu_{x_1} = 10.466$ and $\mu_{x_2} = 15.591$, the same as Selim and Al-Zu'bi [2011][11]. The minimum production cost is shown at the extreme low end of the μ_{x_1} range ($\mu_{x_1} = 8$). This is because production cost includes the cost of production in the first and second stages. If μ_{x_1} was positioned at the low end of the range, the majority of items would be scrap and would never enter the second stage, therefore, they wouldn't incur the second stage production cost.

[10] In this thesis SC_2 is the cost of scrapping a component at the second stage which is inclusive all the value added through the second stage manufacturing process. Thus SC_2 in this thesis is equivalent to SC'_2 in the literature.

[11] The two stage, two feature numerical example given by Bowling et al. [2004] was incorrect due to errors in the expected profit equation detailed in Section 2.5.

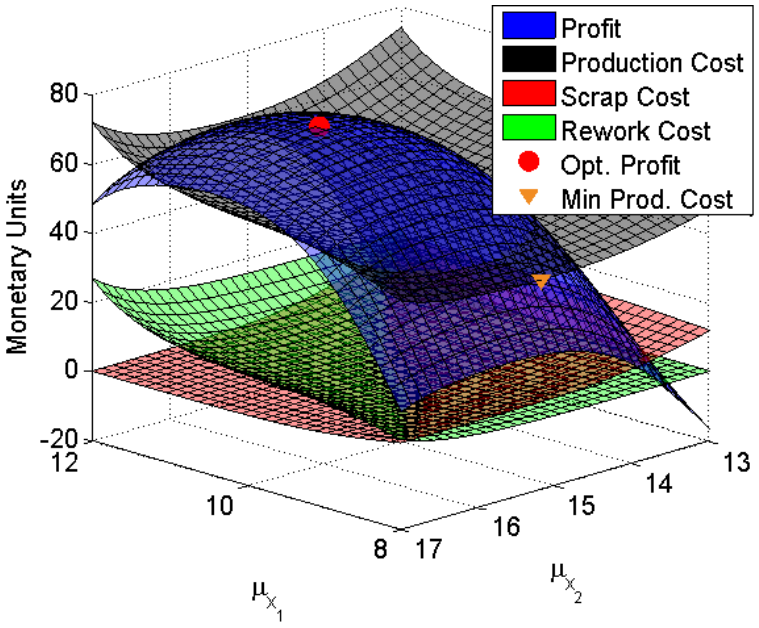

FIGURE 3.25: Variation of expected profit, scrap, rework, and total production costs with the means (μ_{x_1} and μ_{x_2})

However, only a few items would conform after the second stage (few items to sell), hence the profit is low. This highlights the importance of maximising profit rather than attempting to reduce production cost.

3.4.2 Parallel Production

c. Two Features, One Stage Numerical Example

The production of two features in a single manufacturing stage is the simplest type of parallel production, often refereed to as dual quality characteristics in the literature. The value $W = \mathrm{I}$ and the following constants apply,

1-feature	m	β	α	η	δ
$k = 1$	2	0	2	2	2
$k = 2$	1	2	4	4	3

TABLE 3.6: Constants for one stage a two features

The general equation for expected profit for two features manufactured in a single stage is,

$$E(PR) = SP \prod_{i=\mathrm{I}}^{\mathrm{I}} f_{i,C} - \sum_{i=\mathrm{I}}^{\mathrm{I}} \{(PC_i + Sr_i + Rw_i)\} \prod_{l=\mathrm{I}}^{0} f_{l,C}. \tag{3.82}$$

The $\boldsymbol{S}$ and $\boldsymbol{D}$ matrices are for $k = 1$ are given by,

$$
{}^{1}\boldsymbol{S} = \begin{array}{c} \\ 2 \\ 3 \\ 4 \end{array} \begin{array}{c} \begin{array}{cc} x_1 & x_2 \end{array} \\ \left[\begin{array}{cc} 1 & 0 \\ 0 & 1 \\ 1 & 1 \end{array}\right] \end{array} \begin{array}{l} \\ (x_1) \\ (x_2) \\ (x_1, x_2) \end{array} \quad \text{and} \quad {}^{1}\boldsymbol{D} = \begin{array}{c} \\ 2 \\ 3 \\ 4 \end{array} \begin{array}{c} \begin{array}{cc} 2 & 3 \end{array} \\ \left[\begin{array}{cc} p_{\mathrm{I},2} & 0 \\ 0 & p_{\mathrm{I},3} \\ \frac{p_{\mathrm{I},4}p_{\mathrm{I},2}}{1-p_{\mathrm{I},4}} & \frac{p_{\mathrm{I},4}p_{\mathrm{I},3}}{1-p_{\mathrm{I},4}} \end{array}\right] \end{array}.
$$

For $k = 2$ the $\boldsymbol{S}$ and $\boldsymbol{D}$ matrices are,

$$
{}^{2}\boldsymbol{S} = \begin{array}{c} \\ 4 \end{array} \begin{array}{c} \begin{array}{c} x_1, x_2 \end{array} \\ \left[\begin{array}{c} 1 \end{array}\right] \end{array} \begin{array}{l} \\ (x_1, x_2) \end{array} \quad \text{and} \quad {}^{2}\boldsymbol{D} = \begin{array}{c} \\ 4 \end{array} \begin{array}{c} \begin{array}{c} 4 \end{array} \\ \left[\begin{array}{c} p_{\mathrm{I},4} \end{array}\right] \end{array}.
$$

The construction of the scrap terms is more involved for two features produced in parallel, due to the multiple terms in the $\boldsymbol{S}$ and $\boldsymbol{D}$ matrices and the two k-values and consequently α and δ values. The w subscripts are not shown as there is only one stage.

$$
Sr_{\mathrm{I}} = SC_{\mathrm{I}}\, p_{\mathrm{I},S} - \sum_{k=1}^{2} \sum_{j=\alpha}^{\delta+1} \left(SC_j \sum \left[{}^{k}\boldsymbol{S}_{\forall\,[\alpha,4],j}\, {}^{k}\boldsymbol{D}_{\forall\,[\alpha,4],j}\, \frac{p_{j,S}}{1-p_{j,j}} \right] \right).
$$

For $k = 1$ and $k = 2$ the scrap terms are

$$
\begin{aligned}
Sr_{\mathrm{I}} = SC_{\mathrm{I}}\, p_{\mathrm{I},S} &- SC_2 \left[\left(p_{\mathrm{I},2} + \frac{p_{\mathrm{I},4}p_{\mathrm{I},2}}{1-p_{\mathrm{I},4}} \right) \frac{p_{2,S}}{1-p_{2,2}} \right] && \text{for } k = 1 \\
&- SC_3 \left[\left(p_{\mathrm{I},3} + \frac{p_{\mathrm{I},4}p_{\mathrm{I},3}}{1-p_{\mathrm{I},4}} \right) \frac{p_{3,S}}{1-p_{3,3}} \right] \\
&- SC_4 \left[\frac{p_{\mathrm{I},4}\, p_{4,S}}{1-p_{4,4}} \right]. && \text{for } k = 2
\end{aligned}
$$

There are three rework terms for this single manufacturing stage (I), given by,

$$
Rw_{\mathrm{I}} = RC_2\, m_{\mathrm{I},2} + RC_3\, m_{\mathrm{I},3} + RC_4\, m_{\mathrm{I},4}
$$

Thus the expected profit from Equation 3.82 is,

$$
\begin{aligned}
E(PR) \;=\;& SP\, f_{\mathrm{I},C} - PC - SC_1\, p_{\mathrm{I},S} - SC_2 \left(p_{\mathrm{I},4} \left(\frac{p_{\mathrm{I},2}}{1-p_{\mathrm{I},4}} \right) + p_{\mathrm{I},2} \right) f_{2,S} \\
-\;& SC_3 \left(p_{\mathrm{I},4} \left(\frac{p_{\mathrm{I},3}}{1-p_{\mathrm{I},4}} \right) + p_{\mathrm{I},3} \right) f_{3,S} - SC_4 \left(\frac{p_{\mathrm{I},S}}{1-p_{\mathrm{I},4}} \right) p_{\mathrm{I},4} \\
-\;& RC_2\, m_{\mathrm{I},2} - RC_3\, m_{\mathrm{I},3} - RC_4\, m_{\mathrm{I},4}.
\end{aligned}
$$

As before, the transition matrix (P) is required to establish the $\boldsymbol{F}$ and $\boldsymbol{M}$ matrices, which contain the f and m terms. As $k = [1, 2]$, there are two $\boldsymbol{\Gamma}$-matrices corresponding

Stats.	Values	**Costs**	Values
$\boldsymbol{L}$	$[8, 13]$	SP	$[120]$
$\boldsymbol{U}$	$[12, 17]$	PC	$[45]$
$\boldsymbol{\sigma}$	$\sigma_{x_1} = \sigma_{x_2} = 1$	RC	$[15, 12, 27]$
		SC	$[27, 27, 27, 27]$

TABLE 3.7: Specification limits, process variation and cost related for two features produced in parallel in a single manufacturing stage

to each k-value, where the parameters of the $\boldsymbol{J}$ and $\boldsymbol{S}$-matrices vary according to the α and η terms (given in Table 3.6).

$$ {}^{k}\boldsymbol{\Gamma}_w = \sum {}^{1}\boldsymbol{S}_{\forall\,[\alpha,\eta],j}\, {}^{1}\boldsymbol{J}_{\forall\,[\alpha,\eta],j} $$

The k dependent $\boldsymbol{J}$ terms are,

$$ {}^{1}\boldsymbol{J} = \begin{array}{c} \\ 2 \\ 3 \\ 4 \end{array} \begin{array}{c} \begin{array}{cc} 2 & 3 \end{array} \\ \begin{bmatrix} p_{2,2} & p_{2,3} \\ p_{3,2} & p_{3,3} \\ p_{4,2} & p_{4,3} \end{bmatrix} \end{array} \quad \text{and} \quad {}^{2}\boldsymbol{J} = \begin{array}{c} \\ 4 \end{array} \begin{array}{c} \begin{array}{c} 4 \end{array} \\ \begin{bmatrix} p_{4,4} \end{bmatrix} \end{array}, $$

from which the transition matrix (Equation 3.60) can be constructed. The resulting transition matrix is the same as Equation 3.35 shown in Section 3.2.2. The $\boldsymbol{M}$ and $\boldsymbol{F}$ matrices are also illustrated in this Section (Equations 3.38 and 3.37 respectively). This completes the information required to compute the expected profit for two features produced in parallel in a single stage.

The process specification limits, variability and costs are shown in Table 3.7. To make this example comparable to the production of two features in two manufacturing stages the same data was used (Table 3.5 determined by summing the production cost for stage I and II from Table 3.5. Similarly, the rework cost for dual feature rework was the sum of the rework cost for each feature independently and the scrap cost was the sum of the costs associated with scrapping each component independently. The scrap costs were the same irrespective of which feature caused scrap, since a single scrap feature caused the whole component to be designated scrap. Note, although a dual stage process was examined in Section 3.2.2 (see input data in Table 3.1), the input data was changed to match the serial production examples in Section 3.4.1.

Figure 3.26 illustrates the production, scrap and rework costs as well as profit versus the mean settings μ_{x_1} and μ_{x_2}. While profit is given by Equation 3.82, production cost is $E(PR) - SP\, f_{\text{I},C}$. Rework cost and scrap cost are also contained within Equation 3.82. The highest profit 71.17 (obtained using Matlab's *fmincon* function (Mathworks

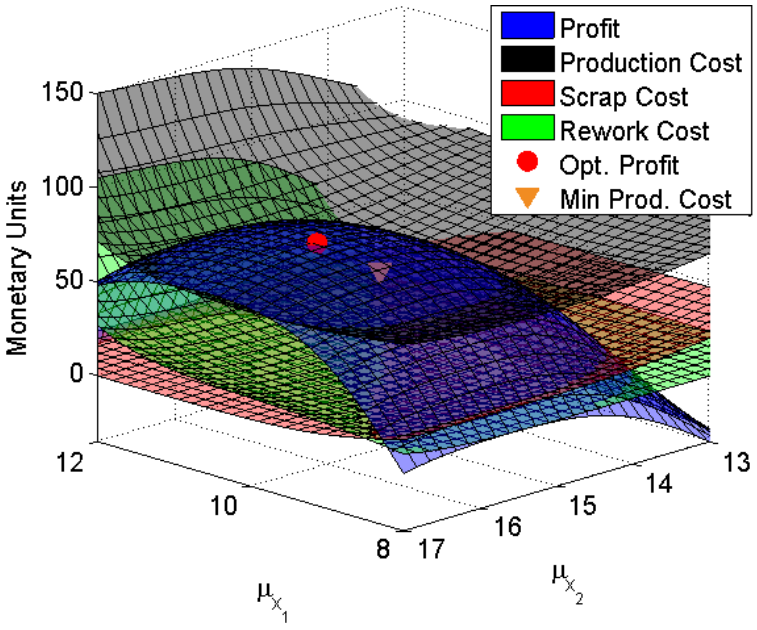

FIGURE 3.26: Variation of expected profit, scrap, rework, and total production costs with the means (μ_{x_1} and μ_{x_2}) in a single manufacturing stage

[2012])), with $\mu_{x_1} = 10.537$ and $\mu_{x_2} = 15.590$ was $\approx 0.3\%$ less than achieved when each feature was manufactured independently (previous example). The minimum production cost was 46.753, located at $\mu_{x_1} = 10.128$ and $\mu_{x_1} = 15.181$. Since there was only one manufacturing stage there was no monetary benefit to biasing scrap for the first feature to reduce production cost, as was observed in the previous example.

d. Multiple Features, Multiple Stages

Equation 3.78 was derived in order to specify the expected profit for the production of any number of features in any combination of serial and parallel operations. The expected profit for all eight possible permutations for the production of four features is illustrated here. This study gives the optimum number of inspection stations to maximise the profit for the production of features. Since parallel operations combine the production of at least two features, this removes at least one dedicated feature inspection stage. Removing an inspection stage may have a financial benefit, but also increases the risk of scrapping a component. Such a principle is analogous to a study by Mittal and McNally [1994] (with a numerical example in Marsh et al. [2010]), where the number of inspection stages were optimised to maximise profit for semiconductor manufacturing. A numerical example is given here, derived from the production of four features used by Bowling et al. [2004] and Selim and Al-Zu'bi [2011].

Bowling et al. [2004] and Selim and Al-Zu'bi [2011] showed the expected profit for the four features produced in series, the other seven combinations of series and parallel

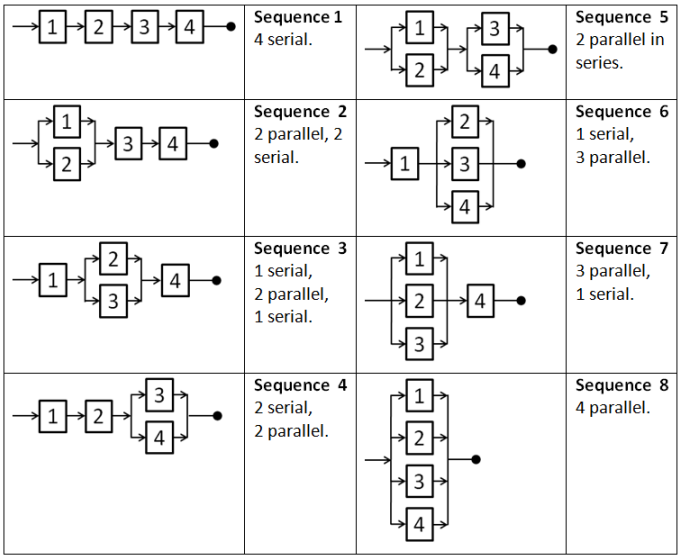

FIGURE 3.27: Possible manufacturing sequences for four features

operations are considered are detailed by Figure 3.27. As was implicitly assumed in the example from Bowling et al. [2004] and Selim and Al-Zu'bi [2011], the order the features are produced is considered important, such that the first feature must be produced before the second and so on. The inspection processes are not shown in Figure 3.27, but an inspection process is implicit after each stage (after each block or column of blocks) and applies just to the feature or features in that block or column. Therefore, Sequence 1 had four inspection processes, Sequence 2 had three inspection processes and Sequence 8 had just one inspection process, inspecting all four features in one inspection operation. Table 3.8 gives the costs, process variations and upper and lower specification limits used by the numerical example, which are the same data used by Bowling et al. [2004] and Selim and Al-Zu'bi [2011]. The selling price was 120 units.

	Feature			
Parameter	**1**	**2**	**3**	**4**
PC	25	20	12	15
RC	15	12	8	10
SC	10	17	5	12
L	8	13	10	7
U	12	17	14	11
σ	1	1	1	1

TABLE 3.8: Cost and process data for the four features

The scrap, processing and rework costs from the serial examples given by Bowling et al. [2004] and Selim and Al-Zu'bi [2011] are not directly applicable to parallel processes. To ensure continuity between the eight manufacturing sequences costs were allocated as follows:

- The scrap costs for parallel processes were cumulative. Therefore, if any one feature was scrap, the sum of all the feature scrap costs in that parallel process were taken as the realised scrap cost. For example, if feature 2 was scrap from Sequence 3 (Figure 3.27), the scrap cost was calculated as $10 + 17 + 5 = 32$. Even though features 1 and 3 may have conformed, the item was still scrap (due to feature 2). Therefore it incurred the feature 3 scrap cost (as feature 3 was still manufactured).

- The processing costs were also cumulative. Thus, the processing cost for a parallel operation was the sum of all the feature processing costs in that parallel operation. Therefore, the processing cost for the second stage of Sequence 3 was, $20+12 = 32$ (the feature 2 and feature 3 PCs).

- Rework created from parallel operations could apply to single or multiple features. For the parallel operation (stage 2) in Sequence 3, the rework operations were either single feature rework on feature 2 or feature 3, or dual feature rework on both features 2 and 3. The rework costs were 12, 8 and 20, respectively.

Equation 3.78 was used to determine the expressions for expected profit for each of the eight sequences shown in Figure 3.27. The means for each feature were then optimised to maximise profit using Matlab's *fmincon* function Mathworks [2012]. Two sets of results were obtained, $E(PR)$ and $E(PR)-I$ (Figure 3.28). The value $E(PR)$ is the result from Equation 3.78 while the $E(PR) - I$ accounts for the cost of an inspection station, given the inspection cost I. The presence of an inspection operation incurred a cost of 0.5 units with a further 0.5 units for each feature inspected. The inspection costs for each sequence are tabulated in Table 3.9. The variation of the inspection costs was designed to represent the likelihood that it would cost less to inspect several features together, than to have a dedicated inspection stop for each feature, before manufacturing the next feature.

The $E(PR)$ results show Sequence 1 was the most profitable method of manufacturing the four features and Sequence 8 the least profitable (Figure 3.28 and Table 3.9). Sequence 1 was more profitable as total scrap cost was minimised, since the failure of any feature to conform only resulted in the scrap cost up to that point. The failure of any feature to conform in Sequence 8 resulted in the scrap cost for all four features, irrespective of which one failed. For example, consider the possibility that feature 2 was designated scrap in both sequences. The total scrap cost for Sequence 1 would be the sum of the scrap costs for the first and second features, 27 units. The total scrap cost for Sequence 2 would be 44 units, since the whole item would be scrapped despite the fact that the other three features may have conformed. The $E(PR) - I$ results show Sequence 1 was the least profitable and Sequence 6 was the most profitable. Reducing

Seq.	Optimal Means	$E(PR)$	I	$E(PR) - I$	Rank 1	Rank 2
1	[10.389, 15.537, 12.674, 9.660]	41.7523	4	37.7523	1	8
2	[10.482, 15.535, 12.667, 9.660]	41.4665	3.5	37.9665	4	7
3	[10.388, 15.570, 12.666, 9.660]	41.6588	3.5	38.1588	2	5
4	[10.388, 15.537, 12.711, 9.659]	41.6501	3.5	38.1501	3	6
5	[10.482, 15.535, 12.711, 9.659]	41.3642	3	38.3642	6	4
6	[10.388, 15.615, 12.710, 9.657]	41.4215	3	38.9215	5	1
7	[10.516, 15.568, 12.664, 9.660]	41.2628	3	38.7628	7	3
8	[10.560, 15.613, 12.708, 9.656]	40.8657	3	38.8657	8	2

TABLE 3.9: Expected profit and means for the eight manufacturing sequences

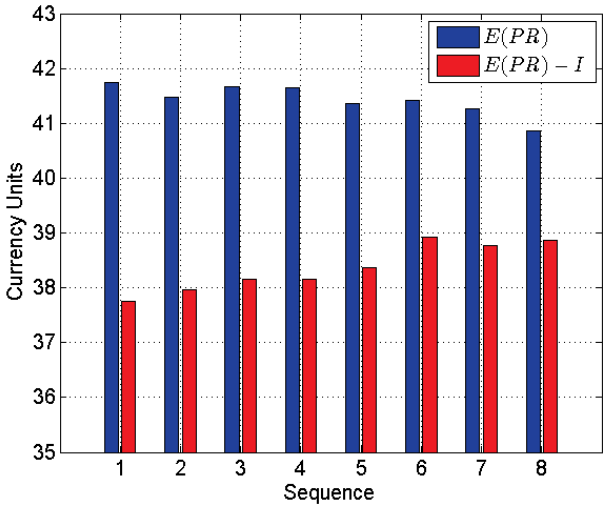

FIGURE 3.28: Expected profit for the eight manufacturing sequences

the number of inspection operations was clearly beneficial, however, not worth the extra scrap cost risk by producing all four features in parallel (Sequence 8). Despite the similarity between Sequences 6 and 7, Sequence 6 was ranked 1 while Sequence 7 was ranked 3 (heading 'Rank 2' on Table 3.9). The relatively high cost of scrap for feature 4 was the primary factor in this. While it was worth the higher scrap cost to reduce the number of inspection operations in Sequence 6, this was not the case in Sequence 7 as the increased scrap cost of feature 4 was too great.

3.5 Optimal Mean Setting for Parallel Production

Section 3.1.2 revealed that greater profit could be gained from parallel production systems by optimising the feature means separately depending on the number of features in a rework stage. This new optimisation procedure for Optimal Mean Setting is referred to a Case II while the conventional methodology present in the literature is referred to

as Case I. In this section the corrected Markovian methodology (from Section 3.2.2) was used to compare the Case II Optimal Mean Setting method with the Case I method.

3.5.1 Comparison of Case I and Case II Optimal Mean Setting Methodologies for Two Features

The flow of features through a dual feature production system was illustrated by Figure 3.5. For the Case I methodology, the mean settings for features x_1 and x_2 in the initial state and state 4 are the same as x_1 in state 2 and x_2 in state 3. In the Case II methodology, the mean settings for features x_1 and x_2 in the initial state and state 4 are optimised separately to the single feature rework in states 2 and 3. Therefore, two means were optimised using the case I methodology and four means were optimised in the case II methodology. Two sets of cost values and statistical moments applicable to the dual feature Optimal Mean Setting problem were available from Khasawneh et al. [2008] and Peng and Khasawneh [2014]. Different values have been used here to better graphically highlight the profit differences between the Case I and Case II methods. The cost values and statistical moments of the problem are shown in Table 3.10. The scrap costs are the same irrespective of which state a component is in when it gets designated scrap. Both Khasawneh et al. [2008] and Peng and Khasawneh [2014] used different values depending on the scrap state. For example, the scrap cost for a component scrapped from state 2 was less than the scrap cost for a component scrapped in state 4. This implies that the rework operations add value to a component. This is true for certain operations such as additive manufacturing processes, however, it is not necessarily true for material removal operations. Ultimately the cost of scrap at various states depends on the specifics of the component, features, process and the manufacturer's contracts in the way scrap cost is determined. A flat cost value for each state was used for this example as it simplifies the subsequent analysis for determining the effect of the Case II optimisation method versus the Case I optimisation method. An example of varying scrap costs for each rework state is given in Appendix D. The expected profit given from Equation 3.78

Variable	***Value***
$\mathbf{U}$	[6 6]
$\mathbf{L}$	[4 4]
Rc	[25 25 50]
Sc	[150, 150, 150, 150]
SP	500
PC	50
$\mathbf{\Sigma}$	$[2, 0; 0, 2]$

TABLE 3.10: Dual feature numerical example input parameters

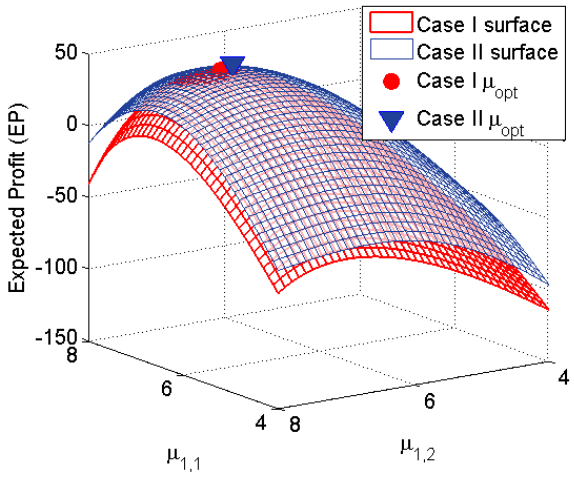

FIGURE 3.29: Profit surfaces for Case I and Case II (optimisation of two and four means respectively)

was plotted for values of $\mu_{1,1}$ and $\mu_{1,2}$ in Figure 3.29. Case I represents the variability of expected profit for $\mu_{1,1}$ and $\mu_{1,2}$. The case II surface was generated by inputting a $\mu_{1,1}$, $\mu_{1,2}$ pair and resolving the $\mu_{2,1}$ and $\mu_{2,2}$ values by satisfying Equation 3.78 for the specified $\mu_{1,1}$ and $\mu_{1,2}$ inputs[12]. The Matlab function '*fmincon*' (Mathworks [2012]) was used to implement this. The case II surface is higher at every point due to optimising the single feature rework means separately from dual feature processing. This also yielded slightly different $\mu_{1,1}$ and $\mu_{1,2}$ optimum values, as there was no compromise between dual feature and single feature cost. The dual feature means were lower than the single feature means, primarily due to the R_{X_1,X_2} rectangle in (Figure 3.31). Components falling into this region (R_{X_1,X_2} rectangle) experienced double the single feature rework cost as well as the increased probability of further rework. The double feature rework state did not exist for a single feature, which allowed the single feature means to be biased to a greater extent towards rework than the double feature case, without incurring a cost penalty. The profits and Optimal Mean Settings are displayed in Table 3.11 which corresponds to the markers on Figure 3.29.

The bar plot in Figure 3.30 shows the rework and scrap costs from the initial and rework states, that were described on Figure 3.5. The initial scrap cost was less for Case I compared to Case II (Sr_I bar in Figure 3.30)) as $\mu^{\text{I}}_{1,1}$ and $\mu^{\text{I}}_{1,2}$ were more rework biased than $\mu^{\text{II}}_{1,1}$ and $\mu^{\text{II}}_{1,2}$. Consequentially, the dual feature rework cost (Rw_4) for Case I was comparatively high due to this rework bias. The last two Case II means, $\mu^{\text{II}}_{2,1}$ and $\mu^{\text{II}}_{2,2}$, which applied to single feature rework, were higher than $\mu^{\text{I}}_{1,1}$ and $\mu^{\text{I}}_{1,2}$, generating less Sr_2 and Sr_3 scrap from Case II, but more Rw_2 and Rw_3 rework. There

[12]For Case II, $\mu_{1,1}$, $\mu_{1,2}$ are the means applied when both features are manufactured or reworked prior to an inspection process. The $\mu_{2,1}$ and $\mu_{2,2}$ means are applied when features are manufactured or reworked independently.

	Value
Case I Profit	40.87
Case II Profit	41.66
Case I Production Cost	146.44
Case II Production Cost	145.75
Case I means $(\mu^{\mathrm{I}}_{1,1}, \mu^{\mathrm{I}}_{1,2})$	6.85, 6.85
Case II means $(\mu^{\mathrm{II}}_{1,1}, \mu^{\mathrm{II}}_{1,2}, \mu^{\mathrm{II}}_{2,1}, \mu^{\mathrm{II}}_{2,2})$	6.75, 6.75, 7.02, 7.02
Case I Final Conformance Prob.	0.5933
Case II Final Conformance Prob.	0.5935
Case I Final Scrap Prob.	0.4067
Case II Final Scrap Prob.	0.4065

TABLE 3.11: Optimisation results

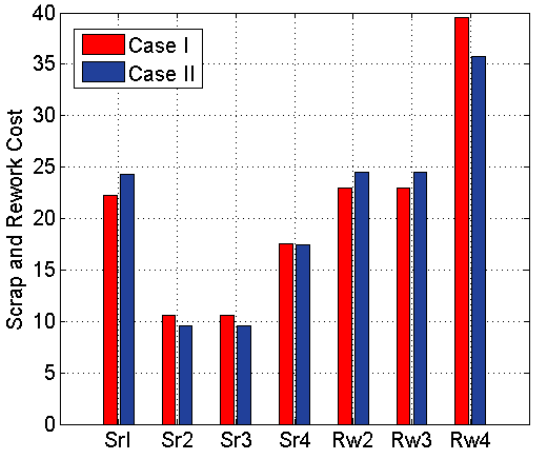

FIGURE 3.30: Scrap and rework costs from the initial and rework states

was a slightly higher production of dual feature scrap, Sr_4, for Case I compared to Case II. The reason for this is multifaceted; firstly the probability of scrap from the dual feature rework state (state 4) for Case I was 0.1481, but greater for Case II at 0.1622. However, the probability of producing dual feature rework was greater for Case I with the probability $p_{\mathrm{I},4} = p_{4,4} = 0.4418$ compared to 0.4171 for Case II. Accounting for the initial probability of components feeding into the dual feature rework state (state 4) and the probability of rework back into the dual feature rework state, the probability for Case I was $p_{\mathrm{I},4}/(1-p_{4,4}) = 0.7914$ and 0.7155 for Case II. Thus the probability of scrap from the state 4, for Case I was $(p_{\mathrm{I},4}/(1-p_{4,4})) * p_{4,S} = 0.7914 * 0.1481 = 0.1172$. For Case II the scrap probability from the state 4 was lower at $(p_{\mathrm{I},4}/(1-p_{4,4})) * p_{4,S} = 0.7155 * 0.1622 = 0.1161$, hence the lower scrap cost for Case II relative to Case I. Overall, the reduced scrap and dual feature rework costs from the case II led to a reduced production cost and a 1.93% increase in profit over Case I. The number of items eventually conforming was also slightly higher in Case II.

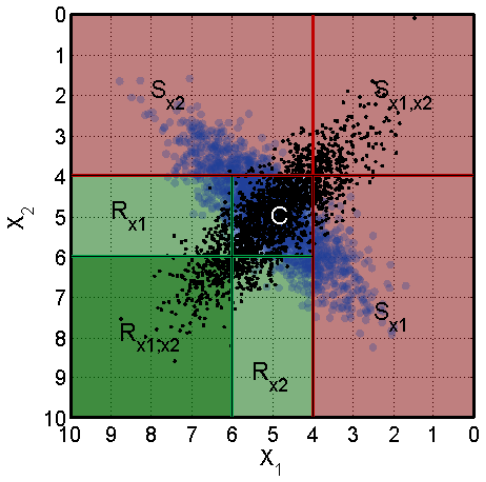

FIGURE 3.31: Scatter plot with correlation ($\rho = -0.8$ and $\rho = 0.8$)

3.5.2 Influence of Correlation

Correlation alters the probability of components falling into single and dual feature rework states, which in turn may influence the optimal means. Figure 3.31 indicates the scatter of points with correlation, $\rho = 0.8$ and $\rho = -0.8$ where the correlation matrix is,

$$\mathbf{\Sigma} = \begin{bmatrix} \sigma_1 & \rho\sigma_1\sigma_2 \\ \rho\sigma_1\sigma_2 & \sigma_2 \end{bmatrix}.$$

The black points correspond to the $\rho = 0.8$ value, while the blue points correspond to $\rho = -0.8$. Table 3.12 indicates the differences between the number of points falling in the various regions after one processing operation (defined in Figure 3.7) compared to the uncorrelated example, where $\rho = 0$. Both positive and negative correlation almost halved the probability of points falling in the single feature rework regions compared to no correlation. Conformance was increased in both cases. The changes in scrap and dual feature rework depended on the sign of the correlation parameter ρ. Positive correlation almost quadrupled the probability of dual feature rework and reduced the probability of scrap by around a quarter. Negative correlation reduced the probability of dual feature rework by a factor of over 500 and slightly increased the probability of scrap. This is clear from the orientations of the point clusters in Figure 3.31.

The effect of correlation on the optimal means and profits are tabulated in Table 3.13. For $\rho = 0.8$, profits were greater for both Case I and II over the uncorrelated example due to a reduced scrap and rework cost and higher overall conformance. The profit increase when $\rho = -0.8$, for Cases I and II, was solely due to the reduction in production cost (scrap and rework cost); the final conformance was slightly lower than the uncorrelated example (Table 3.11).

Region	$\rho = 0.8$	$\rho = 0$	$\rho = -0.8$	Ratio, $\rho = 0.8$	Ratio, $\rho = -0.8$
R_{x1}	0.0610	0.1083	0.0610	0.5632	0.5623
R_{x2}	0.0610	0.1083	0.0610	0.5632	0.5623
$R_{x1,x1}$	0.0976	0.0252	5.62E-5	3.8730	0.0022
C	0.5608	0.4661	0.5608	1.203	1.203
S	0.2196	0.2922	0.3173	0.7515	1.0860

TABLE 3.12: Impact of correlation on the probability of components falling into rework, scrap and conformance

The Case I means for $\rho = 0.8$ were lower than the Case I means with no correlation, $\rho = 0$, to reduce the proportion of components falling into the R_{X_1,X_2} region, given positive correlation increased the probability of R_{X_1,X_2} rework. The $\mu^{\text{II}}_{1,1}$ and $\mu^{\text{II}}_{1,2}$ means for $\rho = 0.8$ were lower than the $\mu^{\text{II}}_{1,1}$ and $\mu^{\text{II}}_{1,2}$ means for $\rho = 0$, for the same reason. They were also lower than the $\mu^{\text{I}}_{1,1}$ and $\mu^{\text{I}}_{1,2}$ means (for $\rho = 0.8$), as they were optimised separately to the single feature means. Note, the $\mu^{\text{II}}_{2,1}$ and $\mu^{\text{II}}_{2,2}$ means are very similar to the uncorrelated case ($\rho = 0$) indicating correlation did not affect the Optimal Mean Setting for the single feature rework means.

The Case I means for $\rho = -0.8$ were also lower than in the uncorrelated case. To reduce cost, the extremities of the negatively correlated scatter region in Figure 3.31 moved to reduce the probability of scrap but not so far to make rework, specifically $R_{x_1}R_{x_2}$ rework, too significant. This was achieved by shifting the mean of the distribution towards to (0,0) compared to the uncorrelated case ($\rho = 0$), but to a lesser extent than in the positive correlated case ($\rho = 0.8$). The $\mu^{\text{II}}_{1,1}$ and $\mu^{\text{II}}_{1,2}$ means of Case II, where $\rho = -0.8$, were also lower than the uncorrelated case for the same reason and again lower than $\mu^{\text{I}}_{1,1}$ and $\mu^{\text{I}}_{1,2}$ due to the differences between the case I and case II methodologies (as explained in Section 3.2.2). The $\mu^{\text{II}}_{2,1}$ and $\mu^{\text{II}}_{2,2}$ means from Case II were the same as the uncorrelated and positive correlated cases as they only applied to single feature rework and therefore were not affected by correlation.

The sensitivity of profit to correlation is plotted in Figure 3.32 for both cases. The difference between the two cases is shown by the orange line and corresponds to the scale on right hand y-axis. In general, the greater the degree of positive or negative correlation the higher the profit with a minimum profit existing at $\rho \approx 0.22$. The actual minimum profit for a given correlation depended on the geometry of the scrap and rework regions and relative standard deviations and tolerance bounds of each feature. As $\rho \to 1$ the difference between the two and four mean case diminished as all components designated rework lay in the dual feature rework region. Thus, the benefit of separately optimising the single feature rework means was lost as there was negligible single feature rework. This is evident by considering Figure 3.31, the black points would converge on a single diagonal as $\rho \to 1$. The same converging effect occurs for $\rho \to -1$, although the line

ρ	Cases	***Value***
0.8	Case I Profit	56.4038
0.8	Case II Profit	58.3309
0.8	Case I Production Cost	140.24
0.8	Case II Production Cost	138.93
0.8	Case I Final Conformance	0.6166
0.8	Case II Final Conformance	0.6181
0.8	Case I means $(\mu^{\mathrm{I}}_{1,1}, \mu^{\mathrm{I}}_{1,2})$	6.65, 6.65
0.8	Case II means $(\mu^{\mathrm{II}}_{1,1}, \mu^{\mathrm{II}}_{1,2}, \mu^{\mathrm{II}}_{2,1}, \mu^{\mathrm{II}}_{2,2})$	6.52, 6.52, 7.02, 7.02
−0.8	Case I Profit	45.11
−0.8	Case II Profit	47.10
−0.8	Case I Production Cost	139.65
−0.8	Case II Production Cost	136.60
−0.8	Case I Final Conformance	0.5869
−0.8	Case II Final Conformance	0.5842
−0.8	Case I means $(\mu^{\mathrm{I}}_{1,1}, \mu^{\mathrm{I}}_{1,2})$	6.80, 6.80
−0.8	Case II means $(\mu^{\mathrm{II}}_{1,1}, \mu^{\mathrm{II}}_{1,2}, \mu^{\mathrm{II}}_{2,1}, \mu^{\mathrm{II}}_{2,2})$	6.57, 6.57, 7.02, 7.02

TABLE 3.13: Optimisation results for correlated features

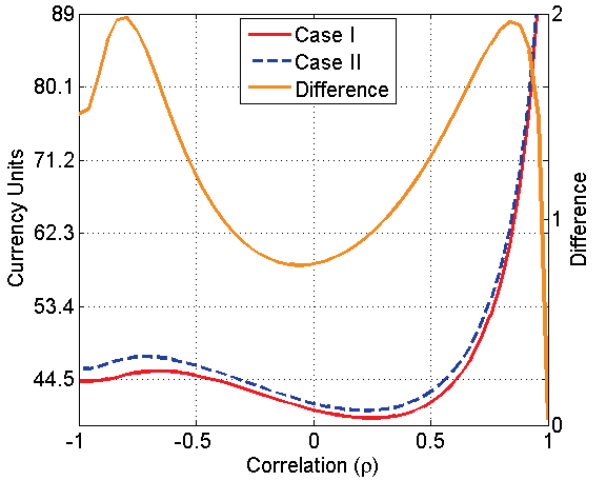

FIGURE 3.32: Profit vs. correlation

orientation is changed by 90 degrees. However, as can be seen from Figure 3.31, the blue points would remain in the single feature rework regions as $\rho \to -1$. It is also likely dual feature rework would exist (depending on the geometry of the scrap and rework regions and the standard deviation), thus there would still be a benefit to optimising dual and single feature means separately. This led to the profit difference between Case I and II for negative correlation.

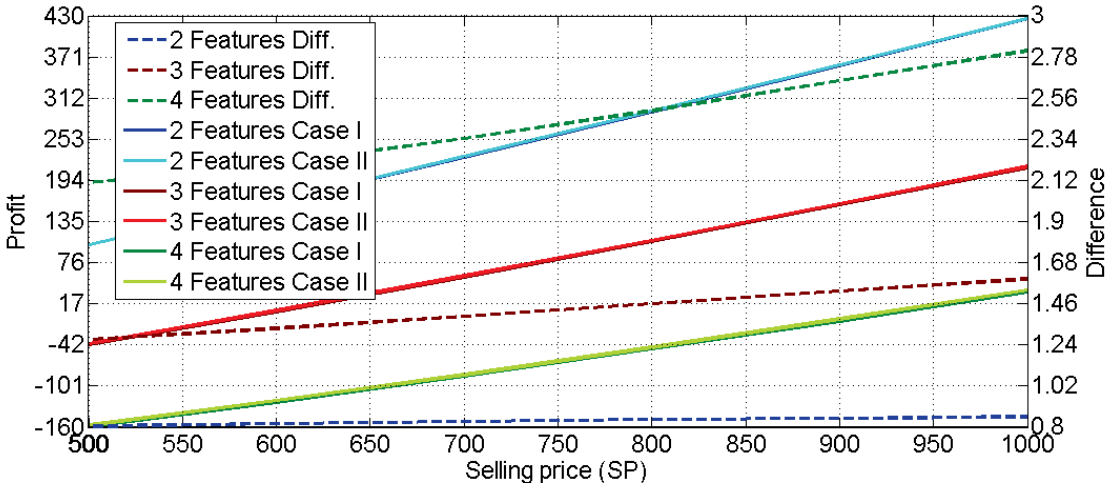

FIGURE 3.33: Profit and profit differences between Case I and Case II methodologies for two, three and four features

3.5.3 Multiple Features - Case I and Case II Comparison

The greater the number of features being manufacturing prior to an inspection operation (parallel production), the greater the potential benefit of the Case II methodology over the Case I methodology. This statement is supported by Figure 3.33. Profit is shown in the left y-axis while the difference between the Case I and Case II methodologies is indicated on the right y-axis. The x-axis represents selling price which determines the maximum profit for each two, three and four feature example. The profits for each of the two, three and four feature examples were optimised with both the Case I and Case II methodologies (solid lines on Figure 3.33). The profit differences between Case II and Case I methods are illustrated by the dashed lines on Figure 3.33. As the number of features increased, there was a clear trend for the differences between the profits (Case II minus Case I) to also increase for all profit levels. The difference for the two feature example was around 0.8, while the profit difference for the four features case varied between ~ 2.1 to ~ 2.8. The statistical moments and costs were kept consistent for each example where $L = 4$, $U = 6$, $\sigma = 2$ and correlation was kept at zero ($\rho = 0$). As the number of features increased, the processing and rework costs remained at $PC = 25$, $RC = 25$ respectively. Scrap cost (SC) was 100 plus the processing cost for each feature (25). Thus, for two features, $SC = 150$, three features, $SC = 175$ and for four features $SC = 200$. Multi-feature rework cost was the sum of the rework costs for each feature, thus for two features $RC = 50$, three feature $RC = 75$ and four features $RC = 100$.

The Case II methodology has clear profit advantage over the Case I methodology used in the literature. The increased effectiveness of the Case II methodology has sound principles discussed in detail in Section 3.1.2 but stems from the fact the Optimal Mean

Settings to maximise profit are different for multi-feature rework compared to single feature rework. The means optimised via the Case I method are a compromise between all rework costs.

The practicality of using the Case II methodology is limited by the ability of the optimisation algorithm to handle large numbers of dimensions due to the matrix inversion (To find the $\boldsymbol{M}$-matrix, shown in Section 3.2). The number of means required to be optimised with the Case II methodology scales as N^2, where N is the number of features. In contrast, the number of means required to be optimised with the Case I methodology scales with the number of features, N. As was shown in Appendix A, the profit function is convex and therefore local search optimisation algorithms are suited to the task such as Matlab's *fminsearch* (Mathworks [2012]). If speed of optimisation is critical (for high N) it may be possible to reduce the dimensionality of the problem, since the probability of rework for single and low combinations of features is higher than for rework involving all or most of the features. Therefore, it may be practical to leave out the means for rework with high numbers of features, as these are unlikely to make a significant impact on profit. Alternatively Section 5.2.3 of the Future Work section discusses a method to avoid the matrix inversion in the first place removing this limitation.

The performance of the Case II method over the Case I method is dependent on the exact nature of the problem in terms of statistical moments, specification limits and the costs and selling price. The conditions under which the Case II method has advantages over the Case I method are:

a. Where the cost of rework involving multiple features is greater than the cost of rework involving low numbers of features, or single features.

b. Where correlation biases the probability of particular type or types of rework. If all types of rework were equally probable, and the rework costs were all equal, the Case II method would return the same result as the Case I method.

Chapter 4

Uncertainty Modelling with Non-Normal Distributions

This Chapter investigates the outcome of using Optimal Mean Setting on the distribution of the manufactured geometry. The act of processing rework modifies the feature distribution from the original normal distribution to some truncated form. In the case of parallel production utilising Optimal Mean Setting several optimal means exist (depending on the type of rework), which make the feature distribution non-normal. These features either progress to subsequent manufacturing stages or form part of the final geometry of the component. It is important to establish the shape of feature distributions as it may impact the rework and scrap probabilities of subsequent manufacturing operations and will affect the performance distribution of the finished component.

The effect of non-normal distributions (created from applying Optimal Mean Setting) on the final manufactured distribution of components has not been studied in the literature. Although Bowling et al. [2004], Khasawneh et al. [2008], Selim and Al-Zu'bi [2011] and Peng and Khasawneh [2014] all studied the final shape of feature distributions after rework, the final shape of the manufactured component, comprising of several features is only given by studying the joint distribution. Parametric distributions, like the normal distribution, often have multivariate forms which can be used to model the joint distribution for several features. However, this requires that all of the component's feature distributions can be represented by a univariate (marginal) version of the joint parametric distribution. As was seen in Section 3.1.2 in Chapter 3, Optimal Mean Setting for parallel production will not give normal feature distributions (even if the process variation is inherently normal), as the single feature rework mean is different to the dual feature mean. Furthermore, the manufacturing process variation may not be normal in the first place. In these cases the joint distribution cannot be given by a

multivariate parametric distribution, as the distributions for the features may be from different parametric families[1]. For variations of truncated normal distributions this problem can be solved by utilising mixture models, this is investigated in Section 4.1. However, for generalised cases the mathematical concept of copulas functions are used to create joint distributions for any general feature distribution (Section 4.2). This Chapter describes the application of copula functions to the area of Optimal Mean Setting which is the primary contribution to knowledge, (as implied in point 4, Section 1.6 in Chapter 1). A practical case study is used in Section 4.3 to illustrate how copulas can be utilised in conjunction with Optimal Mean Setting to produce the inner diameters of the big and small ends of a connecting rod to high precision. The Chapter closes with an in-depth case study of how Optimal Mean Setting may be applied to maximise the performance of a film cooling hole by tolerance tightening (Section 4.4). A comparison is made between the cost of producing the cooling hole using Optimal Mean Setting and a standard production technique. The manufacturing cost is vastly reduced by using Optimal Mean Setting.

4.1 Mixture Models for Truncated Normal Distributions

An illustration of the truncated distribution of a single feature subject to rework was shown in Figure 3.2 (pink line). Given the variation of the manufacturing process is normally distributed the equation for such a distribution follows from the definition of the normal probability density and cumulative density distributions (Wilhelm et al. [2010]),

$$f(\boldsymbol{x},\boldsymbol{\mu},\boldsymbol{\sigma},\boldsymbol{L},\boldsymbol{U}) = \frac{\exp\{-\frac{1}{2}(\boldsymbol{x}-\boldsymbol{\mu})^T\boldsymbol{\Sigma}^{-1}(\boldsymbol{x}-\boldsymbol{\mu})\}}{\int_{\boldsymbol{L}}^{\boldsymbol{U}} \exp\{-\frac{1}{2}(\boldsymbol{x}-\boldsymbol{\mu})^T\boldsymbol{\Sigma}^{-1}(\boldsymbol{x}-\boldsymbol{\mu})\}\,\mathrm{d}\boldsymbol{x}} \tag{4.1}$$

This distribution assumes the nominal mean for the reworked features is the same as the nominal mean for the initial operation. Chapter 2 showed the maximum profit for parallel manufacturing systems was generated by optimising the means separately depending on the number of features being processed. Thus the nominal mean for the reworked components was not necessarily the same as the initial operation. Consequently the distribution of conforming components after rework, for parallel operations, is highly likely to be non-normally distributed[2]. One way to model the shape of the distribution

[1] If there is no correlation between the features the joint distribution is simply the product of the two univariate distributions for each feature.

[2] Unless the costs and statistical moments of the problem happen to generate the same optimal means for all rework states, which is highly improbable.

of conforming components, where the means have been optimised using the Case II (multiple mean) methodology, is to construct a Gaussian mixture model,

$$f(\boldsymbol{x}|\boldsymbol{\lambda}) = \sum_{i=I}^{N} w_i \, f(\boldsymbol{x}|\boldsymbol{\mu}_i, \boldsymbol{\Sigma}_i) \tag{4.2}$$

where $\lambda = \{w_i, \boldsymbol{\mu}_i, \Sigma_i\}$ for $i = 1, 2, \ldots, N$ and $f(\boldsymbol{x}|\boldsymbol{\mu}_i, \boldsymbol{\Sigma}_i)$ is given by Equation 3.19 if the features are normally distributed and Equation 4.1 if the feature distributions are truncated. The weighting term, w_i, is the probability of features exiting a particular rework state or the initial operation. For example, in dual feature case, $w_{\text{I}} = p_{\text{I},C}$, $w_2 = f_{2,C}\left(\frac{p_{\text{I},4}p_{\text{I},2}}{(1-p_{\text{I},2})} + p_{\text{I},2}\right)$, $w_3 = f_{3,C}\left(\frac{p_{\text{I},4}p_{\text{I},3}}{(1-p_{\text{I},3})} + p_{\text{I},3}\right)$ and $w_4 = p_{\text{I},4}\left(\frac{p_{\text{I},S}}{1-p_{\text{I},4}}\right)$ corresponding to the quantities labelled in Figure 3.16 in Section 3.2.2. At the end of each stage in a multi-stage system the probability density, $f(\boldsymbol{x}|\boldsymbol{\lambda})$, must also be multiplied by $f_{\text{i},C}$ to give the distribution of only conforming components.

The difference between the manufactured geometry for a two feature parallel production example, obtained using the Case I and Case II optimisation methodologies, is illustrated by Figure 4.1. The specification limits were, $L = [3, 3]$, $U = [7, 7]$, standard deviations were $\sigma_{\mu_1} = \sigma_{\mu_2} = 1$, there was no correlation ($\rho = 0$) and the Case I means were $\boldsymbol{\mu}^{\text{I}} = [5.5, 5.5]$ while the Case II means were, $\boldsymbol{\mu}^{\text{II}} = [5.5, 5.5, 7.0, 7.0]$. The means were arbitrarily chosen (no cost data or optimisation was performed) to illustrate the different geometry distributions, but are similar to what would be expected from an optimisation, where the Case II single feature rework means are more rework biased than the dual feature means. The integral under both surfaces is one, however, the Case II (blue) surface has a flatter peak skewed towards the upper specification limits. This was due to the optimal mean of single feature reworks having values of 7.0 as opposed to 5.5 for the initial operation and dual feature rework stage (stage 4).

In order to establish the distribution of the individual features it is possible to integrate over the probability density surface. The marginal distribution for the x_1-feature can be obtained by integrating f (Figure 4.1) over x_2. Similarly, integrating over x_1 gives the marginal density for the x_2-feature. Since the x_1 and x_2 features have the same distributions it is only necessary to perform the integration over one feature. The marginal distribution for the Case I surface was computed from,

$$f^{\text{I}}_{X_1}(x_1) = \int_{-\infty}^{\infty} \frac{\exp\{-\frac{1}{2}(\boldsymbol{x} - \boldsymbol{\mu}^{\text{I}})^T \boldsymbol{\Sigma}^{-1}(\boldsymbol{x} - \boldsymbol{\mu}^{\text{I}})\}}{\int_{-\infty}^{\boldsymbol{U}} \exp\{-\frac{1}{2}(\boldsymbol{x} - \boldsymbol{\mu}^{\text{I}})^T \boldsymbol{\Sigma}^{-1}(\boldsymbol{x} - \boldsymbol{\mu}^{\text{I}})\} \, \mathrm{d}\boldsymbol{x}} \, \mathrm{d}x_2. \tag{4.3}$$

For the Case II surface let the means for manufacturing dual and single features be differentiated by subscripts α and β. Thus, dual feature manufacturing means are $\mu^{\text{II}}_{\alpha} =$

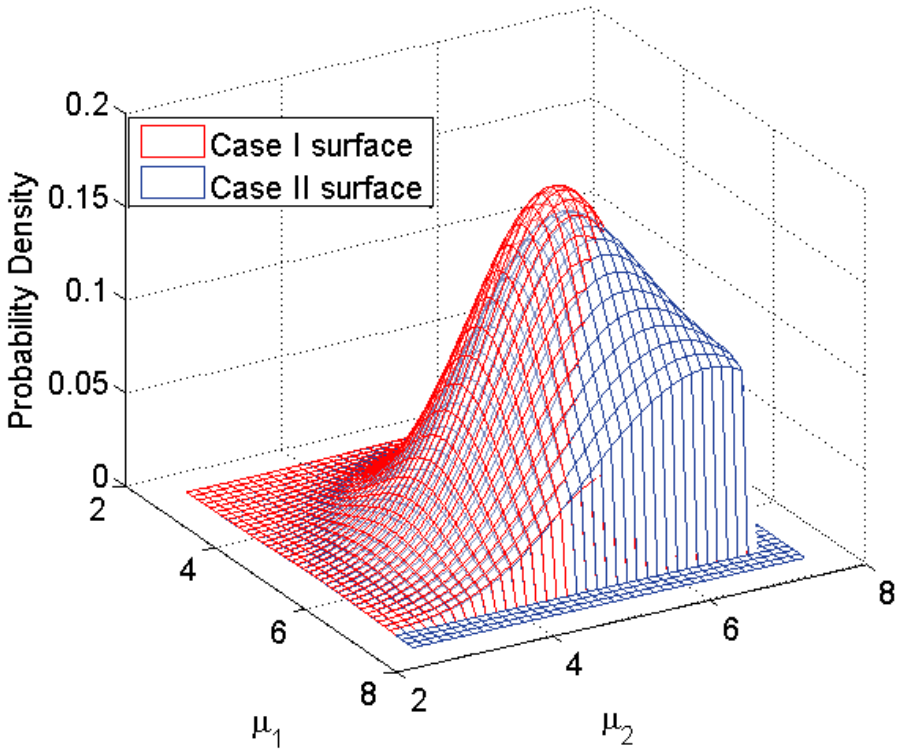

FIGURE 4.1: Difference between the manufactured geometry distributions using the Case I and Case II optimal mean optimisation methodologies

$[5.5, 5.5]$ and the single feature manufacturing means are $\mu_\beta^{\text{II}} = [7, 7]$. The distribution of the x_1-feature is then,

$$f_{X_1}^{\text{II}}(x_1) = \int_{-\infty}^{\infty} \left\{ \left[\frac{\exp\{-\frac{1}{2}(\boldsymbol{x} - \boldsymbol{\mu}_\alpha^{\text{II}})^T \boldsymbol{\Sigma}^{-1} (\boldsymbol{x} - \boldsymbol{\mu}_\alpha^{\text{II}})\}}{\int_{-\infty}^{\boldsymbol{U}} \exp\{-\frac{1}{2}(\boldsymbol{x} - \boldsymbol{\mu}_\alpha^{\text{II}})^T \boldsymbol{\Sigma}^{-1} (\boldsymbol{x} - \boldsymbol{\mu}_\alpha^{\text{II}})\} \, \mathrm{d}\boldsymbol{x}} \right] (w_{\text{I}} + w_4) \right. \\ \left. + \left[\frac{\exp\{-\frac{1}{2}(\boldsymbol{x} - \boldsymbol{\mu}_\beta^{\text{II}})^T \boldsymbol{\Sigma}^{-1} (\boldsymbol{x} - \boldsymbol{\mu}_\beta^{\text{II}})\}}{\int_{-\infty}^{\boldsymbol{U}} \exp\{-\frac{1}{2}(\boldsymbol{x} - \boldsymbol{\mu}_\beta^{\text{II}})^T \boldsymbol{\Sigma}^{-1} (\boldsymbol{x} - \boldsymbol{\mu}_\beta^{\text{II}})\} \, \mathrm{d}\boldsymbol{x}} \right] (w_2 + w_3) \right\} \mathrm{d}x_2, \tag{4.4}$$

with a similar expression for the $x_2 - feature$ marginal distribution. Notice in both cases the limits of the integral in the denominator were set at $-\infty$, this includes all the scrap that would be produced during manufacture. If subsequent manufacturing stages followed it would be necessary to include the lower specification limits L, to truncate the distribution at the lower specification limits. The shape of the marginal distributions are shown in Figure 4.2 for both cases (the distributions for the x_1-feature and x_2-feature are the same hence only one feature for each case is plotted). The introduction of the single feature rework with higher means skewed the distribution mean and mode towards the upper specification limit.

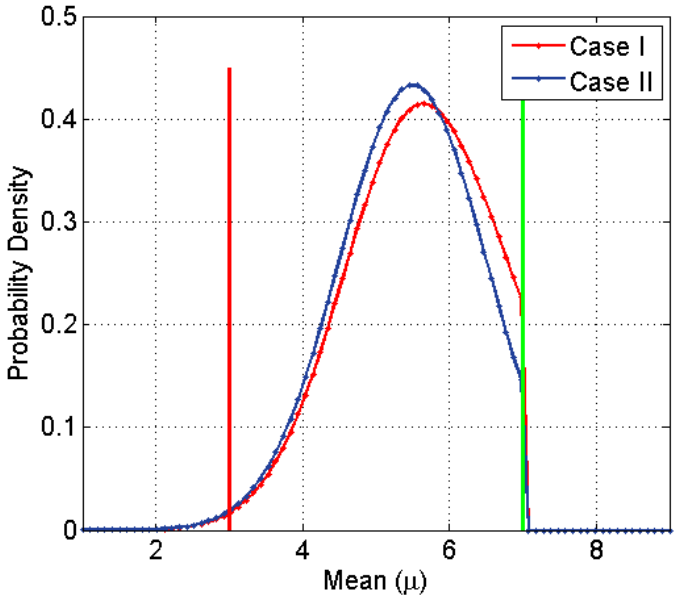

FIGURE 4.2: caption

The weighted sum model (Equation 4.2) is effective in modelling the resulting joint distribution where the Case II optimal mean methodology is applied. However, the multivariate normal distribution model (Equations 4.3 and 4.4) is restrictive in describing the possible shape of variation of manufacturing processes as manufacturing processes are not necessarily normally distributed. One of the earliest examples in the published literature relating to the shape of manufacture geometry is Mansoor [1963]. Here, the likely statistical variations for typical engineering processes such as milling, grinding and reaming were discussed. In more recent examples, Aparisi et al. [1999] and Shorey et al. [2014] indicated the process itself may define the shape of the variation while Singh et al. [2009] noted even inherently normal processes may yield non-normal distributions due to factors such as tool wear and variation in material properties. Ideally it would be possible to model any manufacturing distribution and combine it with other types of distribution to build an exact multivariate representation from the unique marginal distributions. This prohibits the use of parametric distributions, such as the multivariate normal and Student-t distributions, as the marginals must also be part of the multivariate distribution family[3]. Fortunately, a Mathematical construct known as a copula allows any univariate (marginal) distribution to be combined with any other univariate

[3]Often the maximum likelihood function is used to fit parametric distributions to observed data (see Cousineau et al. [2004] for a review and applications of such methods). The same principle could be applied to build fitted multivariate distributions by sampling non-similar parametric marginal distributions, however, the resulting multivariate distribution is only an approximation to the real (observed) distribution. Thus, the scrap, rework and conformance probabilities would not be exact using a fitted model. This would lead to inaccurate optimal means and potentially great differences between theoretical and actual profits. Since copulas allow exact multivariate representations to be generated the fitting of multivariate parametric models is not considered.

distribution, with a specified dependence structure to give a joint (multivariate) distribution. Different copulas allow a wide variety of dependence structures between the univariate distributions. Where there is no dependence between univariate distributions, the joint distribution is the product of the univariate distributions (as shown in Section 4.2.3). Copula modelling allows the probabilities of scrap, rework and conformance to be calculated exactly (providing the dependence between the univariate distributions can be modelled) for multivariate distributions. Recall multivariate distributions are created where two or more features are manufactured prior to inspection (parallel processing).

4.2 Copulas

Copulas are functions for modelling the dependence and interrelationships between random variables, first introduced by Sklar [1959]. They allow one to construct a multivariate distribution from any combination of univariate distributions and apply a range of dependence structures, including non-linear dependence.

The most cited paper in copula literature is David X. Li's paper on default correlation (Li [2000]) which transformed the way collateralised debt obligations (CDOs) were accessed and traded in the early 2000s. More recently the use of copula statistics in financial mathematics has been widely criticised in popular literature. Copula modelling and Li's paper are generally attributed to the collapse of the global financial system in 2008 (Salmon [2009], Jones [2009], Lohr [2009]). It is important to note copula statistics is mathematically sound and many criticisms of the application of the model to CDO pricing are based on an inherent misunderstanding of mathematical modelling [4]

4.2.1 Introduction to Copulas

As demonstrated at the beginning of Chapter 4, processing rework can affect the shape of the manufacturing feature variation resulting in a truncated normal distribution, which represents the variability of the finished manufactured feature. If two or more dependent features have such a distribution, the variability of the manufactured geometry (comprising of two or more features) is modelled by a multivariate truncated normal distribution. Such a distribution can be constructed using a copula function, or alternatively one could use the multivariate truncated normal distribution, however the types

[4] Li's model used the Gaussian copula dependence structure to map correlations between various assets in a CDO portfolio. It was assumed future correlations would follow a similar structure but were subject to change. While the original assumption proved successful for some five years, the dependence structure between assets did alter, thus the inherent CDO risk was miscalculated. Due to the popularity of the model most CDOs were accessed using Li's model which lead to a cascade of defaults in 2007/2008.

of dependence structure are limited. Copulas allow complete freedom of the univariate distribution shape and dependence structure, making them more versatile enough to fit to any manufacturing variation. Furthermore, if an inspectable feature is a result of two or more manufacturing distributions, the resulting variation is unlikely to be a standard parametrised distribution type. Unless this unique distribution can be modelled, it is not possible to accurately calculate the rework, conformance and scrap probabilities or determine the shape of the manufactured geometry variation. Such a situation can be avoided by using copulas to build an exact multivariate representation from the unique marginal distributions.

4.2.2 Definition

Consider the joint cumulative distribution of a set of random variables. In order to gain an understanding of copulas, a bivariate case is considered where the set of random variables are X and Y. The marginal distributions are found from,

$$F_X(x) = \Pr[X \leq x] \quad \text{and} \quad F_Y(y) = \Pr[Y \leq y].$$

These univariate marginal distributions are joined to form the joint distribution function,

$$F_{XY}(x, y) = \Pr[X \leq x, Y \leq y].$$

A copula is a function that represents this joint distribution F_{XY} which exists on the unit cube $[0, 1]^n$ where n characterises the dimensionality of the distribution. By definition $F_X(x)$ and $F_Y(y)$ are restricted to the bound $[0, 1]$ so that a pair of real numbers (x, y) leads to a point $(F_X(x), F_Y(y))$ on the unit cube $[0, 1]^2$. This is depicted in Figure 4.3 where a copula is the mapping which assigns a value to each pair of real numbers of the marginal distributions to form the joint distribution $F(x, y)$. Thus the joint distribution F_{XY}, represented by a copula is,

$$F_{XY}(x, y) = C\left(F_X(x), F_Y(y)\right) = C(u, v). \tag{4.5}$$

where $u = F_X(x)$ and $v = F_Y(y)$.

4.2.3 Sklar's Theorem

Sklar's theorem [Sklar, 1959] asserts that irrespective of the shape of the joint distribution there will be a unique copula satisfying Equation 4.5 given X, Y are continuous. If X, Y are not continuous C is unique for the range $\operatorname{Ran} F_1 \times, \ldots, \times \operatorname{Ran} F_n$ where $\operatorname{Ran} F_n$

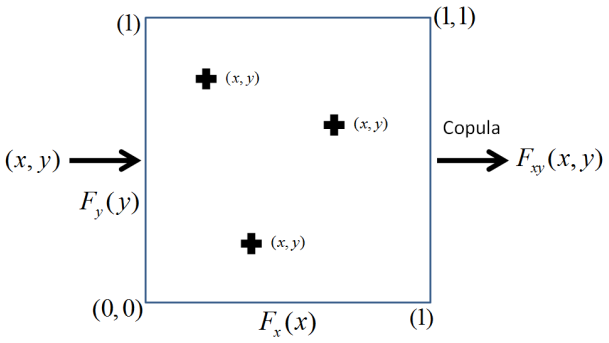

FIGURE 4.3: Mapping of random variables to joint distribution

is the range of the n$^{\text{th}}$ CDF. Note that u, v are uniformly distributed variables on $[0, 1]$, regardless of the functions F_X and F_Y. The arguments of C are also uniformly distributed random variables so all that remains is the dependence structure between the distributions which is modelled by C. Equation 4.5 can be rewritten in terms of C by recognising $x = F_X^{-1}(u)$ and $y = F_Y^{-1}(v)$,

$$C(u, v) = F_{XY}(F_X^{-1}(u), F_Y^{-1}(v)).$$

If F_1 and F_2 are independent then the copula becomes the product of the random variables $C(u, v) = uv$. This is expected as it is analogous to the probability of two independent events occurring simultaneously. The form of the function C is restricted under the following definitions:

(i) $C(0, u) = C(v, 0) = 0$:- Grounded.

(ii) $C(u, 1) = u$ and $C(1, v) = v$:- For $v = 1$, $C(u, 1) = u$ increases from 0 to 1 as u increases from 0 to 1 and similarly for v.

(iii) $C(u_2, v_2) - C(u_2, v_1) - C(u_1, v_2) + C(u_1, v_1) \geq 0$,
$\forall \quad 0 \leq u_1 \leq u_2 \leq 1 \quad \text{and} \quad 0 \leq v_1 \leq v_2 \leq 1$:- 2-increasing, where $C(u, v)$ is increasing for both u and v.

It should be noted these conditions apply for a copula with n dimensions although considerably harder to visualise. Nelsen [2006] and Schmidt [2006] are useful references for the general formulations. The three conditions are graphically represented for the bivariate case in Figure 4.4(a). The copula in this figure is the independent copula $C(u, v) = uv$, thus the surface is simply the product of u and v. Figure 4.4(b) indicates the shape of a copula where there is positive dependence between u and v. Positive dependence implies for any given value of u there is a higher probability that $u = v$ than would be expected if the events were independent. This leads to the distinct ridge or pyramidal shape of Figure 4.4(b)

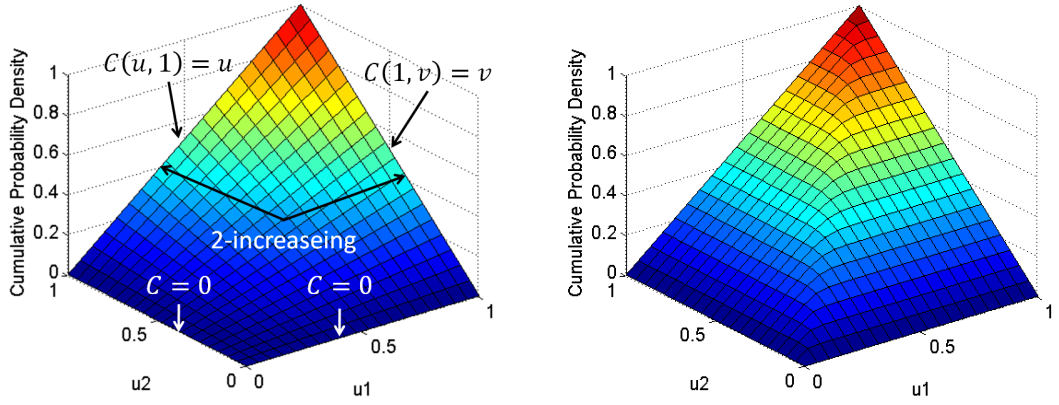

(a) Copula CDF with no correlation

(b) Copula CDF with correlation

FIGURE 4.4: Copula CDFs

The joint density function from the copula formulation is required to model the final manufactured geometry distribution of the component once rework has been carried out on non-conforming features. The density distribution is the derivative of the cumulative distribution,

$$f_{XY}(x,y) = \frac{\partial^2 F_{XY}(x,y)}{\partial x\, \partial y}.$$

Noting Equation 4.5 and recognising,

$$\frac{\partial}{\partial v}\left(\frac{\partial}{\partial u}C(u,v)\right) = \frac{\partial}{\partial x}F_X(x) \quad \text{and} \quad \frac{\partial}{\partial u}\left(\frac{\partial}{\partial v}C(u,v)\right) = \frac{\partial}{\partial y}F_Y(y)$$

the joint density function in terms of a bivariate copula can be written

$$f_{XY}(x,y) = \frac{\partial^2 C(u,v)}{\partial u\, \partial v}\frac{\partial F_X(x)}{\partial x}\frac{\partial F_Y(y)}{\partial y} = c(u,v) f_X(x) f_Y(y) \tag{4.6}$$

where f_X and f_Y are the univariate density distributions of X and Y, respectively. Both this and Equation 4.5 are used in the Optimal Mean Setting process. Equation 4.6 can be used to determine the distribution of the final manufactured geometry after rework with dependence, while Equation 4.5 may be used to determine the scrap and rework probabilities if the marginal distributions are not normal. Such a case would arise if the inspectable parameters were a result of two or more manufacturing features. Alternatively it is possible for a feature to have dependence on another feature produced by a process with a different form of univariate margin. Thus the probability of rework, conformance and scrap is the joint distribution of the two different univariate marginals including the dependence structure.

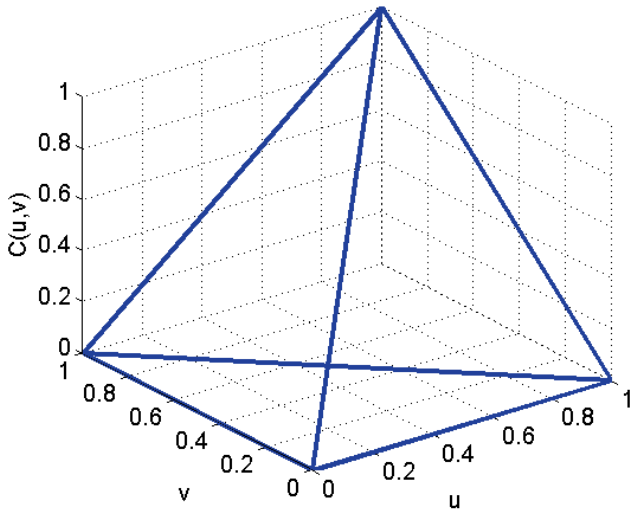

FIGURE 4.5: Graphical representation of the Fréchet-Hoeffding bounds for a bivariate copula

4.2.4 Fréchet-Hoeffding bounds

The Fréchet-Hoeffding bounds restrict the shape of the bivariate copula, such that it lies within a pyramid as shown in Figure 4.5. This comes about due to the extremes of dependence between variables. Consider the extreme monotonic case, where two uniformly distributed random variables are dependent such that $U = V$, the copula is given by,

$$C(u, v) = \Pr(U \leq u, V \leq v) = \min(u, v).$$

This gives rise to the front face of the pyramid in Figure 4.5. The independence case shown graphically in Figure 4.4(a) actually sits in the middle of this pyramid structure. The back face of the pyramid is achieved from the opposite dependence such that the uniformly distributed random variables are $V = 1 - U$. This gives,

$$\begin{aligned} C(u, v) &= \Pr(U \leq u, 1 - U \leq v) \\ &+ \Pr(U \leq u, 1 - v \leq U) = u + v - 1, \end{aligned}$$

leading to the bound,

$$\max(u + v - 1, 0) \leq C(u, v) \leq \min(u, v),$$

which also exists for n dimensions.

4.2.5 Types of Copula

The principal difference between copulas is the types of dependence they model between random variables. Dependence between random variables may occur when two or more features are produced on the same machine. Datum planes or fixings are also likely to be correlated to other features. The choice of copula determines the type and variety of dependence structures one wishes to model. The most common copula types are the Gaussian copula and the Archimedean family of copulas that include Clayton, Gumbel, Frank, Ali-Mikhail-Haq and Joe varieties, where each characterises a particular form of dependence (Nelsen [2006]). The independence copula is also part of the Archimedean family of copulas. A particularly useful characteristic of Archimedean copulas is that they are described by explicit expressions, permitting analytical solutions, unlike the Gaussian copula.

The dependency structure of the Gaussian, Clayton and Frank copulas are considered in this report. The discussion is limited to these copulas principally because the dependence structure these copula models exhibit is not unlike the dependence structure from the covariance matrix used in the multivariate normal distribution model (Equation 3.17). Ultimately, the dependency between features in a production environment and thus the choice of copula requires a copula fitting process. Such techniques are not examined in this report but an overview is given by Schmidt [2006] with a detailed analysis in Matteis [2001]. The three copulas discussed here are sufficient to demonstrate the power of using copula techniques in Optimal Mean Setting analysis. However, they are by no means the only copulas that could be used to model dependence between manufacturing features in practice.

In order to compare different copulas, it is important to measure dependence independent of the marginal distributions. There are a number of ways to quantify dependence but the most common are; the Pearson product-moment correlation, Spearman rank correlation and Kendall rank correlation. The Pearson correlation coefficient is defined as,

$$\rho_p = \frac{\operatorname{cov}(X, Y)}{\sigma_X \, \sigma_Y} = \frac{E[(X - \mu_X)(Y - \mu_Y)]}{\sigma_X \, \sigma_Y}$$

which, for a sample size of n is,

$$\rho = \frac{\sum_{i=1}^{n}(X_i - \bar{X})(Y_i - \bar{Y})}{\sqrt{\sum_{i=1}^{n}(X_i - \bar{X})^2}\sqrt{\sum_{i=1}^{n}(Y_i - \bar{Y})^2}}$$

where $\bar{X}, \bar{Y}$ refer to the means of the X and Y variables. This is a linear measure of dependence between the two variables X and Y where $\rho = [-1, 1]$. However, it is also dependent on the marginal distributions as illustrated in Section 2.2 of Tops

[2010], although first described by Lehmann [1966]. Since it is dependent on the univariate distribution, it is not a suitable coefficient for comparing copula dependence. The Spearman correlation coefficient is derived from the Pearson correlation coefficient and has the same form except the variables are ranked. For a sample of size n, the raw variables X_i, Y_i are converted into ranks x_i, y_i to give

$$\rho_s = \frac{\sum_{i=1}^{n}(x_i - \bar{x})(y_i - \bar{y})}{\sqrt{\sum_{i=1}^{n}(x_i - \bar{x})^2}\sqrt{\sum_{i=1}^{n}(y_i - \bar{y})^2}}$$

where $\rho_s = [-1, 1]$. The Spearman rank coefficient measures the monotone dependence between variables rather than the linear dependence and thus can be defined using a copula function independent of the marginal distributions such that,

$$\rho_s = 12 \int_0^1 \int_0^1 [C(u, v) - u\, v]\, \mathrm{d}u\, \mathrm{d}v. \tag{4.7}$$

This result is considered in more detail by Schweizer and Wolff [1981] but also discussed in more modern literature Fredricks and Nelsen [2007] and Tops [2010]. Another popular correlation coefficient is Kendall's tau which, like Spearman's coefficient, is a rank correlation independent of the marginal distributions. Kendall's tau is the difference between the number of concordant pairs ($\boldsymbol{C}$) and discordant pairs ($\boldsymbol{D}$), divided by the total number of pair combinations. Concordance and discordance are defined as follows: Let $(x_1, y_1), (x_2, y_2), \ldots, (x_n, y_n)$ be a set of observations from the joint random variables X, Y. Assuming x_i and y_i are unique, any pair of joint observations (x_i, y_i) and (x_j, y_j) are concordant if $x_i > x_j$ and $y_i > y_j$ or alternatively if $x_i < x_j$ and $y_i < y_j$. A pair is discordant if $x_i > x_j$ and $y_i < y_j$ or conversely if $x_i < x_j$ and $y_i > y_j$. Hence the Kendall correlation coefficient is given by

$$\tau = \frac{\boldsymbol{C} - \boldsymbol{D}}{n(n-1)}$$

where $\tau = [-1, 1]$ and n is the sample size. As shown by Schweizer and Wolff [1981], Fredricks and Nelsen [2007] and Tops [2010], Kendall's correlation coefficient can be written in terms of copulas as,

$$\tau = 4 \int_0^1 \int_0^1 [C(u, v)\, \c{C}(u, v) - 1.$$

The Spearman rank correlation and the Kendall tau correlation are both commonly used to define correlation between sets of data and in general there is no strong reason to prefer one over the other as commented by Colwell and Gillett [1982]. Typically, the Spearman rank coefficient is larger in absolute value than Kendall's tau, while Kendall's tau coefficient is generally harder to calculate. There are subtle practical difference

between the coefficients: Kendall's tau penalises a disparity between the two ranks as the distance of that disparity, whereas, Spearman's rho penalises the same disparity as the square of the distance. For example let the ranks between two sets of correlated data be $x = [1, 2, 3, 4]$, $y_a = [2, 1, 4, 3]$. Kendall's correlation coefficient $\tau = 0.33$ and Spearman's $\rho = 0.6$. However, if the ranks are changed to represent a different set of data $y_b = [3, 1, 2, 4]$ Spearman's coefficient reduces to $\rho = 0.4$ while Kendall's tau remains at $\tau = 0.33$. The reason for this is the difference between the ranks x and y_a was one, for each element. However, for the second data set x and y_b, the rank of the first element was greater by two and the second and third elements differed by one, while the fourth element remained unchanged. Since the distance of the disparity of the first element is twice as great, Spearman's coefficient penalises this to a greater extent than Kendall's tau. The total distance of disparities in each case is four, hence Kendall's tau remains the same.

In order to compare the dependency structure of the Gaussian, Clayton and Frank copulas, the dependency parameter for each copula was set using Equation 4.7, where $\rho_s = 0.8$. This was solved numerically using Matlab's *fzero* function (Mathworks [2012]), although it is possible to find an analytical solution provided $C(u, v)$ can be expressed explicitly. Figures 4.6(a), 4.6(b) and 4.6(c) show how Spearman's and Kendall's coefficients relate to the Gaussian, Clayton and Frank copulas, respectively. The values of the three copula dependence parameters for $\rho_s = 0.8$ are shown in the table in Figure 4.6(d).

4.2.6 Gaussian Copula

A Gaussian coupla is written as,

$$C(u, v) = \mathbf{\Phi}_{\mathbf{\Sigma}}(\mathbf{\Phi}^{-1}(u), \mathbf{\Phi}^{-1}(v)), \tag{4.8}$$

where $\mathbf{\Sigma}$ is the bivariate covariance matrix,

$$\mathbf{\Sigma} = \begin{bmatrix} \sigma_u^2 & \rho\sigma_u\sigma_v \\ \rho\sigma_u\sigma_v & \sigma_v^2 \end{bmatrix}$$

and $\rho \forall \in [0, 1]$ is the Pearson correlation coefficient. We can investigate the type of dependence structure this copula gives by generating the u and v values from this copula. Recall the bivariate density function was given in Equation 3.17. Under the normalisation $z_1 = (x_1 - \mu_1)/\sigma_1$ and $z_2 = (x_2 - \mu_2)\sigma_2$ the bivariate density function

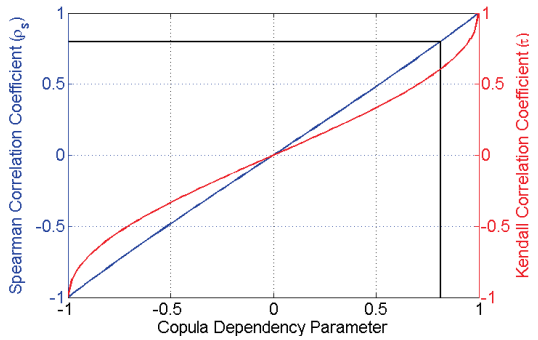

(a) Spearman's and Kendall's correlation versus Gaussian copula dependence

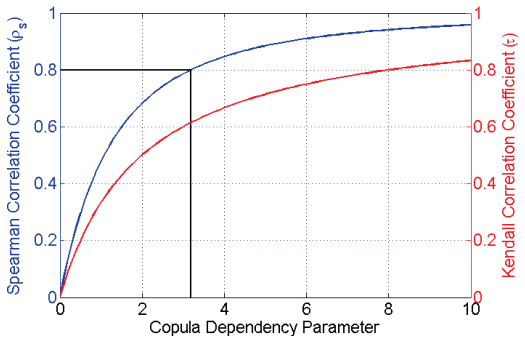

(b) Spearman's and Kendall's correlation versus Clayton copula dependence

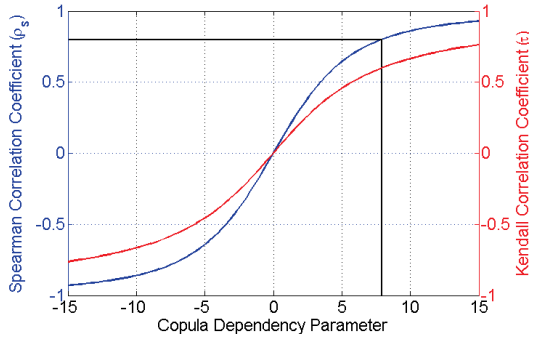

(c) Spearman's and Kendall's correlation versus Frank copula dependence

Copula Type	Dependency Parameter
Gaussian Copula	$\rho = 0.8135$
Clayton Copula	$\theta = 3.1819$
Frank Copula	$\theta = 7.9019$

(d) Copula dependency parameter values

FIGURE 4.6: Relationships between Spearman's and Kendall's correlation coefficients and copula dependency parameters

(Equation 3.17) can be written as,

$$f(x_1, x_2) = \frac{1}{2\pi\sqrt{1-\rho^2}} \exp\left(-\frac{z_1^2 + z_2^2 - 2\rho z_1 z_2}{2(1-\rho^2)}\right).$$

Integrating z_1 and z_2 from $-\infty$ to the inverse CDFs the Gaussian copula can be written [Nelsen, 2006],

$$C(u, v) = \int_{-\infty}^{\Phi^{-1}(u)} \int_{-\infty}^{\Phi^{-1}(v)} \frac{1}{2\pi\sqrt{1-\rho^2}} \exp\left(-\frac{z_1^2 + z_2^2 - 2\rho z_1 z_2}{2(1-\rho^2)}\right) z_1 z_2$$

which has no general closed form solution but can be solved efficiently with standard routines in most numerical software packages. When $\rho = 0$ the fraction inside the integral goes to zero, thus the Gaussian copula reduces to the independent copula $C(u, v) = uv$. To investigate the dependence structure of this copula, V was plotted against U, for positive correlation between the random variables where $\rho \geq 0$. The procedure for this plot was as follows: From Equation 4.8, $U = \mathbf{\Phi}(X)$ and $V = \mathbf{\Phi}(Y)$ where X, Y are the

random vectors created by $\mathbf{\Phi}^{-1}(u)$ and $\mathbf{\Phi}^{-1}(v)$. Most numerical packages, such as Matlab, efficiently generate these random vectors from a multivariate normal distribution (*mvnrnd*). Once vectors U and V are generated, the cumulative distribution functions for each vector can be computed. Figure 4.7(a) plots for V against U, where $\rho = 0.8$ and shows a concentration of points towards the tails. The PDF of the same copula is represented in Figure 4.7(b). The sharp peaks towards $u = v = 0$ and at $u = v = 1$ mirror the high dependence shown in Figure 4.7(a), where the concentration of the points is greater. For $\rho = 0$, the surface in Figure 4.7(b) would be a flat surface and the adjacent scatter plot would show no clustering.

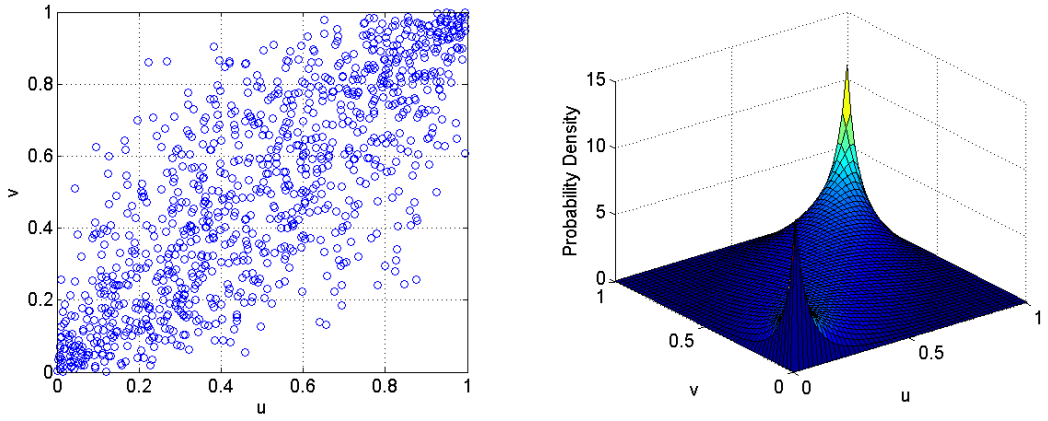

(a) u versus v from a Gaussian copula with $\rho = 0.8135$

(b) Gaussian copula PDF with $\rho = 0.8135$

FIGURE 4.7: Gaussian copula dependence

4.2.7 Archimedean Copulas

Archimedean copulas differ from the Gaussian copula in that they can be written explicitly. For clarity, only bivariate copulas are discussed, but a primary advantage of Archimedean copulas is their ability to model dependence for an arbitrary number of dimensions. All bivariate Archimedean copulas $C(u, v)$ can be generated from [Nelsen, 2006],

$$\boldsymbol{\phi}(C) = \boldsymbol{\phi}(u) + \boldsymbol{\phi}(v) \tag{4.9}$$

where ϕ is known as a generator whose inverse is ϕ^{-1}. The function ϕ is monotone, strictly decreasing from $[0, 1]$ to $[0, \infty]$ where $\phi(0) = \infty$ and $\phi(1) = 0$ as discussed in Nelsen [2006] pages 91 to 92. The copula $C(u, v)$ is given by

$$C(u, v) = \boldsymbol{\phi}^{-1}(\boldsymbol{\phi}(u) + \boldsymbol{\phi}(v)). \tag{4.10}$$

With a generator function it is possible to construct a number of copulas from the Archimedean family. Although only the Clayton and Frank copulas are considered here Nelsen [2006] and Schmidt [2006] offer a more in-depth discussion.

4.2.7.1 Clayton Copula

The generator function for the Clayton copula is,

$$\boldsymbol{\phi}(z) = \frac{-1}{\theta}(1 - z^{-\theta}) \tag{4.11}$$

where z is a place-holder. From Equation 4.11 we require ϕ^{-1} given by,

$$z = \frac{-1}{\theta}(1 - \boldsymbol{\phi}^{-1}(z))^{-\theta} \Rightarrow \boldsymbol{\phi}^{-1}(z) = (1 + \theta z)^{-1/\theta}.$$

Therefore from Equation 4.11,

$$\begin{aligned} C(u,v) &= \boldsymbol{\phi}^{-1}(\boldsymbol{\phi}(u) + \boldsymbol{\phi}(v)) = [1 + \theta\,(\boldsymbol{\phi}(u) + \boldsymbol{\phi}(v))]^{-1/\theta} \\ &= \left[1 + \theta\left(\frac{-1}{\theta}(1 - u^{-\theta}) + \frac{-1}{\theta}(1 - v^{-\theta})\right)\right]^{-1/\theta} \\ &= [u^{-\theta} + v^{-\theta} - 1]^{-1/\theta} \end{aligned} \tag{4.12}$$

where $\theta \in \mathbb{R}[-1, \infty]\backslash 0$. It is possible to rearrange Equation 4.9 so that $\boldsymbol{\phi}(v) = \boldsymbol{\phi}(C) - \boldsymbol{\phi}(u)$ to get,

$$v = \boldsymbol{\phi}^{-1}(\boldsymbol{\phi}(C) - \boldsymbol{\phi}(u)). \tag{4.13}$$

To define the argument C in $\boldsymbol{\phi}(C)$ let $\xi = \partial C/\partial u$ and let h represent the inverse of ϕ' where the $'$ notation is used to represent the first derivative with respect to the argument. Therefore $\boldsymbol{h}(\partial\boldsymbol{\phi}(z)/\partial z) = \boldsymbol{h}(\boldsymbol{\phi}'(z)) = z$. From Equation 4.10 we can determine $\partial C/\partial u$ so that

$$\boldsymbol{\phi}'(C)\,\frac{\partial C}{\partial u} = \boldsymbol{\phi}'(u) \Rightarrow \boldsymbol{\phi}'(C) = \frac{\boldsymbol{\phi}'(u)}{\xi}.$$

Using the function h (defined above), it is possible to define the argument C in terms of u and ξ such that,

$$\boldsymbol{h}(\boldsymbol{\phi}'(C)) = C = \boldsymbol{h}\left(\frac{\boldsymbol{\phi}'(u)}{\xi}\right).$$

Equation 4.13 can now be written in terms of the calculable augments

$$v = \boldsymbol{\phi}^{-1}\left\{\boldsymbol{\phi}\left[\boldsymbol{h}\left(\frac{\boldsymbol{\phi}'(u)}{\xi}\right)\right] - \boldsymbol{\phi}(u)\right\}. \tag{4.14}$$

As the composite function is relatively complex[5] , it is easiest to tackle in stages, thus

$$\boldsymbol{\phi} \circ \boldsymbol{h}(z) = \frac{-1}{\theta}(1 - \boldsymbol{h}^{-\theta}).$$

where $\boldsymbol{h}$ is defined from,

$$\begin{aligned} \boldsymbol{\phi}'(z) &= -z^{-\theta-1} \Rightarrow z = -\boldsymbol{h}(z)^{-\theta-1} \\ \boldsymbol{h}(z) &= -z^{1/(-\theta-1)}. \end{aligned}$$

Therefore,

$$\boldsymbol{\phi} \circ \boldsymbol{h}(z) = \frac{-1}{\theta}(1 + z^{\frac{\theta}{\theta+1}}).$$

Replacing the argument z with $\boldsymbol{\phi}(u)/\xi$ from Equation 4.14 yields,

$$\boldsymbol{\phi} \circ \boldsymbol{h}\left(\frac{\boldsymbol{\phi}'(u)}{\xi}\right) = \frac{-1}{\theta}\left[1 + \left(\frac{\boldsymbol{\phi}'(u)}{\xi}\right)^{\frac{\theta}{\theta+1}}\right].$$

Considering $\boldsymbol{\phi}'(u) = -u^{-\theta-1}$ the argument of $\boldsymbol{\phi}^{-1}$ from Equation 4.14 can now be written as,

$$\boldsymbol{\phi} \circ \boldsymbol{h}\left(\frac{\boldsymbol{\phi}'(u)}{\xi}\right) - \boldsymbol{\phi}(u) = \frac{-1}{\theta}\left[1 + \left(\frac{u^{-\theta-1}}{\xi}\right)^{\frac{\theta}{\theta+1}}\right] + \frac{1}{\theta}(1 - u^{-\theta}) = \Omega.$$

Substituting this expression onto the inverse function completes the right hand side of Equation 4.14,

$$\begin{aligned} v &= \boldsymbol{\phi}^{-1}(\Omega) = \left\{1 - \tfrac{\theta}{\theta}\left[1 + \left(\tfrac{u^{-\theta-1}}{\xi}\right)^{\frac{\theta}{\theta+1}}\right] + \tfrac{\theta}{\theta}(1 - u^{-\theta})\right\}^{-1/\theta} \\ &= \left[\xi^{-\theta/(1+\theta)}u^{-\theta} - u^{-\theta} + 1\right]^{-1/\theta} \end{aligned}$$

giving an expression for v in terms of u and ξ.

To examine the dependence structure created by this copula, we can plot V against U. For a uniformly distributed set of random variables $u, \xi \in [0, 1]$ we can generate the corresponding vector v where the dependence between the two random vectors is defined by 4.12. Figure 4.8(a) shows u and v are closely correlated for small values but the correlation becomes less pronounced as the values become larger. The PDF of this Clayton copula is represented in Figure 4.8(b) (note the axes have been reversed for clarity of visualising the spike). The spike towards $u = v = 0$ reflects the high dependence shown in Figure 4.8(a) at low values of u and v. Like the Gaussian copula, if the dependence

[5]The '$\circ$' symbol is the function composition operator

parameter $\theta = 0$, the surface in Figure 4.8(b) would be a flat surface representing no dependence between the random variables. Due to the restriction on the dependence parameter θ noted under Equation 4.12, the Clayton copula cannot be used to model negative dependence.

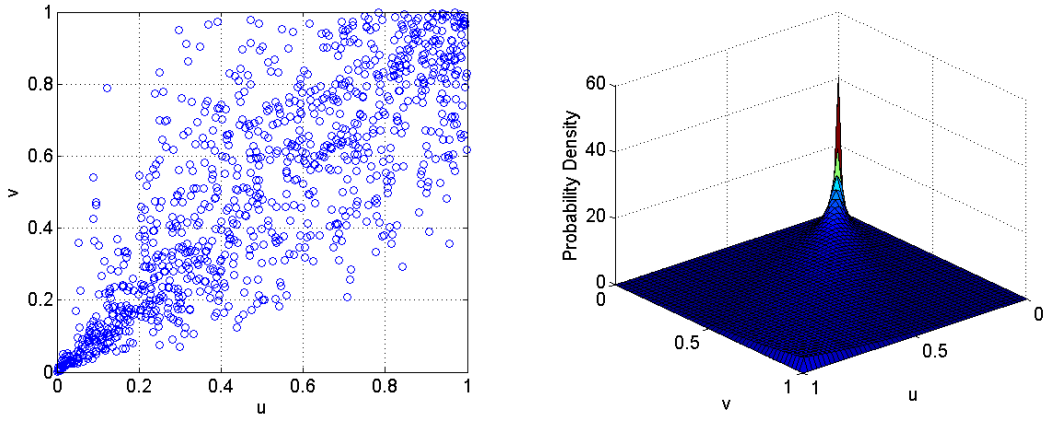

(a) u versus v from a Clayton copula with $\theta = 3.1819$

(b) Clayton copula PDF with $\theta = 3.1819$

FIGURE 4.8: Clayton copula dependence

4.2.7.2 Frank Copula

The Frank copula is generated in a similar fashion to the Clayton copula above. The generator function for the Frank copula as given by Nelsen [2006] is,

$$\phi(z) = -\log\left(\frac{1 - e^{-\theta z}}{1 - e^{-\theta}}\right) \tag{4.15}$$

Using the Equation 4.9 the Frank copula is generated from,

$$-\log\left(\frac{1 - e^{-\theta C}}{1 - e^{-\theta}}\right) = -\log\left(\frac{1 - e^{-\theta u}}{1 - e^{-\theta}}\right) - \log\left(\frac{1 - e^{-\theta v}}{1 - e^{-\theta}}\right),$$

which needs to be rearranged making C the subject. Taking the exponent of both sides and simplifying gives,

$$\frac{-1 + e^{-\theta}}{-1 + e^{-\theta C}} = \frac{(-1 + e^{-\theta})^2}{(-1 + e^{-\theta u})(-1 + e^{-\theta v})},$$

which can be rearranged into the Frank copula,

$$C(u, v) = \frac{-1}{\theta}\log\left[1 - \frac{(1 - e^{-\theta u})(1 - e^{-\theta v})}{1 - e^{-\theta}}\right], \tag{4.16}$$

where $\theta \in \mathbb{R}\backslash\{0\}$. Again, in order to gain an understanding of the dependence structure of this copula, as before v is sought for an input u. Equation 4.14 can be used to determine v for a given u input, as was shown with the Clayton copula. In order to compute Equation 4.14, the functions $\boldsymbol{\phi}$, $\boldsymbol{\phi}^{-1}$, $\boldsymbol{\phi}'$ and $\boldsymbol{h}$ are required. The generator function $\boldsymbol{\phi}$ is given in Equation 4.15, where the inverse is given by,

$$\boldsymbol{\phi}^{-1}(z) = \frac{-1}{\theta}\log(e^{-z+\theta} - e^{-z} + 1).$$

The derivative of $\boldsymbol{\phi}$ with respect to z is,

$$\boldsymbol{\phi}'(z) = \frac{-\theta e^{-\theta z}}{1 - e^{-\theta z}} = \frac{\theta}{1 - e^{\theta z}}.$$

The inverse of this derivative is $\boldsymbol{h}$ given by

$$\boldsymbol{h}(z) = \frac{1}{\theta}\log\left(1 - \frac{\theta}{z}\right).$$

The argument of ϕ^{-1} in Equation 4.14 is broken down into stages, firstly

$$\begin{aligned}
\boldsymbol{\phi} \circ \boldsymbol{h}(z) &= -\log\left(\frac{1 - e^{-\theta \boldsymbol{h}}}{1 - e^{-\theta}}\right) \\
&= -\log\left(\frac{1 - \exp\left\{-\theta\left[1/\theta(\log(1 - \theta/z))\right]\right\}}{1 - e^{-\theta}}\right) \\
&= \log\left[\left(\frac{z}{\theta} - 1\right)\left(1 - e^{-\theta}\right)\right].
\end{aligned}$$

The argument $\boldsymbol{\phi}'(u)/\xi$ can now be inserted for the place-holder z,

$$\begin{aligned}
\boldsymbol{\phi} \circ \boldsymbol{h}\left(\frac{\boldsymbol{\phi}'(u)}{\xi}\right) &= \log\left[\left(\frac{\boldsymbol{\phi}'(u)}{\xi\,\theta} - 1\right)\left(1 - e^{-\theta}\right)\right] \\
&= \log\left[\left(\frac{1}{(1 - e^{\theta u})\xi\,\theta} - 1\right)\left(1 - e^{-\theta}\right)\right].
\end{aligned}$$

The whole argument for $\boldsymbol{\phi}^{-1}$ is,

$$\begin{aligned}
\boldsymbol{\phi} \circ \boldsymbol{h}\left(\frac{\boldsymbol{\phi}'(u)}{\xi}\right) - \boldsymbol{\phi}(u) &= \log\left[\left(\frac{1}{(1 - e^{\theta u})\xi\,\theta} - 1\right)\left(1 - e^{-\theta}\right)\right] + \log\left(\frac{1 - e^{-\theta u}}{1 - e^{-\theta}}\right) \\
&= \log\left[\frac{1 - e^{-\theta u}}{(1 - e^{\theta u})\xi - 1}\right] = \Omega.
\end{aligned}$$

An expression for v is therefore written,

$$\begin{aligned} v = \phi^{-1}(\Omega) &= \frac{-1}{\theta}\log[1 - e^{-\Omega}(1 - e^{-\theta})] \\ &= \frac{-1}{\theta}\log\left[1 - \frac{1 - e^{-\theta}}{1 + e^{-\theta u}(\xi^{-1} - 1)}\right] \end{aligned} \tag{4.17}$$

Equation 4.17 is used to generate the vector v from a set of uniformly distributed random variables $u, \xi \in [0, 1]$. The scatter plot in Figure 4.9(a) allows the visualisation of the dependence structure modelled by this Frank copula (Equation 4.16). The adjacent Figure 4.9(b) shows the probability density plot which is not unlike the Gaussian copula. The principal differences are in tail dependences, which are less pronounced and a more uniform dependence along the diagonal $u = v$. Like the Gaussian copula, the Frank copula can account for negative dependence but not for $\theta = 0$, as noted under Equation 4.16.

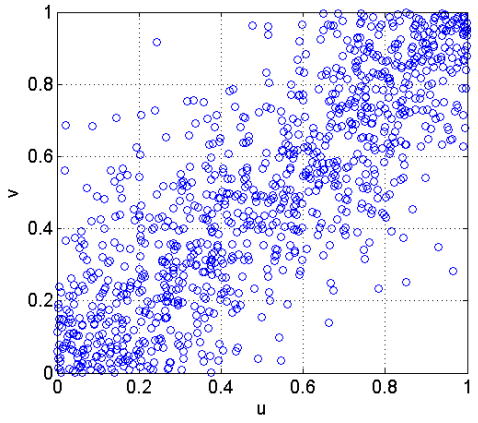

(a) u versus v from a Frank Copula with $\theta = 7.9019$

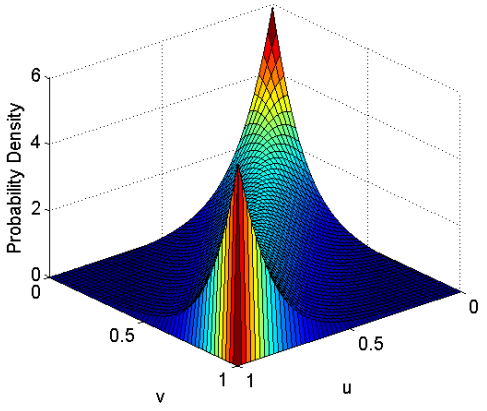

(b) Frank copula PDF with $\theta = 7.9019$

FIGURE 4.9: Clayton copula dependence

4.2.8 Multivariate Copula Construction

The geometry distribution of manufactured features can be modelled using a copula. To demonstrate this, the multivariate distribution created using the Gaussian mixture model (Equation 4.2) depicted by Figure 4.1 was recreated using a copula. The approach is very similar to the method used to obtain the results shown in Figure 4.1 however, a multivariate truncated distribution is built from the two normal marginal distributions using a copula. The weighted sum of the multivariate distributions form the complete

multivariate distribution analogous to Figure 4.1. The weights are determined by evaluating the probability of conformance and scrap from the initial state and each rework state (as was done for Figure 4.1)

The truncated copula distribution has the form[6].

$$f_{X_1X_2} = \frac{C(F_{X_1}(x_1), F_{X_2}(x_2)) f_{X_1}(x_1) f_{X_2}(x_2)}{C(F_{X_1}(U_1), F_{X_2}(U_2)) - C(F_{X_1}(L_1), F_{X_2}(L_2))} \tag{4.18}$$

for all $\boldsymbol{L} \leq x_1, x_2 \leq \boldsymbol{U}$, where the marginal distributions f_{X_1} and f_{X_2} are given by the normal distribution function,

$$f_{X_1} = \frac{1}{\sigma_1\sqrt{2\pi}} \exp\left(-\frac{(x_1-\mu_1)^2}{2\sigma_1^2}\right) \quad \text{and} \quad f_{X_2} = \frac{1}{\sigma_2\sqrt{2\pi}} \exp\left(-\frac{(x_2-\mu)^2}{2\sigma_2^2}\right). \tag{4.19}$$

The cumulative distributions, F_{X_1} and F_{X_2} are the integrals of the respective marginal distributions thus,

$$F_{X_1} = \int_{-\infty}^{t_1} f_{X_1}\, \mathrm{d}t_1 \quad \text{and} \quad F_{X_2} = \int_{-\infty}^{t_2} f_{X_2}\, \mathrm{d}t_2. \tag{4.20}$$

The CDFs in the denominator of Equation 4.18 are the CDFs evaluated at specific points corresponding to the upper and lower specification limits (U_1, U_2 and L_1, L_2); this involves changing the upper integral limits in Equation 4.20 to the appropriate U or L values. Thus, the denominator acts to truncate the PDF at the lower and upper specification limits. The copula function, C, can take a number of forms depending on the correlation between the two features, X_1 and X_2. In this first case a Gaussian copula is used as described in Equation 4.8. Figure 4.10 shows the comparison between the PDF surfaces created with the truncated Gaussian copula (Equations 4.18 and 4.8) and the truncated normal distribution function (Equation 4.4), evaluated at the red points. The two functions create the same PDF with and without correlation given by Spearman's ρ. The maximum difference between red points and the surface evaluated at the same locations was 8.327^{-17}, which is less than machine precision verifying the equivalence between the Gaussian copula distribution and truncated multivariate normal distribution. As alluded to at the beginning of Chapter 4, a significant advantage of copula models is their flexibility with regards to modelling dependencies between variables as well as permitting any form for the marginal distributions. The following Case Study examines the manufacture of a connection rod from a reciprocating engine which demonstrates the use of copula statistics on a physical product.

[6]Note a numerical index is used for variables from henceforth as this approach is more applicable to multivariate cases. The variable x is referred to as x_1 while y becomes x_2. Similarly u becomes u_1 and v becomes u_2.

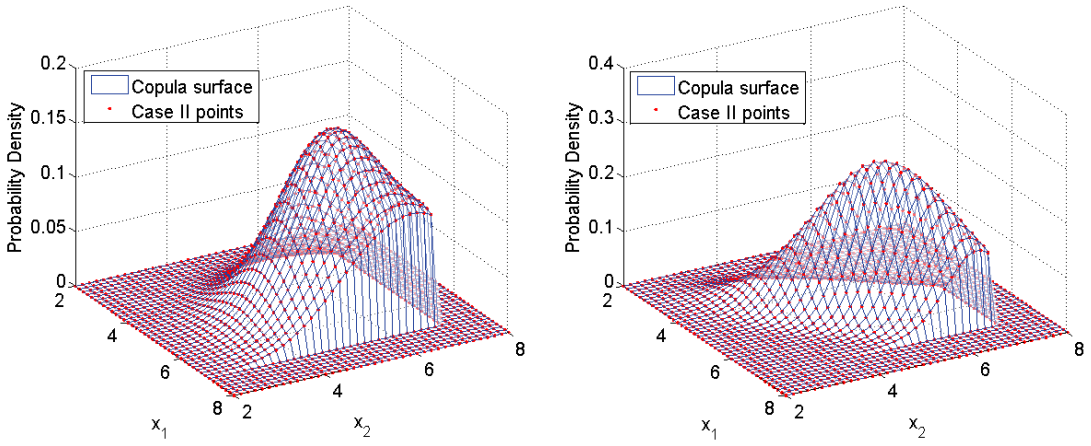

(a) PDF truncated at $U_1 = 7$ and $U_2 = 7$, with no correlation

(b) PDF truncated at $U_1 = 7$ and $U_2 = 7$, with correlation ($\rho = 0.8$)

FIGURE 4.10: Comparison between the PDF surfaces created using a Copula function (Equation 4.18) and the truncated normal distribution (Equation 4.4)

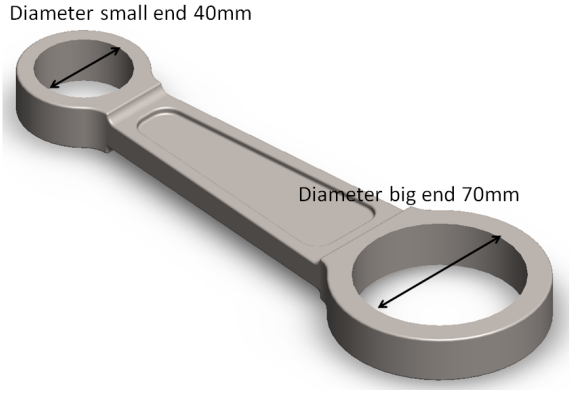

FIGURE 4.11: Connection Rod from Aparisi et al. [1999]

Feature	Nominal (mm)	Mean (mm)	LSL (mm)	USL (mm)	σ	C_{pk}
Diameter big end (x_1)	70.00	70.02	69.00	71.00	1.362	0.24
Diameter small end (x_2)	40.00	40.13	39.25	40.75	0.50	0.71

TABLE 4.1: Data for the connecting rod case study

4.3 Case Study - Connecting Rod

Aparisi et al. [1999] introduced a case study of a connecting rod visualised in Figure 4.11. There were two inspectable features; the diameter of the big end (x_1) and the diameter of the small end (x_2). The nominal means for these features were given in the data contained in Aparisi et al. [1999], but the specification limits were not. For the purposes of this Case Study the specification limits were chosen arbitrarily and are given in Table 4.1. The manufactured values for each of the two features were tabulated

Distribution	BIC	AIC
t-location scale	-113.3	-119.5
Logistic	-113.1	-117.3
Log log logistic	-112.6	-116.8
Rician	-105.6	-109.8
Normal	-105.6	-109.8

TABLE 4.2: BIC and AIC values for the top five best fit distributions returned by *allfitdist* (Sheppard [2012])

by Aparisi et al. [1999] (also available in Costa and Machado [2008]). Histograms of the raw manufacturing data for each feature are given in Figures 4.12 and 4.13. A Chi-Squared test was used to establish if the distributions were likely to come from a normal distribution. The x_1 feature passed the test to a 1% confidence interval indicating it was probable the variations in the diameter of the big end (x_1) were normally distributed. The p-values and fitted normal distribution are shown for the x_1 feature in Figure 4.12. The x_2 feature failed the Chi-Squared test so an alternate continuous probability distribution was sought. A best fitting probability distribution was determined by testing a number of parametric distributions (17 in total). The Matlab function *allfitdist*, developed by Sheppard [2012] was used for this task. The goodness of fit was determined by the Bayesian Information Criterion (BIC) and Akaike Information Criterion (AIC) metrics. These metrics are based on minimising the log-likelihood but account for the number of parameters in the fitted model and therefore offer a justifiable comparison between different parametric distributions (Helie [2006], Dziak et al. [2012]). As noted by Dziak et al. [2012], the most likely modelling error when minimising BIC is under-fitting the model, whereas the most likely modelling error in minimising AIC is an over-fitted model. The fact that the tLocation-Scale distribution was judged to be the best fit to the x_2 feature data by both the BIC and AIC metrics, helps to justify its use. The distribution is commonly used for distributions with heavy tails, prone to outliers (Walck [2007])[7]. Figure 4.13 indicates the difference in shape of the tLocation-Scale distribution (blue line) in comparison to the best fit Gaussian distribution (red line). The PDF for the tLocation-Scale distribution (as given in Section 38 of Walck [2007]) is,

$$f(x,\mu,\sigma,\nu) = \frac{\Gamma\left(\frac{\nu+1}{2}\right)}{\sigma\sqrt{\nu\pi}\,\Gamma\left(\frac{\nu}{2}\right)} \left(\frac{\nu + \left(\frac{x-\mu}{\sigma}\right)^2}{\nu}\right)^{-\left(\frac{\nu+1}{2}\right)},$$

[7]The machining process used to finish the small end (x_1 feature) was different to the process used to finish the big end (x_1 feature), hence the different distributions. Although the manufacturing processes are not specified it is likely the big end (x_1 feature) was reamed, while the small end finishing process was grinding

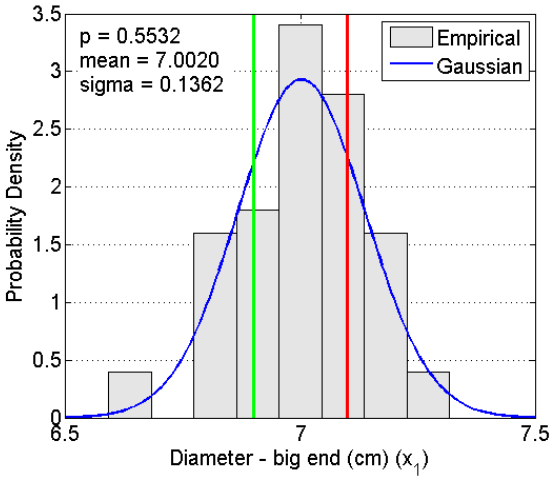

FIGURE 4.12: Histogram and best fit continuous distribution for the diameter of the big end (x_1)

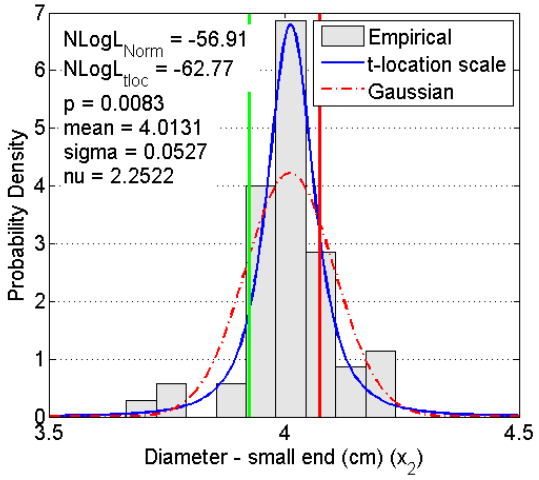

FIGURE 4.13: Histogram and best fit continuous distribution for the diameter of the small end (x_3)

where Γ is the gamma function given by,

$$\Gamma(t) = \int_0^\infty x^{t-1} e^{-x}\, \mathrm{d}x.$$

The upper and lower specification limits in Table 4.1 are visualised by the green and red lines in Figures 4.12 and 4.13. The variations for the two diameter distributions (x_1 and x_2) are outside the specification limits indicating the manufacturing processes are incapable ($C_{pk} < 1$, Table 4.1) and non-conforming features would be produced. It would be beneficial to apply Optimal Mean Setting to the manufacture of these features to maximise profit. Since the univariate (marginal) distributions are different, copula

modelling was utilised to create an exact multivariate model of the x_1 and x_2 features including the dependence structure[8]. Figures 4.14 to 4.16 illustrate the dependence between the x_1 and x_2 features modelled using a Gaussian, Clayton and Frank Copula. The most appropriate copula model to chose depends on a number of factors such as:

- Whether the model will be used as a predictive model outside the current data range or within the current data range.
- The quality of the source data.
- The quantity of the source data, for example some data could be used for cross validation.
- Causal relations between the features may influence the copula choice. For example, the Clayton copula would be a suitable model if there was a causal reason why smaller values of x_1 would imply smaller values for x_2, whilst larger values of x_1 would not influence x_2. This is not the case for the connecting rod case study.

For this case study, the Matlab function *copulafit* (Mathworks [2012]) was used to determine the value of the correlation parameter for each copula (ρ for the Gaussian copula and θ for the Clayton and Frank copulas). The *copulafit* function minimises the negative log likelihood (NLogL) in order to determine the correlation parameter using the procedure outlined by Bouye et al. [2000][9]. The red points on Figures 4.14 to 4.16 show the original data while the blue points are 5000 random sample points drawn from the fitted copula model using the Matlab function *copularnd* (Mathworks [2012]). As indicated in the captions of each figure the Gaussian copula yielded the lowest NLogL, so this copula was chosen as the 'best model' of the data. Fitting copula models to data is an active area of research and several papers discuss suitable ways to establish the 'goodness of fit' (Yan [2007]). The maximum likelihood method is often general practice in evaluating the fit of a Copula to sampled data (Yan [2007]) and considered sufficient for this illustrative example. Nevertheless, there are several alternative approaches, such as Bootstrap methods, probability integral transformation and distance based methods. Fermanian et al. [2012] provides a comprehensive overview. Genest and Favre [2007] offers a good overview of graphical goodness of fit tests and Wang [2010] investigated goodness of fit test for Archimedean copula models.

[8]The tLocation-Scale distribution approaches normal distribution as $\nu \to \infty$. Therefore it would be possible to define the x_1 distribution using a tLocation-Scale distribution and create a multivariate model of the x_1 and x_2 features using a multivariate tLocation-Scale distribution. However, changes to either of the univariate distributions, which may come as a result of reviewing data or alternative fitting techniques, would render the multivariate parametric model inaccurate. A copula model allows any form of marginal distribution and allows any changes in dependence to be updated independently.

[9]As there is only one parameter to change in each copula model, the minimisation of negative log likelihood is a valid comparison between the different copula models, one does not have to use the BIC or AIC metrics to account for differing numbers of parameters in the different models.

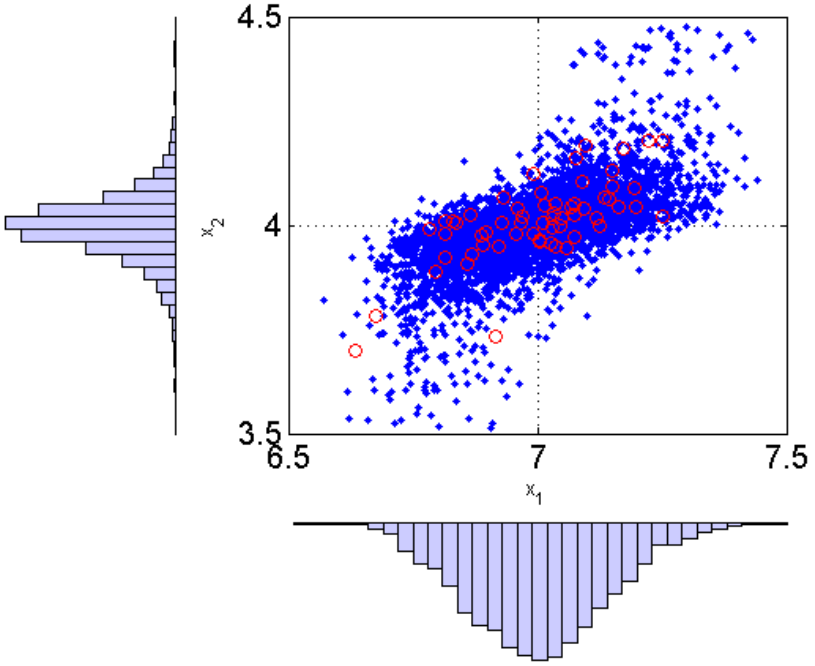

FIGURE 4.14: Dependence between the x_1 and x_2 features described by the Gaussian copula with $\rho = 0.7052$ which returned NLogL = -20.5485

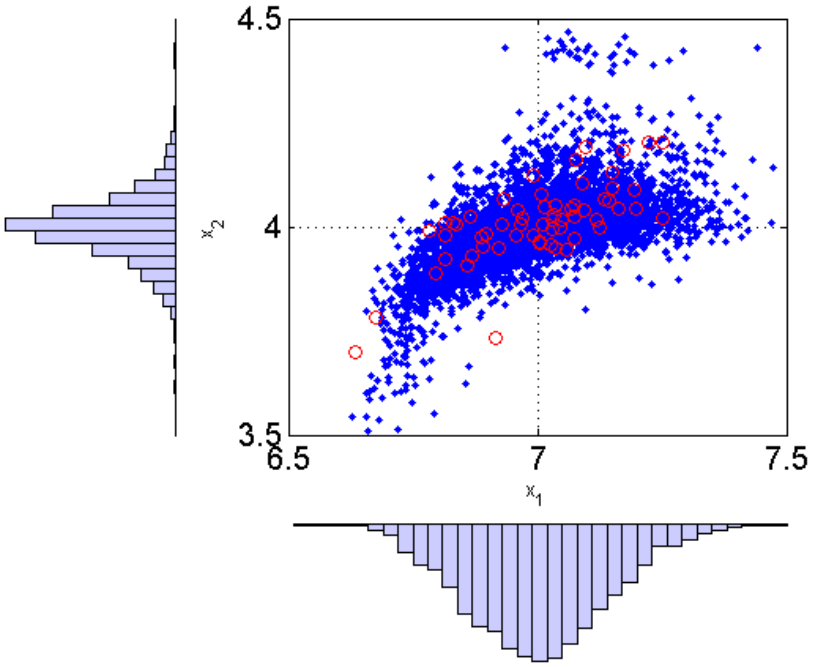

FIGURE 4.15: Dependence between the x_1 and x_2 features described by the Clayton copula with $\theta = 1.5955$ which returned NLogL = -17.8684

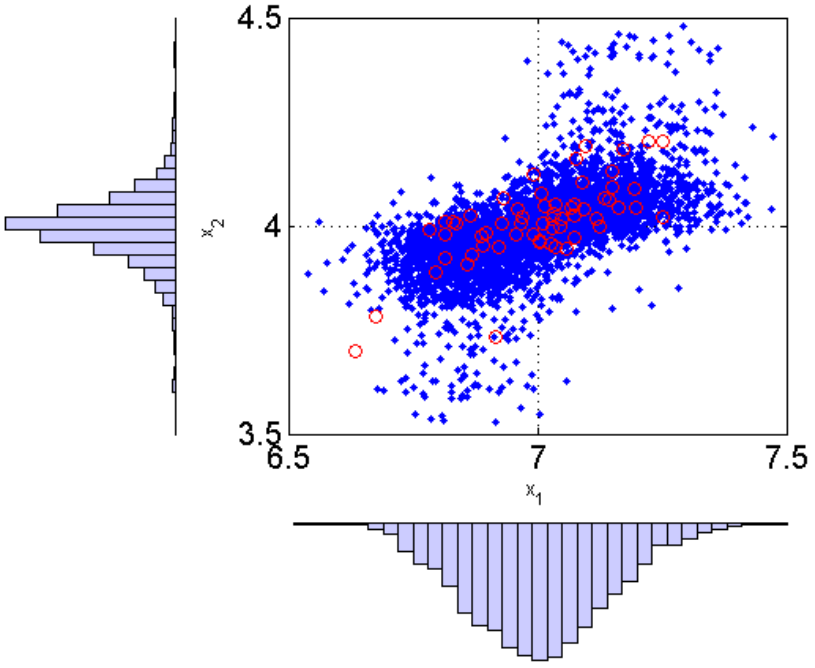

FIGURE 4.16: Dependence between the x_1 and x_2 features described by the Frank copula with $\theta = 5.8142$ which returned NLogL = -17.8611

The costs parameters required for the Optimal Mean Setting procedure are given in Table 4.3, these were chosen arbitrarily as there were no cost data given in the original data source (Aparisi et al. [1999]). The Optimal Mean Setting and achieved profit are also presented in Table 4.3. The first two values in the $\boldsymbol{\mu}$ vector correspond to dual feature rework, while the last two values correspond to single feature rework. The profit achieved through Optimal Mean Setting was 83% higher than the profit achieved by setting all the means to the nominal mean settings (given in Table 4.1). The final distribution of the manufactured geometry is illustrated by the blue joint distribution in Figure 4.17, this includes components that would be scrapped (diameters larger than the upper specification limits) but models the joint distribution where rework has been completed.

Variable	***Value***
Rc	[5 5 10]
Sc	[50 50 50 50]
SP	100
PC	20
$\boldsymbol{\mu}$	[6.8737 3.9514 6.8441 3.9486]
Profit	44.47

TABLE 4.3: Costs for the manufacture of the big end and small end diameters (features x_1 and x_2) of the connecting rod in Figure 4.11

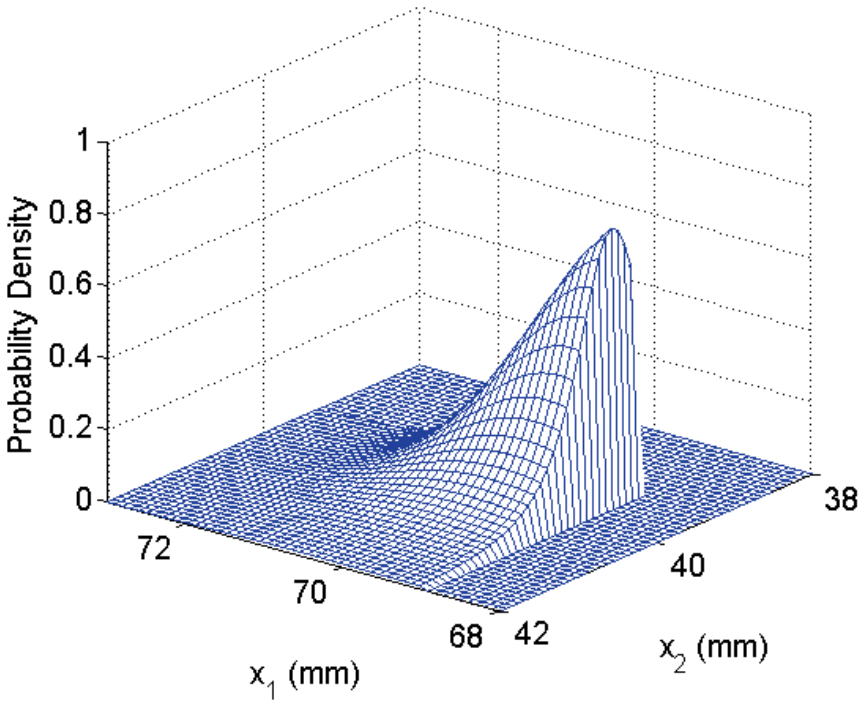

FIGURE 4.17: Finial Geometry distribution of the connecting rod x_2 and x_3 features

The case study demonstrates the applicability of copula modelling to the field of Optimal Mean Setting, where the different manufacturing processes used to create the x_1 and x_2 features produced manufacturing variability best modelled using different parametric distributions. Such an exercise is simply not achievable using a parametric multivariate distributions, as the marginal distributions are from separate parametric families. The benefit of copula functions is also explored in a case study in Appendix F. Here a non-normal distribution is created where a feature is created as a result of another feature. This additional case study also demonstrates how easily the Optimal Mean Setting framework and Equation 3.78 can be fitted to a non-standard example.

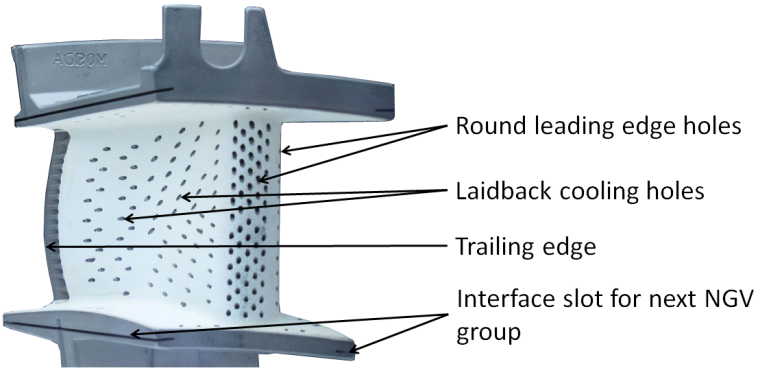

FIGURE 4.18: A V2500 gas turbine NGV (Cleynen [2013])

4.4 Optimal Mean Setting for Cooling Holes

Modern gas turbine engines rely on film cooling to ensure components in the 'hot' part of the engine stay within the material's thermal limits. Typically the combuster, turbine blade and nozzle guide vanes (NGVs) experience the greatest temperatures and film cooling research is devoted heavily to these components. In this thesis, the film cooling holes associated with high pressure turbine blade and guide vanes are studied. The geometry of these film cooling holes is designed to release coolant air in such a way that it forms a protective layer of cool air between the surface of the component and the hot gas. The effectiveness of this coolant layer depends very much on the geometry of the hole where small variations in the hole geometry can lead to large changes in the film cooling effectiveness. The effectiveness of the film cooling determines the surface temperature of the blade which has a significant impact on blade life. Indeed, Bunker [2009] estimated the variations that occur during manufacture could lead to a 20^oC increase in surface temperature (worst case) which would decrease blade life by up to 33%.

4.4.1 Cooling Hole Geometry

Cooling holes are manufactured through the surface of a hollow blade or vane and allow coolant air (taken from the compressor stage) form a film over the surface. Figure 4.18 illustrates these holes on a V2500 engine nozzle guide vane (NGV). Two types of hole are present, straight round holes and laidback holes which have an expansion angle relative to the main hole. The white coating is the ceramic thermal barrier coating used to protect the nickel alloy from excessive heat on the surface. The influence of hole geometry and hole configuration in relation to cooling effectiveness has been studied since the 1960s (Goldstein et al. [1968], Goldstein et al. [1974]). There are a variety of hole shapes that have been developed in the literature, the main variations are shown

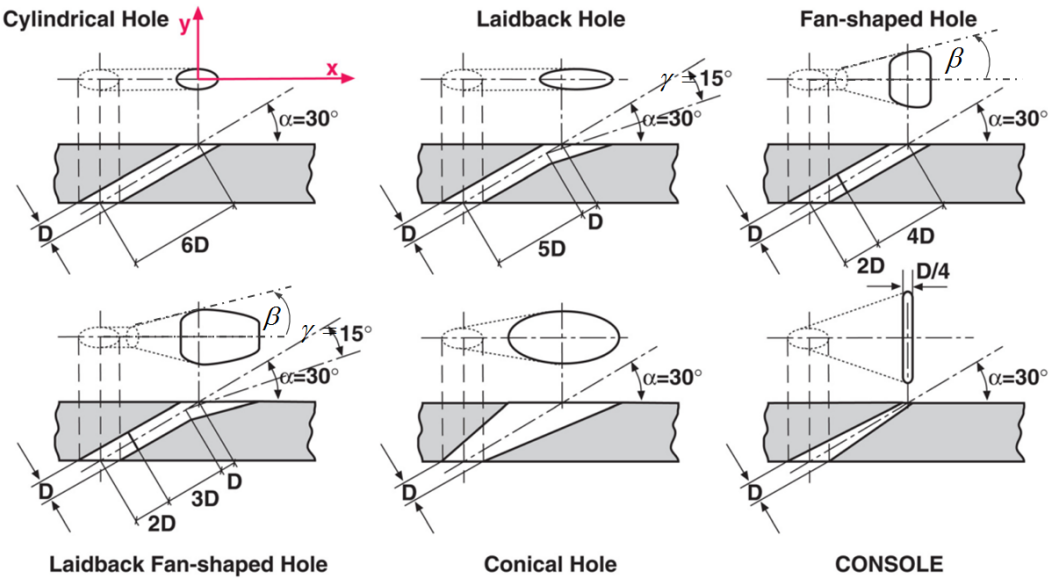

FIGURE 4.19: Types of film cooling holes from Saumweber and Schulz [2012]

in Figure 4.19 from Saumweber and Schulz [2012]. Goldstein et al. [1974], Makki and Jakubowski [1986] and Yu et al. [2002] were among the first to investigate the differences between round (Cylindrical Holes in Figure 4.19) and laidback holes, where the exit of the hole is expanded to diffuse the coolant flow. Gritsch et al. [1998], Thole et al. [1998] and Gritsch et al. [2000] confirmed the advantages of diffuser type holes with regard to cooling effectiveness. Holes that diffused in the lateral direction as well as in the stream-wise direction (laidback fan-shaped hole, Figure 4.19) were also favoured compared to holes that expanded only in one direction (laidback and fan-shaped hole, Figure 4.19). Guangchao et al. [2008] also offers an illustrative comparison between round and diffusing holes with regard to cooling effectiveness downstream of the hole. The benefit of diffusion shaped holes was also confirmed through an extensive review by Bunker [2005] who noted: "*The benefits of shaped hole film cooling are real and substantial, so much so that these types of film holes are used whenever possible in the practice of cooling gas turbines.*". A relatively modern class of hole was developed at Oxford University (Sargison et al. [2001] and Sargison et al. [2002]), where, as opposed to expanding the coolant flow, the coolant was accelerated as the hole morphed from a cylindrical entrance into a convergent slot exit. The principle of this CONverging Slot hOLE (CONSOLE) was to re-laminarize the flow as it passed from the internal passages of the blade (or vane), through the hole onto the airfoil surface. The goal was to establish a laminar boundary layer at the slot exit to reduce mixing with the hot gas. Although the cooling performance of CONSOLE holes is similar to fan shaped holes, the aerodynamic losses are far less. This is because the coolant emitted from a CONSOLE hole forms a laminar boundary layer far less thick than the turbulent boundary layer that forms behind a fan-shaped hole.

As well as changing the type of hole (say, from cylindrical to a laidback fan-shape), the geometric parameters of a particular class of hole can also impact the cooling effectiveness. Such a study was performed by Kohli and Thole [1998] and Hyams and Leylek [2000] where the flow field was found to be highly complex and heavily influenced by the hole's geometric parameters which had a major impact on the cooling effectiveness. Gritsch et al. [2005] was the first to specifically analyse the effects of geometry parameters on cooling effectiveness and Bunker [2009] gave a highly comprehensive review regarding the effects of manufacturing tolerances on film cooling. Lee and Kim [2010], Lee et al. [2010] and Lee and Kim [2011] also investigated multiple variations of fan and laidback fan holes to find an optimum hole geometry. They considered inclination angle (α in Figure 4.19), laidback angle (γ in Figure 4.19), lateral expansion angle (β in Figure 4.19) and length to diameter ratio (L/D). Saumweber and Schulz [2012] gave a detailed investigation regarding the influence of several geometric hole parameters on cooling effectiveness, and analysed the local effectiveness in response to these to geometry changes. The lateral expansion angle (β in Figure 4.19), inclination angle (α in Figure 4.19) and the length to diameter ratio (L/D) parameters were studied. Significant changes to the local cooling effect lead to large differences in the average cooling effectiveness although the variations were typically much greater than would be seen due to manufacturing variation (4 degree increments in β, 15 degree increments in α and $L/D = [6, 10]$). The relationships between cooling effectiveness and hole shape are also influenced by variation in the external flow (such as cross flow and turbulence intensity (Saumweber et al. [2003], D Ammaro and Montomoli [2013])), variations in the inlet conditions and hole entrance (Saumweber and Schulz [2008] and D Ammaro and Montomoli [2013]), as well as operating conditions such as the density ratio between the hot gas and coolant and the blowing ratio of the holes. It is also important to consider the amount of air required for cooling, ideally one aims for low mass flow of coolant and high cooling effectiveness but exactly what the trade-off should be depends on the overall engine performance and operating conditions The overall relationship between a hole's geometric parameters and the cooling efficiency is therefore complex and it is necessary to carefully consider the operating conditions in evaluating the effects of a hole's geometry on cooling performance (see Conclusion of Saumweber and Schulz [2012]).

4.4.2 Cooling Hole Manufacture

Cooling holes are often manufactured by electro discharge machining (EDM), or laser drilling (Bunker [2009]). In this case study the laser drilling process is considered. A detailed review of the Laser drilling process is available from Dhar et al. [2006] and Kreutz [2007] giving more details regarding 5-axis Laser drilling for the creation of

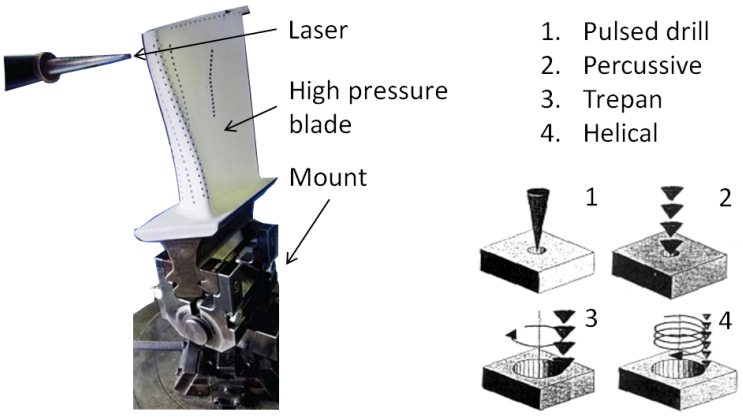

FIGURE 4.20: A laser drilled blade (left picture Wos [2010]) and an illustration of laser drilling techniques (right figure Dhar et al. [2006])

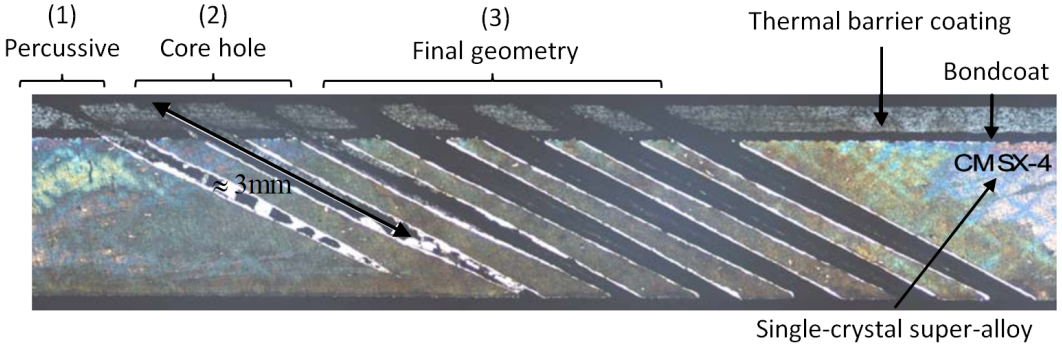

FIGURE 4.21: Laser drilling process steps from Poprawe et al. [2008])

shaped holes. McNally et al. [2004] discussed some of the challenges of Laser drilling particularly in regard to drilling through the thermal barrier coating. Poprawe et al. [2008] also details the Laser drilling process of a shaped hole (which was designed for easy manufacture) with a thermal barrier coating. In general, there are several steps to creating a shaped hole, which vary depending on the hole geometry. The steps involved in creating a laidback fan-shaped hole are detailed in Figure 4.21, from Poprawe et al. [2008] (the laidback angle is small for this hole ($\gamma = 10$, which makes it difficult to visually differentiate this as a laidback hole). The first stage (1) involves percussive drilling to form the centre of the hole. The diameter of the hole is increased by two trepanning cycles (step (2)), which results in a near net shape hole. The third step (3), involves four trepanning cycles at an increasing feed rate to finalise the hole geometry.

Inspecting cooling holes to ensure geometric conformance is problematic due to their diminutive nature, typically diameters are tenths of millimetres (< 1 mm). Nevertheless, there are several methods for ensuring cooling holes conform to the specification limits. A holistic measure to verify that the average hole geometry is within the specification, can be achieved through flow rate analysis, where the mass flow rate of air through the blade is measured. This does not establish if individual holes conform, as a blockage in

one hole may be compensated for by an oversized hole elsewhere. Bunker et al. [2011] offered an advance on standard mass flow rate inspection by measuring the transient thermal response of an internal surface beneath the downstream jet emitted from the cooling hole. If the geometry of the hole performed correctly, the transient response would match the theoretical calculation for transient heating. A more direct method of evaluating the geometry of holes is though direct inspection with calibrated pins. The diameters of these pins increases incrementally and the 'snuggest' fit indicates the approximate diameter of the hole (Shetty et al. [2008]). This method is time consuming and only reveals the smallest hole diameter, it does not pick up defects and cannot be used to verify angles accurately. Shetty et al. [2008] developed an approach to optically determine the diameter and depth of holes. A camera and image recognition algorithm was used to visualise and inspect the hole diameter, while a precision diffractive light tube was used to determine the hole depth. A camera inspection system was also developed by Ho et al. [2012], to determine breakthrough (when the laser penetrates the total thickness of the surface). It is important to monitor breakthrough to help ensure the quality of the hole and prevent damage to the internal geometry of the blade. Another type of visual inspection was developed by Schneider et al. [2010], where x-ray radiography was used to analyse the cross-section of the holes, known as DODO (Direct Observation of Drilled hOle). The method allows measurement of all hole characteristics as well as manufacturing imperfections such as the re-cast layer formed due to melt rather than vaporisation during the Laser drilling process.

4.4.3 Feasibility of Optimal Mean Setting to Film Cooling Hole Manufacture

The following Section considers the parameter and tolerance design of a film cooling hole in relation to Optimal Mean Setting. The literature discussed hitherto indicates the cooling effectiveness of cooling holes can be highly dependent on the geometry of the hole. Tightening the tolerances controlling the geometry of the hole can lead to improvements in the cooling effectiveness. Optimal Mean Setting can be applied to maximise the profit when these tight tolerances lead to non-conformance due to the variation of the manufacturing process.

A fundamental requirement of Optimal Mean Setting is the ability to inspect and rework features. The discussion in Section 4.4.2 clearly indicate it is possible to rework and inspect holes[10]. However, there are challenges to implementing such a system in an industrial environment.

[10]The current laser drilling method illustrated by Figure 4.21 is tantamount to a series of rework steps where the hole is created over a number of drilling cycles

- Inspection of the hole's geometric parameters should take place in-situ to prevent large increases in manufacturing time (if components have to be removed, inspected and then repositioned for re-drilling). In-situ inspection would also prevent inaccuracies emerging from variation in the positioning of components on an inspection jig and then replacement on the drilling jig.
- Rework must also take place in-situ to avoid large increases in manufacturing time and inaccuracies due to replacement of components. This leads to potential complications with regard to adjusting hole inclination angles or diameters as the beam may damage the internal geometry of the blade or vane if breakthrough had already occurred. It may be possible to fill the blade with a substance to block or absorb the beam or ensure breakthrough would not occur until rework on other parameters has been completed.

The application of Optimal Mean Setting to the manufacture of features ultimately depends on whether the benefits achievable through tighter tolerances outweigh the extra manufacturing costs. All tolerances would be tightened (provided there was some benefit to doing so) if the cost was low enough. There is no intrinsic technical reason why inspection and rework could not be applied to the manufacture of film cooling holes, although the expense may be prohibitive. With this in mind an Optimal Mean Setting analysis was implemented to establish the likely performance benefits and a sensitivity analysis was performed to determine when such a strategy would be economically beneficial.

4.4.4 Cooling Hole - 2D, Two parameter

An initial study was set up to investigate the application of Optimal Mean Setting to a cylindrical hole governed by two geometric parameters, the inclination angle (α) and the hole diameter d. The performance of a cooling hole was evaluated by calculating the adiabatic film effectiveness down-stream of the hole where adiabatic effectiveness was given by,

$$\eta = \frac{(T_g - T_s)}{T_g - T_j}. \tag{4.21}$$

The temperature of the hot gas in the main duct was T_g, T_s was the temperature at the surface of the airfoil and T_j was the temperature of the coolant jet. A two-dimensional analysis was performed rather than a three-dimensional study, due to computational constraints in solving the thermal effectiveness at enough design points to ensure the variation in thermal effectiveness scaled realistically with the small variations in α and d. An illustration of the 2D domain is given in Figure 4.22, which follows the conventions of the majority of the literature discussed above. The domain is somewhat

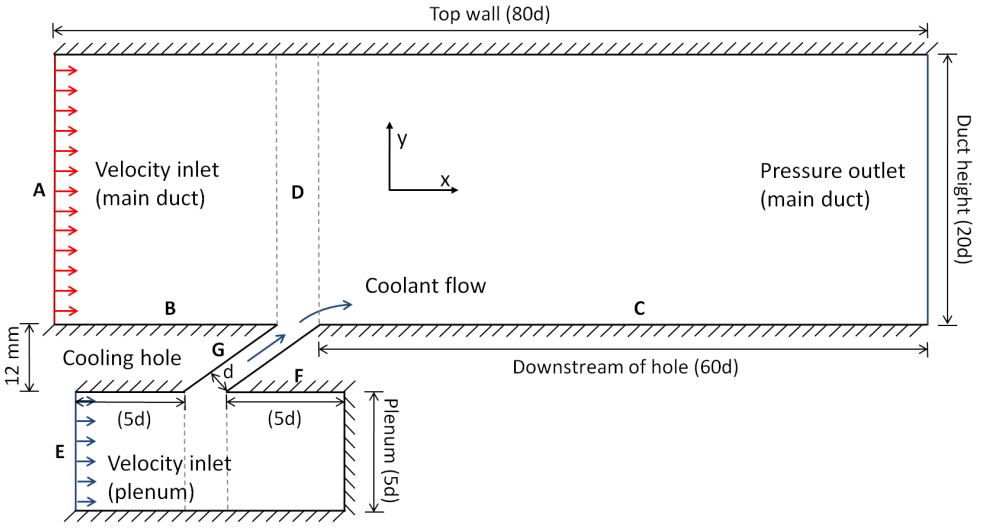

FIGURE 4.22: Overview of the 2D cooling hole computational domain (not to scale)

simplified from a hole on a curved airfoil surface, nor is there any global pressure differential between the main duct velocity inlet and pressure outlet, as would occur on the suction side of an airfoil surface as flow would be accelerated. The principle reason for limiting the complexity of the domain was to ensure the numerical results obtained from computation fluid dynamics (CFD) could be compared to the experimental observations from laboratory experiments in the published literature. Laboratory conditions also used lower temperatures, pressures, heat flux and lower velocity than real engine conditions[11]. Furthermore, the airfoil wall material and holes themselves differ from real engines conditions. Typically, laboratory experiment holes are > 4 mm for manufacturability (Schroeder and Thole [2014]), while real engines cooling holes are < 1 mm. Nevertheless, the discussions are based on normalised values of thermal effectiveness (η) and the fundamental flow physics is broadly unchanged between laboratory conditions and elevated real engine conditions (Wang and Zhao [2011]).

Appendix G details the numerical aerothermal approach taken to establish the jet, gas and surface temperatures downstream of the hole (required in Equation 4.21). The commercial CDF package, Ansys Fluent 14.5 was used to evaluate discrete design points and a Gaussian process regression (Kriging) response surface methodology was used to produce a surrogate model to map changes in the cooling effectiveness with the design features.

[11] A significant challenge in modelling film cooling effectiveness at real engine conditions is acquiring accurate surface temperature readings at elevated temperature. Measuring surface temperatures using thermocouples or film gauges is near impossible due to the extreme temperatures. Infra red techniques can lead to large errors in readings and ensuring access or line of sight for infra red spectrometers or cameras is challenging due to high temperature and pressures (Reagle [2009])

4.4.5 Laser Drilling Costs

A percussive laser drilling process can be used for the production of round holes, as illustrated by process 2 in Figure 4.20. The industry standard technique to produce such holes relies on the use of a flash-lamp pumped Nd:YAG laser. Based on discussions in McNally et al. [2004], Chien and Hou [2006], Kreutz [2007] and Walther et al. [2008] a pulse frequency of 14 Hz and 10 pulses per hole were chosen a suitable drilling parameters. Typically holes with diameters in the range 0.5 mm to 1 mm can be drilled in this way[12].

An illustration of the laser drilling process is shown by the flow chart in Figure 4.24. The drilling process itself is contained by the green box and is generally representative of a percussive drilling process. The inspection process is optically based and is believed to be representative. However, no such process currently exists for the optical inspection of film cooling holes at Rolls-Royce. Nevertheless, a similar optical inspection process is used (in a trial capacity) for the inspection of combuster cooling holes. The inspection process illustrated in Figure 4.24 is based on this combuster cooling hole inspection routine. Typically a blade or vane is also filled with a beam blocking substance to prevent the laser from damaging the internal surfaces of the blade or vane. Often this is a wax as described by Philby and Davies or a gel type substance as shown by Williams [2012]. It is assumed filling the blade with a beam blocking substance is done prior to loading the component in the laser drilling cell and the quality of the beam blocking substance is assumed to maintain its properties irrespective of the number of rework cycles. Thus, the blade does not have to be refilled with a beam blocking substance before rework. Any changes to these assumption simply increase the cost of rework which would affect the positioning of the optimal means but not effect the fundamentals of Optimal Mean Setting (provided a rework method can be implemented).

A breakdown of the times and total time for the drilling and inspection operations are given in Table 4.4. A pulse frequency of 14 Hz and a total of 10 pulse was used to calculate the drill time. Approximately half the total drilling time is accounted for by communication between the machine controller and drill head (coms), the shutter movement, dwell time and index time in order to move the component or drill head to the new position. The image analysis and communication time make up around 80% of the total inspection time. A factory cost rate of 60 £/hr was assumed thus the total drilling processing cost was estimated at 0.0196 £ per hole while the inspection cost was

[12]The diameters of the holes from the CFD study were in the range 6.46 mm to 8.8 mm, to ensure the CDF results could be compared directly to experimental evidence.

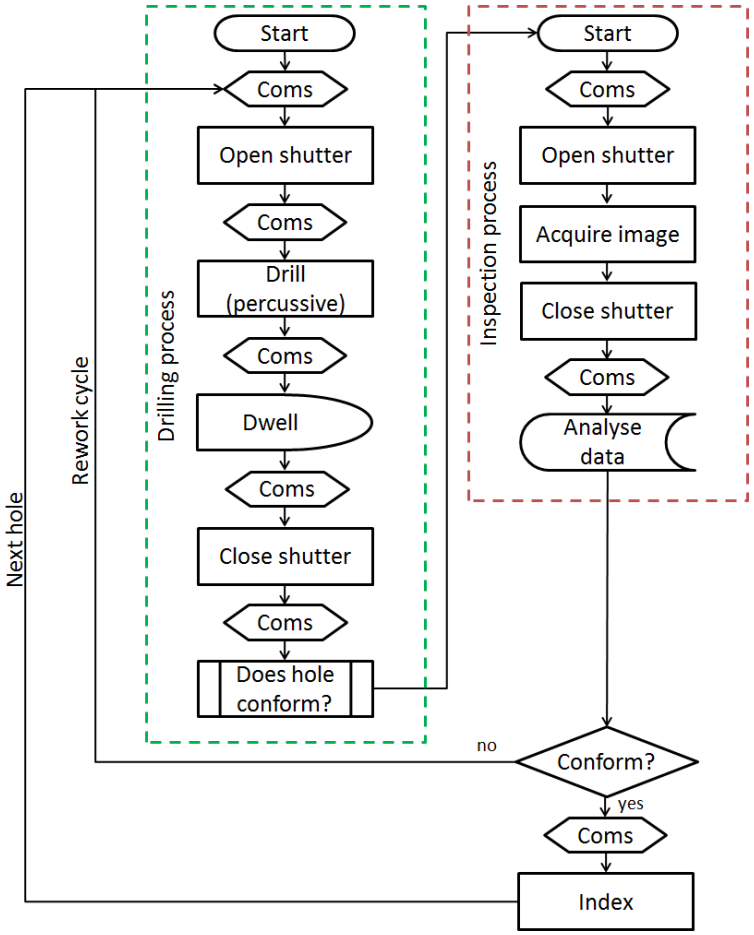

FIGURE 4.23: Flow chart of the laser drilling, inspection and rework process

estimated to be 0.0125 £ per hole[13]. A rework operation was determined by the sum of the drilling process cost and inspection cost of 0.0321 £.

Drill Processes	**Time (s)**	**Inspect Processes**	**Time (s)**
Drill	0.714	Communication	0.1
Communication	0.25	Take image	0.1
Shutter move	0.1	Analyse image	0.5
Dwell	0.1		
Index	0.01		
TOTAL	1.174	TOTAL	0.75

TABLE 4.4: Laser drilling and inspection times

The costs required for Optimal Means Setting are given in Table 4.5.

[13]This inspection cost figure is less reliable than the drilling time figure as there is no such inspection process currently in operation so it is based on the optical inspection process for the inspection of combuster holes.

Rc (£)	[0.0321, 0.0321, 0.0642]
Sc (£)	[1000 1000 1000 1000]
SP (£)	0.03914
PC (£)	0.0321

TABLE 4.5: Costs of rework, processing and selling price for the α and d parameters of the film cooling hole

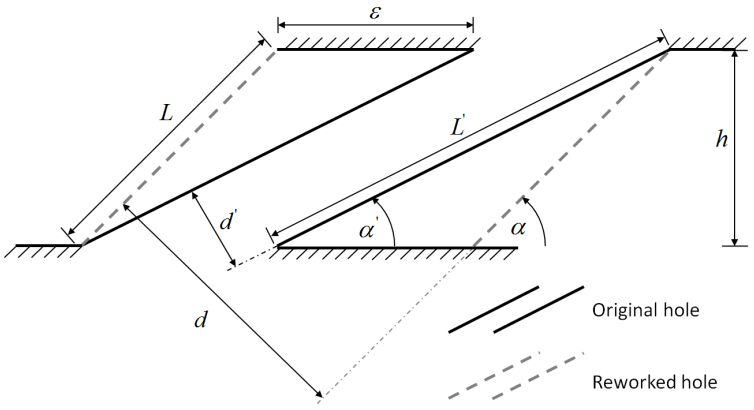

FIGURE 4.24: Rework of the hole inclination angle

4.4.6 Optimal Mean Setting - Film Cooling Hole

As the laser drilling process creates the two features (the inclination angle α and diameter d) in a single process, there is a deterministic relationship between the reworking of the angle and the diameter. It is not possible to rework the angle independently of the diameter, as illustrated by Figure 4.24. Here, the angle of the drilled hole, $\alpha^{'}$ is less than the required angle α. The hole may be reworked to increase this angle, however, in doing so the diameter d will also change by $2\,\varepsilon$ where ε is given by,

$$\varepsilon = \tan(|\alpha - \alpha^{'}|)\frac{h}{\cos(90-\alpha)}.$$

The same formula is applicable if the drilled angle were greater than the required angle, where rework would be required to reduce the inclination angle to ensure conformance. Since the inclination angle may always be reworked (in the range of the variation in the study), the only scrap probability was due to the increase in diameter from reworking the angle, and the probability the diameter was too large from the initial operation. Figure 4.24 illustrates the dependence between the diameter and reworking the angle. Small alterations to α will result in small ε values and hence small increases to the diameter d relative to $d^{'}$. However, large differences between $\alpha^{'}$ and α lead to large ε values which substantially increased d. The joint probability of scrap, conformance and rework is illustrated by Figure 4.25 where the angle can be reworked if it is greater than the upper specification limit or lower than the lower specification. limit. It follows that $p_{\mathrm{I},2} =$

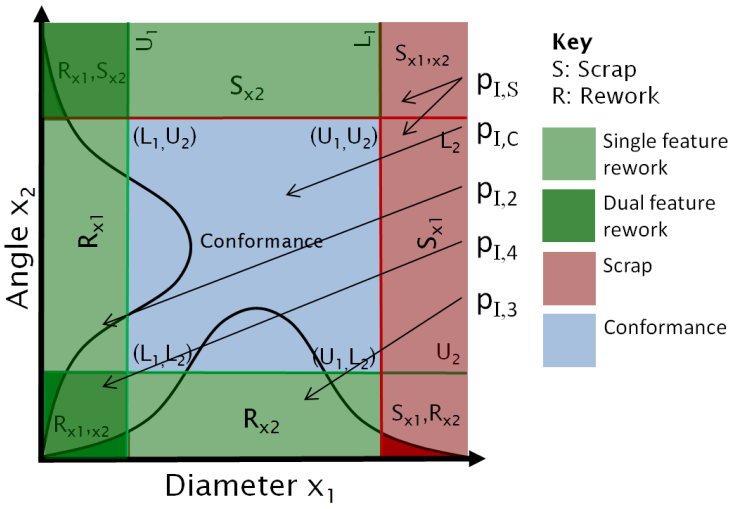

FIGURE 4.25: Joint distribution of the diameter (x_1) and inclination angle (x_2) parameters

$F(L_1, U_2) - F(L_1, L_2)$, $p_{\text{I},3} = 0$, $p_{\text{I},C} = F(U_1, U_2) - F(L_1, U_2) - F(U_1, L_2) - F(L_1, L_2)$, $p_{\text{I},4} = F(U_1) - p_{\text{I},C} - p_{\text{I},2}$ and $p_{\text{I},S} = 1 - F(U_1)$. The $p_{\text{I},3}$ term is zero because there can be no '*angle only*' rework. Any rework of the angle implicitly involves rework of the diameter, thus the probability of features being in the $p_{\text{I},3}$ region in Figure 4.25 ($F(U_1, L_2) - F(L_1, L_2)$) is incorporated in $p_{\text{I},4}$ term (dual feature rework).

The process flow and rework stages are illustrated by Figure 4.26 where the feed-in to state 3 from the initial processing state (I), goes into the dual feature rework state (4). Despite the slight change in the joint distribution from the standard set up (comparing Figure 4.25 to Figure 3.6 on page 57) the same model and subsequent expected profit equations can be used (Equation 3.78) by just modifying the probabilities associated with state 3.

The variation in cooling efficiency was plotted against the α and d parameters in Figure 4.27, which was created using the response surface methodology discussed in Section G.4. The black points are the CDF evaluations of the initial sample points from the DoE.

Parameter and Tolerance Design

The trade-off study was performed to establish the Pareto front of profit versus cooling efficiency. Eight minimum cooling efficiency points were selected in the range $0.77270 \leq \eta \leq 0.77345$. The means and tolerances for the angle and diameter of the hole were optimised to yield highest profit for standard and Optimal Mean Setting production techniques. A Monte-Carlo simulation was performed for each set of means and standard deviations (defined from the optimiser) and the proportion of points yielding

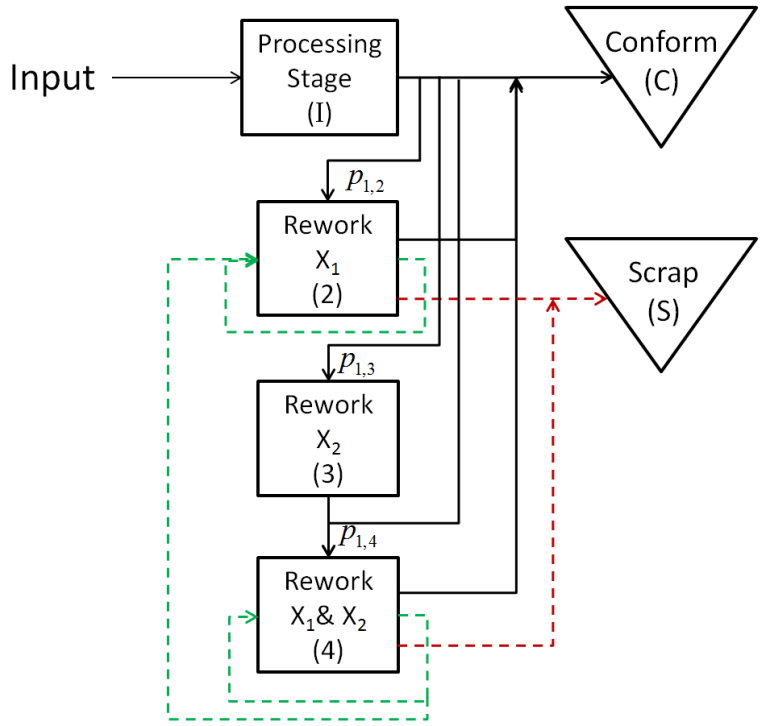

FIGURE 4.26: Process flow and rework stages for the cooling hole diameter (x_1) and inclination angle (x_2) parameters

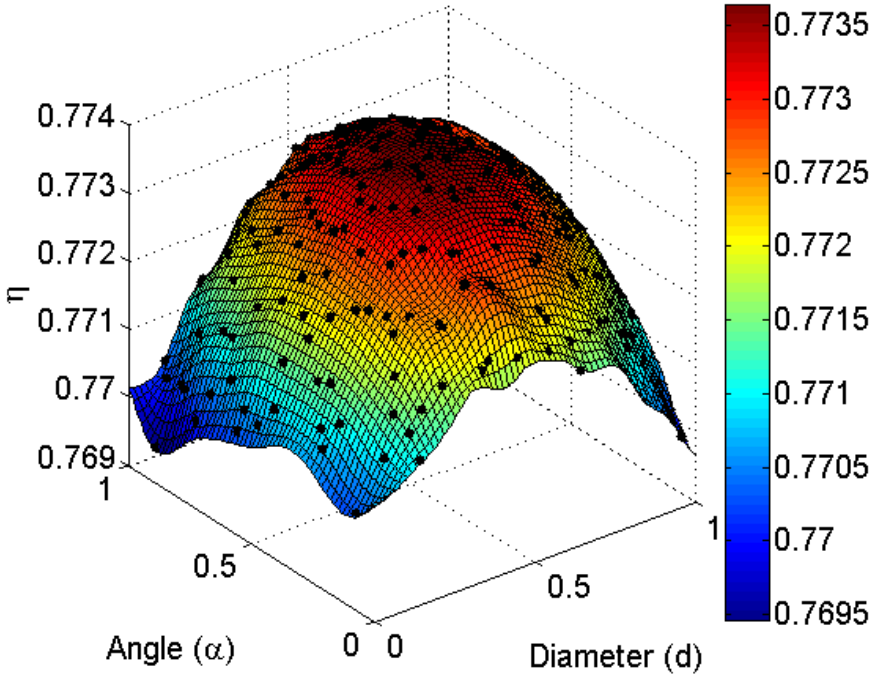

FIGURE 4.27: Cooling effectiveness in response to changes in the α and d parameters

better or equal to the minimum cooling effectiveness was verified. The optimisation strategy is outlined in Equation 4.22 where $EP(\bullet)$ is the expected profit function, $\eta(\bullet)$ is the function of a cooling effectiveness and r is a reliability constraint specifying the required conformance from the Monte-Carlo run. The reliability constraint $R = 0.9938$ corresponding to a 4 sigma level, which implies 99.38% of the points would meet the minimum cooling effectiveness level, $\eta_{\min}$. Failure to comply with this requirement invoked a penalty for the expected profit of -1×10^9 units

$$\begin{cases} \text{find:} & \boldsymbol{\mu} \text{ and } \boldsymbol{\sigma} \\ \text{maximise:} & EP(\boldsymbol{\mu}, \boldsymbol{\sigma}), \\ \text{subject to:} & P[\eta(\boldsymbol{\mu}, \boldsymbol{\sigma}) \geq \eta_{\min}] \leq r \\ & \boldsymbol{L} \leq \boldsymbol{\mu} \leq \boldsymbol{U}. \end{cases} \tag{4.22}$$

Optimisation Strategy

For each $\eta_{\min}$, a set of initial starting means and z values were given, where $\boldsymbol{\mu} = [0.5, 0.5, 0.5]$ and $\boldsymbol{z} = [1, 1]$. Since the standard deviations of the manufacturing process were set at $\boldsymbol{\sigma} = [0.1097, 0.1026]$[14] the z-values determined the upper and lower specification limits, where $\boldsymbol{L} = \boldsymbol{\mu} - \boldsymbol{z}\,\boldsymbol{\sigma}$ and $\boldsymbol{U} = \boldsymbol{\mu} + \boldsymbol{z}\,\boldsymbol{\sigma}$. Four parameters were optimised for the standard production technique, two related to the angle and diameter means. There was no angle rework mean as there was no benefit to allowing the angle mean to deviate from the nominal and there was no option to rework the angle independently of the diameter. Rework for the diameter was set using the same mean as the initial processing for this standard production technique. The remaining two parameters related to the z-values for the angle and diameter, determining the specification limits. Two extra optimisation parameters were included for the Optimal Mean Setting production; a diameter rework mean, and a separate z-value parameter allowing the mean to be off-centre relative to the specification limits. This allowed the diameter to be biased towards the upper or lower specification limits by specifying the upper and lower specification limits as $U = \mu_d + z_{d_u}\,\sigma_d$ and $L = \mu_d - z_{d_l}\,\sigma_d$, respectively.

A two stage optimisation approach was used, where a genetic algorithm was applied to find the local optima in the design space, followed by a local optimiser. The Matlab genetic algorithm (*ga.m*) was used with a population size of 50 for the standard production technique and 60 for the Optimal Mean Setting technique, the mutation rate

[14]The process standard deviations for the hole angle and diameter were defined from a nominal hole with absolute dimensions $\alpha = 33$ degrees and $d = 7.7$ mm. Normalising the standard deviation and assuming all values would be encompassed by $\pm = 3\sigma$ from the nominals gave the standard deviations noted above.

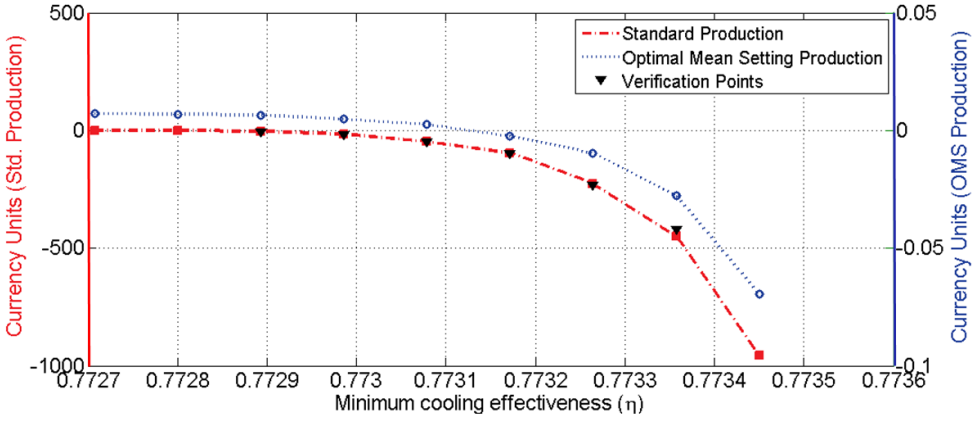

FIGURE 4.28: Cooling effectiveness in response to changes in the α and d parameters

and crossover probability were kept at the default setting. The optimiser was run for 100 generations equating to 5000 evaluations for the standard production technique and 6000 evaluations for the Optimal Mean Setting technique. The optimum means and z-values formed the inputs for the local optimisation run which used the *fmincon.m* algorithm (Mathworks [2012]). This was run for a maximum of 800 evaluations or until the change in expected profit (EP) was no more than 1×10^{-4}. Each Monte-Carlo run was performed with 1×10^6 which lead to each function evaluation taking approximately 1.1 seconds on a 3.4 GHz Intel Core i7 processor.

Figure 4.28 illustrates the expected profit from the standard production system and Optimal Mean Setting method for increasing cooling effectiveness. Six verification points were run to justify the use of 1×10^6 points for the Monte-Carlo runs. Each verification point was evaluated with 1×10^7 points. The absolute values from the two Monte-Carlo

	$\eta = 0.7729$	$\eta = 0.7730$	$\eta = 0.7731$	$\eta = 0.7732$	$\eta = 0.7733$	$\eta = 0.7734$
10^6 pnts	-4.02	-15.81	-48.33	-95.80	-225.66	-448.27
10^7 pnts	-4.00	-15.62	-40.46	-95.04	-229.41	-419.94
difference	0.51%	1.21%	0.28%	0.80%	1.64%	6.75%

TABLE 4.6: Monte-Carlo verification results

resolutions are given in Table 4.6, where the percentage differences were considered sufficiently small to justify the use of 1×10^6 points for each Monte-Carlo run.

Figure 4.28 clearly demonstrates the benefit of using Optimal Mean Setting to increase profit relative to a standard production technique. At the lowest value of η, the expected profit from both techniques was the same, 0.0070. As the minimum η value was increased, the production cost of the standard production technique rose rapidly, consequently reducing profit to a greater extent than the Optimal Means Setting method. At the highest level of cooling effectiveness, $\eta = 0.77345$, the profit from Optimal Mean Setting was -0.070 £ while the profit from a hole produced using conventional methodology

was −957.35 £[15]. The difference in surface temperature between these two extremes is 0.6 K using the real engine conditions given in Wang and Zhao [2011] where the temperature of the gas in the duct was 1400 K and the coolant jet was at 750 K. For reasons discussed Section G.3, the response surface is likely have a greater gradient for 3D conditions, thus the surface temperature difference between the two design is likely to be exaggerated. The 0.6 K improvement is not economic for a standard production technique, incurring a production cost of 957.35 £ per hole. The Optimal Mean Setting technique indicates a production cost for the same minimum η of just 0.086 £ per hole. This is 2.7 times greater than the cost of producing a hole which incurs no scrap or rework, but the extra cost is relatively insignificant compared to the value of a blade. The means, z-values, profits and production costs from the standard production and Optimal Means Setting techniques are shown in Tables 4.7 and 4.8 respectively.

		Means		**z-values**		**Currency (£)**	
η	ρ	μ_d	μ_α	$z_{d_{l,u}}$	z_α	$E(PR)$	Prod. cost
0.77252	0	0.6105	0.5602	9.0299	8.4327	0.0070	0.0321
0.77261	0	0.6500	0.6346	8.5249	9.1047	0.0070	0.0321
0.77271	0	0.5671	0.5156	7.4019	3.9059	0.0070	0.0321
0.77280	0	0.5599	0.4881	4.5472	0.7156	-0.0471	0.0677
0.77289	0	0.5671	0.5517	2.8315	0.8082	-4.0225	4.0452
0.77299	0	0.5494	0.5421	2.2913	1.0305	-15.8104	15.8374
0.77308	0	0.5304	0.5646	1.9382	0.7398	-48.3268	48.3474
0.77317	0	0.5068	0.5543	1.4989	1.0711	-95.7987	95.8247
0.77326	0	0.4894	0.6004	1.0974	0.8568	-225.6591	225.6791
0.77336	0	0.4534	0.5376	0.6585	0.7909	-448.2683	448.2830
0.77345	0	0.4154	0.5390	0.0909	0.2232	-957.3500	957.3508
0.77336	-.8	0.5756	0.6015	1.9096	0.4291	-78.1628	78.1758
0.77336	.8	0.5654	0.5734	1.7036	0.7393	-76.3840	76.4050

TABLE 4.7: Optimisation results for a cooling hole manufactured using a standard production technique

Finished geometry with no correlation between d and α

The positioning of the means and tolerance limits (given from the z-values) is illustrated by the three Figure pairs representing the standard production technique and Optimal Mean Setting in Figure 4.29. The solid green points represent the optimal means for initial processing, while the green star on the right hand plots illustrate the optimal means for the single feature rework. Each plot also displays contours illustrating the final distribution of the manufactured geometry after rework. The hole diameter distributions are truncated towards the diameter rework specification limit (left white line) while the inclination angle distributions are truncated at both specification limits. This was

[15]The profit is negative due to the relatively low selling price of 0.03914 £ in Table 4.5.

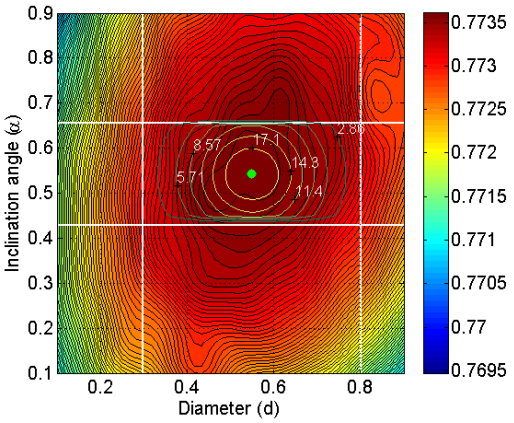

(a) Standard production with $\eta = 0.77299$

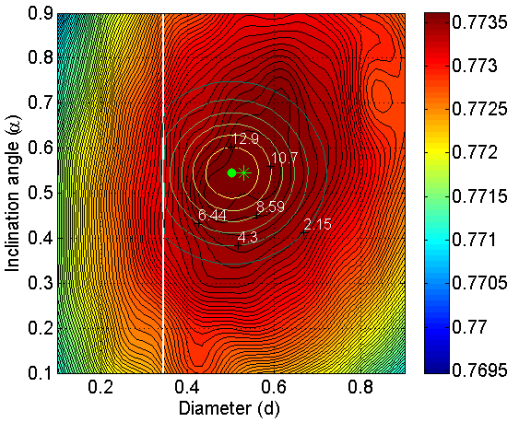

(b) Optimal Mean Setting production with $\eta = 0.77299$

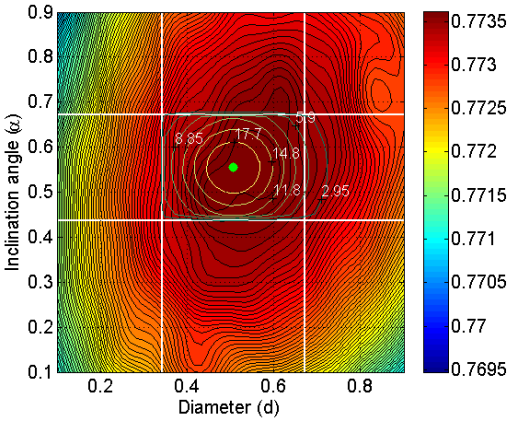

(c) Standard production with $\eta = 0.77317$

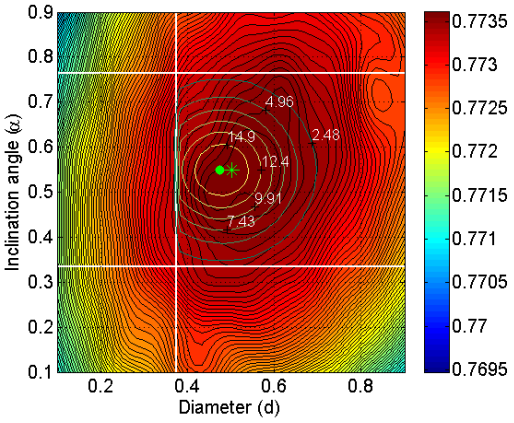

(d) Optimal Mean Setting production with $\eta = 0.77317$

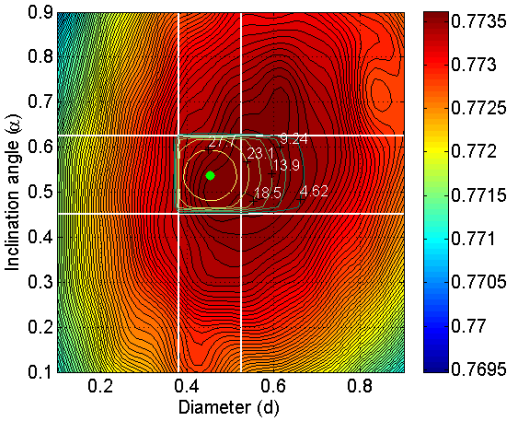

(e) Standard production with $\eta = 0.77336$

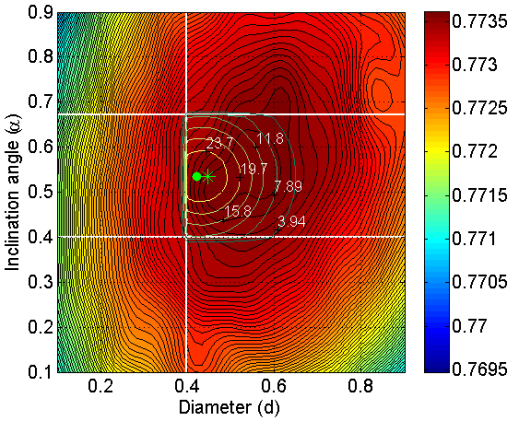

(f) Optimal Mean Setting production with $\eta = 0.77336$

FIGURE 4.29: Optimal means and geometry distributions for varying cooling effectiveness (η)

		Means			**z-values**			**Currency (£)**	
η	ρ	μ_d	μ_α	$\mu_{d_{\text{rework}}}$	z_{d_l}	z_{d_u}	z_α	$E(PR)$	Prod. cost
0.77252	0	0.5807	0.5866	0.6294	8.3502	9.4241	8.4647	0.0070	0.0321
0.77261	0	0.6058	0.5764	0.4307	8.2938	8.5425	9.1149	0.0070	0.0321
0.77271	0	0.5958	0.5994	0.4280	8.3307	9.1901	8.6448	0.0070	0.0321
0.77280	0	0.5314	0.5461	0.6709	2.5341	9.9954	9.2156	0.0069	0.0323
0.77289	0	0.5292	0.5365	0.5844	2.1123	9.9091	9.9972	0.0065	0.0327
0.77299	0	0.5012	0.5452	0.5294	1.5232	9.7337	9.3185	0.0049	0.0342
0.77308	0	0.4933	0.5519	0.5165	1.2423	9.7009	2.6737	0.0026	0.0363
0.77317	0	0.4747	0.5490	0.5018	0.9694	9.9257	2.0922	-0.0025	0.0402
0.77326	0	0.4445	0.5293	0.4519	0.6342	9.5717	1.8807	-0.0096	0.0464
0.77336	0	0.4213	0.5353	0.4477	0.2260	9.9546	1.3290	-0.0278	0.0597
0.77345	0	0.4121	0.5245	0.3811	0.0099	9.6017	0.5592	-0.0697	0.0863
0.77336	-.8	0.5006	0.5947	0.5017	9.5944	9.4981	1.2743	-0.0248	0.0561
0.77336	.8	0.4977	0.5131	0.4877	0.7947	9.9010	1.8665	-0.0072	0.0439

TABLE 4.8: Optimisation results for a cooling hole manufactured using Optimal Mean Setting

because it was always possible to rework the inclination angle if it were less than or greater than the lower and upper specification limits respectively. However, rework on the inclination angle enlarged the hole diameter, hence scrap was produced due to too great a hole diameter. The increase in η from 0.77299 to 0.77336 was accompanied by a shift left of both the standard production and Optimal Means Setting means (Figures 4.29(a) to 4.29(f)). In a pragmatic sense, an initially undersized hole diameter was created, to allow rework and reduced the probability of scrap if the angle (α) did not initially conform. There was very little variation in the optimal mean for the hole angle (α), as the rework cost was equal for features greater than the upper specification limit and less than the lower specification limit. It is noticeable only one specification limit is shown on Figure 4.29(b) and the diameter upper specification limit is not visible in the remaining Optimal Mean Setting Figures (Figures 4.29(d) and 4.29(f)). The generic reason for this is the absence of non-conformance for the specified optimal means and reliability constraint of $R = 99.38\%$. Both the initial and rework means for the diameter (d) parameter are lower in Figure 4.29(b) than the adjacent Figure 4.29(a), which reduced the probability of components falling into the response surface hollow, located around [0.85 0.72] and the yellow shaded region around [0.8 0.4]. This negated the requirement for angle (α) specification limits. The upper specification limit for Figures 4.29(b) to 4.29(f) are never required as the left hand bias of the optimal means reduced the probability of non-conformance (due to too large a diameter), to less than 0.62%.

The shape of the performance distribution between the standard and Optimal Mean Setting production techniques is visualised in Figures 4.31(a) to 4.31(d). In addition to

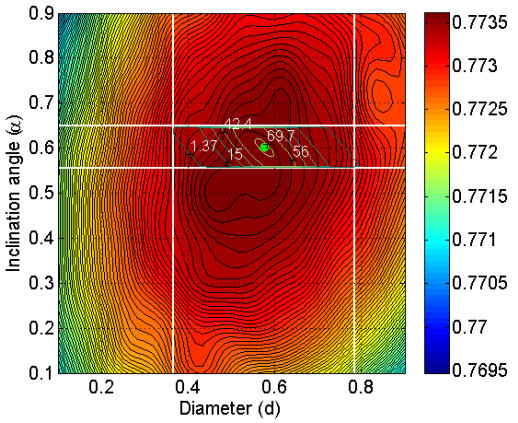

(a) Standard production with $\eta = 0.77336$ and $\rho = -0.8$

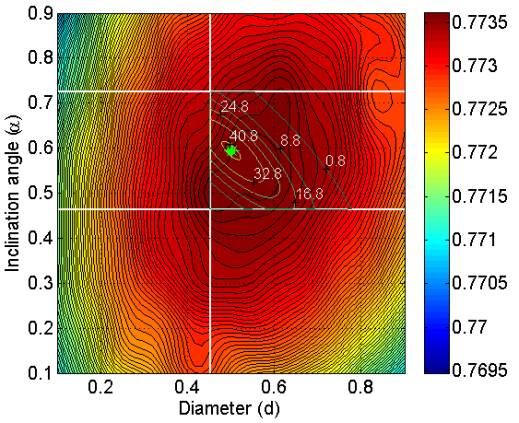

(b) Optimal Mean Setting production with $\eta = 0.77336$ and $\rho = -0.8$

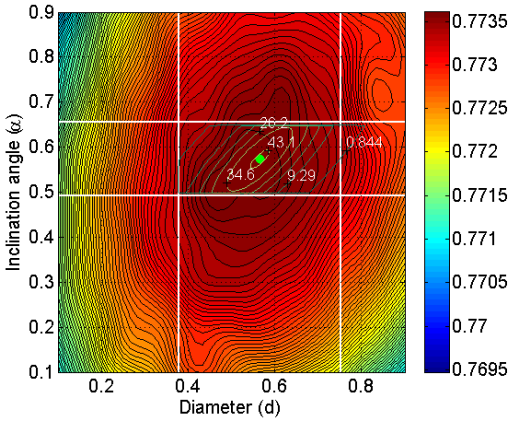

(c) Standard production with $\eta = 0.77336$ and $\rho = 0.8$

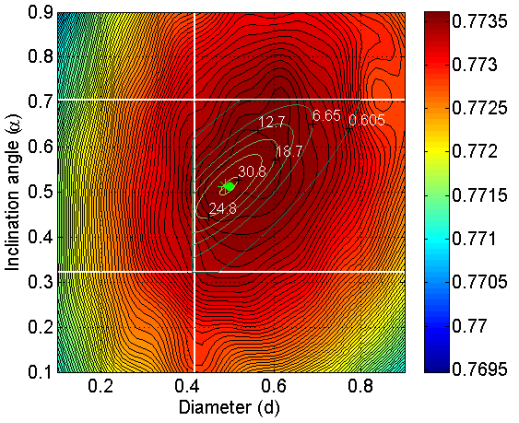

(d) Optimal Mean Setting production with $\eta = 0.77336$ and $\rho = 0.8$

FIGURE 4.30: Optimal means and geometry distributions for varying cooling effectiveness (η) and correlation (ρ)

the three η values chosen for the plots in Figure 4.29, an additional η-value ($\eta = 0.77280$) was plotted (Figure 4.31(a)) to give a holistic picture of the change in the performance distribution with increasing η. The mean performance (η) was always less for the Optimal Mean Setting production technique compared with the standard production. This was because μ_d was always less for Optimal Mean Setting production, which produced components with slightly lower η on average. Additionally, Figures 4.31(a) to 4.31(d) for the Optimal Mean Setting production technique, show a greater number of components with middling values of η compared to the standard production technique. This was again due to the lower μ_d value (for the Optimal Mean Setting technique), which corresponds to lower η values than the standard production technique. The Optimal Mean Setting technique also exhibited slightly bimodal behaviour particularly in Figures 4.31(c) and 4.31(d), where an inflection point formed for middling η values (due to the lower μ_d), before the peak for high η values. The higher peak was bolstered by

the rework mean μ_{rwd}, where the mean for the reworked diameters was larger than the initial mean (μ_d), and more in-line for μ_d for the standard production technique. Since only a proportion of the initial batch of components were reworked the high η peak is lower for Optimal Mean Setting than the standard production technique.

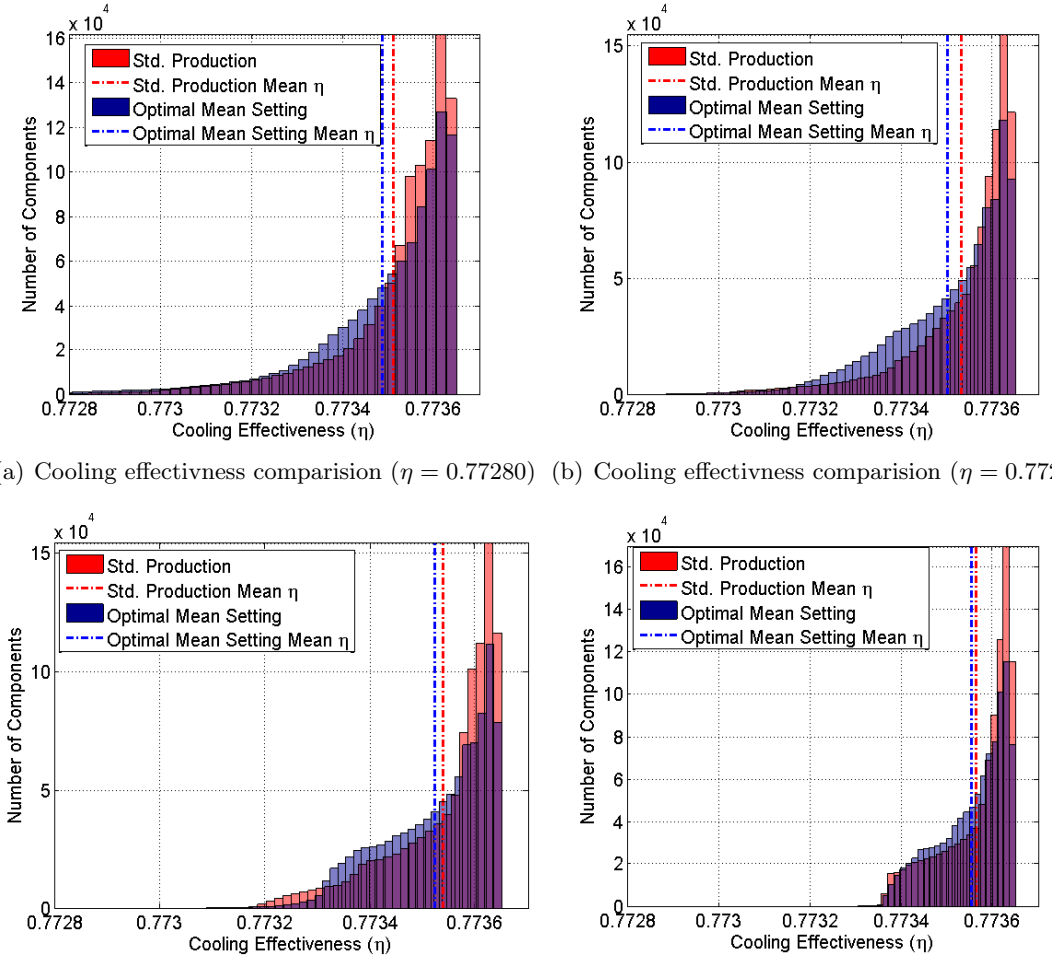

(a) Cooling effectivness comparision ($\eta = 0.77280$) (b) Cooling effectivness comparision ($\eta = 0.77299$)

(c) Cooling effectivness comparision ($\eta = 0.77317$) (d) Cooling effectivness comparision ($\eta = 0.77336$)

FIGURE 4.31: Performance distributions for varying cooling effectiveness (η)

Correlation between d and α

The effect of negative and positive correlation between the d and α parameters is illustrated by Figure 4.30(a) to 4.30(d). In practice the correlation between the hole diameter and inclination angle would be fitted from data, as shown in Section 4.3. As no data existed for this case, two prospective negative and positive correlations were specified where a Gaussian dependence structure was implemented via a Gaussian copula. Positive correlation effectively caused a diagonal ridge of high probability density with a negative slope (Figures 4.30(a) and 4.30(b)). In contrast the areas of high η for

the response surface were aligned with a slightly positive diagonal. This mismatch between the natural orientation of the manufactured geometry distribution and the ridge of high η significantly reduced the tolerance of the inclination angle (α) compared to the uncorrelated case. Conversely, the hole diameter (d) tolerances were widened since the variation along the α dimension was reduced. The geometry produced using the Optimal Mean Setting method (Figure 4.30(b)), showed the means were shifted closer to the diameter rework specification limit, this reduced the probability of geometry being created with too large a diameter (right hand side of the response surface). As a consequence, the inclination angle upper and lower specification limits were relaxed compared to the standard production case (Figure 4.30(a)), as the discrete variation of the hole diameter was lower [16]. Hence, there was a reduced probability of producing nonconforming geometry at the corners, where the diameter and angle specification limits intersect.

Figures 4.30(c) and 4.30(d) illustrate the geometry distribution and response surface for positive correlation. The better alignment between the diagonal slope of the geometry distribution and the response surface led to an improvement in expected profit for both the standard and Optimal Mean Setting techniques. The tolerances were set wider apart in Figures 4.30(c) and 4.30(d) compared to 4.30(a) and 4.30(b). Tables 4.7 and 4.8 also verify lower production costs and high profits for the positively correlated cases. The distribution of the performance of the manufactured geometry is shown in Figures 4.32(a) and 4.32(b) for negative and positive correlation, respectively. The principle difference between the correlated and uncorrelated cases is the truncation around $\eta = 0.7734$. Both the d and α distributions are truncated in the uncorrelated case (Figures 4.29(e) and 4.29(f). The distributions are less truncated for the correlated cases (Figure 4.30) particularly in regard to the hole diameter. This leads to a less truncated shape for the performance distributions (Figure 4.32).

Cooling Hole Study Conclusion

The average performance of a cooling hole could be improved by tightening the tolerances for the hole diameter and inclination angle. The cost of doing this using a standard method of manufacture was economically infeasible. The same minimum performance was achieved using Optimal Mean Setting with an increased of production cost of 0.086 £ per hole, compared to the original cost of 0.032 £. The mean hole performance was slightly less using Optimal Mean Setting compared to the standard production technique. The degree to which the average performance was lower depended on the minimum cooling effectiveness (η) and the correlation between the hole diameter and

[16] The total variation remained unchanged but the probability was less dense at the periphery. Notice the largest diameter contour on Figure 4.30(b) has a density of 0.8 and the equivalent contour on Figure 4.30(a) has a density of 1.37.

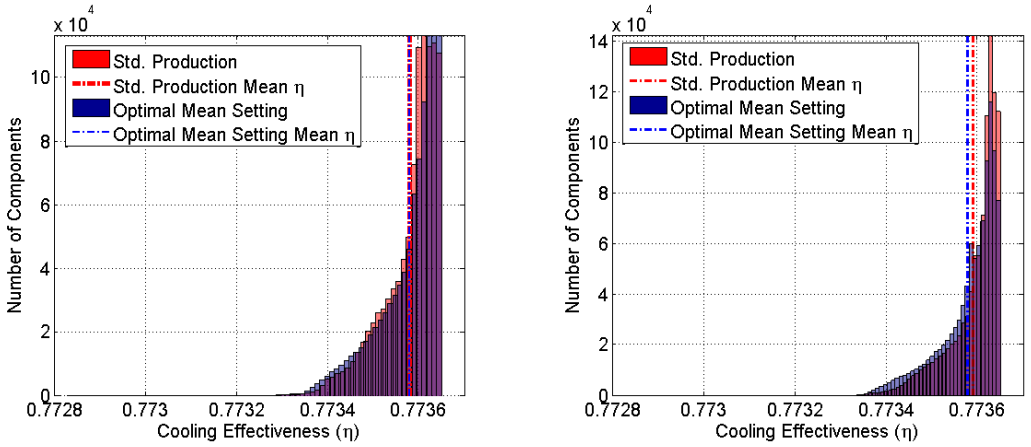

(a) Cooling effectivness comparision for $\eta = 0.77336$ and $\rho = -0.8$

(b) Cooling effectivness comparision for $\eta = 0.77336$ and $\rho = 0.8$

FIGURE 4.32: Performance distributions for positive and negative correlation (ρ)

inclination angle. In summary, performance gains by tolerance tightening using standard production techniques would be economically impractical, Optimal Mean Setting makes such a suggestion economically possible.

Chapter 5

Conclusions and Future Work

5.1 Conclusion

Optimal Mean Setting is a technique that can be used to reduce the cost of manufactured features and components when the manufacturing variation is greater than the tolerance limits. It has applications where the performance of the feature or component necessitates tight tolerances and it is not practical or possible to reduce the inherent variation in the manufacturing process. Typically, this would lead to non-conformance and the expense of reworking and scrapping components. Optimal Mean Setting can be used to ensure the non-conformance that is created is primarily rework, as opposed to more costly scrap. In this manner, the tolerances can remain tight but the cost of production can be minimised. This thesis sets out the framework necessary to determine the feature mean values to maximise profit. The process effectively modifies the shape of the manufacturing feature distributions to achieve the most profitable component geometry within the specification limits. Chapter 3 developed the ideas of a generalised approach to Optimal Mean Setting for idealised examples. The case studies in Chapter 4 and in Appendix F showed how the method could be applied to non-ideal real components. Several contributions to five key topics were made and are detailed below.

- A literature review uncovered an error in the methodology of previous research, related to the application of Optimal Mean Setting to parallel manufacturing processes. A part of the research in this thesis was devoted to correcting this error and generalising the methodology. The generalisation enabled a mixture of serial and parallel processes to be considered for n-features. This is the first time a robust, generalised method has existed and does not restrict the application of Optimal Mean Setting to a small number of features (two for parallel production) and a specific sequence of manufacture (serial or parallel).

- The optimisation methodologies discussed in previous literature were found to be sub-optimal for determining the mean settings to maximise profit for features produced in parallel. An optimal strategy was discussed in Section 3.1.2 and proven to outperform the literature in Section 3.5.1 using like-for-like examples.

- A fundamental restriction identified in previous work was the inability to evaluate the scrap, conformance and rework probabilities for parallel production where the feature distribution were not normally distributed or where different distributions families modelled the manufacturing variably of each feature[1]. Copulas were introduced to remove this restriction, which allowed the joint distribution to be calculated (to yield the scrap, conformance and rework probabilities) irrespective of the type of distribution used to model the variation of the manufacturing features.

- The effect Optimal Mean Setting has on the final manufactured distribution had not been considered previously. Optimal Mean Setting yields means that are usually biased towards one of the specification limits. Moreover, the mean of rework processes can be different to the original mean, which can further modify the distribution of the manufactured geometry. Since it is the final manufactured geometry that governs the performance distribution of the components, it is important to be able to predict the distribution. Again copula functions were used to model the final distribution of the manufactured geometry, as there was no restriction of the shape of the feature distributions.

The source of uncertainties in manufactured products will never be eliminated (Wilson [1980]). Therefore, the performance of products will vary depending on the sensitivity to the product's geometry and to the precision the geometry can be manufactured to. Thus, there will always be potential to improve a product's functional performance through tolerance tightening and manufacturing a more precise product. The change of a product's geometry through service must also be considered to prevent over precision engineering components that will immediately deform in service. Nevertheless, the generalised approach of Optimal Mean Setting presented in this thesis allows engineers to consider increasing the precision of a product through a coupling of design and manufacturing knowledge. It allows manipulation of the shape of uncertainty to create better value engineering products.

[1]More correctly the literature is limited to features where the variation is approximated by the same distribution family for each feature. In parallel production, the joint probability of scrap, conformance and rework must be evaluated which involves solving the multivariate distribution function. Most parametric distribution families have a multivariate distribution function but different distribution families cannot be mixed, unless copulas are used.

5.2 Future Work

5.2.1 Optimise Functional Distributions

Much of the literature inspired by Taguchi discussed in Chapter 2 is associated with achieving desirable functional distributions, such as larger-the-better, nominal-the-best and smaller-the-better. The cooling effectiveness distribution of the film cooling hole case study, in Chapter 5, is an example of a larger-the-better distribution. A further area for investigation would be to attempt to optimise the functional distribution by applying Optimal Mean Setting. By altering the proportion of rework on a feature, and modifying the mean values for different rework iterations, Optimal Mean Setting can modify the feature distributions, ultimately changing the functional distribution of the component. This is in contrast to the well established principles of Six Sigma, where one of the implementation corollaries is to acknowledge variation exists but set up processes to minimise the affect on the product. Future work should examine the benefits of implementing Optimal Mean Setting to achieve desirable performance characteristics. One significant advantage of the Optimal Mean Setting approach is tolerance tightening and product performance can be improved without expensive re-design or vast capital expenditure to improve manufacturing capability.

Trade-offs between performance gains brought about through Optimal Mean setting, improved manufacturing capability or redesign are all value related and fall into the remit of Value Drive Design (Collopy and Hollingsworth [2009] and Cheung et al. [2010]). The objective of this area of research aims to quantify 'best' design and decisions by maximising value.

The performance of assemblies can also be associated with Optimal Mean Setting. For example, many gas turbine assemblies are annular in nature and composed of several components, such as a ring of nozzle guide vanes. Variation in the geometry of these vanes or vane pairs impacts how cylindrical this annular assembly is. Variation at component level and the affect of assembly performance is an active research area (Lowth and Axinte [2014]). Optimal Mean Setting could be applied to such areas of research to guarantee assembly performance by impacting tolerances at component level

5.2.2 Copula Modelling Manufacturing Distributions

The research presented in this thesis was the first application of copula functions to model the variation in manufacturing features. There is great potential in this approach to propagate manufacturing variation through to performance variation in engineering

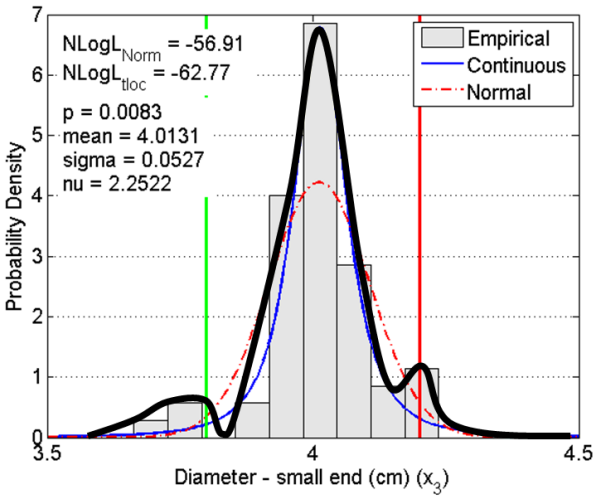

FIGURE 5.1: Illustration of a customised distribution fitted to the data points

quantities such as stress, aerodynamic performance and thermal transfer. As examined in this thesis, different families of parametric distributions can be used to model the manufacturing variation. However, it is not even necessary to fit a parametric distribution to data, the data could be used explicitly. This concept is expressed in Figure 5.1 which illustrates how a distribution might be explicitly fitted to the sample points from the manufacturing data in Section 4.3 (black line). There are two potential challenges:

- There is a danger of over customizing distributions to data samples. Although the distribution in Figure 5.1 represents the variation in the feature (x_3) well for this sample, it is questionable if this is really representative of the process variation if a larger number of samples were taken. If enough data samples were available it would be possible to use a proportion to customise a distribution and the remainder to verify if the customized distribution really was representative of the manufacturing process variation.
- Optimal Mean Setting also requires the mean to be shifted. If customizable distributions were created, it would be important to establish how the shape of the distribution would change with the process mean.

5.2.3 Alternative Strategy to Evaluate $\boldsymbol{F}$-matrix terms

One of the time consuming elements of the Optimal Mean Setting methodology set-out in this thesis is the matrix inversion $(\boldsymbol{I}-\boldsymbol{Q})^{-1}$ which is used to determine the $\boldsymbol{M}$-matrix terms the $\boldsymbol{F}$-matrix. As the number of features increase, the $\boldsymbol{I}$ and $\boldsymbol{Q}$ matrices become larger, increasing the time it takes to execute the inversion.

While the $\boldsymbol{M}$-matrix probabilities follow a sequence related to the geometric series, the $\boldsymbol{F}$-matrix probabilities are more complex to determine without the Markovian method. Rudolph [1999] and Uem [2009] offer tantalising mathematical models of random walks that have similar characteristics to the rework, scrap and conformance states involved in Optimal Mean Setting. It may be possible to adapt and further their research and avoid the matrix inversion, which has the potential to reduce the computational time for greater numbers of features. This is a purely mathematical exercise but a comparison of computational time versus number of features for the Markovian method and an alternative would be of practical benefit.

5.2.4 Non-Exhaustive Mean Search

Selim and Al-Zu'bi [2011] introduced a method to enable the optimal means for the manufacture of components in series to be found without exhaustive search. This is advantageous as it reduces the computational time necessary to find the optimal mean setting. It is possible this work could be incorporated with the research in this thesis in two main ways.

- Although the methodology presented in Selim and Al-Zu'bi [2011] is restricted to a the manufacturing of a single feature at each stage, it may be possible to apply a similar strategy to parallel production. The mathematical framework regarding parallel production presented in this thesis is a starting point for such an investigation.
- If the preceding bullet point could be achieved, it would then be possible to derive a method to allow the means for n-features in any combination of serial and parallel operations to be found, utilising the basis of Selim's method

5.2.5 Inclusion of Measurement Error

The Optimal Mean Setting framework discussed in this thesis did not model the effect of measurement uncertainty due to the inherent design of measurement systems and fluctuation in environmental conditions. Measurement error would predominately influence the measurements that were in close proximity to the specification limits. This topic has been associated with Optimal Mean Setting and process targeting, for example, Duffuaa and Siddiqui [2003] investigated the losses in profit due to product misclassification. Feng and Kapur [2008] developed a model to specify optimum specification limits for bivariate quality characteristics with penalty costs for misclassification. An

area for future study is the inclusion of measurement error to the generalised Optimal Mean Setting approach developed in this thesis.

5.2.6 Holistic Integration

As described by Shukor and Axinte [2009], *"Traditionally, the translation of a conceptual design into a final product has been accomplished by repetitive iterations between design and manufacturing stages of the product development life cycle"*. Designers may operate with little knowledge of the manufacturing process, which can lead to non-manufacturable designs resulting in time-consuming iterations between the design department and manufacturing. The specification of tolerances is one such area. To better design for manufacture, Manufacturing Analysis Systems (MAS) have been developed to pull manufacturing aspects into the design stages (Gupta et al. [1997] reviewed in Shukor and Axinte [2009]). In the case of tolerance specification and Optimal Mean Setting, the manufacturing capability and variation distribution are required at the design stage. A complex but powerful research area would be to bring such information into the design environment which would empower designers and manufacturing engineers to optimise products in light of the likely variation they would encounter during manufacture.

Appendix A

The Nature of the Stationary Points

Theorem 3.1 was proven and total profit is maximised when the same optimal mean is applied over all rework iterations such that, $\mu = \mu_{\text{opt}}$. Thus, the expression for total profit, Equation 3.4, can be formulated as a geometric series and written,

$$\begin{aligned} TP = SP &\left(\frac{F(U,\mu,\sigma) - F(L,\mu,\sigma)}{1-[1-F(U,\mu,\sigma)]}\right) \\ &- PC - Sc\left(\frac{F(L,\mu,\sigma)}{1-[1-F(U,\mu,\sigma)]}\right) \\ &- Rc\left(\frac{1}{1-[1-F(U,\mu,\sigma)]} - 1\right). \end{aligned} \tag{A.1}$$

The nature of the stationary point which maximises TP is given by,

$$\begin{aligned} \frac{\mathrm{d}^2 TP}{\mathrm{d}\mu^2} = \frac{\sqrt{2}}{\sqrt{\pi}\sigma^3 G(\mu)} &\Big((L-\mu)A(\mu)\xi(\upsilon)\alpha \\ &-(U-\mu)B(\mu)\xi(\varphi)\alpha - (2Rc+\alpha)(U-\mu)B(\mu) \\ &+(L-\mu)A(\mu)\Big) + \frac{4B(\mu)}{\pi\sigma^2 G(\mu)^3}\left(A(\mu)\xi(\upsilon)\alpha\right. \\ &\left.-B(\mu)\xi(\varphi)\alpha + (2Rc+\alpha)B(\mu) - A(\mu)\alpha\right). \end{aligned} \tag{A.2}$$

The functions A, B and G are given by,

$$A(\mu) = \exp\left(-\frac{(L-\mu)^2}{2\sigma^2}\right),$$

$$B(\mu) = \exp\left(-\frac{(U-\mu)^2}{2\sigma^2}\right),$$

$$G(\mu) = 1 + \frac{2}{\sqrt{\pi}} \int_0^{\frac{(U-\mu)\sqrt{2}}{2\sigma^2}} e^{-t}\,\mathrm{d}t$$

The stationary point of Equation A.1 is only a maximum when $\mathrm{d}^2TP/\mathrm{d}\mu^2 < 0$. This condition is generally satisfied for $SP > Sc > Rc$, which ensures that the optimal mean lies to the right of the nominal mean, μ_{nom}. While $\mu_{\text{opt}} < USL$, there are only two positive contributing terms in Equation A.1, the third and eighth terms, $-(U-\mu)B(\mu)\xi(\varphi)\alpha$ and $-B(\mu)\xi(\varphi)\alpha$, because $\xi(\varphi)$ may be negative as indicated by Figure A.1. However, the absolute value of the fourth and ninth terms is always greater than the third and eighth respectively such that,

$$|(2Rc+\alpha)(U-\mu)B(\mu)\xi(\varphi)| > |(U-\mu)B(\mu)\xi(\varphi)\alpha|$$

and

$$|(2Rc+\alpha)B(\mu)| > |B(\mu)\xi(\varphi)\alpha|$$

making the sum negative, and thus Equation A.2 remains negative.

While $\mu_{\text{opt}} > USL$, the second and seventh terms from Equation A.2 make a positive contribution due to $\xi(\upsilon)$ becoming negative, as illustrated on Figure A.1. Nevertheless the absolute value of the fifth term and tenth terms are greater than the second and seventh terms respectively such that,

$$|(L-\mu)A(\mu)| \geq |(L-\mu)A(\mu)\xi(\upsilon)|$$

and

$$|A(\mu)\alpha| \geq |A(\mu)\xi(\upsilon)\alpha|$$

which again ensures Equation A.2 is negative confirming the stationary point is a maximum $\forall\,\mu \in \mathbb{R}$ where $\mu_{opt} > \mu_{nom}$. It is worth clarifying in practical cases $\mu_{opt} > \mu_{nom}$ is generally satisfied, since the selling price must be greater than the scrap cost, which in turn is greater than the rework cost ($SP > Sc > Rc$).

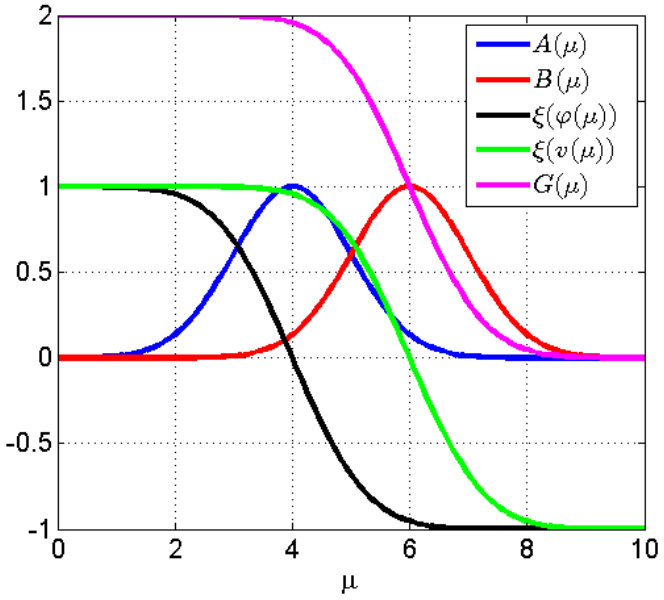

FIGURE A.1: Illustration of the $A, B, \xi(\varphi), \xi(v), G(\mu)$ functions for $L = 4$, $U = 6$ and $\sigma = 1$

Appendix B

Total Profit for a Given Iteration

Equations 3.5 to 3.7 were derived from specific instances of the single feature total profit expression, Equation 3.4. These specific instances for total profit for $n = 1$, $n = 2$ and $n = 3$ are derived in this Appendix. Given the process standard deviation (σ) and the feature specification limits (U and L) remained constant, the following substitutions were made to condense the notation. Let $\mathcal{U}_i = F(U, \mu_i, \sigma)$ and $\mathcal{L}_i = F(L, \mu_i, \sigma)$, where i is an iteration number, such that $i = 1, 2, \ldots, n$. The optimal mean for a single iteration is considered below.

Optimal mean for n=1

$$TP = SP(\mathcal{U}_1 - \mathcal{L}_1) - PC - Sc(\mathcal{L}_1) + Rc(1 - \mathcal{U}_1) \tag{B.1}$$

To determine the optimal mean, the expression must be differentiated with respect to μ_1, thus it is convenient to rearrange Equation B.1 in terms of $\mathcal{U}_1(\mu_1)$ and $\mathcal{L}_1(\mu_1)$.

$$TP = \mathcal{U}_1(SP + Rc) - \mathcal{L}_1(SP + Sc) - PC - Rc. \tag{B.2}$$

Setting Equation B.2 to zero and differentiating with respect to μ_1, yields the maximum of the TP_1 expression (note this was shown to be a maximum in Appendix A),

$$\frac{\partial TP}{\partial \mu_1} = \frac{\sqrt{2}}{2\sqrt{\pi}\sigma} \left\{ (SP + Sc) \exp\left[\frac{-(\mu_1 - L)^2}{2\sigma^2}\right] - (SP + Rc) \exp\left[\frac{-(\mu_1 - U)^2}{2\sigma^2}\right] \right\} = 0.$$

This can be rearranged by making μ_1 the subject to give,

$$\mu_1 = \frac{1}{2(L-U)}\left\{2\sigma^2 \ln\left[\frac{SP+Rc}{SP+Sc}\right] + L^2 - U^2\right\},$$

which is the optimal mean setting for a single iteration.

Optimal mean for n=2

The total profit for $n = 2$ is given by,

$$\begin{aligned} TP = {} & SP\left\{(\mathcal{U}_1 - \mathcal{L}_1) + (\mathcal{U}_2 - \mathcal{L}_2)(1-\mathcal{U}_1)\right\} \\ & - PC - \left\{[Sc(\mathcal{L}_1) + Rc(1-\mathcal{U}_1)]\right. \\ & \left. + [Sc(\mathcal{L}_2)(1-\mathcal{U}_1) + Rc(1-\mathcal{U}_2)(1-\mathcal{U}_1)]\right\}. \end{aligned} \tag{B.3}$$

Collecting like terms of $\mathcal{U}$ and $\mathcal{L}$ gives,

$$\begin{aligned} TP = {} & \mathcal{U}_1(SP+2Rc) - \mathcal{L}_1(SP+Sr) \\ & - 2Rc - PC + \mathcal{U}_2(SP+Rc) - \mathcal{L}_2(SP+Sc) \\ & + \mathcal{L}_2\mathcal{U}_1(SP+Sc) - \mathcal{U}_2\mathcal{U}_1(SP+Rc). \end{aligned} \tag{B.4}$$

By setting Equation B.4 to zero and differentiating with respect to μ_1 and μ_2 yields,

$$\begin{aligned} \frac{\partial TP}{\partial \mu_1} = {} & \frac{\sqrt{2}}{2\sqrt{\pi}\sigma}\left\{\frac{1}{2}\left[(SP+Sc)\,\xi(-\varphi_1)\right.\right. \\ & \left. -(SP+Rc)\,\xi(-\upsilon_1) - Sc - 2SP - 3Rc\right] \\ & \left. \exp\left[\frac{-(\mu_1-U)^2}{2\sigma^2}\right] + \exp\left[\frac{-(\mu_1-L)^2}{2\sigma^2}\right](SP+Rc)\right\} = 0. \end{aligned} \tag{B.5}$$

$$\begin{aligned} \frac{\partial TP}{\partial \mu_2} = {} & \frac{\sqrt{2}}{4\sqrt{\pi}\sigma}\left(\xi(-\upsilon_1)+1\right)\left(\exp\left[\frac{-(\mu_2-L)^2}{2\sigma^2}\right](SP+Sc)\right. \\ & \left. -\exp\left[\frac{-(\mu_2-U)^2}{2\sigma^2}\right](SP+Rc)\right) = 0. \end{aligned} \tag{B.6}$$

Both Equations B.5 and B.6 can be solved for μ_1 and μ_2 respectively yielding,

$$\begin{aligned}\mu_1 = \frac{1}{2(L-U)}\Bigg\{2\sigma^2 \ln\Bigg[\frac{1}{2(SP+Sc)}\Bigg((SP+Sc)\xi(\varphi_2) \\ -(SP+Rc)\xi(\upsilon_2)+3Rc+2SP+Sc\Bigg)\Bigg] \\ +L^2-U^2\Bigg\},\end{aligned} \tag{B.7}$$

and

$$\mu_2 = \frac{1}{2(L-U)}\left\{2\sigma^2 \ln\left[\frac{SP+Rc}{SP+Sc}\right]+L^2-U^2\right\}. \tag{B.8}$$

The last iteration (Equation B.8), where $i=2$, is the same as the iteration from $n=1$. The first iteration, where $n=2$ (Equation B.7), is dependent on the last iteration.

Optimal mean for n=3

The total profit for $n=3$ is given by,

$$\begin{aligned}TP = SP\{(\mathcal{U}_1-\mathcal{L}_1)+(\mathcal{U}_2-\mathcal{L}_2)(1-\mathcal{U}_1) \\ +(\mathcal{U}_3-\mathcal{L}_3)(1-\mathcal{U}_2)(1-\mathcal{U}_1)\}-PC \\ -\{[Sc(\mathcal{L}_1)+Rc(1-\mathcal{U}_1)]+[Sc(\mathcal{L}_2)(1-\mathcal{U}_1) \\ +Rc(1-\mathcal{U}_2)(1-\mathcal{U}_1)]+Sc(\mathcal{L}_3)(1-\mathcal{U}_2)(1-\mathcal{U}_1) \\ +Rc(1-\mathcal{U}_3)(1-\mathcal{U}_2)(1-\mathcal{U}_1)\}.\end{aligned} \tag{B.9}$$

Collecting like terms of $\mathcal{U}$ and $\mathcal{L}$ gives,

$$\begin{aligned}TP = \mathcal{U}_1(SP+3Rc)-\mathcal{L}_1(SP+Sr) \\ -3Rc-PC+\mathcal{U}_2(SP+2Rc)-\mathcal{L}_2(SP+Sc) \\ +\mathcal{L}_2\mathcal{U}_1(SP+Sc)-\mathcal{U}_2\mathcal{U}_1(SP+Rc) \\ +\mathcal{U}_3(SP+Rc)-\mathcal{L}_3(SP+Sc) \\ -\mathcal{U}_3\mathcal{U}_2(SP+Rc)-\mathcal{U}_3\mathcal{U}_1(SP+Rc)+\mathcal{L}_3\mathcal{U}_2(SP+Sc) \\ +\mathcal{L}_3\mathcal{U}_1(SP+Sc)+\mathcal{U}_3\mathcal{U}_2\mathcal{U}_1(SP+Rc)-\mathcal{L}_3\mathcal{U}_2\mathcal{U}_1(SP+Sc)\end{aligned} \tag{B.10}$$

Setting Equation B.10 to zero and differentiating with respect to μ_1, μ_2 and μ_3 yields,

$$\begin{aligned}\frac{\partial TP}{\partial \mu_1} =& \frac{\sqrt{2}}{2\sqrt{\pi}\sigma}\left\{\frac{1}{4}\left(\left[(SP+Sc)\,\xi(-\varphi_3)-(SP+Rc)\,\xi(-\upsilon_3)\right.\right.\right.\\ &\left.-Sc-2SP-3Rc\right]\xi(-\upsilon_2)+(SP+Sc)\xi(-\varphi_2)\\ &-(SP+Rc)\xi(-\upsilon_3)+(2SP+2Sc)\xi(-\varphi_2)\\ &\left.-3Sc-4SP-7Rc\right)\exp\left[\frac{-(\mu_1-U)^2}{2\sigma^2}\right]\\ &\left.+\exp\left[\frac{-(\mu_1-L)^2}{2\sigma^2}\right](SP+Rc)\right\}=0,\end{aligned} \tag{B.11}$$

$$\begin{aligned}\frac{\partial TP}{\partial \mu_2} =& \frac{\sqrt{2}}{4\sqrt{\pi}\sigma}\left(\xi(-\upsilon_1)+1\right)\left\{\frac{1}{2}\left[(SP+Sc)\,\xi(-\varphi_3)\right.\right.\\ &\left.-(SP+Rc)\,\xi(-\upsilon_3)-Sc-2SP-3Rc\right]\\ &\left.\exp\left[\frac{-(\mu_2-U)^2}{2\sigma^2}\right]+\exp\left[\frac{-(\mu_2-L)^2}{2\sigma^2}\right](SP+Rc)\right\}=0\end{aligned} \tag{B.12}$$

and

$$\begin{aligned}\frac{\partial TP}{\partial \mu_3} =& \frac{\sqrt{2}}{8\sqrt{\pi}\sigma}\left(\xi(-\varphi_1)+1\right)\left(\xi(-\varphi_2)+1\right)\\ &\left(\exp\left[\frac{-(\mu_3-L)^2}{2\sigma^2}\right](SP+Sc)\right.\\ &\left.-\exp\left[\frac{-(\mu_3-U)^2}{2\sigma^2}\right](SP+Rc)\right)=0.\end{aligned} \tag{B.13}$$

Solving Equations B.11, B.12 and B.13 for μ_1, μ_2 and μ_3 respectively gives,

$$\begin{aligned}\mu_1 = \frac{1}{2(L-U)}&\left\{2\sigma^2\ln\left[\frac{1}{4(SP+Sc)}\left(-(SP+Sc)(\xi(\upsilon_2)-1)\xi(\varphi_3)\right.\right.\right.\\ &-(SP+Rc)(\xi(\upsilon_2)-1)\xi(\upsilon_3)+2(SP+Sc)\xi(\varphi_2)\\ &\left.\left.-(3Rc+2SP+Sc)\xi(\upsilon_2)+7Rc+4SP+3Sc\right)\right]\\ &\left.+L^2-U^2\right\},\end{aligned} \tag{B.14}$$

$$\mu_2 = \frac{1}{2(L-U)}\left\{2\sigma^2 \ln\left[\frac{1}{2(SP+Sc)}\left((SP+Sc)\xi(\varphi_3)\right.\right.\right.$$
$$\left.\left.\left.-(SP+Rc)\xi(\upsilon_3)+3Rc+2SP+Sc\right)\right] \qquad \text{(B.15)}$$
$$\left.+L^2-U^2\right\}$$

and

$$\mu_3 = \frac{1}{2(L-U)}\left\{2\sigma^2 \ln\left[\frac{SP+Rc}{SP+Sc}\right]+L^2-U^2\right\}.$$

It is evident a pattern is emerging, where the last mean, μ_n, is always a function of the selling price, scrap and rework costs, manufacturing variation and the upper and lower specification limits. The second to last term is also a function of these variables as well as the μ_n. The third to last term is a function of the costs, manufacturing variation, specification limits as well as the last and second to last terms, μ_n and μ_{n-1}. The form of the terms remains constant. This pattern was generalised in Equations 3.10 and 3.61 in Section 3.1.1.

Appendix C

Equivalence of Profit Equations

Equation 2 from Selim and Al-Zu'bi [2011] expanded for two features is,

$$\begin{aligned} E(PR) =& SP\,\frac{p_{1,A}}{1-p_{1,A}}\,\frac{p_{2,A}}{1-p_{2,A}} - \left(PC_1 + PC_2\,\frac{p_{1,A}}{1-p_{1,A}}\right) \\ &- \left[SC_1\left(\frac{p_{1,S}}{1-p_{1,R}}\right) + SC_2\left(\frac{p_{1,S}}{1-p_{1,R}}\right)\frac{p_{1,A}}{1-p_{1,A}}\right] \\ &- \left[RC_1\,\frac{p_{1R}}{1-p_{1,R}} - RC_2\,\frac{p_{2,R}}{1-p_{2,R}}\,\frac{p_{1,A}}{1-p_{1,A}}\right] \end{aligned} \tag{C.1}$$

this is equivalent Equation 3.77,

$$\begin{aligned} E(PR) =& SP\,f_{\mathrm{I},C}f_{\mathrm{II},C} - (PC_{\mathrm{I}} + PC_{\mathrm{II}}\,f_{\mathrm{I},C}) \\ &- \left[SC_{\mathrm{I}}\left(\frac{p_{\mathrm{I},S}}{1-p_{2_{\mathrm{I}},2_{\mathrm{I}}}}\right) + SC_{\mathrm{II}}\left(\frac{p_{\mathrm{II},S}}{1-p_{\mathrm{II},2_{\mathrm{II}}}}\right)f_{\mathrm{I},C}\right] \\ &- RC_1\,m_{\mathrm{I},2_{\mathrm{I}}} - RC_2\,m_{\mathrm{II},2_{\mathrm{II}}}\,f_{\mathrm{I},C} \end{aligned} \tag{C.2}$$

since

$$\begin{aligned} f_{\mathrm{I},C} &= \frac{p_{\mathrm{I},C}}{1-p_{\mathrm{I},2_{\mathrm{I}}}} = \frac{p_{1,A}}{1-p_{1,A}} \\ f_{\mathrm{II},C} &= \frac{p_{\mathrm{II},C}}{1-p_{\mathrm{II},2_{\mathrm{II}}}} = \frac{p_{2,A}}{1-p_{2,A}} \\ m_{\mathrm{I},2_{\mathrm{I}}} &= \frac{p_{\mathrm{I},2_{\mathrm{I}}}}{1-p_{\mathrm{I},2_{\mathrm{I}}}} = \frac{p_{1R}}{1-p_{1,R}} \\ m_{\mathrm{II},2_{\mathrm{II}}} &= \frac{p_{\mathrm{II},2_{\mathrm{II}}}}{1-p_{\mathrm{II},2_{\mathrm{II}}}} = \frac{p_{2,R}}{1-p_{2,R}}. \end{aligned} \tag{C.3}$$

Substitution of the expressions in Equation C.3 show Equation C.2 and Equation C.1 are equivalent.

Appendix D

Optimal Mean Setting for Parallel Production - Alternative Scrap Cost Structure

This appendix offers an alternative formulation to the example in Section 3.5.1. In a similar manner to the literature (Khasawneh et al. [2008] and Peng and Khasawneh [2014]), the scrap cost was adjusted depending on the state at which a component was deemed to be scrap. In a parallel production system, this implicitly implies the rework operations add value to the component. Normally a manufacturing process does add value to a component, however, a rework operation is a repeat or partial repeat of the original process. Thus, rework has a cost due to machine utilisation, tool wear, energy use and operator time but it does not necessarily increase the value over a similar component that conformed in the first iteration. An exception would be additive manufacturing processes, where the material volume increases with each rework operation, hence the value of the component will increase. The literature (Khasawneh et al. [2008] and Peng and Khasawneh [2014]) used a static scrap cost for each state, here a dynamic scrap cost is used where the scrap cost at each state is proportional to the number of times a feature was reworked as shown in Table D.1 (Section 3.5.1 used a flat cost of 150 units irrespective of which state caused the scrap). It was assumed rework cost per feature was 25 units , and 50 units for dual feature rework. All other costs were the same as the example in Section 3.5.1.

The expected profit versus the dual feature means were plotted in Figure D.1 in a similar manner to Figure 3.29 from Section 3.5.1. As the scrap cost structure is different, the two examples are not directly comparable. Nevertheless some observations can be made relating to impact of the two different cost structures. The location of the optimal means

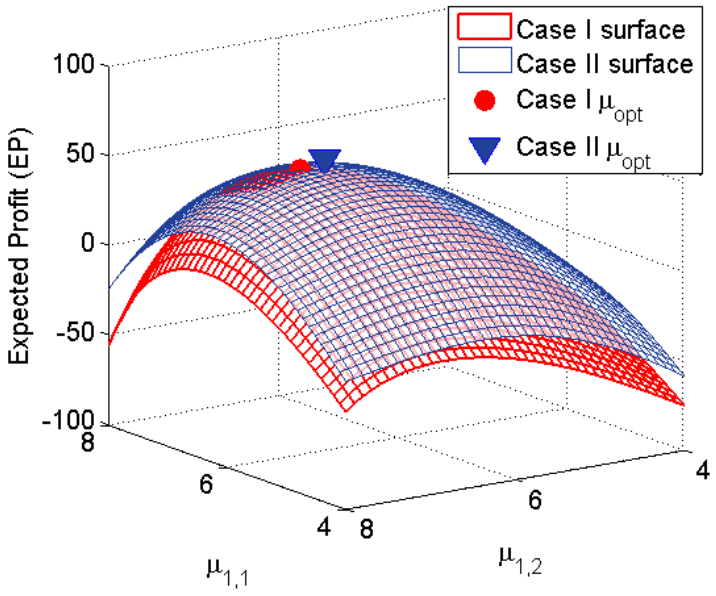

FIGURE D.1: Profit surfaces for Case I and Case II (optimisation of two and four means respectively)

between the two Cases (Case I and Case II) followed the same principles as the example in Section 3.5.1. The Case I means were greater than the dual feature Case II means and the Case II single feature rework means were more rework biased than the Case I means. However, the difference between the dual and single feature rework means were greater than the example from Section 3.5.1. The reason for this lies in the difference between the single and dual feature scrap costs. The dual feature rework cost is at least 150 units, while the single feature rework cost is at least 125 units; the rework cost in the example in Section 3.5.1 was 150 units irrespective of whether the rework was single or dual feature. Therefore, the single feature rework means in Table D.1 could afford to be more rework biased relative to the dual feature rework means in the example in Section 3.5.1.

Variable	***Value***
U	[6 6]
L	[4 4]
Rc	[25 25 50]
Sc	$[100,\ 100+25(1+m_{\mathrm{I},2}),\ 100+25(1+m_{\mathrm{I},3}),\ 100+50(1+m_{\mathrm{I},4})]$
SP	400
PC	50
$\boldsymbol{\Sigma}$	$[2, 0; 0, 2]$

TABLE D.1: Dual feature numerical example input parameters

The bar plot in Figure D.2 shows the rework and scrap costs from the initial and rework states. There are two primary differences between the plot in Figure D.2 and Figure

3.30 from Section 3.5.1, relating to the values of the rework costs and the value of the dual feature scrap cost (Sr_4). (1) The total rework costs Rw_2 to Rw_4 are all lower in Figure D.2 compared to Figure 3.30. The rework costs in both examples are the same but the means for both Cases (Case I and Case II) in Section 3.5.1 are higher than the equivalent means in the current example. (2) The absolute value of Sr_4 in Figure D.2 is greater than in Figure 3.30. The values of Sr_4 relative to Sr_2 and Sr_3 from Figure D.2 are also higher compared to the relative differences in Figure 3.30. The increase in Sr_4 was caused by the lower means relative to the example in Section 3.5.1. The Sr_2 and Sr_3 values remain approximately the same between both examples due to the different cost structure. While the probability of producing Sr_2 and Sr_3 scrap in the example in Section 3.5.1 is low, the scrap cost is also higher at 150 units compared to at least 125 units in the current example. Thus, the differences approximately cancel out for Sr_2 and Sr_3. This also explains why the difference between the Sr_4, and Sr_2 and Sr_3 values are greater in the current example. The scrap costs for Sr_4 are approximately the same for both examples but the probability of dual feature scrap is greater in the current example, leading to a greater difference between the Sr_4, and Sr_2 and Sr_3 values.

	Value
Case I Profit	45.20
Case II Profit	47.27
Case I Production Cost	131.77
Case II Production Cost	129.48
Case I means $(\mu^{\mathrm{I}}_{1,1}, \mu^{\mathrm{I}}_{1,2})$	6.67, 6.67
Case II means $(\mu^{\mathrm{II}}_{1,1}, \mu^{\mathrm{II}}_{1,2}, \mu^{\mathrm{II}}_{2,1}, \mu^{\mathrm{II}}_{2,2})$	6.50, 6.50, 6.97, 6.97
Case I Final Conformance Prob.	0.5674
Case II Final Conformance Prob.	0.5669
Case I Final Scrap Prob.	0.4326
Case II Final Scrap Prob.	0.4331

TABLE D.2: Optimisation results

D.1 Influence of Correlation

Correlation alters the probability of components falling into single and dual feature rework states, in the same way as described by Figure 3.31 from Section 3.5.1.

The effect of correlation on the optimal means and profits are tabulated in Table D.3. Profits for both cases were higher with the new scrap cost structure, due to reduced production cost, which was also observed in Table D.2 for no correlation. The difference between the dual feature and single feature means was also increased relative to the example from Section 3.5.1. However, there was no fundamental change to the results as a consequence of the alternative scrap cost structure. Nevertheless, Figure D.3 illustrates

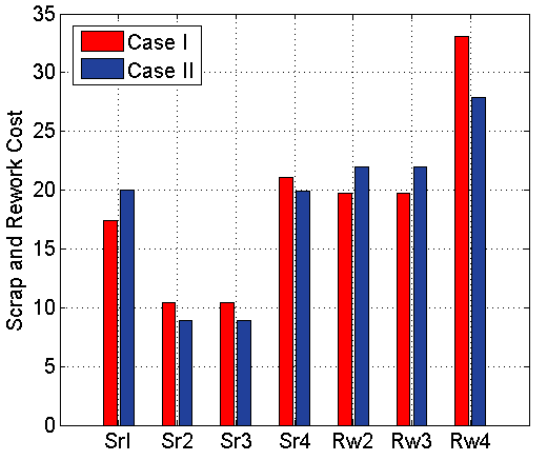

FIGURE D.2: Scrap and rework costs from the initial and rework states

the difference between the profits of the Case I and Case II optimisation methods was greater with the dynamic scrap cost structure, compared to Figure 3.32 from Section 3.5.1. The reason for this was due to the less costly single feature scrap cost compared to dual feature scrap cost. The means settings in the Case I methodology was a compromise between single and dual feature rework. Since the Case II methodology could optimise both rework types independently it could take advantage of the lower single feature rework cost rate. Since a flat scrap cost was used in the Section 3.5.1 example, the advantage of optimising the single feature rework means separately was not as pronounced.

ρ	Cases	***Value***
0.8	Case I Profit	57.15
0.8	Case II Profit	60.55
0.8	Case I Production Cost	128.97
0.8	Case II Production Cost	126.14
0.8	Case I Final Conformance	0.5903
0.8	Case II Final Conformance	0.5917
0.8	Case I means $(\mu^{\mathrm{I}}_{1,1}, \mu^{\mathrm{I}}_{1,2})$	6.44, 6.44
0.8	Case II means $(\mu^{\mathrm{II}}_{1,1}, \mu^{\mathrm{II}}_{1,2}, \mu^{\mathrm{II}}_{2,1}, \mu^{\mathrm{II}}_{2,2})$	6.26, 6.26, 6.97, 6.97
-0.8	Case I Profit	52.63
-0.8	Case II Profit	57.81
-0.8	Case I Production Cost	119.40
-0.8	Case II Production Cost	111.81
-0.8	Case I Final Conformance	0.5551
-0.8	Case II Final Conformance	0.5491
-0.8	Case I means $(\mu^{\mathrm{I}}_{1,1}, \mu^{\mathrm{I}}_{1,2})$	6.57, 6.57
-0.8	Case II means $(\mu^{\mathrm{II}}_{1,1}, \mu^{\mathrm{II}}_{1,2}, \mu^{\mathrm{II}}_{2,1}, \mu^{\mathrm{II}}_{2,2})$	6.21, 6.21, 6.97, 6.97

TABLE D.3: Optimisation results for correlated features

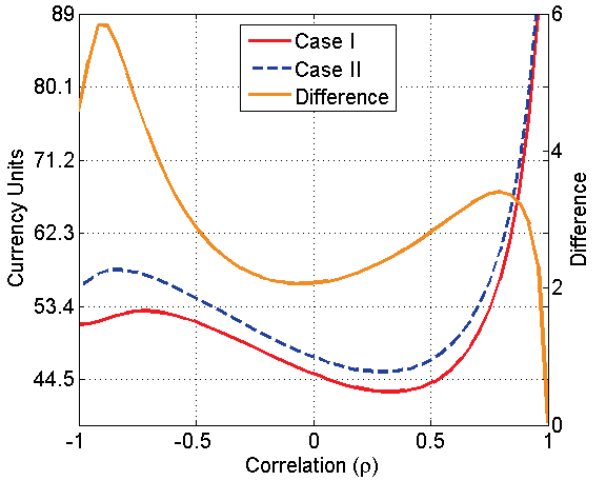

FIGURE D.3: Profit vs. correlation

Appendix E

Matlab Code

The *StageCostFun* function

```
function [F_stageC,pIC,Rwi,Sri] = StageCostFun_MultiMu(MU,sigs,rho,U,L,R_Cost,S_Cost)
% Computes the final probability items through a manufacturing process with
% rework will conform.
% Christopher Dodd - 2014 - Chris.S.Dodd@Gmail.com
% INPUTS -  MU:     A 1 by n vector of process means
%           sigs:   Correlation matrix with size n by n
%           U:      A 1 by 2 vector of upper specification limits
%           L:      A 1 by 2 vector of lower specification limits
%           RC:     The rework costs for each rework stage
%           SC:     The scrap costs for each rework stage and inital stage

% OUTPUTS - F_stageC:   Final probability of conformance
%           pIC:        Probability of conformance from the inital
%                       operation
%           Rwi:        Vector of rework probabilities
%           Sri:        Vector of scrap probabilities

N = size(MU,2); % Total number of features at stage
eta = 1;        % Initiate eta value
for k = 1:N     % eta for given N and k - Equation 2.45 Dodd [2014]
    eta_c = factorial(N)/(factorial(k)*(factorial(N-k)));
    eta = eta + eta_c;
end
% Determine all possible permutations
for k = 1:N
    UP{k} = combinator(N,k,'c');
end

% create an Upsilon vector with all the combinations
```

```
% i.e.  [1]
%       [2]
%       [3]
%       [1 2]
%       :
%       [1 2 3]
c = 1;
for k = 1:N
    Coms = combinator(N,k,'c');
    sizeComs = size(Coms);
    for j = 1:sizeComs(1)
        UPv{c,:} = Coms(j,:);
        c = c+1;
    end
    k=k+1;
end

%% calculate S-Matrix
beta = 0;
for k = 1:N % Generate S-matrix for each k- value
    for i = 1:k-1 % Calculate beta
        beta_c = factorial(N)/(factorial(i)*(factorial(N-i)));
        beta = beta + beta_c;
    end
    alpha_l = 0;
    for i = N:-1:k % Calculate alpha
        alpha_c = (factorial(N)/(factorial(i)*(factorial(N-i))));
        alpha_l = alpha_l + alpha_c; % Determine last term in alpha eqn
    end                              % alpha is k-dependent
    alpha = 2 + (eta-1) - alpha_l;   % alpha eqn
    m = (factorial(N)/(factorial(k)*(factorial(N-k)))); % m equation
    delta = beta+m;
    SMat = kSMatrix(k,alpha,eta,m,UP,UPv); % S-Matrix function
    SMat_Cell{k} = SMat;                % Store S-Matrices in a cell array
    beta = 0; % reset beta to zero

end

%% probability vecotrs
[PIs PSs PMat] = Probs_nVars_MultiMu(MU,L,U,sigs,rho);
%% Transition Matrix
P=PMat;
Q = P(1:eta,1:eta);     % Q Matrix (prob of transient to transient)
R = P(1:eta,eta+1:end); % R Matrix (prob of transient to absorbing)
I = eye(length(Q));     % Identiy matrix
M = (I-Q)^-1;           % average time in transient states
F = M*R;                % Final probabilities of absorbtion
temp = Q.*eye(eta,eta); PRR = temp(temp>0)'; % Determine the
```

```
                                        % state-back-to-state rework
                                        % vector from Q matrix

%% Scrap costs
SCP_Cost = 0; % initilize Scrap cost
for k = 1:N
    for i = 1:k-1 % Calculate beta
        beta_c = factorial(N)/(factorial(i)*(factorial(N-i)));
        beta = beta + beta_c;
    end
    alpha_l = 0;
    for i = N:-1:k % Calculate alpha
        alpha_c = (factorial(N)/(factorial(i)*(factorial(N-i))));
        alpha_l = alpha_l + alpha_c; % Determine last term in alpha eqn
    end                              % alpha is k-dependent
    alpha = 2 + (eta-1) - alpha_l;   % alpha eqn
    m = (factorial(N)/(factorial(k)*(factorial(N-k)))); % m equation
    delta = beta+m;                                     % delta equation
    DMat = kDMatrix(m,PIs,alpha,delta,eta); % compute the D-matrix
   % JMat = kJMatrix(m,PIs,alpha,delta,eta)
    SDMat = SMat_Cell{k}.*DMat;
    beta = 0; % reset beta to zero
    for j = 1:m
        a = alpha + j - 2;
        % Scrap cost Equation
        % Note for 1 state (p_Is/(1-p_Ir))*p_Ir + p_Is = p_Is/(1-p_Ir)
        % where p_Is: prob from I to scrap, p_Ir: prob from I to rework
        kSCPi = S_Cost(a+1)*sum([SDMat(:,j).*(PSs(a+1)/(1-PRR(a)))]);
        % Scrap cost for each k
        SCP_Cost = SCP_Cost + kSCPi; % total scrap cost for all k
    end
end

%% Rework Costs
for i = 1:eta-1 % Rework cost
    rw(i) = R_Cost(i)*M(1,i+1);
end
SCPCOST = SCP_Cost;
Sri = SCP_Cost + PSs(1)*S_Cost(1);
Rwi = sum(rw);
pIC = 1-PSs(1);
F_stageC = F(1,1);
```

The *kSMatrix* function

```
function SMat = kSMatrix(k,alpha,eta,m,UP,UPv)
% Compute the S matrix
% Christopher Dodd - 2014 - Chris.S.Dodd@Gmail.com
% INPUTS -  k:      Scalr giving the k conbination, e.g. 1,2,3,...,n.
%                   There is an S-matrix for each k value.
%           alpha:  Scalar computed from Equation 3.50
%           eta:    Total number of rework states including inital process
%           m:      Scalar computed from Equation 3.46
%           UP:     The Upsilon set, Equation 3.48
%           UPv     A k subset from the Upsilon set.
%
% OUTPUTS - SMat:   The S-Matrix
Ctemp = UP{k};
for i = 1:eta - alpha + 1
    z = alpha - 2 + i;
    for j = 1:m
        mem = ismember(Ctemp(j,:),UPv{z}); % check is C vals are part of
                                           % UPSILON set
        gamma = all(mem == 1);          % make sure all member of C are
                                        % part of UPSILON set
        SMat(i,j) = gamma;              % populate S-matrix.  Recall there
    end                                 % is an S-matrix for every k-value.
end
```

The *kDMatrix* function

```
function DMat = kDMatrix(m,PIs,alpha,delta,eta)
function DMat = kDMatrix(m,PIs,alpha,delta,eta)
% Compute the S matrix
% Christopher Dodd - 2014 - Chris.S.Dodd@Gmail.com
% INPUTS -  m:      Scalar computed from Equation 3.46
%           PIs:    Vector of transistion probabilities, e.g for 2
%                   features PIs = [pI2,pI3,pI4,pIC,pIS].  Computed from
%                   the Probs_nVars_MultiM.m function
%           alpha:  Scalar computed from Equation 3.50
%           delta:  Scalar given from beta + m, where beta is given from
%                   Equation 3.47.
%           eta:    Total number of rework states including inital process
%
% OUTPUTS - SMat:   The D-Matrix

DMat = ones(eta-(alpha-1),m);

DMat(1:m,1:m) = bsxfun(@times,eye(m),PIs(alpha-1:delta));
w = delta+1;              % counter for accessing relevent elemts from PIs
```

```
for i = m+1:eta-(alpha-1) % i goes from 4:7, 4:4 and 2:1 (i.e. 0) for N=3.
    v = alpha-1;          % counter for accessing relevent elemts from PIs
    for j = 1:m
        DMat(i,j) = PIs(w)*PIs(v)/(1-PIs(w)); % probabiliy fraction
        v = v+1;
    end
    w = w + 1;
end
```

The *Probs_nVars* function

```
% Determine the probabilities in the transition matrix
% for any number of features.
% Christopher Dodd - 2014 - Chris.S.Dodd@Gmail.com
% INPUTS -  MU:     A 1 by n vector of process means
%           U:      A 1 by n vector of upper specification limits
%           L:      A 1 by n vector of lower specification limits
%           sigs:   Correlation matrix with size n by n
%           rho:    Correlation parameter
%
% OUTPUTS - PIs:    Vector of transistion probabilities, e.g for 2
%                   features PIs = [pI2,pI3,pI4,pIC,pIS]
%           PSs:    Vector of transition to scrap probabilities, eg for 2
%                   features PSs = [pIS,p2S,p3S,p4S]
%           PMat:   Transition matrix

num_vars = size(MU,2); % Number of variables
%% Determine the Multi feature means through to single feature means
% e.g. 2 features MU = [mu1_2f, mu2_2f;
%                       mu1_1f, mu2_1f] where f:=feature

for i=1:size(MU,1)
    MU_R(i,:) = L+(U-MU(i,:)); % reverse the axes
end

eta = 1;
for i = 1:num_vars
    eta_c = factorial(num_vars)/(factorial(i)*(factorial(num_vars-i)));
    eta = eta + eta_c;
end
eta;

%% ---------- Pps probs  ----------
% This section determines the probabilities of the rework regions
% e.g. in 3D:
```

```
%       pI2 = F([-inf L2 L3],[L1 U2 U3])      x_1 rework only
%       pI3 = F([L1 -inf L3],[U1 L2 U3])      x_2 rework only
%       pI4 = F([L1 L2 -inf],[U1 U2 L3])      x_3 rework only
%       pI5 = F([-inf -inf L3],[L1 L2 U3])    x_1 & x_2 rework
%       pI6 = F([-inf L2 -inf],[L1 U2 L3])    x_1 & x_3 rework
%       pI7 = F([L1 -inf -inf],[U1 L2 L3])    x_2 & x_3 rework
%       pI8 = F([-inf -inf -inf],[L1 L2 L3])  x_1, x_2 & x_3 rework


ic = 1;  % initiate 'ic' counter
Rw_vars{1,:} = combinator(num_vars,num_vars,'c');
for i = 1:num_vars-1    % determine all possilbe combinations of reworks
    ic = ic+1; % counter to define rows of pRWs
    %'----------------- All possilbe RW combos-----------------'
    Rw_vars{ic,:} = combinator(num_vars,i,'c');  % e.g. x1,x2,x3 and x1,x2
                                                 % or x1,x3 or x2,x3 etc
end
c = 0;  % initiate 'c' counter
cc = 0; % initiate 'cc' counter
for j = 1:size(Rw_vars,1)

    %'----------------- Local Rw Operations -----------------'
    RwIter = Rw_vars{j};
    for k = 1:size(RwIter,1)
       %r = r+1
    %'----------------- Define Local MUs and Sigmas -----------------'
        MU_Ri = MU_R(j,RwIter(k,:));  % only selct the mean for the
                                      % relevant features
        % Build covariance matrix for all featuers including correlation
        % (rho)
        CorrMatrix = rho.*(ones(length(MU_Ri),length(MU_Ri)));
        CorrMatrix(logical(eye(size(CorrMatrix))))=1;
        SIGMA = corr2cov(sigs(RwIter(k,:)), CorrMatrix);
        Lvars = L(RwIter(k,:));  % Get the right Lower and upper bounds for
        Uvars = U(RwIter(k,:));  % the particular means.
        LocalVars = length(MU_Ri);% Length of the mean vector, for the
                                  % relevant means
        cc = cc+1;
        % Probabilities from state to conformance
        PCs(cc) = mvncdf(Lvars,Uvars,MU_Ri,SIGMA);
        % Probabilities from state to scrap
        PSs(cc) = 1-mvncdf(Uvars,MU_Ri,SIGMA);
        for m = 1:LocalVars%:-1:1
        %'----------------- Define Combins-----------------'
            nvar = nchoosek(LocalVars,m);
            combins = combinator(LocalVars,m,'c');
            for v = 1:nvar
                c = c+1; % counter i++
```

```
                % substitute -inf for relevent lower limits
                Llim = Lvars; Llim(combins(v,:)) = -inf;
                % subsitute L for relevent upper limits
                Ulim = Uvars; Ulim(combins(v,:)) = Lvars(combins(v,:));
                Pps(c) = mvncdf(Llim,Ulim,MU_Ri,SIGMA); % these are all the
                % probability terms in the P-Matrix but just a long vector
                % not in the correct places
            end
        end
    end
end


%% calculate S-Matrix
SMAT = zeros(eta-1,eta-1);
for k = 1:num_vars
    UP{k} = combinator(num_vars,k,'c');
end
% create an Upsilon vector with all the combinations
% i.e.  [1]
%       [2]
%       [3]
%       [1 2]
%       :
%       [1 2 3]
c = 1;
for k = 1:num_vars
    Coms = combinator(num_vars,k,'c');
    sizeComs = size(Coms);
    for j = 1:sizeComs(1)
        UPv{c,:} = Coms(j,:);
        c = c+1;
    end
    k=k+1;
end
beta = 0;
%SCP_Cost = 0; % initilize Scrap cost

for k = 1:num_vars % Generate S-matrix for each k- value
    for i = 1:k-1
        beta_c = factorial(num_vars)/(factorial(i)*(factorial(num_vars-i)));
        beta = beta + beta_c;
    end
    alpha_l = 0;
    for i = num_vars:-1:k
        alpha_c = (factorial(num_vars)/(factorial(i)*(factorial(num_vars-i))));
        alpha_l = alpha_l + alpha_c; % Determine last term in alpha eqn
    end                              % alpha is k-dependent
```

```
    alpha = 2 + (eta-1) - alpha_l;   % alpha eqn
    % Compute the m equation (k-dependent)
    m = (factorial(num_vars)/(factorial(k)*(factorial(num_vars-k))));
    delta = beta+m;
    SMat = kSMatrix(k,alpha,eta,m,UP,UPv);   % S-Matrix function
    % Store S-Matrices in a cell array
    SMAT(alpha-1:eta-1,alpha-1:delta) = SMat;
    beta = 0; % reset beta to zero

end


%% Compute the tranistion (Pmatrix)
[col row] = find(SMAT(1:eta-2,:)'==1);

PMat = zeros(eta+2,eta+2);
for i = 1:length(row)
    PMat(row(i)+1,col(i)+1) = Pps(eta-1+i);
end

PMat(1,2:eta) = Pps(1:eta-1);  %input the values for the first row
PMat(eta,2:eta) = Pps(1:eta-1); % input the values for the eta row
PMat(end,end) = 1; PMat(end-1,end-1) = 1; % Input 1s for absorbing states

%% Now we need the Probs to conformance and probs to scrap
% Conformance prob vector, e.g. 2 vars PSs = [pIC,p2C,p3C,p4C];
PCs = [PCs, PCs(1)];
% Scrap  vector, e.g. 2 vars PSs = [pIS,p2S,p3S,p4S];
PSs = [PSs, PSs(1)];
PMat(1:eta,eta+1) = PCs;
PMat(1:eta,eta+2) = PSs;

%% Define PIs vector
% Define the PIs vec, e.g 2 vars PIs = [pI2,pI3,pI4,pIC,pIS];
PIs = [Pps(1:eta-1) PCs(1) PSs(1)];
```

Appendix F

Case Study - Optimal Mean Setting

The primary purpose of this case study was to demonstrate the use of copula functions when the distributions of inspectable features were not normal. Additionally the case study demonstrates the application of Optimal Mean Setting to a non-standard case, where one manufacturing operation produced more than one inspectable feature[1]. A boring operation was used to create a hollow cylinder with an inspectable inner diameter. As a result a wall thickness was created, which also required inspection. Optimal Mean Setting was used to establish the economically optimal target mean for the inner diameter, given the inner diameter and wall thickness tolerances. The distribution of the wall thickness was a convolution between the outer and inner diameters and not a parametric distribution, thus a copula function was necessary to establish the final geometry distribution. An alternative method of manufacture would be to create the wall thickness by turning the outer diameter (d_1) after boring the inner diameter (d_3). However, this would have added an extra manufacturing operation, which was avoided using the aforementioned method.

Figure F.1 illustrates a test casing for solid or hybrid rocket motors. The left opening permits a variety of graphite nozzles to be tested; while the right opening allows a plug and oxidizer injector to be fitted as well as an opening to insert the graphite nozzle. There are two critical dimensions, the inner diameter (d_3) and casing thickness (t_1). An upper tolerance was specified on the inner diameter to prevent the presence of a gap between the graphite nozzle and the inner wall, which would allow the ingress of combustion gasses. A lower tolerance was specified to ensure the graphite nozzle could be inserted into the casing. Tolerances were specified on the wall thickness to ensure

[1]The Optimal Mean Setting framework presented hitherto dealt with independent features.

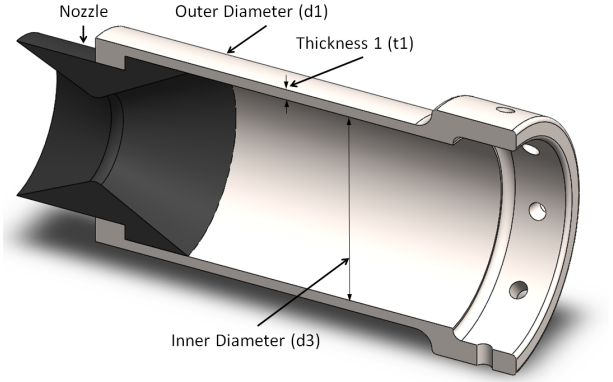

(a) Casing cut-through

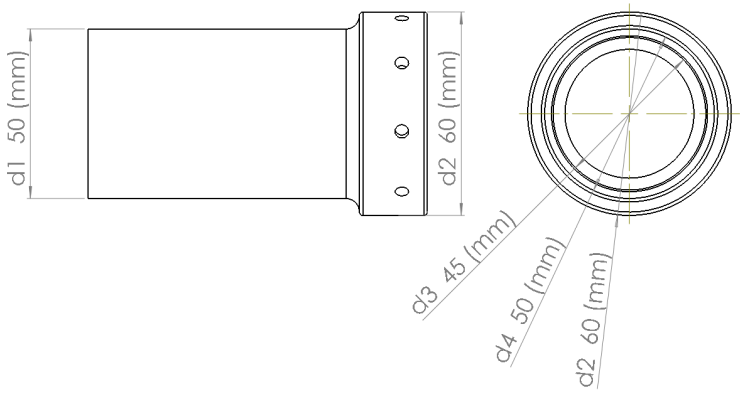

(b) Casing dimensional drawing

FIGURE F.1: Case study - rocket motor test casing

Stats.	Values	**Costs**	Values
$\boldsymbol{L}$	$L_{d_3} = 3.9,\ L_{t_1} = 0.8$	SP	[100]
$\boldsymbol{U}$	$U_{d_3} = 4.3,\ U_{t_1} = 1.0$	PC	[10]
$\boldsymbol{\sigma}$	$\sigma_{d_1} = 0.05,\ \sigma_{d_3} = 0.08$	RC	$[0, -, -, 10]$
$\boldsymbol{\mu}_{\text{nominal}}$	$\mu_{d_1} = 5,\ \mu_{d_3} = 4.1,\ \mu_{t_1} = 0.9$	SC	$[15, -, -, 15]$
$\mu_{\text{opt } d_3}$	4.0304	EP_{opt}	80.8982
ρ_{D_3,T_1}	-0.8480		

TABLE F.1: Specification limits, process variation and costs for the rocket casing case study

the wall was thick enough to withstand the pressure created through combustion but excessive thickness increased mass. The nominal means, upper and lower specification limits and standard deviation of the manufacturing operations are given in Table F.1.

The Optimal Mean Setting equation for this two feature case is similar to Equation 3.44 from Chapter 3. However, there are differences since it was not possible to rework the inner diameter or wall thickness independently of each other. The $f_{2,S}$ and $f_{3,S}$ terms

are zero and the $p_{\mathrm{I},4}$ term becomes,

$$p_{\mathrm{I},4} = F([L_1, U_2], \boldsymbol{\mu}, \boldsymbol{\Sigma}) + F([U_1, L_2], \boldsymbol{\mu}, \boldsymbol{\Sigma}) - F([L_1, L_2], \boldsymbol{\mu}, \boldsymbol{\Sigma}).$$

This accounts for the proportion of single feature rework components where both features were reworked, since the inner diameter and wall thickness were not independent. Expected profit for the manufacture of the inner diameter and wall thickness was given by,

$$\begin{aligned} E(PR) &= SP\, f_{\mathrm{I},C} - PC - SC_1\, p_{\mathrm{I},S} \\ &- SC_4 \left(\frac{p_{\mathrm{I},S}}{1 - p_{\mathrm{I},4}} \right) p_{\mathrm{I},4} - RC_4\, m_{\mathrm{I},4}. \end{aligned} \tag{F.1}$$

The casing was assumed to be a near net shape forging, where machining was only required to complete the inner diameter (d_3). The outer diameter (d_1) was assumed to have a normal distribution where the mean and standard deviation are given in Table F.1. Equation F.1 was optimised with Matlab using *fminsearchcon.m* developed by Errico [2006], recognising scrap occurred if features were produced greater than the upper specification limits and rework occurred where features were produced lower than the lower specification limit. The distribution of the wall thickness (f_{t_1}), is given by the difference between the outer diameter distribution (f_{d_1}) and the inner distribution (f_{d_3}). Since both the outer and inner diameter distributions are normal, the initial wall thickness distribution is also a normal distribution where the mean is $\mu_{t_1} = \mu_{d_1 - d_3} = \mu_{d_1} - \mu_{d_3}$ and the variance is $\sigma^2_{t_1} = \sigma^2_{d_1 - d_3} = \sigma^2_{d_1} + \sigma^2_{d_3}$. The probability of scrap, rework and conformance was given by the joint normal distribution f_{d_3,t_1}, as was first discussed in Section 3.1.2 in Chapter 3. The dependence between d_3 and t_1 was modelled using correlation of the form,

$$\rho_{D_3,T_1} = \frac{E[(D_3 - \mu_{D_3})(T_1 - \mu_{T_1})]}{\sigma_{D_3}\sigma_{T_1}},$$

where D_3 and T_1 are random variables of the inner diameter and thickness. The random variables, D_3, were generated by using the Matlab *normrnd.m* function Mathworks [2012] while $T_1 = D_1 - D_3$, where *normrnd.m* was also used to generate the D_1 vector. The value for correlation was given in Table F.1.

Figure F.2(a) shows the probability density distribution for the initial operation. The upper and lower specification limits are represented by the red and green lines, respectively. There was non-conformance caused from the inner diameter (the variance was such that scrap and or rework were always created), thus rework was required which led to a truncated inner diameter distribution (f_{d_3}). Since the inner diameter was truncated the distribution of wall thickness was no longer given by a normal distribution

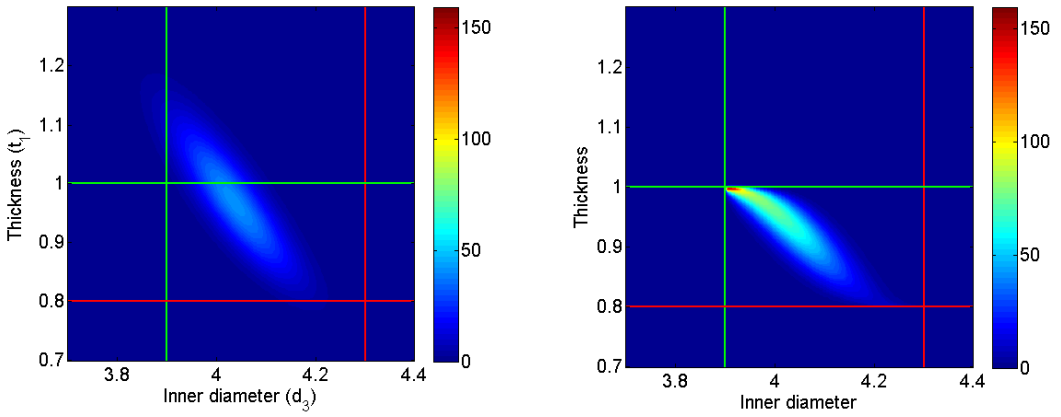

(a) Inner diameter and thickness distributions from the inital processing

(b) The fianl inner diameter and thickness distributions after rework

FIGURE F.2: Inner diameter and wall thickness probability plots for the distributions before and after rework

but from the convolution difference between the outer and inner diameters, such that $f_{t_1} = f_{d_1} + (-f_{d_3})$. The distribution of wall thickness is written,

$$f_{t_1}(t_1) = \int_{-\infty}^{\infty} f_{d_3}(d_3)\, f_{d_1}(t_1 - (-d_3))\, \mathrm{d}_3, \tag{F.2}$$

where the outer diameter, $f_{d_1}(d_1)$ is a normal distribution,

$$f_{d_1}(d_1) = \frac{1}{\sqrt{2\pi\sigma_{d_1}^2}} \exp\left(-\frac{(d_1 - \mu_{d_1})}{2\sigma_{d_1}^2}\right). \tag{F.3}$$

Let,

$$\kappa = \frac{\mu_{d_3} - \mathrm{USL}_{d_3}}{\sigma_{d_3}} \quad \text{and} \quad \lambda = \frac{\mu_{d_3} - \mathrm{LSL}_{d_3}}{\sigma_{d_3}},$$

allowing $f_{d_3}(d_3)$ from Equation F.2 to be written as the truncated normal distribution due to rework,

$$f_{d_3}(d_3) = \frac{1}{\sqrt{2\pi\sigma_{d_3}^2}\left[\mathbf{\Phi}(\lambda) - \mathbf{\Phi}(\kappa)\right]} \exp\left(-\frac{(d_3 - \mu_{d_3})}{2\sigma_{d_3}^2}\right). \tag{F.4}$$

To simplify the expression for the thickness distribution f_{t_1}, let

$$\Gamma = \frac{1}{2\pi\sigma_{d_1}\sigma_{d_3}\left[\mathbf{\Phi}(\lambda) - \mathbf{\Phi}(\kappa)\right]}.$$

Then substituting Equation F.3 and F.4 into Equation F.2 yields,

$$f(t_1) = \Gamma \int_{\mathrm{LSL}_{d_3}-t_1}^{\mathrm{USL}_{d_1}-t_1} \exp\left[-\frac{(d_3-\mu_{d_3})^2}{2\sigma_{d_3}^2}\right] \exp\left[-\frac{(t_1-d_3-\mu_{d_1})^2}{2\sigma_{d_1}^2}\right] \mathrm{d}_3. \tag{F.5}$$

This has no closed form solution but can be solved in terms of the error function which has the general form,

$$\mathrm{erf}(x) = \frac{2}{\sqrt{\pi}} \int_0^x \exp(-t^2)\, \mathrm{t}.$$

Maple was used to determine the integral in terms of the error function giving,

$$\begin{aligned} f(t_1) =& \frac{\sqrt{2\pi}\,\sigma_{d_1}\sigma_{d_3}}{\sqrt{\sigma_{d_1}^2+\sigma_{d_3}^2}} \exp\left(-\frac{(\mu_{d_1}-\mu_{d_3}+t_1)^2}{2({\sigma_{d_1}}^2+{\sigma_{d_3}}^2)}\right)\times \\ & \left[\mathrm{erf}\left(\frac{\sqrt{2}}{2}\frac{\left((\mathrm{USL}_{d_3}-\mu_{d_3})\,\sigma_{d_1}^2+\sigma_{d_3}^2\,(\mathrm{USL}_{d_3}-t_1-\mu_{d_1})\right)}{(\sigma_{d_1}\sigma_{d_3}\sqrt{{\sigma_{d_1}}^2+{\sigma_{d_3}}^2})}\right)\right. \\ & \left. -\,\mathrm{erf}\left(\frac{\sqrt{2}}{2}\frac{\left((\mathrm{LSL}_{d_3}-\mu_{d_3})\,\sigma_{d_1}^2+\sigma_{d_3}^2\,(\mathrm{LSL}_{d_3}-t_1-\mu_{d_1})\right)}{(\sigma_{d_1}\sigma_{d_3}\sqrt{{\sigma_{d_1}}^2+{\sigma_{d_3}}^2})}\right)\right]. \end{aligned} \tag{F.6}$$

The μ_{d_3} parameter was optimised to maximise the expected profit given by Equation F.1; the optimal mean ($\mu_{\mathrm{opt}\ d_3}$) and expected profit (EP_{opt}) are given in Table F.1. The resulting f_{d_3} distribution is illustrated by Figure F.3(a). The initial distribution (before rework), truncated distribution (after rework and without scrap), and the optimal mean are shown by the grey, blue and black lines respectively. The upper and lower specification limits are also shown. The green line represents the rework limit, where outside this limit rework is possible, the red line indicates the scrap limit. The thickness distribution, resulting from the convolution between the outer and inner diameter distributions is shown in Figure F.3(b). The shape of the initial distribution (grey line) is not normal, there is some positive skew. The distribution became truncated due to rework on the d_3 parameter, as illustrated by the blue line in Figure F.3(b). Both the μ_{d_3} and μ_{t_1} parameters shifted toward the respective rework limits as due to the reduced cost of rework compared to scrap. The final distribution of the geometry was determined by establishing the joint distribution between the correlated truncated normal, f_{d_3}, and the truncated skewed f_{t_1} distribution (Figure F.2(b)).

This example demonstrated the use of optimal mean setting where one of the design parameters (wall thickness) was a result of another design feature (inner diameter). Although the optimisation of expected profit did not follow the standard set-up described in Chapter 3, it was simple to fit the case study to the existing framework. The final manufactured geometry was obtained and shown in Figure F.2(b). Due to the

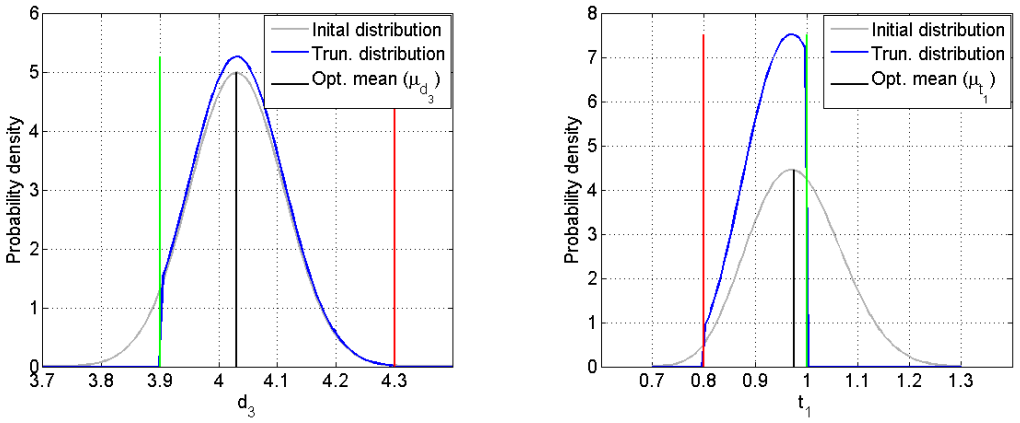

(a) Casing diameter distributions before and after rework

(b) Casing thickness distributions before and after rework

FIGURE F.3: Distributions of the inner diameter and thickness features before and after rework

non-normal wall thickness distribution, the joint distribution of the final manufactured geometry was only calculable due to the freedom offered by copula functions.

Appendix G

Aerothermal Analysis and Response Surface Methodology of a Film Cooling Hole

G.1 Numerical Model

The temperature on the lower duct surface, down stream of the hole (T_S), was computed by solving the 2-D time-averaged steady-state Navier-Stokes equations where continuity was given by,

$$\frac{\partial}{\partial x_i}\left(\overline{\rho u}_i\right) = 0 \tag{G.1}$$

and momentum was,

$$\frac{\partial}{\partial x_j}\left(\overline{\rho u_i u}_j\right) = -\frac{\partial \bar{P}}{\partial x_i} + \frac{\partial}{\partial x_j}\left[\mu\left(\frac{\partial \bar{u}_i}{\partial x_j} + \frac{\partial \bar{u}_j}{\partial x_i} - \frac{2}{3}\delta_{ij}\frac{\partial \bar{u}_l}{\partial x_l}\right)\right] + \frac{\partial}{\partial x_j}\left(-\overline{\rho u_i' u_j'}\right). \tag{G.2}$$

In Equations G.1 and G.2, $\bar{\rho}$ is mean density, $\bar{u}$ is the mean component of velocity, $\bar{P}$ is mean pressure and μ is the molecular viscosity. The δ_{ij} term in the Kronecker delta, which is 0 when $i \neq j$ and 1 if $i = j$. The $-\overline{\rho u_i' u_j'}$ are the Reynolds stresses accounting for the turbulent fluctuation in the fluid momentum. The Reynolds stress terms must be modelled to satisfy the so called 'closure problem' (Pope [2009]). The Boussineq hypothesis is employed to related the Reynolds stresses with the mean velocity gradient of the flow, such that the Reynolds stresses become,

$$-\overline{\rho u_i' u_j'} = \mu_t\left(\frac{\partial \bar{u}_i}{\partial x_j} + \frac{\partial \bar{u}_j}{\partial x_i}\right) - \frac{2}{3}\left(\rho k + \mu\frac{\partial \bar{u}_i}{\partial x_i}\right)\delta_{ij}. \tag{G.3}$$

The k term is the turbulent kinetic energy and μ_t is the turbulent viscosity given by,

$$\mu_t = \rho C_\mu k^2/\varepsilon, \tag{G.4}$$

for which C_μ is a constant and ε is the dissipation rate. The Realizable k-ε model (Shih et al. [1995] based on the original k-ε model proposed by Launder and Spalding [1972]), was chosen to model the turbulence. While the standard k-ε model is robust and offers reasonable accuracy over a wide range of turbulent flows, the realizable formulation more accurately predicts the spreading rate for planar and round jets (Fluent [2012]) and therefore beneficial for the modelling of a coolant jet.

G.2 Turbulence Model

The turbulent kinetic energy (k) and dissipation rate (ε) can obtained from the transport equations. For steady-state incompressible flow the transport equation given in Fluent [2012] reduce to,

$$\frac{\partial}{\partial x_i}(\rho k \bar{u}_i) = \frac{\partial}{\partial x_j}\left[\left(\mu + \frac{\mu_t}{\sigma_k}\right)\frac{\partial \varepsilon}{\partial x_j}\right] + G_k - Y_k \tag{G.5}$$

$$\frac{\partial}{\partial x_i}(\rho \varepsilon \bar{u}_i) = \frac{\partial}{\partial x_j}\left[\left(\mu + \frac{\mu_t}{\sigma_\varepsilon}\right)\frac{\partial \varepsilon}{\partial x_j}\right] + G_\varepsilon - Y_\varepsilon \tag{G.6}$$

The σ_k and σ_ε terms are the turbulent Prandtl number for the turbulent kinetic energy (k) and dissipation rate (ε), respectively. The G_k term represents the generation of turbulent kinetic energy ($G_k = -\overline{\rho u_i' u_j'}\frac{\partial u_j}{\partial x_i}$) due to the average velocity gradient. In is approximated using the Boussinesq hypothesis such that,

$$G_k = \mu_t S^2,$$

where S is the average rate-of-strain tensor given by,

$$S = \sqrt{2 S_{ij} S_{ij}}, \quad \text{where} \quad S_{ij} = \frac{1}{2}\left(\frac{\partial \bar{u}_j}{\partial x_j} + \frac{\partial \bar{u}_i}{\partial x_j}\right).$$

The Y_k term accounts for the dissipation of turbulent kinetic energy defined by $Y_k = \rho\varepsilon$. The 'k' part of the transport equation (Equation G.5) for the standard k-ε model and the realisable k-ε model are the same. However, the production and diffusion terms in the 'ε' part of the transport equation (Equation G.6) differ between the standard and realisable forms of the k-ε model. For the realisable model,

$$G_\varepsilon = \rho C_1 S \varepsilon, \quad \text{where} \quad C_1 = \max\left[0.43, \frac{\zeta}{\zeta + 5}\right] \quad \text{and} \quad \zeta = S\frac{k}{\varepsilon}. \tag{G.7}$$

The diffusion term is given by,

$$Y_\varepsilon = \rho C_2 \frac{\varepsilon^2}{k + \sqrt{\nu\varepsilon}} \tag{G.8}$$

where C_2 is a constant. Turbulent viscosity is computed using Equation G.4 however, C_μ is not constant for the realisable k-ε model but found from,

$$C_\mu = \frac{1}{A_0 + A_s \dfrac{kU^*}{\varepsilon}} \tag{G.9}$$

The velocity component U^* is given by,

$$U^* \equiv \sqrt{S_{ij}S_{ij} + \bar{\Omega}_{ij}\bar{\Omega}_{ij}} \quad \text{where} \quad \bar{\Omega}_{ij} = \frac{1}{2}\left(\frac{\partial \bar{u}_i}{\partial x_j} - \frac{\partial \bar{u}_j}{\partial x_i}\right). \tag{G.10}$$

The A_0 term is a constant and the remaining term A_s is given by

$$A_s = \sqrt{6}\cos\left(\frac{1}{3}\cos^{-1}\left(\sqrt{6}\frac{S_{ij}}{\sqrt{S_{ij}S_{ij}}}\right)\right) \tag{G.11}$$

The constants for the model, as given by Fluent [2012], are $A_0 = 4.04$, $C_2 = 1.9$, $\sigma_k = 1.0$ and $\sigma_\varepsilon = 1.2$.

The realisable k-ε model is generally valid for fully turbulent flows which is not necessarily the case at the wall, where the Reynolds number is low in the vicinity of the boundary layer. For this reason an Enhanced Wall Function (Fluent [2012]) treatment was used to model the near wall flow downstream of the hole (a similar approach was used for the 2D analysis conducted by Li and Wang [2007] and Wang and Zhao [2011]). The whole domain was segregated into a viscosity-affected region and a fully turbulent region by specifying the turbulent Reynolds number,

$$\mathrm{Re}_y \equiv \frac{\rho y\sqrt{k}}{\mu},$$

where y was the normal distance from the wall. For $\mathrm{Re}_y > 200$ the realisable k-ε model was used. Towards the wall, where $\mathrm{Re}_y < 200$ in the viscosity-affected region the one-equation Wolfstein model was used (Wolfshtein [1969]). The transition between the turbulent viscosities in the fully turbulent and viscosity-affected regions were smoothed by using the blending function proposed by Jongen [1998],

$$\mu_{t,\text{enhanced}} = \lambda_\varepsilon \mu_t + (1 - \lambda_\varepsilon)\mu_{t,\text{one}}.$$

Viscosity from the realisable k-ε model is μ_t while $\mu_{t,\text{one}}$ represents the viscosity form the one-equation model.

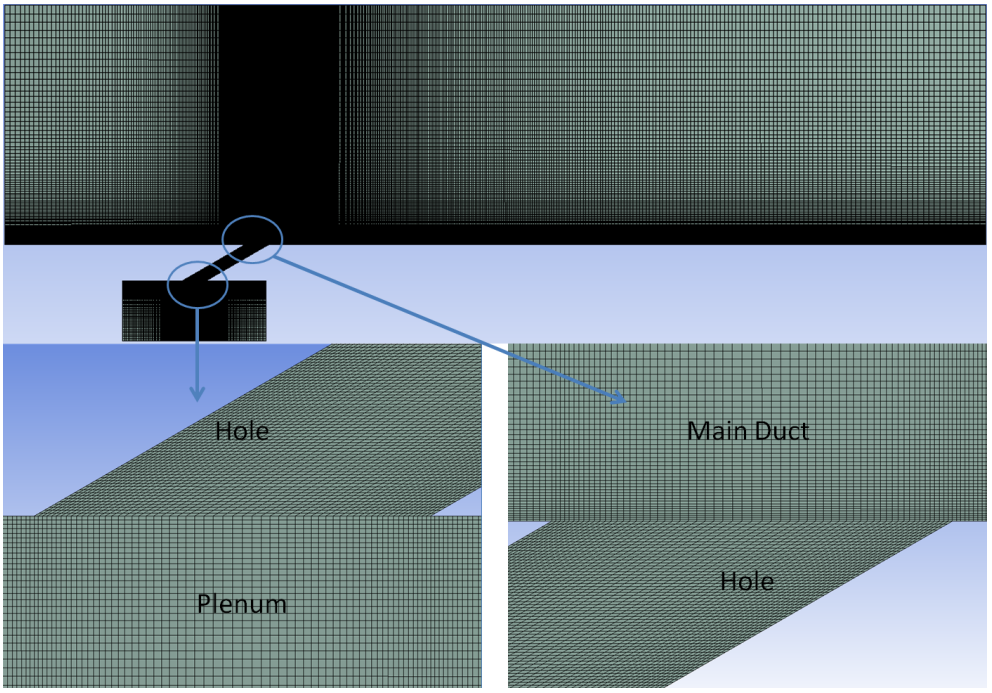

FIGURE G.1: Overview of the 2D mesh

G.3 Mesh Generation and Results Validation

The domain illustrated in Figure 4.22 was meshed using the Ansys meshing tool where the domain sizing broadly follows that of Li and Wang [2007]. The mesh was updated parametrically with changes to the domain geometry (α and d parameters), which required the addition and removal of cells to maintain the mesh density and cell aspect ratios. The density of the mesh was bias towards the lower section of the main duct to capture the coolant and hot gas mixing, and satisfy the condition of the enhanced wall treatment method, which required a $y^+ \approx 1$ (Section G.2). The value y^+ was calculated from $y^+ \equiv u_f y/\nu$, where y was the distance to the nearest wall, u_f was friction velocity and ν was the local kinematic viscosity. Since the last two terms are properties of the fluid and global domain, the only way to ensure $y^+ \approx 1$ was to run the case, measure y^+ and resize until $y^+ \approx 1$ was achieved. The mesh density also increased in the vicinity of the hole to capture the mixing of the coolant and hot gas. Sargison et al. [2001] found the geometry at the hole entry could impact the flow in the hole and affect the cooling effectiveness. Therefore, the grid density close to the hole in the plenum was increased to ensure the flow was accurately modelled at the hole entrance.

Three mesh densities were tested to ensure mesh convergence, the details regarding the edge sizing and biases are tabulated in Table G.1. The hole was defined in accordance with the standardised public hole described by Schroeder and Thole [2014], where the laidback angle was set to zero. The diameter, $d = 4$, and the inclination angle, $\alpha = 30$,

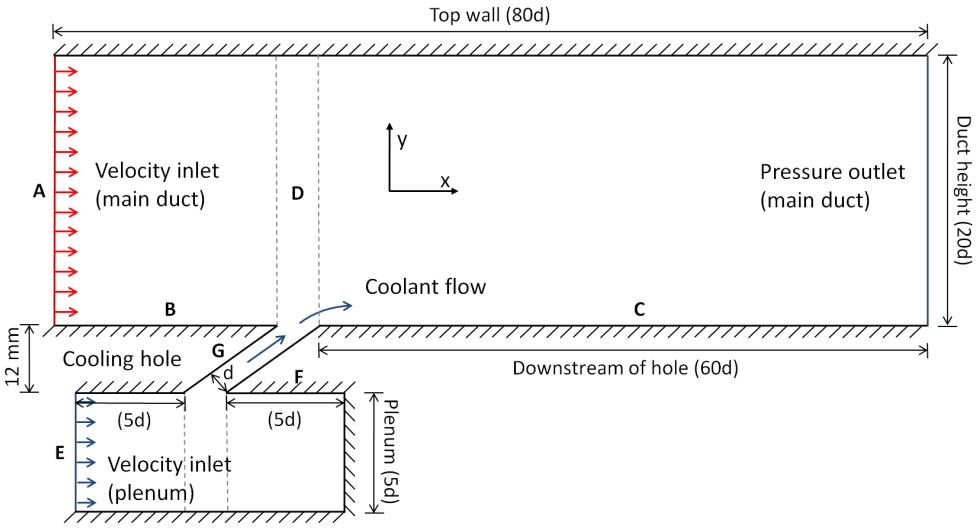

FIGURE G.2: Overview of the 2D cooling hole computational domain (not to scale)

in accordance with Schroeder and Thole [2014]. The boundary conditions noted in Table G.2 were also taken from Schroeder and Thole [2014]. Based on these condition the blowing ratio, $M = 0.98$, and the density ratio was 1.51, which are representative of engine conditions (Schroeder and Thole [2014]). Following the 2D analysis by Wang and Zhao [2011], the air was modelled as an incompressible ideal gas, where specific heat capacity was modelled as a piecewise polynomial function with two temperature sub ranges of 100 - 1000 K and 1000 - 2000 K respectively. The thermal conductivity was 0.0242 (w/mK) and viscosity was modelled using a piecewise polynomial with values dependent on the temperature in the plenum and the duct (see table G.2). The Reynolds number based on the hydraulic diameter of the main duct, was $\mathrm{Re}_{\mathrm{duct}} = 83500$ and the Reynolds number, based on the inlet hole velocity and hole diameter was $\mathrm{Re}_{\mathrm{hole}} = 3580$. The commercial CDF package, Ansys Fluent 14.5 was used to solve the Reynolds Averaged Navier-Stokes (RANS) equations (Detailed in Section G.1). The computational time was between seven and 15 minutes (dependent on the number of cells which changed depending on the α and d parameters), running on seven cores of a 3.4 GHz Intel Core i7 processor with 16 GB of installed RAM.

The thermal effectiveness (η) obtained from the three meshes was plotted in Figure G.3. Experimental results from Schroeder and Thole [2014] and Rhee et al. [2002] (blue crosses and magenta points) are also shown, where cooling effectiveness was measured along the centreline, downstream of the holes. Numerical results from Wang and Zhao [2011] are also shown. Clearly there is a mismatch between the numerical solutions and the results obtained by Schroeder and Thole [2014], which had the same boundary conditions and hole geometry. The results from Rhee et al. [2002] also indicate a lower η than

	Low Density		**Medium Density**		**High Density**	
Edge	Spacing	Bias	Spacing	Bias	Spacing	Bias
A	1.0×10^{-3}	1.04	0.667×10^{-3}	1.37	0.667×10^{-3}	1.037
B	1.185×10^{-3}	1.03	0.79×10^{-3}	1.03	0.60×10^{-3}	1.02
C	1.185×10^{-3}	1.03	0.79×10^{-3}	1.01	0.60×10^{-3}	1.008
D	0.27×10^{-3}	1.03 b	0.18×10^{-3}	1.03 b	0.1×10^{-3}	1.03 b
E	0.285×10^{-3}	1.03	0.285×10^{-3}	1.03	0.285×10^{-3}	1.03
F	0.285×10^{-3}	1.03	0.285×10^{-3}	1.03	0.285×10^{-3}	1.03
G	0.27×10^{-3}	1.01	0.18×10^{-3}	1.01	0.12×10^{-3}	1.03

TABLE G.1: Mesh sizing for each edge given in Figure 4.22 where the number of elements for each mesh were: LD= 38,962, MD= 73,427 and HD= 97,622. The letter 'b' indicates bilateral bias, i.e. the mesh density increased in both positive and negative x-directions.

	Duct	**Plenum**
Inlet Velocity	10.0 (m/s)	1.13 (m/s)
Turbulent intensity	0.5 %	0.5 %
Turbulent length scale	0.0090 (m)	0.0020 (m)
Temperature	295 (K)	195 (K)
Viscosity	1.846×10^{-5} (kg/ms)	1.307×10^{-5} (kg/ms)
Hydraulic diameter	0.1288 (m)	0.0286 (m)

TABLE G.2: Boundary conditions

predicted by the numerical analysis[1]. Wang and Zhao [2011] attributed this mismatch to a conjugate heat transfer effect, where the surface temperature was higher than the coolant, due to heat transfer from the hot gas to the surface, further downstream or upstream in the test section. Wang postulated conduction through the surface increased the surface temperature near the hole, above what would be expected if only mixing had occurred between the coolant and hot gas. Immediately adjacent to the hole the surface temperature would be expected to be the same as the coolant, as no mixing would have taken place. However, this explanation is not valid for the difference between the numerical results and the data from Schroeder and Thole [2014], as a foam surface was used with a thermal conductivity of just 0.029 W/mK, making any conductive transfer negligible. Schroeder and Thole [2014] also calculated an uncertainty of ± 0.024 for the η measurement, but this is insufficient to explain the higher η obtained by the numerical solutions. The most likely explanation is due to lateral mixing in the 3D coolant (z-direction) jet, lowering the centreline effectiveness. Clearly these 3D effects are not applicable to the 2D numerical studies. The 3D effects on the centreline effectiveness are

[1]The results from Rhee et al. [2002] and Wang and Zhao [2011] were obtained using slightly different boundary conditions and hole geometry to Schroeder and Thole [2014] and the numerical results run for this thesis. The inclination angle was 35 degrees (5 degrees greater), higher turbulence intensity of 5% was used, the density ratio was 1.3 as opposed to 1.5 and the blowing ratio was 1.3 as opposed to ~ 1. Nevertheless as η is a normalised value, provided the flow physics is captured correctly the differences are minimal as indicated by Figure G.3

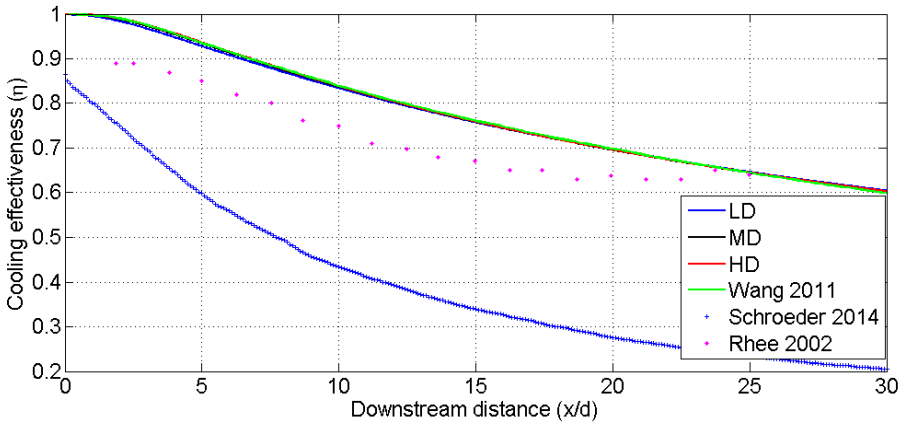

FIGURE G.3: Cooling effectiveness versus downstream distance from the hole

likely to be greater for the cylindrical fan shaped hole exits of Schroeder and Thole [2014] than for the wider rectangular holes from Rhee et al. [2002], which may explain why the experimental η values predicted by Rhee et al. [2002] are greater than those predicted by Schroeder and Thole [2014]. Despite the differences between the numerical solutions and the experimental evidence, the numerical solutions (in this thesis) generally agree well with the numerical solution from Wang and Zhao [2011]. Since the application of Optimal Mean Setting for the cooling hole geometry only requires the relative differences in cooling effectiveness, ensuring the numerical solutions match the lab solutions is not essential, provided the global flow physics is modelled correctly (indeed the lab solutions only approximate real engines conditions). Figures G.4(a) and G.4(b) provide greater detail on the differences between the η values from the three meshes and the numerical solution from Wang and Zhao [2011]. The low density mesh (LD) produced lower values of η close to the hole and higher values further downstream. The difference between the medium and high density meshes (MD and HD) was 0.0022 at three diameters downstream, as opposed to 0.0061 and 0.0083 for the LD mesh compared to the MD and HD meshes respectively. At 30 diameters downstream the difference between the MD and HD meshes was 0.0003 while the difference between the LD mesh and the MD and HD meshes was 0.0021 and 0.0018 respectively. The HD mesh was considered to be converged due to the closeness of the η values at all points downstream of the hole between the MD and HD meshes. Figure G.5 shows the variation in y^+ with downstream distance from the hole. The LD mesh exhibited values of $y^{\sim}3$. The size of the elements in close proximity to the surface were reduced for the MD and HD meshes giving a $y^+ < 1$ everywhere on the surface, in accordance with the use of the enhanced wall treatment discussed in Section G.2. Figure G.6 illustrates the velocity temperature and turbulent kinetic energy in the domain. There is a clear segregation between the hot gas and coolant which gradually becomes less contrasting as the coolant and hot gas mix. The flow becomes turbulent at the hole entrance and develops in the hole itself. The

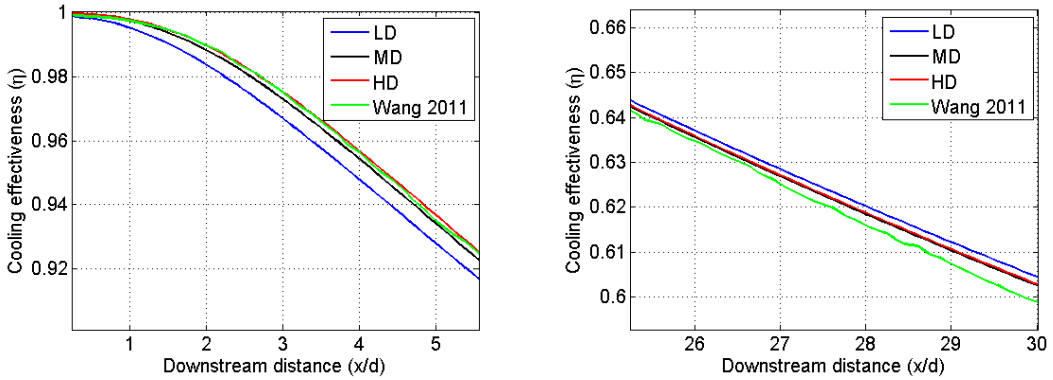

(a) Cooling effectiveness versus downstream distance close to the hole opening

(b) Cooling effectiveness at 25 to 30 diameters down stream

FIGURE G.4: Cooling effectiveness close to the hole and around 25 to 30 diameters downstream

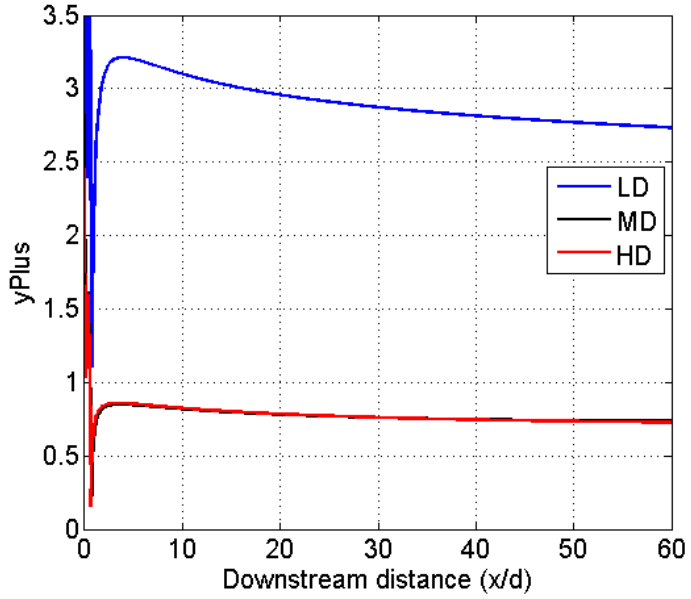

FIGURE G.5: Cooling effectiveness versus downstream distance from the hole

turbulent kinetic energy is broadly representative of the turbulent intensity illustrated by Gritsch et al. [1998]. Figures G.7(a) and G.7(b) illustrate the flow through the hole in greater detail. The presence of the separation bubbles and jetting effects were similarly shown by Saumweber and Schulz [2012]. The separation bubble at the downstream exit of the hole is similar to that predicted by the standard k-ε turbulence model detailed by Li and Wang [2007].

Overall the flow characteristics are in good agreement with experimental data and other numerical results available in the literature. The discrepancies between the predicted η values and the experimental results (particularly Schroeder and Thole [2014]) are

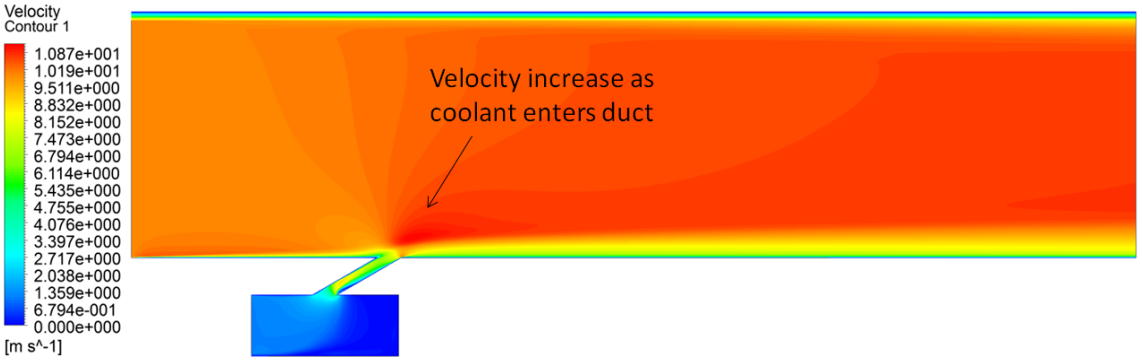

(a) Contours of velocity over the whole domain

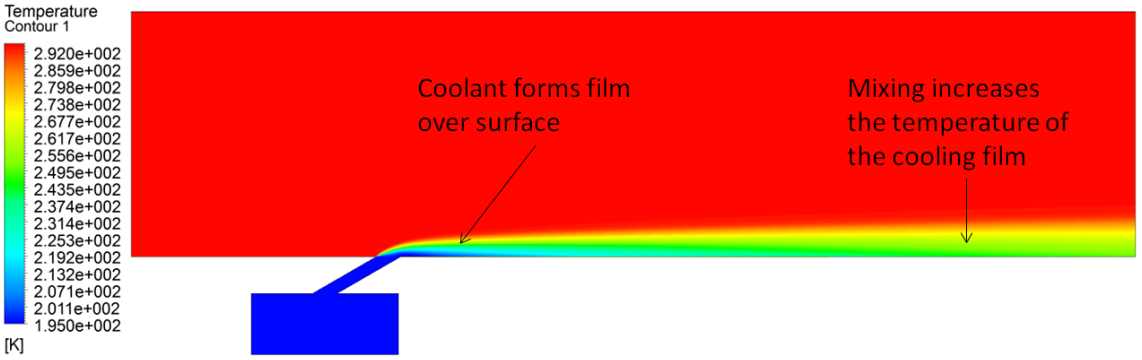

(b) Contours of temperature over the whole domain illustraties the effect film cooling has on segregating the hot gas from the airfoil surface

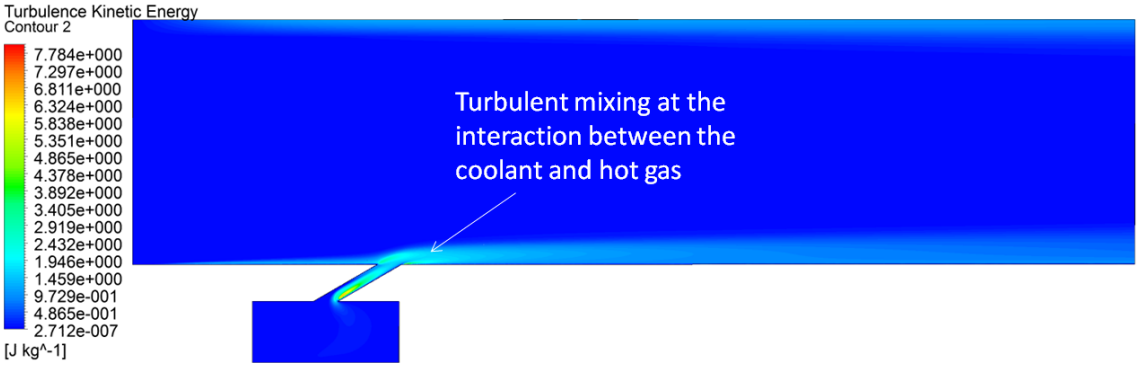

(c) Turbulent kinetic energy over the whole domain illustrating turbulent forming in the hole and the turbulent mixing between the coolant and hot gas

FIGURE G.6: Contour plots illustrating the velocity, temperature and turbulent kinetic energy over the whole domain

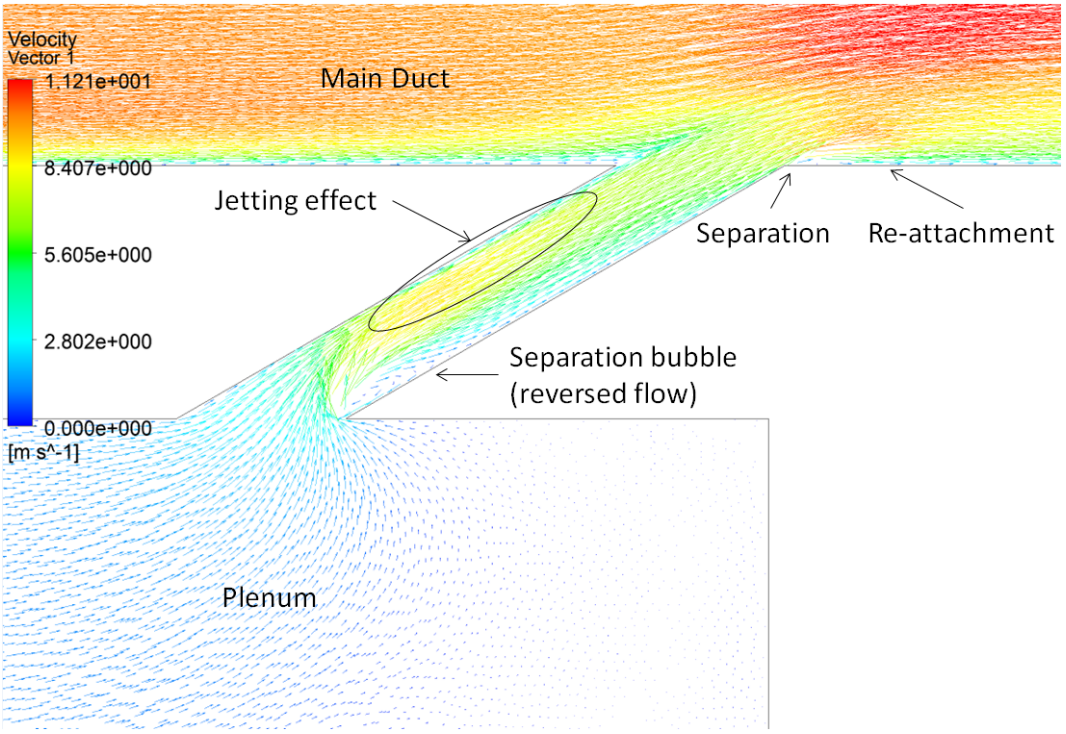

(a) Velocity vectors in the cooling hole illustrating the major flow features

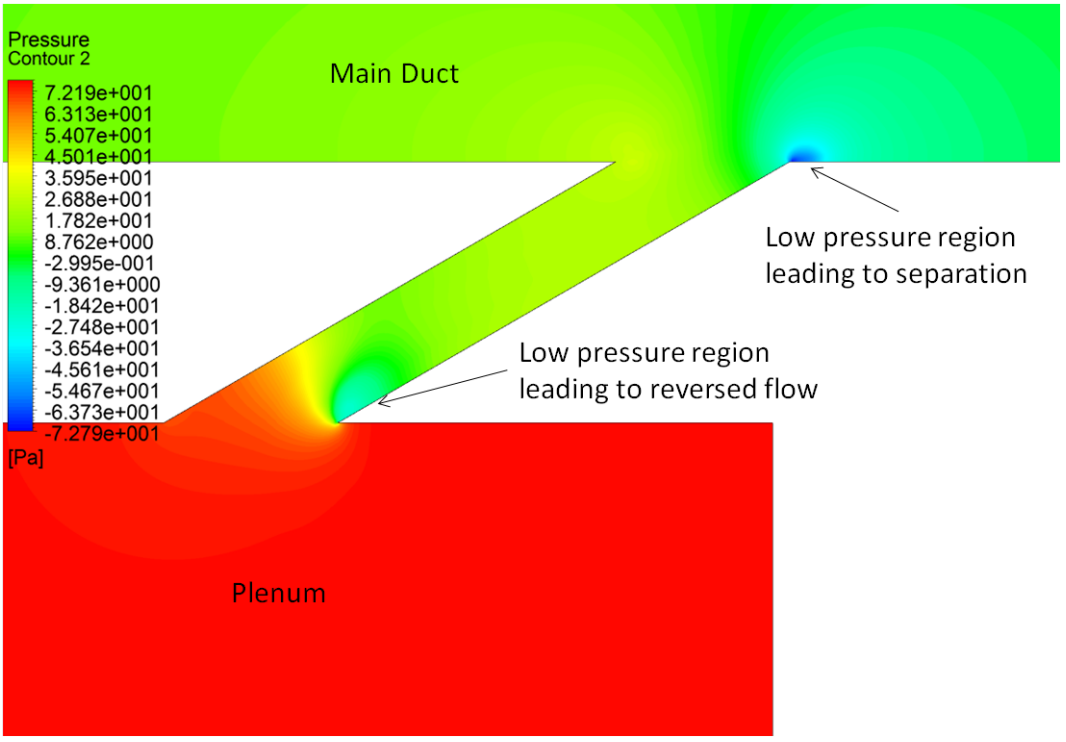

(b) Pressure contours in the cooling hole

FIGURE G.7: Detailed illustration of the velocity and pressure in the cooling hole

most likely due to 3D effects that were not modelled in the 2D scheme presented here. Nevertheless they do correspond well to the 2D numerical results from Wang and Zhao [2011].

G.4 Response Surface Methodology

A response surface was created to establish the variation in cooling efficiency (η) with the cooling hole's inclination angle (α) and diameter (d). The cooling hole geometry and mesh were built parametrically in Ansys Workbench 14.5 with α and d parameters. The α and d sample points were selected following design of experiment principles using a space filling Latin hypercube (following Forrester et al. [2008]). A total of 177 samples points were chosen, where $6.46 \leq d \leq 8.8$ and $27.75 \leq \alpha \leq 37.5$. The minimum hole diameter was larger than the nominal hole diameter used for the mesh convergence study. This was not planned, but it was observed that cooling efficiency improved with the hole diameter despite a reduced blowing ratio (as the coolant inlet velocity remained fixed). A greater hole diameter allowed a thicker film over the surface, which increased the separation between the hot gas and the surface leading to a better cooling efficiency. This was beneficial until the movement of coolant was sufficiently slow that the heat transfer from the hot gas heated the coolant before new coolant passed through. For a 3D hole the coolant is heated and mixing occurs from the sides as well as from the top surface, reducing the cooling effectiveness of the coolant faster. Thus, the benefit of a thicker but slower coolant layer would be less prolonged for a 3D hole.

A response surface was created using a Kriging estimate following the methodology presented in Section 2.4 of Forrester et al. [2008]. The text also provides a Description of the Matlab code necessary to implement the procedure.

Bibliography

Abdolshah, M.; Yusuff, R.M.; Hong, S. H., and M.Y.B., Ismail. New Process Capability Index using Taguchi Loss Functions. *Journal of Applied Sciences*, 9(20):3775–3779, 2009.

Abdolshah, M.; Yusuff, R.M., and Hing, T.S. Loss-based process capability indices : a review. *International Journal of Productivity and Quality Management*, 7(1), 2011.

Abdul-Kader, Walid; Ganjavi, Ozhand, and Solaiman, Aim. An integrated model for optimisation of production and quality costs. *International Journal of Production Research*, 48(24):7357–7370, December 2010.

Akao, Y. New product development and quality assurance – quality development system. *Standardization and Quality Control*, 25(4):7–14, 1972.

Akpose, Wole. A history of Six Sigma. *IEEE -USA Tolday's Engineer*, December 2010.

Al-Sultan, K.S. An algorithm for the determination of the optimum target values for two machines in series with quality sampling plans. *International journal of production research*, 32(1):37–45, 1994.

Al-Sultan, K.S. and Pulak, M.F.S. Optimum target values for two machines in series with 100 % inspection. *European Journal of Operational Research*, 120:181–189, 2000.

Aldrich, John. Information and Economics in Fisher's Design of Experiments. *International Statistical Review*, 75(2):131–149, August 2007.

Anbari, Frank T; Ph, D; George, The, and Kwak, Young Hoon. Success Factors in Managing Six Sigma Projects. pages 1–14, 2004.

Antony, J. Multi-Responce Optimization in Industrial Experiments Using Taguchi's Quality Loss Function and Principal Component Analysis. *Quality and Reliability Enigneering International*, (16):3–8, 2000.

Antony, J. Simultaneous Optimisation of Multiple Quality Characteristics in Manufacturing Processes Using Taguchi's Quality Loss Function. *The International Journal of Advanced Manufacturing Technology*, 17(2):134–138, January 2001.

Aparisi, Francisco; Jabaioyes, Jose, and Carrion, Andres. Statistical properties of the lsi multivariate control chart. *Communications in Statistics - Theory and Methods*, 28(11):2671–2686, January 1999.

Arcelus, F J and Rahim, M A. Reducing Performance Variation in the Canning Problem. 2217(95):477–487, 1996.

Arcelus, F.J. Uniformity of Production vs. Conformance to Specifications in the Canning Problem. In Al-Sultan, K.S. and Rahim, M.A., editors, *Optimization in Quality Control*, chapter 9, pages 243–258. Kluwer Academic Publishers, 1996.

Arcelus, F.J. and Rahim, M.A. Optimal process levels for the joint control of variables and attributes. *European Journal of Operational Research*, 45(2-3):224–230, 1990.

Bettes, D.C. Finding an Optimum Target Value in Relation to a Fixed Lower Limit and an Arbitrary Upper Limit. *Journal of the Royal Statistical Society. Series C (Applied Statistics)*, 11(3):202–210, 1962.

Bisgaard, S.; Hunter, W, and Pallensen, L. Economic Selection of Quality of Manufactured Product. *Technometrics*, 26(1):9–18, 1984.

Boucher, Thomas and Jafari, Mohsen. The Optimum Target Value for Single Filling Operations with Quality Sampling Plans. *Journal of Quality Technology*, 23(1):44–47, 1991.

Bouye, E.; Durrleman, V.; Nikeghbali, A.; Riboulet, G., and Roncalli, T. Copulas for Finance A Reading Guide and Some Applications. 2000.

Bowling, S.R.; Khasawneh, M.T.; Kaewkuekool, S., and Cho, B.R. A Markovian approach to determining optimum process target levels for a multi-stage serial production system. *European Journal of Operational Research*, 159(3):636–650, December 2004.

Bunker, Ronald S. A Review of Shaped Hole Turbine Film-Cooling Technology. *Journal of Heat Transfer*, 127(4):441, 2005.

Bunker, Ronald S. The Effects of Manufacturing Tolerances on Gas Turbine Cooling. *Journal of Turbomachinery*, 131(4):041018, 2009.

Bunker, R.S.; Allen, J.R., and Jared, M. *Method for Quantifying Hole Flow Rates in Film Cooled Parts*, volume 2. US Patent, 20040037344 A1, 2011.

Carlsson, . Determining the most profitable process level for a process under different sales conditions. *Journal of Quality Technolgy*, 16(1):44–49, 1984.

Carlsson, Olle. Economic Selection of a Process level Under Acceptance. *Engineering Costs and Production Economics*, 16:69–78, 1989.

Cavalieri, S. Parametric vs. neural network models for the estimation of production costs: A case study in the automotive industry. *International Journal of Production Economics*, 91(2):165–177, September 2004.

Chan, W.M. and Ibrahim, R.N. Evaluating the quality level of a product with multiple quality characterisitcs. *The International Journal of Advanced Manufacturing Technology*, 24(9-10):738–742, April 2004.

Chase, Kenneth W. Least Cost Tolerance Allocation for Mechanical Assemblies with Automated Process Selection. 3(1):49–59, 1990.

Chase, K.W. Design Issues in Mechanical Tolerance Analysis. Technical Report 87, ADCASTS Report No. 87-5, 1988.

Chen, C H. Determining the Optimum Process Mean Based on Asymmetric Quality Loss Function and Rectifying Inspection Plan. In *IEEE: Industiral Engineering Management Conference*, pages 1080–1084. IEEE, 2004. ISBN 0780385195.

Chen, C.H. and Chou, C.Y. Determining the Optimum Process Mean Under the Bivariate Quality Characteristics. *The International Journal of Advanced Manufacturing Technology*, 21:313–316, 2003.

Chen, C.H.; Chou, C.Y., and Huang, K.W. Determining the Optimum Process Mean Under Quality Loss Function. *The International Journal of Advanced Manufacturing Technology*, 20:598–602, 2002.

Chen, Chung-Ho. Determining the optimum process mean for a mixed quality loss function. *The International Journal of Advanced Manufacturing Technology*, 28(5-6): 571–576, June 2005.

Chen, Chung-ho. Model for Product with Quality Loss under the Serial Production System and Rectifying Inspection Plan. 17(2):99–113, 2010.

Chen, Chung-Ho and Lai, Min-Tsai. Determining the optimum process mean based on quadratic quality loss function and rectifying inspection plan. *European Journal of Operational Research*, 182(2):755–763, October 2007a.

Chen, Chung-Ho and Lai, Min-Tsai. Economic manufacturing quantity, optimum process mean, and economic specification limits setting under the rectifying inspection plan. *European Journal of Operational Research*, 183(1):336–344, November 2007b.

Cheung, Julie; Scanlan, James; Wong, James; Forrester, Jennifer; Eres, Hakki; Collopy, Paul; Hollingsworth, Peter; Wiseall, Steve, and Briceno, Simon. Application of Value-Driven Design to Commercial Aero-Engine Systems. In *10th AIAA Aviation Technology, Integration, and Operations (ATIO) Conference*, number September, pages 1–21, Fort Worth, Texas, 2010. AIAA.

Chien, W and Hou, S. Investigating the recast layer formed during the laser trepan drilling of Inconel 718 using the Taguchi method. 33(3):308–316, 2006.

Cho, B.R. and Leonard, M.S. Identification and extensions of quasi-convex quality loss functions. *International Journal of Reliability Quality and Safety Engineering*, 4: 191–204, 1997.

Cho, Byung Rae. Optimum Process Target for Two Quality Characteristics Using Regression Analysis. *Quality Engineering*, 15(1):37–47, September 2002.

Cleynen, O. Repair process for a V2500 high-pressure turbine guide vane. Technical report, 2013.

Collopy, Paul and Hollingsworth, Peter. Value-Driven Design. In *AIAA Aviation Technology, Integration, and Operation Conference (ATIO)*, number September, pages 1–16, Hilton Head, South Carolina, 2009. AIAA.

Collopy, Paul D and Curran, Richard. The Challenge of Modeling Cost: Steps Toward a Solution. In *1st International Conference on Innovation and Integration in Aerospace Sciences 4-5*, Queen's University Belfast, Northern Ireland, UK. CEIAT, 2005a.

Collopy, Paul D and Curran, Richard. The Challenge of Modeling Cost: The Problem. In *1st International Conference on Innovation and Integration in Aerospace Sciences 4-5*, Queen's University Belfast, Northern Ireland, UK. CEIAT, 2005b.

Colwell, D. J. and Gillett, J. R. Spearman versus Kendall. *The Mathematical Gazette*, 66(438):307–309, 1982.

Costa, a. F. B. and Machado, M. a. G. A new chart based on sample variances for monitoring the covariance matrix of multivariate processes. *The International Journal of Advanced Manufacturing Technology*, 41(7-8):770–779, May 2008.

Cousineau, Denis; Brown, Scott, and Heathcote, Andrew. Fitting distributions using maximum likelihood: methods and packages. *Behavior research methods, instruments, & computers : a journal of the Psychonomic Society, Inc*, 36(4):742–56, November 2004.

Curran, R; Raghunathan, S, and Price, M. Review of aerospace engineering cost modelling: The genetic causal approach. *Progress in Aerospace Sciences*, 40(8):487–534, November 2004.

D Ammaro, Antonio and Montomoli, Francesco. Uncertainty quantification and film cooling. *Computers & Fluids*, 71:320–326, January 2013.

Das, C. Selection and Evaluation of Most Profitable Process Targets for the Control of Canning Quality. 28(2):259–266, 1995.

Dhar, Sushant; Saini, Nishant, and Purohit, R. A review on laser drilling and its Techniques. In *International Conference on Advances in Mechanical Engineering*, volume 2006, PunJab, India, 2006. AME.

Dodson, B.L. Determining the Optimal Target Value for a Process with Upper and Lower Specifications. *Quality Engineering*, 5(3):393–402, 1993.

Drain, D. and Gough, A.M. Applications of the Upside-Down Normal Loss Function. *IEEE Transaction on Semiconductor Manufacturing*, 9(1):143–145, 1996.

Duffuaa, Salih O. and Siddiqui, Atiq W. Process targeting with multi-class screening and measurement error. *International Journal of Production Research*, 41(7):1373–1391, January 2003.

Duffuaa, S.O. and El-Ga'aly, a. A multi-objective mathematical optimization model for process targeting using 100% inspection policy. *Applied Mathematical Modelling*, 37 (3):1545–1552, February 2013.

Duffuaa, S.O.; Al-Turki, U.M., and Kolus, A.A. Process-targeting model for a product with two dependent quality characteristics using acceptance sampling plans. *International Journal of Production Research*, 47(14):4031–4046, July 2009.

Dziak, John J; Coffman, Donna L, and Lanza, Stephanie T. Sensitivity and specificity of information criteria. 2012.

Elsayed, E.A. and Chen, A. Optimal levels of Process Parameters for Products with Multiple Characteristics. *International Jounral of Production Research*, 5(31):1117–1132, 1993.

Errico, D. fminsearchcon, 2006. URL http://uk.mathworks.com/help/index.html.

Feng, Qianmei and Kapur, Kailash C. Selection of optimal precision levels and specifications considering measurement error. *The International Journal of Advanced Manufacturing Technology*, 40(9-10):960–970, February 2008.

Fermanian, J-D.; Jaworski, P., and Durant, J. An Overview of the Goodness-of-Fit Test Problem for Copulas. In Hrdle, W., editor, *Copulae in Mathematical and Quantitative Finance*, pages 68–89. Springer, 2012.

Fig, Matt. *Combinator - combinations and permutations.* Matlab Central, 2009. URL http://www.mathworks.co.uk/matlabcentral/fileexchange/24325-combinator-combinations-and-permutations.

Fisher, R.A. *Design of experiments.* Oliver & Boyd, Edinburgh, 1935.

Fisher, R.A. *Statistics in Scientific Though in the Twentieth Century.* Watts, London, 1951.

Fluent, . Fluent 6.3 User's Guide. Technical report, 2012.

Forrester, A.I.J.; Sobester, A., and Keane, A.J. *Engineering Design Via Surrogate Modelling A Practical Guide.* Wiley, Chichester, 2008.

Fredricks, Gregory a. and Nelsen, Roger B. On the relationship between Spearman's rho and Kendall's tau for pairs of continuous random variables. *Journal of Statistical Planning and Inference*, 137(7):2143–2150, July 2007.

Frey, Daniel D; Jahangir, Ebad, and Engelhardt, Fredrik. Computing the Information Content of Decoupled Designs. *Research in Engineering Design*, 12:90–102, 2000.

Genest, Christian and Favre, Anne-catherine. Everything You Always Wanted to Know about Copula Modeling but Were Afraid to Ask. (August):347–368, 2007.

Genz, Alan. Numerical computation of rectangular bivariate and trivariate normal and t probabilities. *Statistics and Computing*, 14(3):251–260, August 2004.

Genz, Alan and Bretz, Frank. Methods for the Computation of Multivariate t-Probabilities. *Journal of Computational and Graphical Statistics*, 11:1–18, 2002.

Goldstein, R.; Eckert, E., and Ramsey Rhine, J. Film cooling with injection through holes: adiabatic wall temperatures downstream of a circular hole. *Journal of Engineering for Power*, 90:384–395, 1968.

Goldstein, R.; Eckert, E., and Burggraf, F. Effects of hole geo metry and density on three-dimensional film coolingitle. *International Journal of Heat and Mass Transfer*, 17:595–607, 1974.

Golhar, DY. Determination of the best means contents for a canning problem. *Journal of Quality Technology*, 19:82–84, 1987.

Golhar, Y.D. and Pollock, S.M. Determination of Optimal process mean and the upper limit for a canning problem.pdf. *Journal of Quality Technology*, 20:188–192, 1988.

Grinstead, Charles M. and Snell, Laurie J. *Grinstead and Snell ' s Introduction to Probability and in memory of.* Number July. The Chance Project, 2nd edition, 2006.

Gritsch, M.; Schulz, A., and Wittig, S. Adiabatic Wall Effectiveness Measurements of Film-Cooling Holes With Expanded Exits. *Journal of Turbomachinery*, 120(3):549, 1998.

Gritsch, Michael; Schulz, Achmed, and Wittig, Sigmar. Film cooling holes with expanded exits near hole heat transfer coefficients. 21:146–155, 2000.

Gritsch, Michael; Colban, Will; Schaar, Heinz, and Doobbeling, Klaus. Effect of Hole Geometry on the Thermal Performance of Fan-Shaped Film Cooling Holes. *Journal of Turbomachinery*, 127(4):718, 2005.

Guangchao, Li; Huiren, Zhu, and Huiming, Fan. Influences of Hole Shape on Film Cooling Characteristics with CO2 Injection. *Chinese Journal of Aeronautics*, 21(5): 393–401, October 2008.

Gupta, S.K.; Regli, W.C.; Das, D., and Nau, S. Automated Manufacturability Analysis : A Survey. *Research in Engineering Design*, 9(3):168–190, 1997.

Helie, Sebastien. An Introduction to Model Selection : Tools and Algorithms. 2(1):1–10, 2006.

Ho, Chao-ching; Chang, Yuan-jen; Hsu, Jin-chen; Kuo, Chia-lung, and He, Jun-jia. Monitoring and breakthrough control of laser drilled holes by means of machine vision. 37(3):355–363, 2012.

Ho, L.L. and Quinino, Roberto C. Optimum Mean Location in a Poor-Capability Process. *Quality Engineering*, 16(2):257–263, January 2003.

Hollinger, Peggy and Powley, Tanya. Rolls-Royce sets out on path to rebuild investor confidence. *Financial Times*, October 2014.

Hong, S. H. Optimum mean value and screening limits for production processes with multi-class screening. *International Journal of Production Research*, 37(1):155–163, January 1999.

Hunter, W.G. and Kartha, C.P. Determining the Most Profitable Value for a Production Process. *Journal of Quality Technology*, 9:176–181, 1977.

Huyse, L. Solving Problems of Optimization Under Uncertainty as Statistical Decision Problems. In *42nd AIAA Structures, Structural Dynamics and Materials Conference and Exhibit*, Seatle, 2001. AIAA.

Hyams, D. G. and Leylek, J. H. A Detailed Analysis of Film Cooling Physics: Part III— Streamwise Injection With Shaped Holes. *Journal of Turbomachinery*, 122(1): 122, 2000.

Jeang, A. An approach of tolerance design for quality improvement and cost reduction. *International Journal of Production Research*, 35(5):1193–1211, May 1997.

Jeang, A. Combined parameter and tolerance design optimization with quality and cost. *International Journal of Production Research*, 39(5):923–952, January 2001.

Jeang, Angus. Tolerance chart balancing with a complete inspection plan taking account of manufacturing and quality costs. *The International Journal of Advanced Manufacturing Technology*, 55(5-8):675–687, December 2010.

Jeang, Angus and Chung, Chien-Ping. Process capability analysis based on minimum production cost and quality loss. *The International Journal of Advanced Manufacturing Technology*, 43(7-8):710–719, September 2008.

Jeang, Angus and Lin, Yang-Kuei. Product and process parameters determination for quality and cost. *International Journal of Systems Science*, (March):1–13, January 2013.

Jenab, K. and Liu, D. A graph-based model for manufacturing complexity. *International Journal of Production Research*, 48(11):3383–3392, June 2010.

Jeyapaul, R.; Shahabudeen, P., and Krishnaiah, K. Quality management research by considering multi-response problems in the Taguchi method – a review. *The International Journal of Advanced Manufacturing Technology*, 26(11-12):1331–1337, April 2004.

Jones, Sam. The Formula that Felled Wall St. *The Financial Times*, April 2009.

Jongen, T. *Simulation and modeling of turbulent incompressible fluid flows*. Phd. thesis, EPF Lausanne, Switzerland, 1998.

Kapur, K.C. and Cho, B.R. Economic Design and Development of Specifications. *Quality Engineering1*, 6(3):401–417, 1994.

Kapur, K.C. and Cho, B.R. Economic design of the specification region for multiple quality characteristics. *IIE Transactions*, 28(3):237–248, March 1996.

Kapur, K.C. and Wang, C.J. Economic design of specifications based on Taguchi's concept of quality loss function. In DeVor, R.E. and Kapoor, S.G., editors, *Quality: Design, Planning, and Control*, pages 23–36, Boston, 1987. The Winter annual meeting of the American Society of Mechanical Engineers.

Keane, A J and Scanlan, J P. Design search and optimization in aerospace engineering. *Philosophical transactions. Series A, Mathematical, physical, and engineering sciences*, 365(1859):2501–29, October 2007.

Keane, A.J. and Nair, P.B. *Computational Approaches for Aerospace Design*. Wiley, Chichester, 2005.

Khasawneh, Mohammad T.; Bowling, Shannon R., and Cho, Byung Rae. A Markovian approach to determining process means with dual quality characteristics. *Journal of System Science and Systems Engineering*, 17(1):66–85, March 2008.

Kohli, A. and Thole, K.A. Entrance Effects on Diffused Film Cooling Holes. In *International Gas Turbine & Aeroengine Congress & Exhibition*, Stockholm, Sweden, 1998. ASME.

Kovach, Jami and Cho, Byung Rae. Solving Multiresponse Optimization Problems Using Quality Function–Based Robust Design. *Quality Engineering*, 20(3):346–360, June 2008.

Kreutz, Ernst Wolfgang. Process Development and Control of Laser Drilled and Shaped Holes in Turbine Components. *Journal of Laser Micro/Nanoengineering*, 2(2):123–127, June 2007.

Krishnaswami, M. and Mayne, R.W. Optimizing tolerance allocation based on manufacturing cost and quality loss. In *Advances in Design Automation*, pages 211–218. ASME, 1994.

Langley, R.S. Unified approach to probabilistic and possibilistic analysis of uncertain systems. *ASCE Journal of Engineering Mechanics*, 126:1163–1172, 1999.

Langmaak, Stephan; Wiseall, Stephen; Bru, Christophe; Adkins, Russell; Scanlan, James, and Sóbester, András. An activity-based-parametric hybrid cost model to estimate the unit cost of a novel gas turbine component. *International Journal of Production Economics*, 142(1):74–88, March 2013.

Launder, B. and Spalding, D.B. *Lectures in Mathematical Models of Turbulence*. Academic Press, London, 1972.

Lee, Ki-Don and Kim, Kwang-Yong. Shape optimization of a fan-shaped hole to enhance film-cooling effectiveness. *International Journal of Heat and Mass Transfer*, 53(15-16): 2996–3005, July 2010.

Lee, Ki-Don and Kim, Kwang-Yong. Surrogate based optimization of a laidback fan-shaped hole for film-cooling. *International Journal of Heat and Fluid Flow*, 32(1): 226–238, February 2011.

Lee, Ki-don; Husain, Afzal, and Kim, Kwang-yong. Multi-objective Optimization of a Laidback Fan Shaped Film-Cooling Hole Using Evolutionary Algorithm. (June): 150–159, 2010.

Lee, Min Koo and Elsayed, Elsayed a. Process mean and screening limits for filling processes under two-stage screening procedure. *European Journal of Operational Research*, 138(1):118–126, April 2002.

Lehmann, E. L. Some Concepts of Dependence. *Annals of Mathematical Statistics*, 37 (11):1137–1153, 1966.

Leung, Bartholomew P.K. and Spiring, Fred a. The inverted beta loss function: properties and applications. *IIE Transactions*, 34(12):1101–1109, December 2002.

Leung, B.P.K. and Spring, F.A. Some Properties of the Family of Inverted Probability Loss Functions Bartholomew. *Quality Technology and Quantitative Management*, 1 (1):125–147, 2004.

Li, David X. On Default Correlation : A Copula Function Approach This draft : April 2000 First draft : September 1999 On Default Correlation : A Copula Function Approach. (99), 2000.

Li, William and Wu, C F J. An Intergrated Method of Parameter Design and Tolerance Design. *Quality Engineering*, 11(3):417–425, March 1999.

Li, Xianchang and Wang, Ting. Effects of Various Modeling Schemes on Mist Film Cooling Simulation. *Journal of Heat Transfer*, 129(4):472, 2007.

Liu, W. and Raghavachari, M. The Target Mean Problem for an Arbitrary Quality Characteristic Distribution. *International Journal of Production Research*, 35(6): 1713–1728, June 1997.

Lohr, Steve. Wall Street's Math Wizards Forgot a Few Variables. *The New York Times*, September 2009.

Lowth, Stewart and Axinte, Dragos. An assessment of "variation conscious" precision fixturing methodologies for the control of circularity within large multi-segment annular assemblies. *Precision Engineering*, 38(2):379–390, April 2014.

Makki, Y. and Jakubowski, G. An experimental study of film cooling from diffused trapezoidal shaped holes. In *4th Thermophysics and Heat Transfer Conference*, number 36, Reston, Virigina, June 1986. American Institute of Aeronautics and Astronautics.

Mansoor, E.M. Proceedings of the Institution of Mechanical Engineers Part H. *Proceedings of the Institution of Mechanical Engineers. Part H, Journal of engineering in medicine*, 222(7):i, October 1963.

Marsh, R.; Jonik, M.; Lanham, J.; Cheung, W. M.; Newnes, L. B., and Mileham, a. R. Modelling an assembly process using a close coupled generative cost model and a discrete event simulation. *International Journal of Computer Integrated Manufacturing*, 23(3):257–269, March 2010.

Marx, William J; Mavris, Dimitri N, and Schrage, Daniel P. A hierarchical aircraft life cycle cost analysis model. In *American Institute of Aeronautics and Astronautics*, pages 1–18, Anaheim, CA, September 19–21., 1995.

Mathworks, . Matlab Functions, 2012. URL http://uk.mathworks.com/help/index.html.

Matteis, Roberto D E. *Fitting copulas to data*. Diploma thesis, University of Zurich, 2001.

McNally, C.a.; Folkes, J., and Pashby, I.R. Laser drilling of cooling holes in aeroengines state of the art and future challenges. *Materials Science and Technology*, 20(7):805–813, July 2004.

Miles, B. L. and Swift, K. Design for manufacture and assembly. *Manufacturing Engineer*, pages 221–224, 1998.

Mittal, Sanjiv and McNally, Peter. Line Defect Control to Maximize Yields. *Intel Technology Journal*, (Q4):1–3, 1994.

Montgomery, D.C. Quality Improvement in the Modern Business Environment. In Welter, J.; Dumas, S, and Sapira, L., editors, *Intorduction to Statistical Quality Control*, chapter 1, pages 5–7. John Wiley & Sons, Jefferson City, 6th edition, 2009.

Moorhead, P.R. and WU, C.F.J. Cost-Driven Parameter Design. *Technometrics*, 40(2): 111–119, 1998.

Mukhopadhyay, Samar K and Chakraborty, Debopam. Optimal process variance under Taguchi loss. 1995.

Myrtveit, Ingunn and Stensrud, Erik. A Controlled Experiment to Assess the Benefits of Estimating with Analogy and Regression Models. *IEEE Transactions on SoftwareEngineering*, 25(4):510–525, 1999.

Naidu, N.V.R. Mathematical model for quality cost optimization. *Robotics and Computer-Integrated Manufacturing*, 24(6):811–815, December 2008.

NASA, . NASA Armstrong Photo Gallery, 2015. URL http://www.nasa.gov/centers/armstrong/multimedia/imagegallery/.

Natrella, M.; Croarkin, C., and Tobias, P. e-Handbook of Statistical Methods, 2012. URL http://www.itl.nist.gov/div898/handbook.

Nelsen, Roger. *An Introduction to Copulas*. Springer, New York, 2nd edition, 2006. ISBN 10: 0-387-28659-4.

Nelson, L.S. Best Target Value for a Production Process. *Journal of Quality Technolgy*, 10(2):88–89, 1978.

Pande, P.S.; Neuman, R.P., and Cavanagh, R.R. *The Six Sigma Way: How GE, Motorola, and Other Top Companies Are Honing Their Performance*. McGraw-Hill, New York, 2000.

Park, G.J.; Hwang, K.H.; Lee, T.H., and Lee, K.H. Robust Design: An Overview. *AIAA Journal*, 44(1):181–191, January 2006.

Park, Gyung-jin. Calculation of information content in axiomatic design. In *The Third International Conference on Axiomatic Design*, pages 1–6, Seoul, 2004. Proceedings of ICAD.

Park, Gyung-jin. *Analytic Method for Design Practice*. Springer, London, 2007.

Peng, Chien-Yi and Khasawneh, Mohammad T. A Markovian approach to determining optimum process means with inspection sampling plan in serial production systems. *International Journal of Advanced Manufacutring Technology*, 72(9-12):1299–1323, March 2014.

Phadke, M.S. *Quality engineering using robust design*. Prentice Hall, Michigan, 1989.

Philby, J.D. and Davies, G.J. UK Patent, CA2041356 A1.

Pope, S.B. *Turbulent Flows*. Cambridge University Press, Cambridge, 6th edition, 2009.

Poprawe, R; Kelbassa, I; Walther, K; Witty, M; Bohn, D, and Krewinkel, R. Optimising and Manufacturing a Laser-Drilled Cooling Hole Geometry for Effustion-Cooled Multi-Laser Plates. In *The 12th International Symposium on Transport Phenomena and Dynamics of Rotating Machinery*, number 1999, Honolulu, Hawaii, 2008.

Pulak, M F S and Al-Sultan, K S. The Optimum Targeting for a Single Filling Operation with Rectifying Inspection. *Omega - The International Journal of Management Science*, 24(6):727–733, 1996.

Pyzdek, T. *The Six Sigma Handbook*. McGraw-Hill, New York, 1st edition, 2001.

Pyzdek, T. *Non-Normal Distributions in the Real World*. Quality America's Online Knowledge Centre, 2002. URL http://www.qualityamerica.com/Knowledgecenter/statisticalinference/non%_normal_distributions_in_the_real_world.asp.

Rackwitz, Rüdiger. Reliability analysis—a review and some perspectives. *Structural Safety*, 23(4):365–395, October 2001.

Rahim, M A and Al-sultan, Khaled S. Joint determination of the optimum target mean and variance of a process. pages 192–199, 2000.

Rao, A. R.; Scanlan, J. P., and Keane, A. J. Technical Review: Applying Multiobjective Cost and Weight Optimization to the Initial Design of Turbine Disks. *Journal of Mechanical Design*, 129(12):1303–1310, 2007.

Reagle, Colin J. *Heat Transfer Measurements Using Thin Film Gauges and Infrared Thermography on a Film Cooled Transonic Vane*. Masters thesis, Virginia Polytechnic Institute and State University, 2009.

Rehman, Sumaira and Guenov, Marin D. A methodology for modelling manufacturing costs at conceptual design. *Computers & Industrial Engineering*, 35(3-4):623–626, December 1998.

Rhee, Dong Ho; Lee, Youn Seok, and Cho, Hyung Hee. Film Cooling Effectiveness and Heat Transfer of Rectangular-Shaped Film Cooling Holes. In *Turbo Expo 2002, Parts A and B*, pages 21–32, Amsterdam, The Netherlands, 2002. ASME. ISBN 0-7918-3608-8.

Robinson, David G. A Survey of Probabilistic Methods Used in Reliability Risk and Uncertainty Analysis. Technical report, Sandia National Laboratories, 1998.

Rudolph, G Unter. The Fundamental Matrix of the General Random Walk with Absorbing Boundaries . Technical Report Sfb 531, Technical Report of the Collaborative Research Center - Comptational Intelligence, University of Dortmund, Dortmund, 1999.

Rush, Christopher and Roy, Rajkumar. Analysis of cost estimating processes used within a concurrent engineering environment throughout a product life cycle. In *Seventh ISPE International Conference on Concurrent Engineering: Research and Application*, volume 44, Lyon, France, 2000. Technomic.

Rush, Christopher and Roy, Rajkumar. Expert judgement in cost estimating: Modelling the reasoning process. *Concurrent Engineering: Research & Applications (CERA)*, 9 (4), 2001.

Salmon, Felix. Recipe for Disaster: The Formula That Killed Wall Street. *Wired Magazine*, 2009.

Sargison, J. E.; Guo, S. M.; Oldfield, M. L. G.; Lock, G. D., and Rawlinson, A. J. A Converging Slot Hole Film Cooling Geometry Part 1 Low Speed Flat-Plate Heat Transfer and Loss. In *Volume 3: Heat Transfer; Electric Power; Industrial and Cogeneration*. ASME, June 2001. ISBN 978-0-7918-7852-1.

Sargison, J. E.; Guo, S. M.; Oldfield, M. L. G.; Lock, G. D., and Rawlinson, A. J. A Converging Slot Hole Film Cooling Geometry Part 2 Transonic Nozzle Guide Vane Heat Transfer and Loss. *Journal of Turbomachinery*, 124(3):461, 2002.

Saumweber, Christian and Schulz, Achmed. Comparison the Cooling Performance of Cylindrical and Fan-Shaped Cooling Holes With Special Emphasis on the Effect of Internal Coolant Cross-Flow. In *Volume 4: Heat Transfer, Parts A and B*, pages 893–903. ASME, 2008. ISBN 978-0-7918-4314-7.

Saumweber, Christian and Schulz, Achmed. Effect of Geometry Variations on the Cooling Performance of Fan-Shaped Cooling Holes. *Journal of Turbomachinery*, 134(6): 061008, 2012.

Saumweber, Christian; Schulz, Achmed, and Wittig, Sigmar. Free-Stream Turbulence Effects on Film Cooling With Shaped Holes. *Journal of Turbomachinery*, 125(1):65, 2003.

Savage, G. J.; Tong, D., and Carr, S.M. Optimal Mean and Tolerance Allocation Using Conformance-based Design. *Quality and Reliability Engineering International*, 22(4): 445–472, June 2006.

Savage, G.J. and Seshadri, R. Minimizing Cost of Multiple Response Systems by Probabilistic Robust Design. *Quality Engineering*, 16(1):67–74, January 2003.

Savage, G.J. and Swan, D.A. Probabilisitc Robust Design with Multiple Quality Characteristics. *Quality Engineering*, 13(4):629–640, June 2001.

Scanlan, James; Rao, Abhijit; Bru, Christophe; Hale, Peter, and Marsh, Rob. DATUM Project: Cost Estimating Environment for Support of Aerospace Design Decision Making. *Journal of Aircraft*, 43(4):1022–1028, July 2006.

Schmidt, R. and Pfeifer, P. Economic Selection of the Mean and Upper Limit for a Canning Problem with Limited Capacity. *Journal of Quality Technology*, 23(4):312–317, 1991.

Schmidt, Thorsten. Coping with Copulas. In Rank, Jorn, editor, *Copulas - From Theory to Applications in Finance*, chapter 1. Risk Books, London, 1st edition, 2006.

Schneider, M.; Berthe, L.; Muller, M., and Fabbro, R. A fast method for morphological analysis of laser drilling holes. *Journal of Laser Applications*, 22(4):127, 2010.

Schroeder, Robert P and Thole, Karen A. Adiabatic Effectiveness Measurements for a Baseline Shaped Film Cooling Hole. pages 1–13, 2014.

Schweizer, B. and Wolff, E.F. On Nonparametric Measures of Dependence for Random Variables. *The Annals of Statistics*, 9(4):879–885, 1981.

Selim, Shokri Z. and Al-Zu'bi, Walid K. Optimal means for continuous processes in series. *European Journal of Operational Research*, 210(3):618–623, May 2011.

Shannon, C E. The mathematical theory of communication. *The Bell System Technical Journal*, 27:379–423, 1948.

Sheppard, Mike. Allfitdist, 2012. URL http://www.mathworks.co.uk/matlabcentral/fileexchange/34943-fit-all-valid-parametric-probability-distributions-to-data/content/allfitdist.m.

Shetty, Devdas; Eppes, Tom; Campana, Claudio; Filburn, Thomas, and Nazaryan, Nikolai. New Approach to the Inspection of Cooling Holes in Aero-Engines. pages 129–135, 2008.

Shewhart, Walter. *Economic control of quality of manufactured product*. D. Van Nostrand Company, Inc., New York, the bell edition, 1931.

Shiau, G.H. A Study of the Sintering Properties of Iron Ores using Taguchi's Parameter Design. *Journal of the Chinese Statistical Association*, 28:253–275, 1990.

Shih, Tsan-Hsing; Liou, William W.; Shabbir, Aamir; Yang, Zhigang, and Zhu, Jiang. A new k-e eddy viscosity model for high reynolds number turbulent flows. *Computers & Fluids*, 24(3):227–238, March 1995.

Shorey, A.B.; Piech, G.A.; Li, X.; Thomas, J.C.; Keech, J.T.; Domey, J.J., and Shustack, P.J. *Sacrificial Cover Layers For Laser Drilling Substrates and Methods Thereof*, volume 1. Corning Incorporated, 2014.

Shukor, S.a. and Axinte, D. Manufacturability analysis system: issues and future trends. *International Journal of Production Research*, 47(5):1369–1390, March 2009.

Singh, P K; Jain, P K, and Jain, S C. Important issues in tolerance design of mechanical assemblies. Part 1: tolerance analysis. *Proceedings of the Institution of Mechanical Engineers, Part B: Journal of Engineering Manufacture*, 223(10):1225–1247, October 2009.

Sklar, A. *Fonctions de repartition a n dimensions e leurs marges.* Publications de l'Institut de Statistique de l'Univiversit´ e de Paris, Paris, 1959.

Spiring, F.A. The reflected normal loss function. *The Canadian Journal of Statistics*, 21(3):321–330, 1993.

Spiring, F.A. and Yeung, A.S. A general class of loss functions with industrial applications. *Journal of Quality Technology*, 30(48):152–162, 1998.

Spotts, W.F. Allocanon of tolerance to minimize cost of assembly. *Journal of Engineering for Industry*, pages 762–764, 1973.

Springer, C. A Method for Determining the Most Economic Position of a Process Mean. *Industrial Quality Control*, 8(1):36–39, 1951.

Stahl, H. Philip. Survey of cost models for space telescopes. *Optical Engineering*, 49(5): 053005, 2010.

Suh, Nam P. On an axiomatic approach to manufacturing systems. *Journal of Engineering for Industry Trans. ASME*, 100:27–130, 1978.

Suh, Nam P. *The Principles of Design.* Oxford University Press, New York, 1st edition, 1990.

Suh, Nam P. *Axiomatic Design - Advances and Applications.* Oxford University Press, New York, 2001.

Sun, F.; Laramee, J., and Ramberg, J. On Spiring's inverted normal loss function. *The Canadian Journal of Statistics*, 24:241–249, 1996.

Sundararajan, C.R. *Probabilistic structural mechanics handbook: theory and industrial applications.* Chapman & Hall, 1st edition, 1995.

Taguchi, G. *Introduction to Quality Engineering.* Asian Producatvity Organization, Minato-ku, Tokyo, 1986.

Tai, C.Y.; Chen, T.S., and Wu, M.C. An Enhanced Taguchi Method for Optimizing SMT Process. *Journal of Electronics Manufacutring*, 2:91–100, 1992.

Tammineni, S. V.; Rao, a. R.; Scanlan, J. P.; a.S. Reed, P., and Keane, a. J. A knowledge-based system for cost modelling of aircraft gas turbines. 20(3):289–305, June 2009.

Taylor, N. I. Cost Engineering. In *85th Meeting of the AGARD Structures and Material Panel*, Neuilly-Sur-Seine France, 1997.

Teeravaraprug, Jirarat. Targets for Multiple Optimum Process Quality Characteristics Analysis Using Regression. 2006.

Teeravaraprug, Jirarat and Cho, Byung Rae. Designing the optimal process target levels for multiple quality characteristics. *International Journal of Production Research*, 40 (1):37–54, January 2002.

Thole, K.; Gritsch, M.; Schulz, A., and Wittig, S. Flowfield Measurements for Film-Cooling Holes With Expanded Exits. *Journal of Turbomachinery*, 120(2):327, 1998.

Tops, Robbin. *Copulas and Correlation in Credit Risk " Who will pay the difference ?"*. PhD thesis, University of Amsterdam, 2010.

Tutorialspoint, . Six Sigma Methodology, 2014. URL http://www.tutorialspoint.com/six_sigma/index.htm.

Uem, Theo Van. Modified discrete random walk with variable absorption probabilties. Technical report, Amsterdam School of Technology, Amsterdam, The Netherlands, 2009.

Walck, Christian. *Hand-book on Statistical Distribtuions for Experimentalists*. Number September. Particle Physics Group - University of Stockholm, Stockholm, 2007.

Walther, K; Brajdic, M; Dietrich, J; Hermans, M; Horn, A; Kelbassa, I, and Poprawe, R. Manufacturing of Shaped Holes in Multi-Layer Plates by Laser Drilling. In *Proceedings of the 3rd Pacific International Conference on Application of Lasers and Optics*, number 1001, Beijing, China, 2008.

Wang, Antai. Goodness-of-fit Test for Archimedean Copula Models. *Statistica Sinica*, 20:441–453, 2010.

Wang, Ting and Zhao, Lei. Discussions of some myths and concerned practices of film cooling research. *International Journal of Heat and Mass Transfer*, 54(9-10):2207–2221, April 2011.

Wen, D and Mergen, A.E. Running a process with poor capability. *Quality Engineering*, 11(4):505–509, July 1999.

Wilhelm, Stefan; Manjunath, B G; Carlo, Monte, and Gibbs, The. tmvtnorm : A Package for the Truncated Multivariate Normal Distribution Generation of random numbers computation of marginal densities. 2(June):25–29, 2010.

Williams, Paul E. *Laser Drilling Components*. US Patent, 8 164 026B2, 2012.

Wilson, David Robert. *An Exploratory Study of Complexity in Axiomatic Design*. PhD thesis, Massachusetts Institute of Technology, 1980.

Wolfshtein, M. The velocity and temperature distribution in one-dimensional flow with turbulence augmentation and pressure gradient. *International Journal of Heat and Mass Transfer*, 12(3):301–318, March 1969.

Wos, F.J. Laser Hole-Shaping Improves Combustion Turbine Efficiency. *POWER*, 2010.

Wright, T. P. Factors affecting the cost of airplanes. *Journal of Aeronautical Science*, 3 (2), 1936.

Wu, C. C. and Tang, G.R. Tolerance design for products with asymmetric quality losses. *International Journal of Production Research*, 36(9):2529–2541, September 1998.

Wu, Chin-Chung; Chen, Zhuoning, and Tang, Geo-ry. Component tolerance design for minimum quality loss and manufacturing cost. *Computer In Industry*, 35:223–232, 1998.

Wu, Ful-Chiang and Chyu, Chiuh-Cheng. Optimization of robust design for multiple quality characteristics. *International Journal of Production Research*, 42(2):337–354, January 2004.

Yan, Jun. Enjoy the Joy of Copulas : With a Package copula. *Journal of Statistical Software*, 21(4), 2007.

Yao, Wen; Chen, Xiaoqian; Luo, Wencai; van Tooren, Michel, and Guo, Jian. Review of uncertainty-based multidisciplinary design optimization methods for aerospace vehicles. *Progress in Aerospace Sciences*, 47(6):450–479, August 2011.

Yates, F. Sir Ronald Fisher and the Design of Experiments. *Biometrics*, 20(2):307–321, 1964.

Younossi, O.; Arena, M.V.; Moore, R.M.; M., Lorell; Mason, J., and Graser, J.C. Military Jet Engine Acquisition: technology basics and cost-estimating methodology. Technical report, US Air Force, RAND, Santa Monica, CA, USA, 153, 2002.

Yu, Y.; Yen, C.H.; Shih, T. I.-P.; Chyu, M. K., and Gogineni, S. Film Cooling Effectiveness and Heat Transfer Coefficient Distributions Around Diffusion Shaped Holes. *Journal of Heat Transfer*, 124(5):820, 2002.

Zang, C.; Friswell, M.I., and Mottershead, J.E. A review of robust optimal design and its application in dynamics. *Computers & Structures*, 83(4-5):315–326, January 2005.

Zang, T.A.; Hemsch, M.J.; Hilburger, M.W.; Kenny, S.P.; Luckring, J.M.; Maghami, P.; Padula, S.L., and Jefferson, W.J. Needs Based and Opportunities Multidisciplinary Vehicles for Uncertainty- Design Methods for Aerospace. Technical Report July, NASA, 2002.

Zhang, Y F; Fuh, J Y H, and Chan, W T. Feature-based cost estimation for packaging networks products using neural networks. *Computers in Industry*, 32:95–113, 1996.